The conferences on piezoelectronics are nearly regularly organized in Poland since 1968. This volume contains selected papers presented at the VII-th Conference on Piezoelectronics which was held on April 25–27, 1990 at Serock near Warsaw. Some of them were delivered to the Programme Committee in polish and russian language and were translated to english on behalf the editors of this volume. The content shows that piezoelectronics is still a developing branch of science and technology far from saturation. A big effort is containning in developing new piezoelectronic sensors of various physical and chemical quantities. Piezoelectric resonators are continuously expanding into the microwave frequency region. Thin films piezoelectric structures find new applications. These is also a continuous effort to develop new piezoelectric materials.

The edition of this volume was possible thanks to the editors of *Archives of Acoustics* and the support given by Institute of Fundamental Technological Research of the Polish Academy of Sciences.

General Editor

Prof. Stefan Hahn

ARCHIVES OF ACOUSTICS
16, 1, 5-9 (1991)

APPLICATION OF ACOUSTOELECTRONIC DEVICES WITH REFLECTIVE ARRAYS TO SIGNAL PROCESSING

M. U. ALEXANDROV, V. I. ROGATCHEV, A. V. YANTCHENKO

Leningrad Institute of Aviation Instrument Making
(Leningrad, 190 000, USSR)

1. Comparative characteristics of devices with reflective arrays and IDT

A typical SAW device with IDT is shown in Fig. 1. When an electrical signal is fed to the fingers of input IDT, a surface acoustic wave propagating to output IDT is excited due to the piezoeffect. In output IDT the acoustic wave is transformed into an electric signal. The layout of IDT fingers determines the transmission coefficient or pulse response of the device. In devices with reflective arrays (RA), surface or bulk

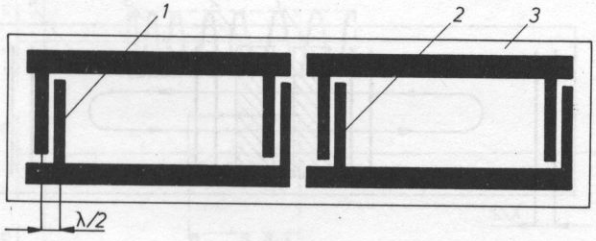

FIG. 1

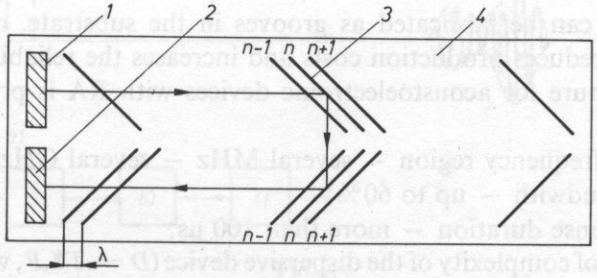

FIG. 2

waves are radiated and received with special transducers, and electrical characteristic are determined by the RA layout (Fig. 2).

A comparative analysis of acustoelectronic devices leads to the following conclusions:

– the distance between adjacent fingers in IDT is equal to $\lambda/2$ (where λ – acoustic wavelength), and the same distance in RA – λ. This make it possible to double operating frequencies with the same technological equipment.

– when IDT has defects (such as shorting or disconnections) the device is unsuitable. The same defects in RA do not affect device performance.

– the minimum absolute passband of a device is determined by pulse response duration which in turn is determined by the length of the piezoplate in a device with IDT. In devices with RA, pulse response duration is doubled due to the double path along the plate.

– in devices with RA, non-piezoelectric substrates can be used; in this way dimensions of the devices can be increased and their costs reduced.

– every sample of pulse response in RA (Fig. 2) is formed by interactions on several reflectors ($n-n$, $n-1-n+1$, $n+1-n-1$), etc.). That averages up all imperfections of their disposition and thus reduces requirements to the equipment [1].

– metal fingers in IDT on the way of SAW propagating cause dispertion or SAW wavefront shift. RA in forms of grooves or strips do not cause dispersion.

– multireflections of acoustic waves in resonators (Fig. 3) considerably increase pulse response duration in smaller devices.

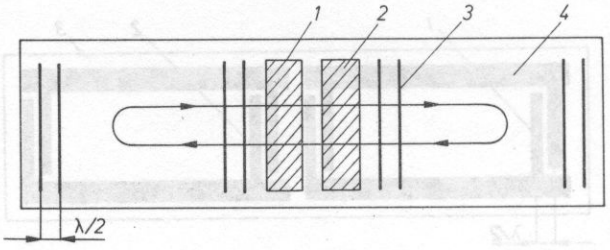

FIG. 3

– as RA can be fabricated as grooves in the substrate, metallization is not required. This reduces production costs and increases the reliability of devices.

A good future for acoustoelectronic devices with RA is proved by their high performance:

operating frequency region – several MHz – several GHz:

relative bandwith – up to 60%;

pulse response duration – more than 100 μs;

coefficient of complexity of the dispersive device ($D = .T^*.F$, where $.T$ – difference of the group delay characteristic in passband $.F$) – more than 10 000.

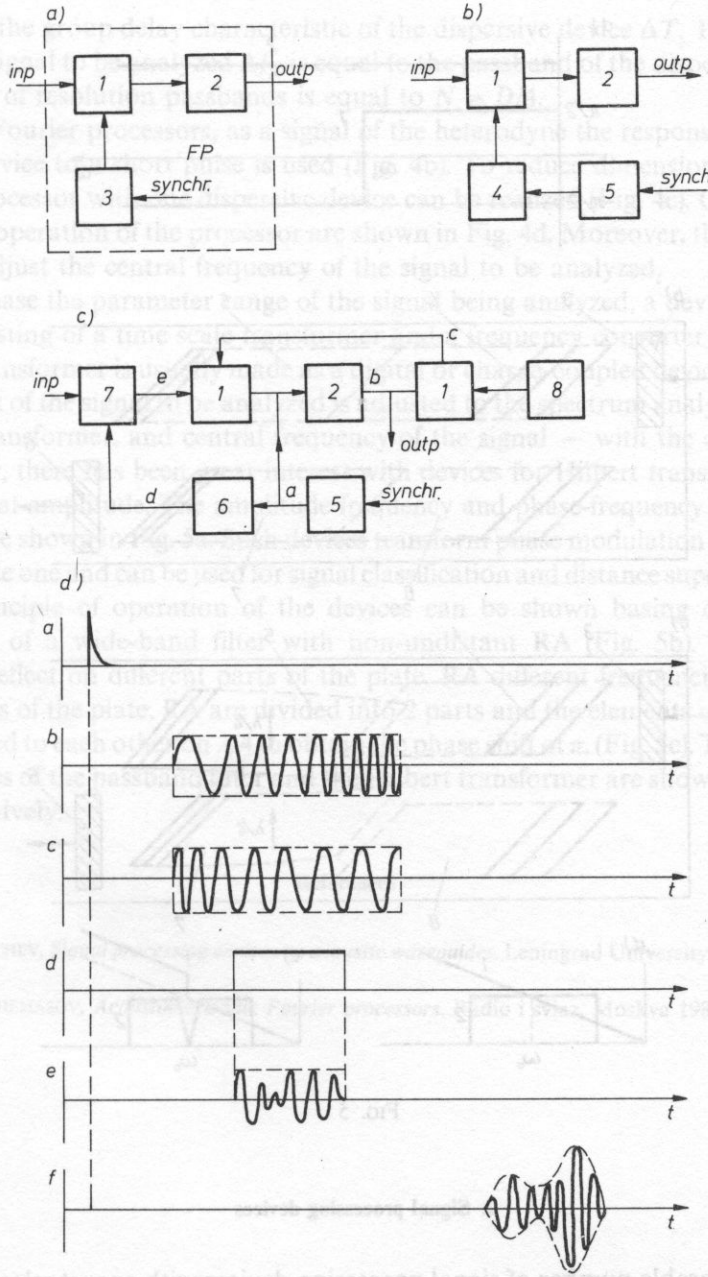
a)
inp
1
2
outp
FP
3
synchr.
b)
inp
1
2
outp
4
5
synchr.
c)
c
inp
7
e
1
2
b
1
8
outp
d
6
a
5
synchr.
d)
a
t
b
t
c
t
d
t
e
t
f
t
e)
9
10
11

FIG. 4

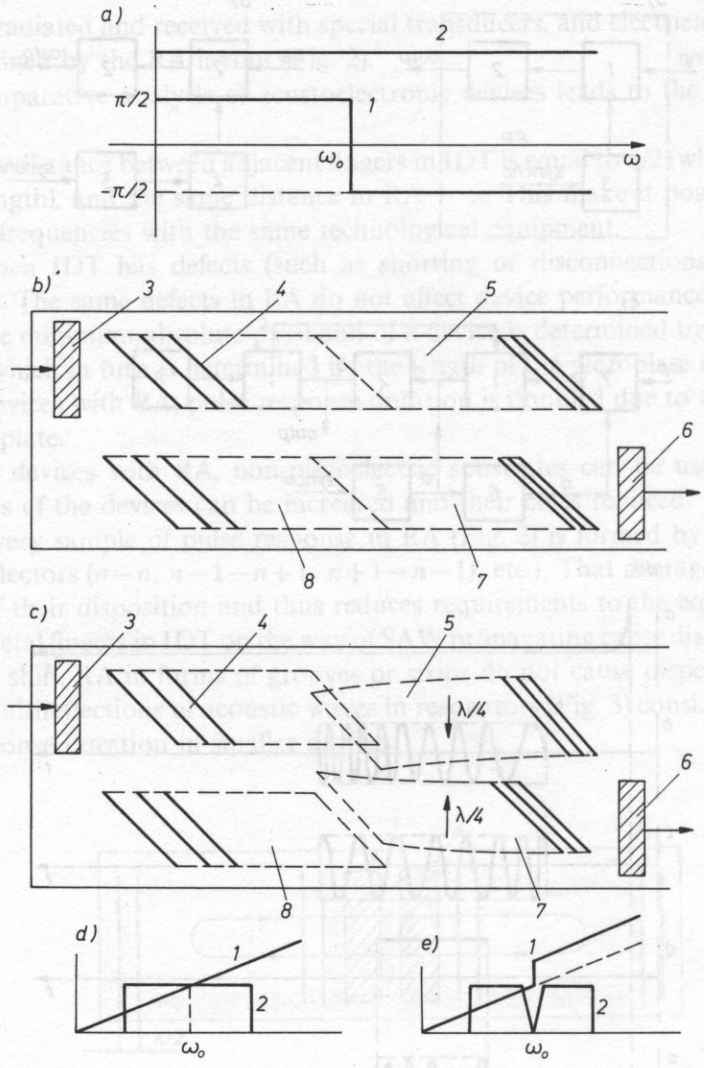

FIG. 5

2. Signal processing devices

A considerable number of signal processing devices with acoustoelectronic components is described in literature [2].

Dispersive Fourier processors operating in real time are widely used (Fig. 4a). They consist of multiplier *1*, churp heterodyne *2*, and dispersive device *3*. The parameters of the spectral analyzer are determined by those of the dispersive device. Frequency resolution $\delta f = 1/T_S$ is determined by sample duration T_S which is equal to half of the

difference of the group delay characteristic of the dispersive device ΔT. The spectrum widthof the signal to be analyzed Δf_S is equal to the passband of the dispersive device. The number of resolution passbands is equal to $N = D/4$.

In real Fourier processors, as a signal of the heterodyne the response of another dispersive device to a short pulse is used (Fig. 4b). To reduce dimensions and costs, a Fourier processor with one dispersive device can be realized (Fig. 4c). Oscillograms showing the operation of the processor are shown in Fig. 4d. Moreover, this processor enables to adjust the central frequency of the signal to be analyzed.

To increase the parameter range of the signal being analyzed, a device shown in Fig. 4e consisting of a time scale transformer and a frequency converter is used. The time scale transformer is usually made as a digital or charge-coupled device [2]. In this case duration of the signal to be analyzed is adjusted to the spectrum analyzer with the time scale transformer, and central frequency of the signal – with the converter.

Recently, there has been great interest with devices for Hilbert transformation of complex signal amplitude. The amplitude frequency and phase-frequency responses of the devices are shown in Fig. 5a. Such devices transform phase modulation (phase hops) into amplitude one and can be used for signal classification and distance superresolution.

The principle of operation of the devices can be shown basing on a certain modification of a wide-band filter with non-undistant RA (Fig. 5b). As different frequencies reflect on different parts of the plate. RA different frequencies reflect on different parts of the plate, RA are divided into 2 parts and the elements of the second part are shifted to each other on $\lambda/4$ to obtain the phase shift of π. (Fig. 5c). The resulting characteristics of the passband filter and the Hilbert transformer are shown in Figs. 5d and e respectively.

References

[1] V. I. ROGATCHEV, *Signal processing devices on acoustic waveguides.* Leningrad University pb., Leningrad 1979.

[2] V. N. KOTCHEMASOV, *Acoustoelectronic Fourier processors*, Radio i sviaz, Moskva 1987.

ARCHIVES OF ACOUSTICS
16, 1, 11-30(1991)

SURFACE ACOUSTIC WAVES AND DEVICES

B. A. AULD

Department of Applied Physics Stanford University
(Stanford, California 94305, USA)

The purpose of this paper is to review the basic physics of surface wave propagation on piezoelectric substrates, and to survey the applications of these waves to various types of devices. Smooth, layered, and corrugated substrates will be considered. Methods of analysis will be reviewed, and general characteristics of the solutions (polarization, velocity, piezoelectric coupling, etc.) will be summarized. To conclude, a brief overview of the historical development of surface wave devices (delay lines, resonators, correlators, convolvers etc.) will be presented, and recent trends in applications will be described.

1. History and classification of wave types

The story of surface acoustic wave devices begins with the publication in 1885 of a paper by LORD RAYLEIGH that analyzed the propagation of waves along the plane surface of an isotropic elastic solid [12]. In this paper Rayleigh was influenced by earlier work of LAMB in a paper (1882) on the vibrations of an elastic sphere, and he predicted that these surface waves would probably play an important role in the study

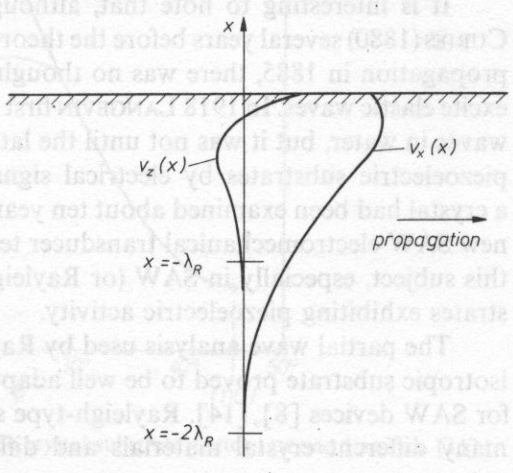

FIG. 1. Particle displacement components for Rayleigh surface wave (SAW) propagation along a smooth surface. (After AULD [17].)

of earthquakes. As will be seen in Section 2, Rayleigh's analysis solved the problem by combining appropriate longitudinal and shear vibrations to satisfy the boundary conditions, thereby anticipating the partial wave method that is now standard in the design surface acoustic wave devices. Figure 1 illustrates the depth variation of the two components of elastic displacement resulting from this combination of partial waves.

The last decade of the 19th century was a period of great activity in elastic vibration research. Rayleigh soon followed his surface wave paper with a second paper (based on the same analytical approach) on wave propagation along a free isotropic plate [13]. In this paper he identified the two families of plate solutions now known as horizontal shear (SH) and Lamb waves. The second wave type was named after Lamb, in recognition of his publication in the same year (1889) of a paper on flexural waves in an elastic plate [9], a member of one of the two classes of Lamb wave solutions. The surface wave solutions, now called surface acoustic waves (SAW) in the elastic device community, were named Rayleigh waves some time before 1925.

Rayleigh's prediction that elastic surface waves would play an important role in geophysics was quickly realized. A paper by LAMB in 1904 considered the propagation of tremors over an elastic surface [10]. Several years previously BROMWICH (1898) had introduced the concept of wave propagation on a layered half-space, motivated by the desire to model the effect of the earth's mantel on earthquake propagation. Waves on layered surfaces were the subject of intense investigation in the years to follow (LOVE (1911), STONELY (1924) and SEZAWA (1927)), and were later to prove to be of great practical importance in SAW devices. BREKHOVSKIKH published in 1960 a general reference work on propagation in layered solids [18]. During this same period, interest in the earthquake problem stimulated a series of papers on the excitation of waves on a half-space by localized mechanical surface and volume sources. The excitation problem (treated by LAMB (1904) and later, for example, by NAKANO (1925) and CAGNIARD (1939)) became the subject of renewed interest with the advent of SAW applications to nondestructive testing [27] and signal processing [14], beginning in the 1950's and 1960's.

It is interesting to note that, although piezoelectricity was discovered by the CURIES (1880) several years before the theoretical demonstration of elastic surface wave propagation in 1885, there was no thought until decades later of using this effect to excite elastic waves. In 1918 LANGEVIN first used piezoelectricity to excite acoustic bulk waves in water, but it was not until the late 1960's that SAW were excited directly in piezoelectric substrates by electrical signals. Wave propagation on the surface of a crystal had been examined about ten years previously [5]. But the emergence of this new SAW electromechanical transducer technology led to an explosion of interest in this subject, especially in SAW (or Rayleigh wave) propagation on anisotropic substrates exhibiting piezoelectric activity.

The partial wave analysis used by Rayleigh for surface wave propagation on an isotropic substrate proved to be well adapted to the piezoelectric substrates required for SAW devices [8], [14]. Rayleigh-type surface waves (SAW) were investigated for many different crystal materials and differently-oriented substrates. During these

investigations it was discovered that anomalous behavior can occur for certain propagation directions. It was originally believed that SAW could not propagate in these directions. But more detailed calculations showed a more complex type of behavior (Fig. 2). At the critical direction ([110]) in the figure the normal surface wave becomes a bulk wave that propagates parallel to the surface without radiation (surface skimming wave). At this same point a nonradiating surface wave with a different velocity (pseudo surface wave) exists, but it propagates without radiation loss only in this one critical direction. Elsewhere the wave radiates energy into the substrate and becomes a leaky wave (leaky wave solutions were noted by RAYLEIGH in his 1885 paper but were discarded as nonphysical).

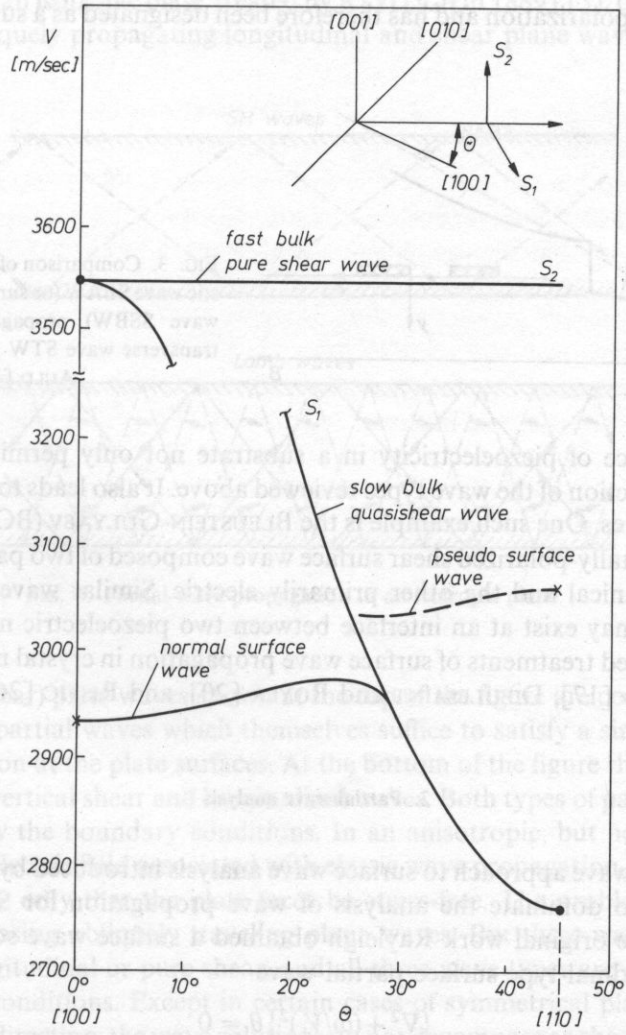

FIG. 2. Pseudosurface wave propagation along a single crystal substrate. (After LIM and FARNELL [11].)

In some crystals, surface skimming bulk waves, SSBW, (alternatively termed shallow bulk acoustic waves, SBAW) exhibit properties, such as a higher propagation velocity than a SAW, that are useful in practical devices. For this reason this type of wave is sometimes used in delay line applications, despite the fact that it is not closely confined to the surface. Confinement may be achieved by depositing a layer on the surface [21] to create a Love wave, or by fabricating a corrugated surface [1], [7], [15]. Figure 3 shows a corrugated surface created by depositing a periodic array of metal strips, where an SBAW stopband is created by BRAGG scattering due to the periodicity of the structure. As seen in the figure, the wave on the corrugated surface propagates at a lower velocity than the SBAW for frequencies below the stopband. Like the SAW, which is also a slow wave, this wave is a surface wave, Unlike the SAW, however, it has horizontal shear polarization and has therefore been designated as a surface transverse wave (STW).

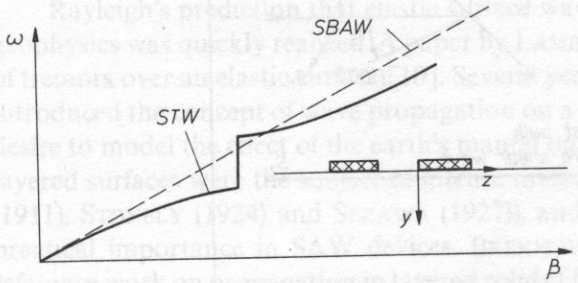

FIG. 3. Comparison of shallow bulk acoustic wave SBAW (or surface skimming bulk wave SSBW) propagation and surface transverse wave STW propagation. (After AULD [17].)

The existence of piezoelectricity in a substrate not only permits electrical excitation and detection of the wave types reviewed above. It also leads to the existence of new types of waves. One such example is the BLEUSTEIN-GULYAEV (BG) wave [4], [6]. This is a horizontally-polarized shear surface wave composed of two partial waves, one primarily mechanical and the other primarily electric. Similar waves, analogous to Stonely waves, may exist at an interface between two piezoelectric media.

More detailed treatments of surface wave propagation in crystal media have been published (AULD [17], DIEULESAINT and ROYER [20], and RISTIC [26]).

2. Partial wave analysis

The partial wave approach to surface wave analysis introduced by RAYLEIGH [12] has continued to dominate the analysis of wave propagation for SAW device applications. In the original work Rayleigh obtained a surface wave solution by combining a longitudinal-type surface partial wave

$$\{\nabla^2 + (\omega/V_l)^2\}\theta = 0 \tag{1a}$$

$$\theta \sim \exp(-\alpha_l z + i\beta x) \tag{1b}$$

and a shear-type surface partial wave

$$\{\nabla^2 + (\omega/V_s)^2\} u_s = 0 \tag{2a}$$

$$u_s \sim \exp(-\alpha_s z + i\beta x) \tag{2b}$$

to satisfy stress-free boundary conditions at the substrate surface. These boundary conditions require that the β's be the same in Eqs. (1) and (2). The relations between the depth decay factors α_l, α_s and β are obtained from the longitudinal and shear dispersion relations. Application of the zero stress boundary condition then leads to a condition linking ω, α_l, α_s and β, which must be solved simultaneously with the longitudinal and shear dispersion relations [16].

In the case of an isotropic plate, treated by RAYLEIGH in 1889 [13], the partial wave solutions are obliquely propagating longitudinal and shear plane waves (Fig. 4). The

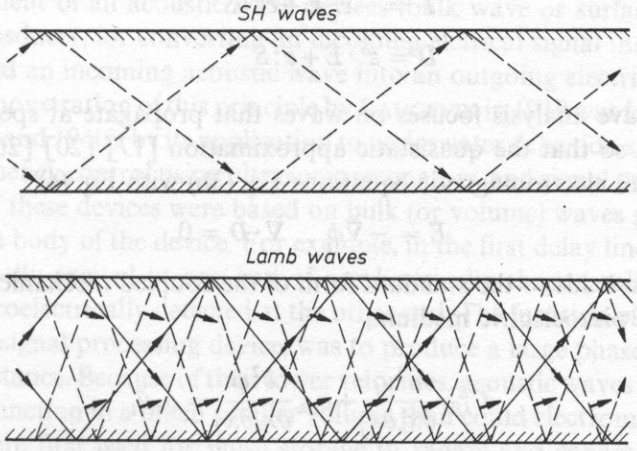

FIG. 4. Partial wave propagation in an isotropic plane.

SH (horizontal shear) plate waves shown at the top of the figure are constructed from horizontal shear partial waves which themselves suffice to satisfy a single zero stress boundary condition at the plate surfaces. At the bottom of the figure the Lamb waves are composed of vertical shear and longitudinal waves. Both types of partial waves are required to satisfy the boundary conditions. In an anisotropic, but nonpiezoelectric plate, there is no electric field associated with elastic wave propagation, and boundary conditions require only that the plate faces be stress-free. The problem can still be solved by superposing obliquely traveling plane waves. But these waves are not, in general, pure longitudinal or pure shear, and all three wave types are coupled by the stress boundary conditions. Except in certain cases of symmetrical plate orientation and propagation direction, the wave solutions do not decompose as shown in Fig. 4. To summarize, elastic wave solutions in nonpiezoelectric crystal plates are most generally

constructed from three partial waves. A similar remark applies to SAW propagation on a nonpiezoelectric crystal substrate.

In the piezoelectric substrates required for SAW devices, coupling between the elastic and electromagnetic requires that both mechanical and electrical boundary conditions be satisfied at the substrate surface. (A similar remark would apply to the case of plate waves in a piezoelectric plate.) The partial wave method may still be applied, but the partial waves must now be solutions to the coupled elastic and electromagnetic equations

$$\nabla \cdot T = \varrho \frac{\partial^2 u}{\partial t^2} \tag{3a}$$

$$\nabla \times E = -\mu_0 \frac{\partial H}{\partial t} \qquad \nabla \times H = \frac{\partial D}{\partial t} \tag{3b}$$

$$\begin{aligned} T &= -e \cdot E + c^E : S \\ D &= \varepsilon^S \cdot E + e : S \end{aligned} \tag{3c}$$

Piezoelectric wave analysis focuses on waves that propagate at speeds close to the elastic velocity, so that the quasistatic approximation [17] [20] [26] can be made, replacing the full electromagnetic equations Eq. (3b) with Eq. (4).

$$E = -\nabla \phi \qquad \nabla \cdot D = 0 \tag{4}$$

Combining then leads to the standard form of the coupled mechanical and electrical equations for a piezoelectric medium,

$$C^E_{ijkl} \frac{\partial^2 u_l}{\partial x_k \partial x_j} + e_{ijk} \frac{\partial^2 \phi}{\partial x_k \partial x_j} = \varrho_m \ddot{u}_i \tag{5}$$

$$e_{ikl} \frac{\partial^2 u_l}{\partial x_k \partial x_i} - \varepsilon^S_{ek} \frac{\partial^2 \phi}{\partial x_k \partial x_i} = 0$$

At a stress-free boundary oriented normal to $\hat{n}$, with arbitrary electrical boundary conditions, the relations

$$T \cdot \hat{n} = 0 \tag{6a}$$

$$\Phi = \Phi'$$

$$D \cdot \hat{n} = D' \cdot \hat{n} \tag{6b}$$

must be satisfied in general. In SAW device analysis, however, it is common to consider only short-circuit boundary conditions (where $\Phi = 0$) or open-circuit boundary conditions (where $D \cdot \hat{n} = 0$) at the surface of the substrate. There are then just four boundary conditions: three mechanical and one electrical. (The number may be further

reduced, as noted above, for particular symmetric substrate orientations and propagation direction). As a consequence, four partial waves are required. Solution of Eq. (5) for plane waves always yields three solutions, corresponding to the three plane elastic wave solutions for a nonpiezoelectric material, but modified by the piezoelectric interaction. However, Eq. (5) also permits the existence of the four piezoelectric surface-type partial waves required to satisfy the four boundary conditions imposed in piezoelectric SAW analysis. Three of these solutions correspond to the three partial waves required for nonpiezoelectric SAW, but modified by piezoelectricity. The fourth solution corresponds to the Laplace solution for Φ in a nonpiezoelectric material, again modified by the piezoelectricity.

3. Surface wave transduction

A basic element of all acoustic wave devices (bulk wave or surface wave) is the piezoelectric transducer, for converting an incoming elctrical signal into an outgoing acoustic wave and an incoming acoustic wave into an outgoing electrical signal. The first practical demonstration of this principle by LANGEVIN in 1918 was followed during the 1920's, 1930's and 1940's by its application to underwater detection systems (sonar), filtering and frequency control using ultrasonic resonators, and signal processing using delay lines. All of these devices were based on bulk (or volume) waves propagating in the interior of the body of the device. For example, in the first delay lines a bulk wave was piezoelectrically excited at one end of a cylindrically-shaped solid body (or in a liquid), and piezoelectrically detected at the other end. The function of the delay line, the first acoustic signal processing device, was to produce a large phase shift or delay time in a short distance. Because of their lower velocities, acoustic waves in solids could accomplish this function in a much smaller volume than could electromagnetic waves. These devices were first used for pulse storage in radars and sonars, as well as in computers and pulse decoders [2].

Interest in the piezoelectric excitation of Rayleigh surface waves (SAW) first arose in the field of nondestructive testing during the 1940's and 1950's. A surface wave generates a much larger pulse echo return from a small surface crack than does a bulk wave, because the wave is more confined to the surface of the test piece, and because the surface crack presents a larger scattering cross section to a wave traveling along the surface. A review of piezoelectric transducers for these applications was published in 1967 by VIKTOROV [27]. Typical transducer structures are illustrated in parts (a) and (b) of Fig. 5. These are based on the concept of exciting the wave by a distribution of forces applied to the surface of the solid, as in the earlier geophysical studies by LAMB (1904) and others. In both examples an external piezoelectric structure was used to generate such forces.

A second impetus to the development of piezoelectric surface wave transducers was provided by the recognition that an ability to tap into an acoustic delay line at

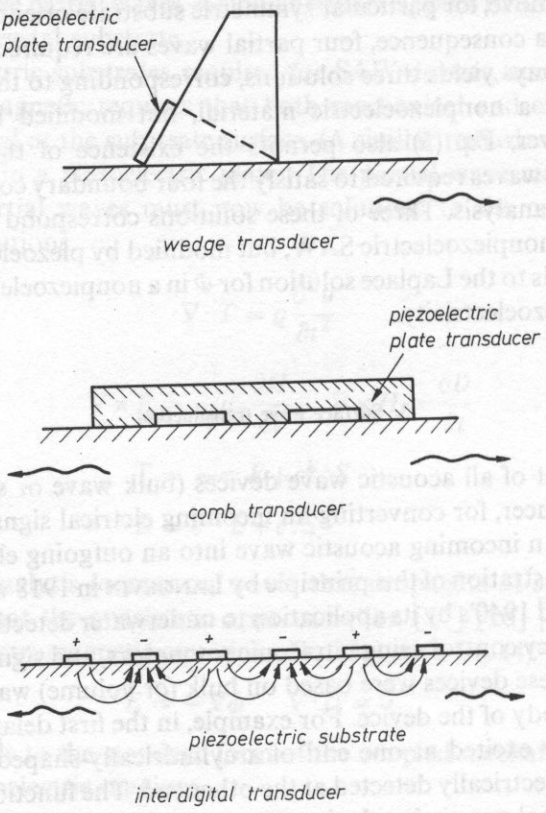

FIG. 5. Methods of surface acoustic wave SAW transduction (a) Wedge, (b) Comb, (c) Interdigital electrodes (IDT)

various points along the propagation path would vastly expand the signal processing capabilities of the device. Surface acoustic delay lines immediately attracted attention because of the ready accessibility of the wave at all points along its propagation path. The unsuitability of wedge and comb transducers for tapped delay lines led quickly to the invention and rapid development of the interdigital transducer, shown in part (c) of Fig. 5. Here, transduction and propagation occur in the same piezoelectric material. A periodic electric field, generated in the medium by a comb electrode structure, with alternate electrodes driven in phase opposition, creates a strain distribution that changes sign spatially with the same period as the surface wave to be excited.

The interdigital transducer (IDT) quickly assumed a major role in SAW technology, because of its suitability for tapped delay line applications and its planar character, which made it compatible with integrated circuit technology. A number of text and reference works dealing with the theory of these transducers appeared in the 1970's and 1980's [17], [20], [24], [25], [26].

4. Surface wave signal processing and resonators

After the perfection of the IDT SAW transduction technique there occurred a virtual explosion in SAW device development. A small sampling will serve to illustrate the richness and variety of the applications. Details may be found in reference works [14], [19], [22], [24], [25] and in the periodical literature.

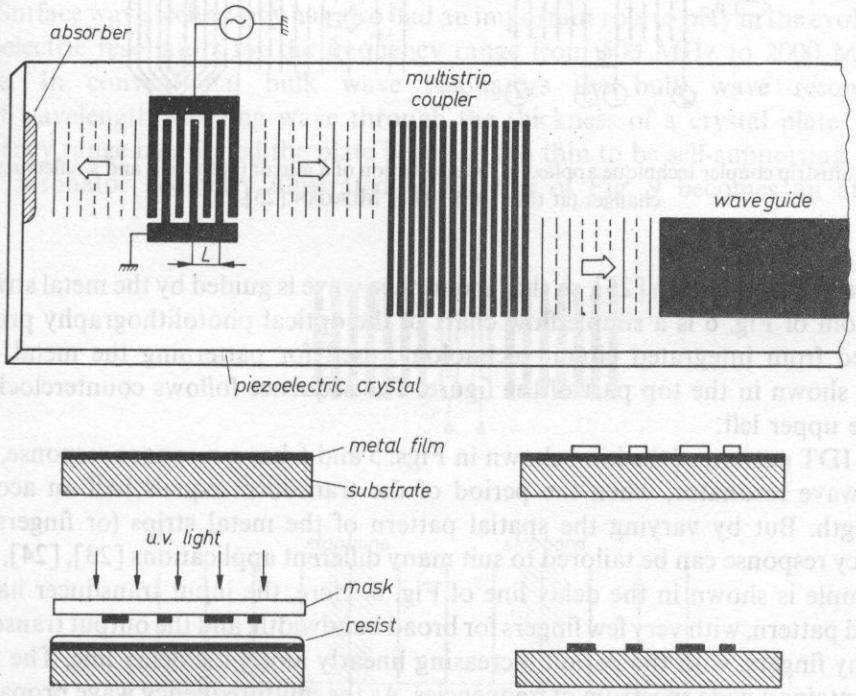

FIG. 6. Typical SAW components and fabrication technique. (After MORGAN [25].)

The top part of Fig. 6 illustrates several kinds of surface wave device components using the piezoelectric effect. They are all realized by depositing metal patterns on a piezoelectric crystal, either coupling to the surface acoustic waves by means of piezoelectrically generated electric fields or perturbing the piezoelectric surface wave by changing the electrical boundary conditions a the substrate surface. At the left is the interdigital transducer structure of Fig. 5 (c). In the center of the figure is a multistrip coupler. This functions essentially as an IDT receiver coupled directly, strip by strip, to an IDT transmitter. In this case it serves to laterally displace the surface wave beam, but many other applications developed from this simple concept [25]. (Figure 7 gives two examples.) At the right of Fig. 6 is a surface wave duct waveguide. The short circuit electrical boundary conditions under the film slow down the wave velocity and create

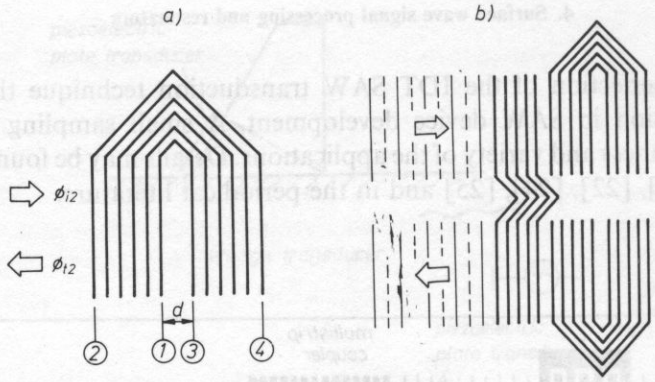

FIG. 7. Multistrip coupler technique applied to the realization of a mirror (at the left) and a reflecting track changer (at the right). (After MORGAN [25].)

a trapped wave condition [25], so that the surface wave is guided by the metal strip. At the bottom of Fig. 6 is a simple flow chart of the optical photolithography process, borrowed from integrated circuit technology, used for patterning the metal components shown in the top part of the figure. The sequence follows counterclockwise from the upper left.

An IDT pattern of the kind shown in Figs. 5 and 6 has a resonant response, as in a bulk wave resonator, when the period of the transducer equals half an acoustic wavelength. But by varying the spatial pattern of the metal strips (or fingers) the frequency response can be tailored to suit many different applications [23], [24], [25]. An example is shown in the delay line of Fig. 8. Here, the input transducer has the standard pattern, with very few fingers for broad bandwidth, and the output transducer has many fingers, with the period increasing linearly along the delay line. The input pulse contains a wide spectrum of frequencies. As the multifrequency wave propagates

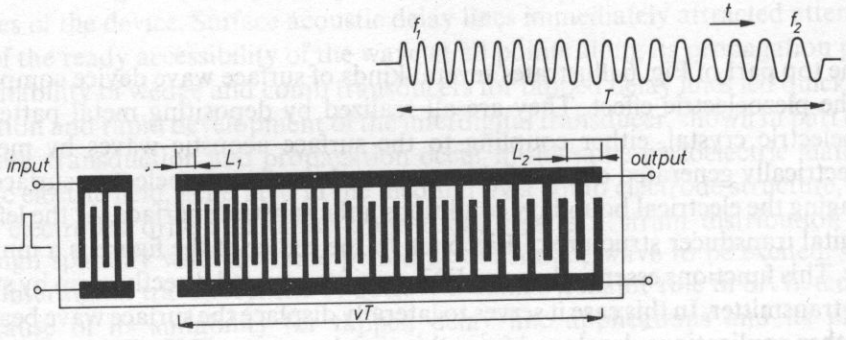

FIG. 8. "Chirp" waveform generated in a SAW delay line. (After MORGAN [25].)

under the output transducer the various frequency components couple out at points where wavelength-period matching to the IDT occurs. High frequencies arrive first and low frequencies last, so that the short input signal is converted into a long signal with a linear frequency modulation. Such so-called "chirp" waveforms are widely used in radar. If this same waveform is fed back into the output of a chirped delay line, with the chirp pattern reversed in time from that shown in the figure, the long waveform is compressed into a narrow pulse again.

Surface wave technology has also had an important role to play in the evolution of piezoelectric resonators for the frequency range from 500 MHz to 2000 MHz and above. In conventional bulk wave resonators the bulk wave resonates in a half-wavelength standing wave through the thickness of a crystal plate. For the frequency range mentioned the plate becomes too thin to be self-supporting, and the SAW resonator geometry illustrated at the top of Fig. 9 becomes an attractive

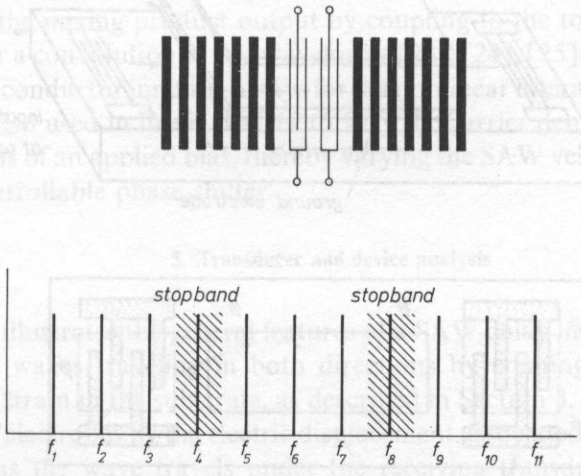

FIG. 9. SAW resonator structure and mode distribution. (After AULD [17].)

alternative. A standing SAW now resonates between two deposited metal strip gratings shown by the heavy vertical lines. These gratings act as strong reflectors within stopbands near the Bragg reflection frequencies, where the metal strip period is equal to a multiple of one-half a SAW wavelength. Standing wave resonances can occur only within a grating stopband. By making the stopband sufficiently narrow one single resonance can be selected in each stopband (Fig. 9, bottom). In this way the central (or resonator) part of the structure can be made long enough for convenience in fabrication and to permit insertion of IDT's. At the same time all but a few of the length resonances are suppressed by the discrete stopband frequency response of the grating mirrors. SAW resonators may also be realized with etched groove gratings, as shown in the top

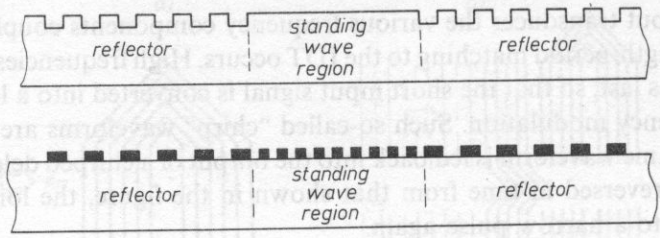

FIG. 10. STW resonator structure. (After AULD [17].)

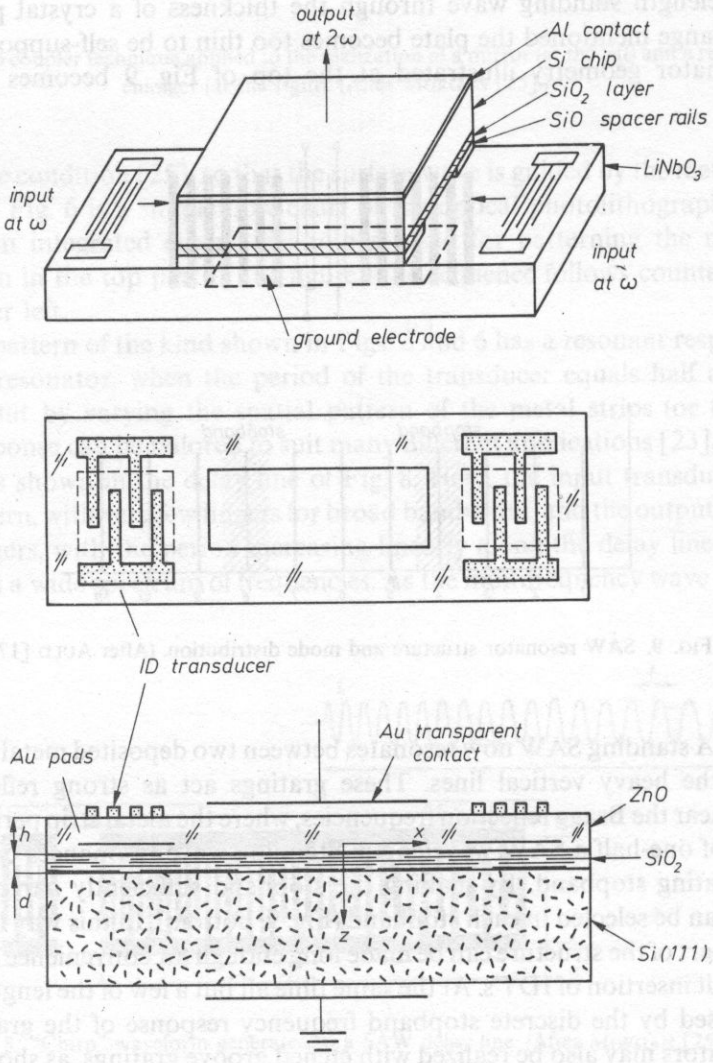

FIG. 11. SAW-semiconductor convolver. (After KINO [24].)

part of Fig. 10. Another alternative is to operate with the STW introduced in Section 1 (Fig. 10, bottom). These resonators are easier to fabricate because the STW wavelength can be longer than the SAW wavelength at the same frequency. They also have certain operational advantages [3].

Another class of SAW devices for signal processing exploits the piezoelectric interaction between surface acoustic waves and charge carriers in semiconductors. Both semiconductor substrates (gallium arsenide) and semiconductor overlays (silicon) on insulating substrates are used. The first efforts in this direction aimed at developing a SAW amplifier by interacting the wave with a stream of drifting carriers. Amplification was observed, but the overall transducer-to-transducer performance was not sufficiently good to make the device attractive for practical applications. A useful class of *nonlinear* SAW/semiconductor devices used the electric field associated with a piezoelectric surface wave to electrically mix two counterpropagating waves. Figure 11 illustrates one version of this type of device. Waves are excited at each end of the delay line, and distributed electrical mixing occurs in the silicon chip overlay. Spatial integration of the mixing product output by coupling to the top electrode generates a correlation or a convolution of two waveforms [23], [24], [25]. Some versions of this device use semiconductor junction arrays for the nonlinear interaction. Semiconductor junctions are also used in linear devices to vary the carrier density in the interaction region by means of an applied bias, thereby varying the SAW velocity and realizing an electrically-controllable phase shifter.

5. Transducer and device analysis

Figure 12 illustrates the general features of a SAW delay line. The IDT at the left excites surface waves traveling in both directions by creating a spatially periodic distribution of strain in the substrate, as described in Section 3. At the right, charge is induced on the electrodes by the electric displacement associated with the piezoelectric surface wave as the wave travels under the receiving transducer thereby creating a current through the electrical load Z_L. The power in the wave not converted to electrical power in the receiver load is transmitted past the transducer, where it must be absorbed by a lossy coating on the substrate to avoid reflection. A reflection of the incident wave also occurs at the front side of the receiving transducer, and this return wave is again reflected at the transmitting transducer. Care must be taken to minimize all these multiple reflections at the transducers, as well as those at the ends of the substrate.

Since the introduction of SAW technology in signal processing devices, a variety of methods have evolved for analyzing the surface wave components such as those in Figs. 6 and 12. It is convenient to unify this theory in a format analogous to that of microwave circuit theory. Microwave circuit formalism deals with ensembles of distributed electromagnetic components that are connected by wave propagation regions to form electromagnetic "circuits", analogous to the ensembles of SAW components in Figs. 6 and 12. It is customary in microwave theory to represent each subelement of the

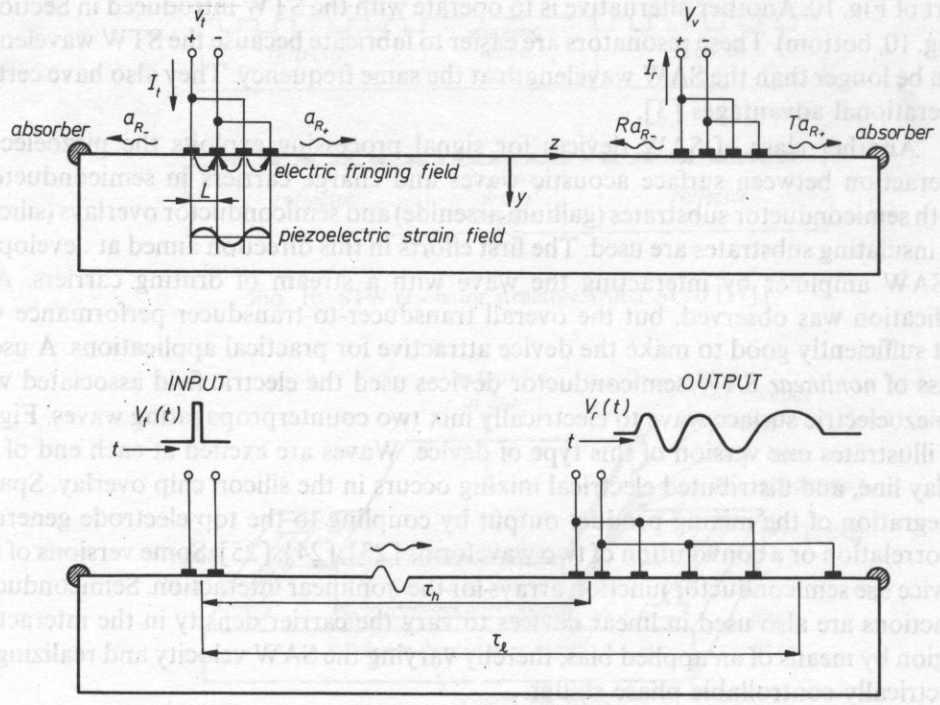

FIG. 12. SAW delay line, with IDT excitation and detection. (After AULD [17].)

ensemble by its scattering matrix. In this scattering matrix, the matrix elements (or *S*–parameters) relate the outgoing wave amplitudes [b] to the incoming wave amplitudes [a] at terminal planes defining the subelement in question (amplitudes are normalized so that unit amplitude corresponds to unit power). This *S*–parameter relation is written as

$$[b] = [S]\,[a] \tag{7}$$

In Fig. 12, for example, the outgoing waves are the surface acoustic waves emitted to the right and left of the left-hand (or transmitting) transducer by an electromagnetic wave incident at the electrical terminals. At the right-hand transducer the wave launched by the transmitter is an incoming wave and the wave passing beyond the transducer is outgoing.

Equation (8) shows a mathematical formulation of the distributed transducer principle briefly outlined in Section 3.

$$\begin{aligned} a_{R+}(z) &= e^{i\beta_R z}/4P_R \int_{-\xi}^{+\xi} e^{i\beta_R \zeta} \{\ \}_{R+} \cdot \hat{\mathbf{y}}\, d\zeta, \qquad z > +\xi \\ \{\ \}_{R+} &= \{\Phi_{R+}^{\infty *}(0)(i\omega D_y(0, z)\} \end{aligned} \tag{8}$$

The amplitude of the emitted wave is expressed an integral over a distribution of sources defined by the driving charge distribution (equal to the normal electric

displacement D_y) induced on the transducer electrodes by the incident electromagnetic wave. This result is derived from a general field theorem that constitutes a basic analytic tool in microwave circuit theory, but extended to include piezoelectric waves [17]. The modified theorem can be stated as

$$\nabla \cdot [\ \ ] = 0 \tag{9}$$

with

$$[\ \ ] = \mathbf{v}_1 \cdot \mathbf{T}_2 - \mathbf{v}_2 \cdot \mathbf{T}_1 \oplus \mathbf{E}_1 \times H_1 \ominus E_2 \times H_1 \tag{10}$$

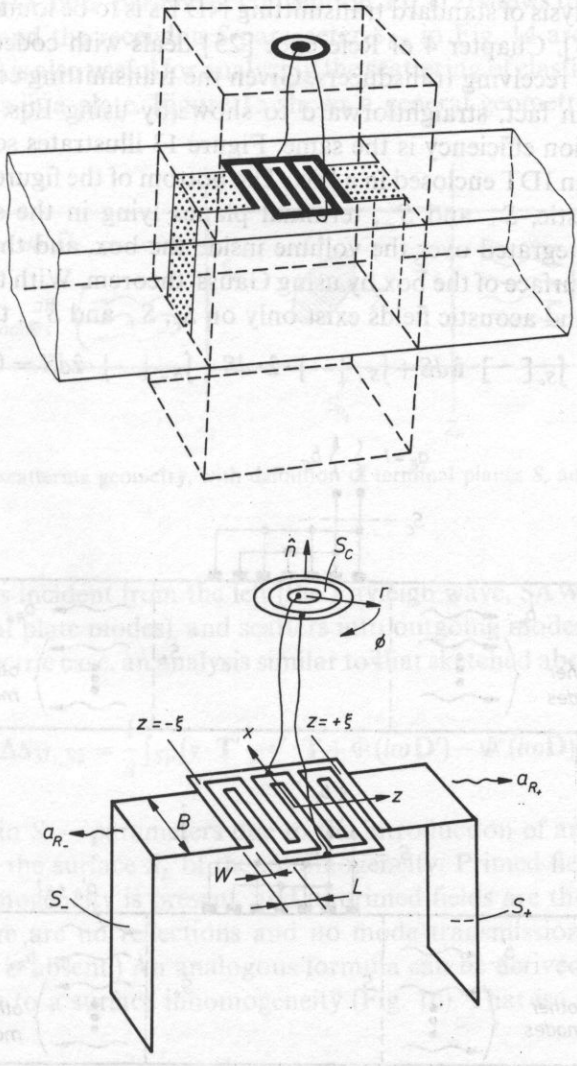

FIG. 13. Construction for proof of IDT reciprocity. General configuration (top). Definition of terminal planes $S \ldots S_-$ and S_c (bottom). (After AULD [17].)

In Eq. (10) the circled plus and minus signs apply for media where the electromagnetic coupling is due to piezoelectricity, as in the cases considered here. The signs are interchanged when the electromechanical coupling is due to magnetostriction (page 176, Vo. II in Reference [17]). For purely electromagnetic problems the displacement velocity and stress terms are suppressed, and Eqs. (9) and (10) reduce to the Lorentz reciprocity relation used in microwave theory. Another variant of Eq. (10), useful for purely piezoelectric problems, replaces Maxwell's equations by the quasistatic equations (Eq. (4)) and which replaces the square bracket in Eq. (8) by

$$\{\quad\} = \{\mathbf{v}_1 \cdot \mathbf{T}_2 - \mathbf{v}_2 \cdot \mathbf{T}_1 + \boldsymbol{\Phi}_1 (i\omega \mathbf{D}_2) - \boldsymbol{\Phi}_2 (i\omega \boldsymbol{D}_1)\} \tag{11}$$

Detailed analysis of standard transmitting NDT's is to be found in references such as [17], [24], [25]. Chapter 4 of Reference [25] deals with coded transducer finger patterns, and also receiving transducers. Given the transmitting conversion efficiency of an IDT it is, in fact, straightforward to show (by using Eqs. (9)–(11)) that the receiving conversion efficiency is the same. Figure 13 illustrates schematically, at the top of the figure, an IDT enclosed in a box. The bottom of the figure defines electric, S_c, and surface acoustic, S_+ and S_-, terminal planes lying in the surface of the box. Equation (9) is integrated over the volume inside the box, and then converted to an integral over the surface of the box by using Gauss' theorem. With the assumption that electromagnetic and acoustic fields exist only on S_c, S_+ and S_-, this reduces to [17]

$$\int_{S_c} [\quad] \cdot \hat{\mathbf{n}} dS + \int_{S_+} \{\quad\} \cdot \hat{\mathbf{z}} \cdot dS - \int_{S_-} \{\quad\} \cdot \hat{\mathbf{z}} dS = 0 \tag{12}$$

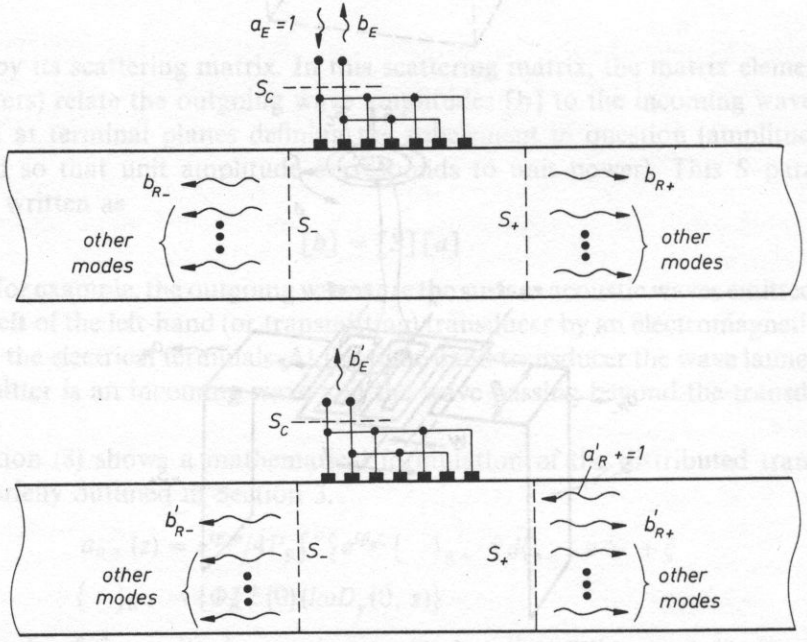

FIG. 14. Solutions used in the reciprocity theorem analysis of an IDT. (After AULD [17].)

At the acoustic terminal planes S_+ and S_- the quasistatic form (Eq. (11)) may be used, while the full electromagnetic form must be used at the electrical terminal plane S_c.

The solutions 1 and 2 in Eqs. (9)–(11) are now selected as in Fig. 14. It can be shown [17] that inside the brackets [ ] and { } cross products involving pairs of outgoing waves cancel, so that the integral over S_- is zero and

$$\begin{aligned} \int_{S_+} \{\ \} \cdot \hat{\mathbf{z}} dS &= b_{R+}\, a'_{R+}\, (4P_{RR}B) \\ \int_{S_c} [\ ] \cdot \hat{\mathbf{n}} dS &= -b'_E a_E \left(\int_{S_c} 2 (E_r)_i (H_\phi)_i dS\right) \end{aligned} \tag{13}$$

When the power flow integrals on the right side of these relations are normalized to unity, according to the S–parameter convention, Eq. (12) shows that the transmitting S-parameter S_{RE} and the receiving S-parameter S_{ER} in Fig. 14 are equal.

Equation (9) is also useful for analyzing the scattering of elastic waves from internal inhomogeneities in a plate. Figure 15 shows a general geometry, where a particular

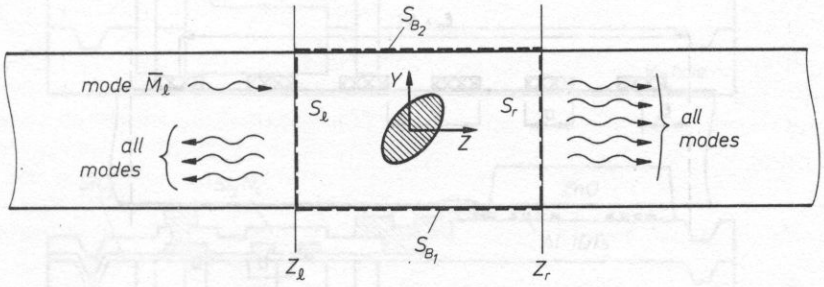

FIG. 15. General scattering geometry, with definition of terminal planes S_r and S_l. (After AULD [17].)

plate mode $\bar{M}$ is incident from the left (the Rayleigh wave, SAW, is in fact one of the family of general plate modes), and scatters into outgoing modes of all types. For the general piezoelectric case, an analysis similar to that sketched above yields the relation

$$\Delta S_{\bar{M}_l, \bar{N}_r} = \frac{1}{4} \int_{S_F} (\mathbf{v} \cdot \mathbf{T}' - \mathbf{v}' \cdot \mathbf{T} + \Phi (i\omega \mathbf{D}') - \Phi' (i\omega \mathbf{D})) \cdot \hat{\mathbf{n}} dS \tag{14}$$

for the change in S – parameters due to the introduction of an inhomogeneity. The integral is over the surface S_F of the inhomogeneity. Primed fields are those existing when the inhomogeneity is present, and unprimed fields are those when it is absent. (Note that there are no reflections and no mode transmission couplings when the inhomogeneity is absent.) An analogous formula can be derived for the change in S–parameters due to a surface inhomogeneity (Fig. 16). That is

$$\Delta S_{Rl,Rl} = \frac{1}{4} \int_{\xi - a/2}^{\xi + a/2} (\mathbf{v} \cdot \mathbf{T}' + i\omega \Phi \mathbf{D}') \cdot \hat{\mathbf{n}} dz \tag{15}$$

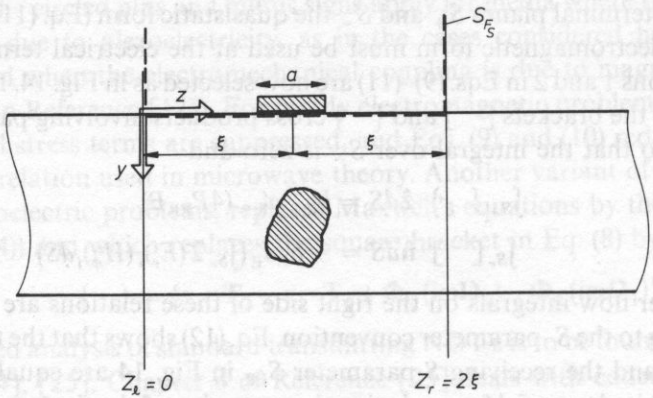

FIG.16. Surface and volume scattering of SAW. (After AULD [17].)

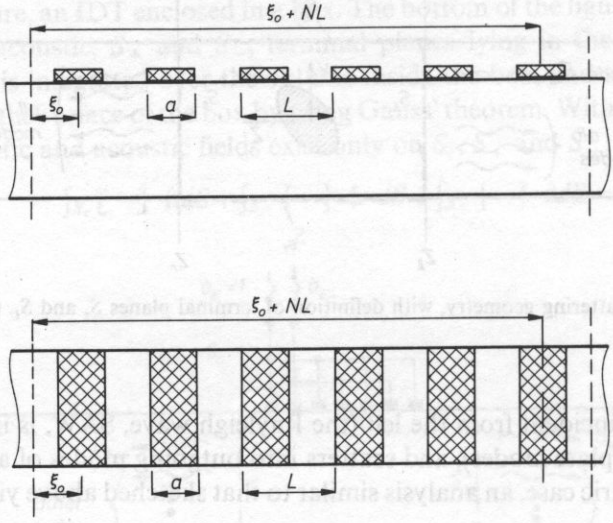

FIG. 17. Scattering of SAW by surface and volume gratings. (After AULD [17].)

The inhomogeneities need not be single, but may take the form of periodic gratings (Fig. 17). In this way Eq. (15) may be used to analyze surface wave scattering from an IDT (Fig. 12).

6. New techniques and future directions

The initial motivation for developing piezoelectric surface wave devices came from the need for better nondestructive testing and signal processing technologies. In these areas the use of SAW devices has become very sophisticated, with widespread ap-

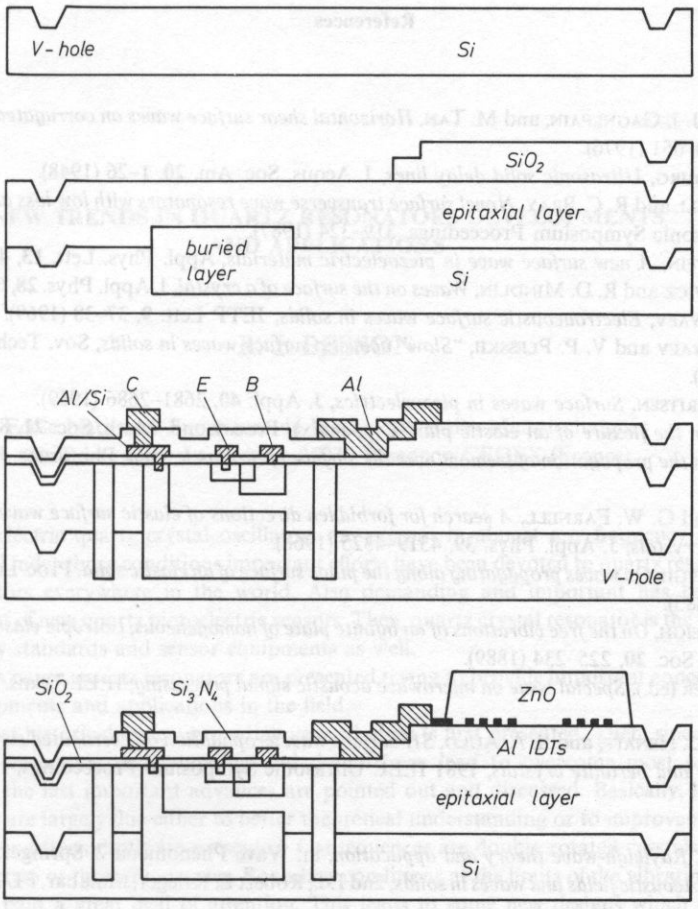

FIG. 18. Integration of a SAW device with integrated circuits. (After VISSER [28].)

plications in the military, in civilian communications, and in the consumer market. A recent trend has begun to exploit the planar compatibility of SAW devices with semiconductor integrated circuits. Figure 18 gives an example, a SAW filter with associated integrated circuitry, showing the process chart for its fabrication (after VISSER [28]). SAW devices are also beginning to play an important role in sensor technology. Delay lines have been deposited on microfabricated silicon diaphragms for pressure sensing. Surface acoustic wave temperature pressure and acceleration sensors utilize the temperature and strain sensitivity of surface acoustic waves on crystal substrates. The extreme sensitivity of SAW delay lines to surface conditions has led to their use in sensors for air pollution and for studies of adsorbed materials. Recent years have also seen a resurgence of interest in SAW/semiconductor devices for electrically controllable phase shifters and oscillators.

References

(a)

[1] B. A. AULD, J. J. GAGNEPAIN, and M. TAN, *Horizontal shear surface waves on corrugated surfaces*, Elec. Lett. **12**, 650–651 (1976).

[2] D. L. ARENBURG, *Ultrasonic solid delay lines*, J. Acous. Soc. Am. **20**, 1–26 (1948).

[3] T. L. BAGWELL and R. C. BRAY, *Novel surface transverse wave resonators with low loss and high Q*, 1987 IEEE Ultrasonic Symposium Proceedings, 319–324 (1987).

[4] J. L. BLEUSTEIN, *A new surface wave in piezoelectric materials*, Appl. Phys. Lett. **13**, 412–413 (1968).

[5] H. DERESIEWICZ and R. D. MINDLIN, *Waves on the surface of a crystal*, J. Appl. Phys. **28**, 669–671 (1957).

[6] Yu. V. GULYAEV, *Electroacoustic surface waves in solids*, JETP Lett. **9**, 37–38 (1969).

[7] Yu. V. GULYAEV and V. P. PLESSKII, *"Slow" acoustic surface waves in solids*, Sov. Tech. Phys. Lett. **3**, 87–88 (1977).

[8] K. A. INGEBRITSEN, *Surface waves in piezoelectrics*, J. Appl. **40**, 2681–2686 (1969).

[9] H. LAMB, *On the flexure of an elastic plane (Appendix)*, Proc. Lond. Math. Soc. **21**, 85 (1989).

[10] H. LAMB, *On the propagation of tremors over the surface of an elastic solid*, Phi. Trans. Roy. Soc. **A203**, 1–42 (1904).

[11] T. C. LIM and G. W. FARNELL, *A search for forbidden directions of elastic surface wave propagation in anisotropic crystals*, J. Appl. Phys. **39**, 4319–4325 (1968).

[12] LORD RAYLEIGH, *On waves propagating along the plane surface of an elastic solid*, Proc. Lond. Math. Soc. **17**, 4–11 (1885).

[13] LORD RAYLEIGH, *On the free vibrations of an infinite plate of homogeneous, isotropic elastic matter*, Proc. Roy. Math. Soc. **20**, 225–234 (1889).

[14] T. M. REEDER (ed.), *Special issue on microwave acoustic signal processing*, IEEE Trans. **MTT-21** (April 1973).

[15] A. RENARD, J. HENAFF, and B. A. AULD, *SH surface wave propagation on corrugated surfaces of rotated Y-cut quartz and berlinite crystals*, 1981 IEEE Ultrasonic Symposium Proceedings, 123–128 (1981).

(b)

[16] B. A. AULD, *Rayleigh-wave theory and application*, in: Wave Phenomena **2**, Springer, Berlin 1985.

[17] B. A. AULD, *Acoustic fields and waves in solids*, 2nd Ed., Robert E. Krieger, Malabar, FL 1990, vols. I and II.

[18] L. M. BREKHOVSKIKH, *Waves in layered media*, Academic Press, New York 1960.

[19] S. DATTA, *Surface acoustic wave devices*, Prentice-Hall, Englewood Cliffs, NJ 1986.

[20] E. DIEULESAINT and D. ROYER, *Elastic waves in solids*, Wiley, New York 1980.

[21] G. W. FARNELL and E. L. ADLER, *Elastic wave propagation in thin layers*, Chapter 2 in Physical Acoustics **9**. W. P. Mason and R. N. Thurston, eds., Academic Press, New York 1972.

[22] M. FELDMAN and J. HENAFF, *Traitement du signal par ondes elastiques de surface*, Masson, Paris 1986.

[23] H. MATTHEWS (ed.), *Surface wave filters*, Wiley, New York, 1977.

[24] G. S. KINO, *Acoustic waves – devices, imaging, and analogue signal processing*, Prentice-Hall, Englewood Cliffs, NJ 1987.

[25] D. P. MORGAN, *Surface wave devices for signal processing*, Elsevier, Amsterdam 1985.

[26] V. M. RISTIC, *Principles of acoustic devices*, Wiley Interscince, New York 1983.

[27] I. A. VIKTOROV, *Rayleigh and Lamb waves*, Plenum, New York 1967.

[28] J. H. VISSER, *Suurface acoustic wave filters* in ZnO-SiO_2-Si *layered structures*, PhD Thesis, Technical University of Delft, December 1989.

ARCHIVES OF ACOUSTICS
16, 1, 31-52(1991)

NEW TRENDS IN QUARTZ RESONATORS DEVELOPMENTS AND APPLICATIONS

R. J. BESSON

Ecole Nationale Superieure de Mecanique et des Microtechniques
(Route de Gray-La Bouloie-25030 Besançon CEDEX (France)

Piezoelectric quartz crystal oscillators are present in almost any frequency control equipment. Under those conditions important efforts have been devoted to quartz resonators and oscillators everywhere in the world. Also demanding and important has been the development of new quartz piezoelectric sensors. Then, quartz crystal resonator is the "heart" of frequency standards and sensor equipments as well.

In this paper, quartz resonators are presented trying to provide important concepts for new developments and applications in the field.

A short historical review providing general ideas is first presented. Then, since recent progress in resonator understanding and design have lead to overcome most previous limitations, the last important advances are pointed out and discussed. Basically, late improvements are largely due either to better theoretical understanding or to improvements of boundary conditions. Both are presented. Consequences are doubly rotated crystals, use of a crystal on two or three frequencies. Boundary conditions at the limits of the vibrating body have to be paid a great deal of attention. This leads to some new designs which include "unelectroded" crystals and "quartz monolithic mount" of resonators.

Recent improvements in low aging, low external pressure variation sensitivity, fast warm-up are discussed in relation with different designs. Improvements of commercially available units are also presented according to several domains of application ranging from watch industry to high precision measurements.

In conclusion, some new developments and applications are pionted out.

Introduction and historical review

Principal milestones in piezoelectricity and its applications may be indicated as follows:

1880: Pierre and Jacques Curie, Discovery of piezoelectricity.
1893: Lord Kelvin, Microscopic theory of piezoelectricity in quartz crystal.
1910: Voigt, Lehrbuch der Kristall Physik.
1914–1918: Langevin, Work on ultrasonic detection in water.

1918: Nicholson (Bell Labs), Patent on oscillating circuit with Rochelle salt crystal (US Patent 2212845, April 10 1918).

1920: W. G. Cady Patent on oscillating cricuit with 3 vacuum tubes and quartz crystal resonator (in feed back circuit).

1921: Pierce's first oscillator.

1926: First crystal controlled radio station in New York city.

1939–1945: 130 millions of crystal resonators and oscillators were manufactured during world war II.

1948: Introduction of coated units by R. A. Sykes.

1952: Introduction of energy trapping by A. W. Warner.

1975: Doubly rotated SC cuts by E. P. Eernisse.

1975: Ceramic flat pack for resonators by Wilcox, Snow, Hafner and Vig.

1976: Electrodeless BVA resonator by R. J. Besson.

1980–1990: Important efforts to obtain ultrapure, dislocation free quartz material.

In fact, piezoelectric resonators are solids (plates, bars,) of a given configuration shape and dimensions prepared from high quality material under precise control of orientation. Geometric shape is fundamental since frequency depends on one or several dimensions of the vibrating solid which turns out to be a cavity for acoustic waves.

Electrodes provide electric field but only certain vibrations are piezoelectrically driven. Electrodes can be deposited on crystal or they can be located very close to the crystal (so said "electrodeless" crystal). To summarize we have:

– a crystal solid vibrating according given modes and frequencies with a given quality factor,

– electrodes used to piezoelectrically drive vibrations and at the same time to detect vibrations. Classical distinction between bulk acoustic waves and surface acoustic waves has of course to be made (in this paper B.A.W. devices will rather be considered).

Notice:

– for resonators used in frequency control, a particular interest is devoted to frequency variations versus temperature. Actually, the user looks for turn over temperatures which provide the working points of the temperature controlled ovens.

– frequency may depend and actually depend on various external parameters (temperature, pressure, acceleration, force etc). The resonator can be made to be sensitive in frequency dependance, then it is used as a sensor.

The first piezoelectric resonators were used by Langevin, Nicholson and Cady. Cady's resonator was invented in 1920 giving rise to fabrication at artisan rate until second world war. Electrodes were not deposited on the crystal but technology could not take advantage of it. Between 1944 and 1948, R. A. Sykes introduced electrodes deposited on the crystal and in 1952, A. W. Warner introduced energy trapping. The Warner's technique is still used nowadays without any major change. After 1975

doubly rotated cuts began to be used following recommandations of Eernisse, Ballato and Besançon's group. These doubly rotated cuts had more or less been previewed since 1938 and they could overcome some limitations of the regular ATcut Warner's resonator. In the last fifteen years several new resonators have been introduced (BVA resonators, flat pack, resonators, miniature resonators, composite resonators, UHF resonators and so on).

In fact, quartz oscillators are present in almost any time or frequency control equipment. Piezoelectric sensors are widely used especially as precision sensors. As a consequence tremendous effort has been made towards better piezoelectric resonators especially during the two last decades. Recent progress in resonator understanding and design leads to overcome most previous limitations. As a result, a single crystal oscillator can now provide, at the same time, excellent short term stability and excellent long term drift. Fast warm-up can be obtained together with other excellent characteristics. Also impressive (and necessary) is the achievement of very small g sensitivity (less than 10^{-10}/g).

Improvements of piezoelectric resonators is particulary necessary for lower aging, better thermal stability, lower thermal transients and lower environmental dependence (vibration shock, acceleration, radiations). Basically, improvements could come from efforts in many domains (better theory, better or new piezoelectric material, better design, better processing. In fact, late improvements are largely due either to better theoretical understanding or to better consideration and achievement of boundary conditions. Both lead to new concepts and new design yielding better short term stability, aging rates, thermal characteristics, g and new environmental sensitivities. Also due to passive methods [1], [2] improvements on resonator alone can be clearly seen. In addition may be time for new concepts in resonator design.

In fact, for somebody who is not too much impressed by the extraordinary amount of available literature on resonators, each step of the resonator design can be reconsidered. This sometimes arises questions which, at first, look almost childish. For example:

Why do crystals have usually circular or rectangular shapes and spherical contours?

The answer is that quartz does not care but it is usually easier to deal with those shapes and contours. If correctly handled this interrogation can lead to interesting new shapes or contours. Technical feasibility or (and) even tradition often determines the fabrication method. In addition, it is so delicate to make excellent resonators that the slightest change can be critical. This does not encourage the use of new concepts; it promotes the advantages of established procedures. But, theoretical understanding has been considerably improved and technology has fast evolved. In other words, important further advances are still possible and probable. But this will be very difficult. Part of the problem is that every step of the fabrication proces has to be excellent; any failure anywhere can mask an improvement nevertheless achieved. To begin with, improvement of the material quality is slow and difficult though very impressive effort is made in that domain and quartz material is not challenged in many applications.

1. Brief presentation of quartz crystal resonators

The resonator outlined in previous section may be represented on Fig. 1. Question marks show the main points of interest and sources of difficulties for crystal manufacturers. Of importance is the fact that the external world unfortunately is a source of vibrations, accelerations, temperature and pressure variations.

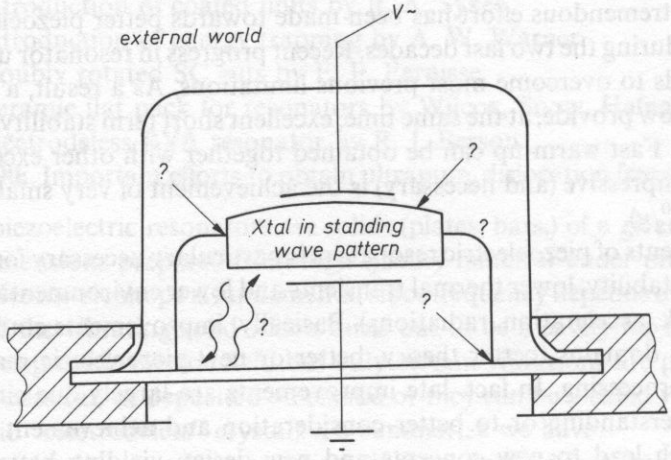

FIG. 1

The usual equivalent circuit of Fig. 2 is valid around a resonant frequency. The intrinsic Q_i factor of a resonator is given by:

$$Q_i = \frac{\bar{c}}{\omega \eta_s}$$

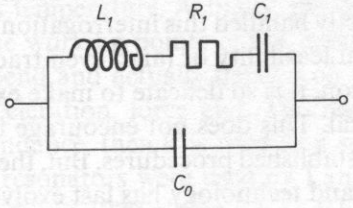

FIG. 2

where c is the rotated elastic coefficient (piezoelectric effect included) η_s is the viscosity constant.

In fact, the previous formula assumes a perfect resonator and Q_i represents an

upper limit since the actual Q factor Q_a is given by:

$$\frac{1}{Q_a} = \frac{1}{Q_i} + \frac{1}{Q_1} + \frac{1}{Q_2} + \ldots + \frac{1}{Q_n}$$

where the Q_n each correspond to a particular phenomenon increasing damping (acoustic losses through fixations, mass loading losses in the surface layers, losses due to imperfections, dislocations, impurities and so on).

Then the quality factor Q_a of an actual resonator depends:

– on the intrinsic Q_i, i.e., on the actual cut, frequency and η_s (a BT cut basically yields 2.3 times the Q factor of an AT cut),

– on the construction of the resonator (ideally on would aim to obtain one single resonant frequency only and introduce no other losses than material losses).

The crystal manufacturer is usually very careful checking the following:

a) *Frequency temperature behaviour*

For a bulk resonator high frequency thickness shear vibrating the frequency f at a temperature T between $-200°C$ and $+200°$ C is given by

$$\frac{f-f_0}{f_0} = a(T-T_0) + b(T-T_0)^2 + c(T-T_0)^3$$

where $f = f_0$ for $T = T_c$.

a, b, c are functions of the rotated material constants for a given mode of vibration.

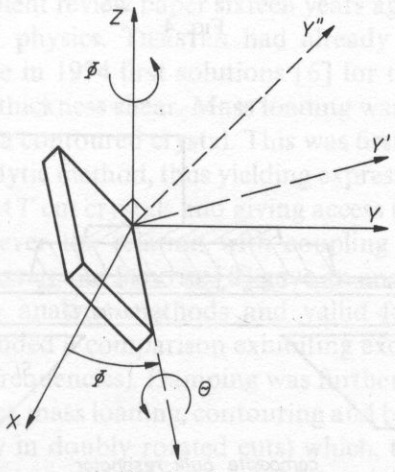

FIG. 3

The singly rotated AT cut (C mode vibrating) is one for which: $a = b = 0$. This cut will provide us with an interesting behaviour versus temperature since two "turn over" points are available on the plot of frequency versus temperature thus giving rise to temperature stabilization. Let us assume now that additional interesting properties are needed. For instance minimal nonlinear effects or independence versus stresses in the plane of the cut are desired. One more degree of freedom must be used thus leading to doubly rotated cuts of Fig. 3. Singly rotated cuts correspond to $\Phi = 0$.

Similar considerations to those developed for bulk resonators can be developed for S.A.W. devices and give very promising cuts as a result.

b) *Modes of motion*

If the crystal vibrates, the corresponding waves propagate and may form standing wave patterns for given frequencies. The corresponding patterns are called resonance of motion. Complete understanding and investigation of those modes are needed for any improvement in quartz crystal design. Usually, the radiofrequency spectrum of a reso-

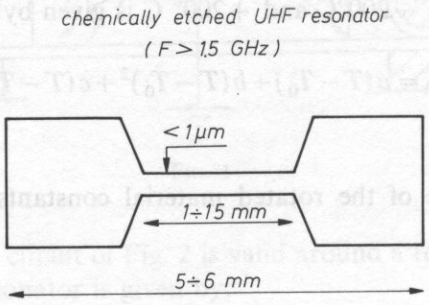

FIG. 4

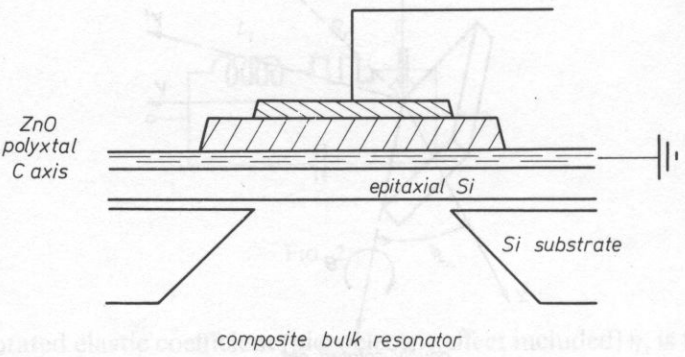

FIG. 5

nator is very complicated (but still does not comprise vibrations which do not give rise to an electric resonance) and its complete investigation needs theoretical developments, together with accurate analysis by X-ray topography scanning electron microscopy interferometry, holography or so.

Before going to more details it is important to point out the extraordinary large variety of crystal resonators. In fact, the piezoelectric resonator domain has been considerably extended for example to watch miniature crystals, UHF resonators for the GHz range (Fig. 4 shows such a crystal chemically etched) or composite bulk resonators (Fig. 5).

Also important is the fact that last two decades improvements have really been tremendous. This will be discussed in the next sections.

2. Resonator understanding together with theory verification is most important and fruitful

A. Better theoretical understanding of resonator have brought in many results during the last decade

A pointed out [3] by Pr. V. E. BOTTOM, one problem, in the quartz crystal business, has been, in the past, a relative lack of research and development together with difficulties for piezoelectricity to be part of programs in Schools of Electrical Engineering. However, the last decade has brought out important advances in fundamental understanding of piezoelectric resonators. We will try to give some examples in the next sections.

1. Analysis of the vibration from a three dimensional point of view. As pointed out by HAFNER [4] in his excellent review paper sixteen years ago, the subject is one of the most difficult in classical physics. TIERSTEN had already indicated many ways to solution [5] when he gave in 1974 first solutions [6] for trapped energy resonators operating in overtones of thickness shear. Mass loading was already involved but not the radius of curvature of a contoured crystal. This was first proposed by WILSON [7] using an approximate analytic method, thus yielding expressions for overtine frequencies and displacements in AT cut crystals and giving access to comparison with X rays Lang's topographs. However the relation with coupling between modes was not investigated. In 1977, TIERSTEN and SMYTHE [8] gave an analytic solution introducing contour and coupling by analytic methods and vallid for AT-cut quartz crystal resonators (the paper included a comparison exhibiting excellent agreement between calculated and measured frequencies). Damping was further introduced in 1978 using [9] Tiersten's model. In fact, mass loading, contouring and boundary conditions imply coupling effects (especially in doubly rotated cuts) which, then, have to be studied.

– Coupling has been investigated between thickness modes themselves

This was the case of work performed by TIERSTEN and STEVENS [10], [11] using an

analytic method which replace mechanical displacement by its decomposition on the eigenvectors triad of Christoffel's problem. This was also the case of work done by BOURQUIN [12] using an analytic method and by DULMET [13] using a semi-analytic perturbation method valid for *AT* and *SC* cuts. Later improvement by introduction of temperature was performed and was presented in 1984 [14] leading to effects of coupling on frequency spectrum and frequency versus temperature behaviour of counteres resonators. The improvement is obtained through use of "effective elastic coefficients" introduced by BOURQUIN and DULMET [15], [16], [17]. It turns out that influence of the choice of the state of reference on temperature coefficients of elastic coefficients is very important. Finally, an interesting special case has been investigated and presented recently [18]. Strong coupling arising from modes having close frequencies and different thermal sensitivities is investigated thus giving one possible mechanism for certain "accidents" occuring on frequency versus temperature curves (Fig. 6).

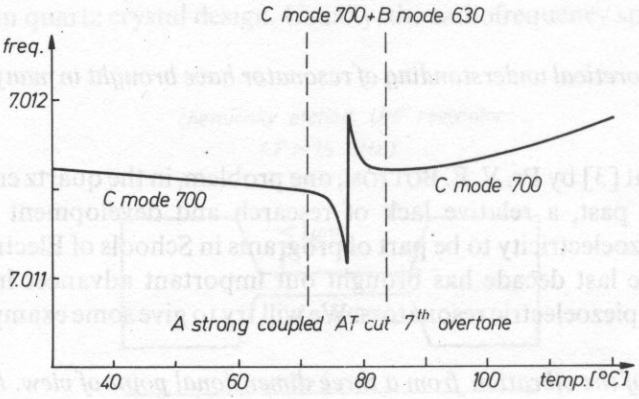

FIG. 6

— Coupling has also been investigated between thickness modes and other kinds of vibration (including flexural).

This has been the case of the work performed by MILSOM, ELLIOTT and REDWOOD [19]. (This three dimensional theory adresses miniature resonators, uses a perturbation method and utilises complex wave numbers). Coupling between thickness modes and other modes is also largely investigated by MINDLIN and his disciples (using Mindlin's special method) [20], [21], [22].

It is to be pointed out that ref. [22] by LEE and YONG adresses doubly rotated plates and shows how frequency temperature behaviour is affected by plate dimensions and orientations.

As a conclusion: it can be said that tremendous advance has been made in the analysis of the vibration from a three dimensional point of view. In our opinion, further

improvements should come from including edge boundary conditions which have not been considered except for choice of mounting points or calculations of force-frequency constants for example by BALLATO [23], [24].

2. *Lagrangian formulation and temperature problems.* This formulation and been extensively used in the analysis of the influence of static stresses on the resonant frequency. It is also very useful to study non linearities such as amplitude frequency effect [25], [26], [27], [28].

This was first done in order to reduce sensitivities to forces and accelerations or in order to make force sensors or accelerometers. A good example is the calculation by LEE and KUANG-MING WU of the effects of acceleration in AT cuts or doubly rotated plates [29], [30]. The method was also used to determine thermal sensitivities either as dynamic temperature variations or as static temperature variations.

Static temperature variations.

Much work has been done in this domain especially by LEE and YONG [31] using material from previous work [32]. It is also used in the case of the stress free temperature variations [15]. In a classical manner, vibration of a resonator by referen-

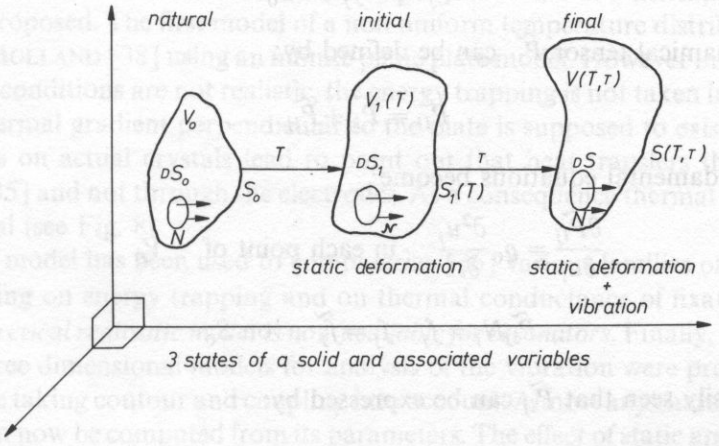

FIG. 7

ce to the 3 states of a solid Fig. 7 is obtained by use of the following equations of equillibrium and boundary conditions:

$$\frac{\partial \tau_{ij}}{\partial x_i} = \frac{\partial^2 u_j}{\partial t^2}, \text{ in each point of } V \tag{1}$$

$$\tau_{ij} n_i = f_j, \text{ in each point of } S \tag{2}$$

with

$$\tau_{ij} = B_{ijkl} \frac{\partial u_k}{\partial x_l} \tag{3}$$

where τ_{ij} is the usual stress in the final state, n_i is the direction cosine of surface element dS and f_j the external force applied on dS.

It is clear that ϱ and n_i depend on static deformation and therefore on temperature. But important advantage can be obtained using the a_i coordinates [25] as independent variables. Equations corresponding to Eq(1) and Eq(2) then make use of Piola tensor P_{ij} [25]:

$$P_{ij} N_i dS_0 = \tau_{ij} \tag{4}$$

where N_i is the direction cosines of dS_0. P_{ij} tensor corresponds to total deformation (static deformation with thermal origin plus dynamical deformation). Without dynamical deformation we obtain the static Piola tensor $\overline{P_{ij}}$:

$$\frac{\partial \overline{P_{ij}}}{\partial a_i} = 0 \quad \text{in each point} \quad V_0 \tag{5}$$

$$\overline{P_{ij}} N_i = f_j \text{ on } S_0. \tag{6}$$

In fact a dynamical tensor $\widetilde{P_{ij}}$ can be defined by:

$$P_{ij} = \overline{P_{ij}} + \widetilde{P_{ij}}. \tag{7}$$

Then the fundamental equations become:

$$\frac{\partial \widetilde{P_{ij}}}{\partial a_i} = \varrho_0 \frac{\partial^2 u_j}{\partial t^2} \quad \text{in each point of} \quad V_0 \tag{8}$$

$$\widetilde{P_{ij}} N_i = f_j - \overline{f_j} = \widetilde{f_j} \quad \text{on } S_0. \tag{9}$$

It can be easily seen that $\widetilde{P_{ij}}$ can be expressed by:

$$\widetilde{P_{ij}} = A_{ijkl} \frac{\partial u_l}{\partial a_k} + \frac{\varrho_0}{\varrho_1} \frac{\partial a_k}{\partial x_l} \frac{\partial a_i}{\partial x_m} \overline{T}_{ml} \frac{\partial u_j}{\partial a_k} \tag{10}$$

where $\overline{T_{ml}}$ represents mechanical stress without vibrations ($u_i = 0$). A_{ijkl} is a tensor of elastic coefficients. If the resonator is free to expand without induced stresses, $\overline{f_j}$ and $\overline{T_{ml}}$ are zero in any point of the solid. Then:

$$\widetilde{P_{ij}} = A_{ijkl} \frac{\partial u_k}{\partial a_l} \tag{11}$$

A_{ijkl} defines new coefficients so called "effective elastic coefficients".

Let us point out advantages obtained by use of those effective coefficients. In fact, everything is refered to a so said "natural state" at the reference temperature To including propagation equation and boundary conditions. This finally turns out to be simpler and at the same time more accurate. For instance, the slight change in orientation due to temperature or the fact that a sphere expands into an ellipsoid are taken into account. This can be of importance especially in the case of some doubly rotated cuts as *RT* cuts. Finally this method entitles to separate dimensional variation of resonator due to temperature from variations of elastic coefficients with temperature. In other words a fictive medium without expansion is considered but its mechanical coefficients have (compared to the actual medium) a different variation with temperature.

Dynamic temperature variations.

Much work has been performed in that domain especially by TIERSTEN, STEVENS and SINHA [33], [34]. It is to be pointed out that the case of doubly rotated cuts is included. Another important advance was recently introduced by VALENTIN [35] and used to predict frequency shifts arising from in-plane temperature gradient distribution [36] in resonators and to achieve fast warm up [37]. In fact, a new thermal model for resonator is proposed. The first model of a non uniform temperature distribution was proposed by HOLLAND [38] using an infinite plane plate model. However in this model the boundary conditions are not realistic, the energy trapping is not taken ino account and only a thermal gradient perpendicular to the plate is supposed to exist. Realistic considerations on actual crystals lead to point out that heat transfers through the quartz itself [35] and not through the electrodes. As a consequence thermal gradient is basically radial (see Fig. 8).

This new model has been used to computerize [36] various families of isotherms either depending on energy trapping and on thermal conductance of fixations.

3. *A theoretical realisatic model is now available for resonators.* Finally, during the last decade three dimensional models for analysis of the vibration were progressively made available taking contour and coupling into account. Almost any characteristic of a resonator can now be computed from its parameters. The effect of static and dynamic temperature variations can be accurately predicted. A new thermal model far from the infinite plane plate is also available. In other words, in every domain, theoretical models are much more realistic and differ from the old infinite plane plate model which however is the basic of determination of mechanical coefficients C_{ij} and their temperature coefficients. It would probably be interesting to remarke the experiments of BECHMANN, BALLATO, and LUKASZEK [39] using accurate energy trapping models to redetermine some coefficients and their derivatives by respect to temperature. (In fact, improvements in accuracy of these coefficients are now needed to define new cuts or design new resonators and sensors).

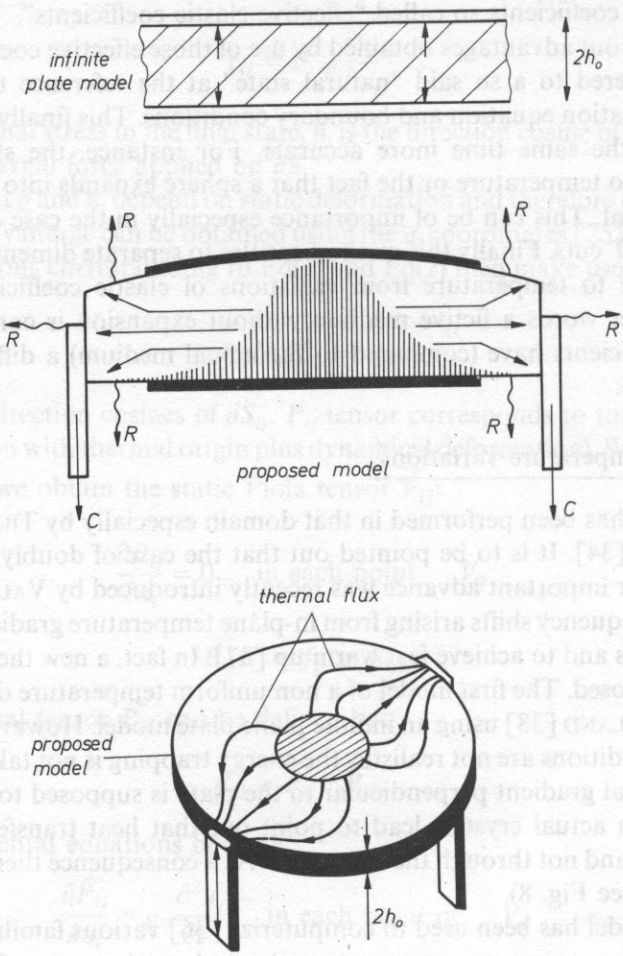

FIG. 8

B. Theory verification feeds back theory and prepares for new designs

Theoretical analysis is complex and difficult; it may have to be completed by finite elements techniques but it always has to be confronted in detail with actual figures. Various diagnostics and measurements have to be performed at each step of fabrication (on raw material, water, surface, interface, fixation, electrode, deposition, cleaning, enclosing, and on final resonator). For simplicity, only visualization of crystal's vibrations will be considered here.

1. X *ray topographic techniques.* When an actual resonator has been designed, it is possible to get, from theory, every resonant frequency with it's associated vibration pattern, in the whole needed frequency domain. Then, the actual resonant frequencies

and vibration patterns have to be obtained, for instance, through Lang's or similar X ray topographic techniques [40]. Though many exciting new results can still be found in that field, the technique is now well known. It needs very well trained people using expensive equipment. However, even if is time consuming there is no way properly design a new resonator such a technique (or a similar one). On the pattern of Fig. 9, theoretical results and topographs appear at the same time. The engineer and the theoretician need to discuss for design evolution trying to avoid or explain unexpected patterns. The technique can also be used for study of coupling between modes under variation of temperature provided an adequate oven transparent to X rays is used [18].

2. *Other techniques.* Many other techniques have been used recently to visualize or computerize actual vibration patterns. This is the case in laser interferometric measurement of vibration displacements [41] or in measurements using speckle effects [42].

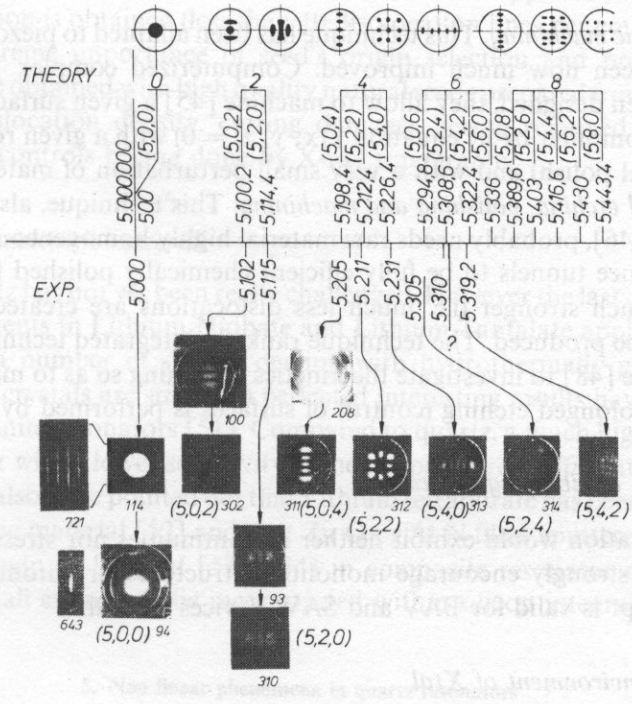

FIG. 9

3. Better consideration and achievement of boundary conditions

A crystal resonator is a solid limited by surfaces connected to outside changing world by fixations, electrodes and surrounding medium (Fig. 1). Interactions are mechanical and thermal and electric. Obviously boundary conditions have to be paid a great deal of attention and care [43], [44]. Important improvements are still ahead.

As we have seen in Sect. 2, theory now includes much more realistic boundary conditions. But also new techniques are developed with much better achievement of surface limits, much better mounting of piezoelectric crystal. Some examples will be considered here.

A. Surface of piezoelectric medium

In an ideal situation, one would create a surface corresponding exactly to a given shape (or equation), whithout any perturbed layer and nevertheless exhibiting optical polish. Very close to the surface the material properties should be unperturbed. No defect should be created by machining or by electrode deposition i.e. "electrodess" crystals are desirable. From that point of view, at least two techniques have been found promisive.

1. Ultrasonic machining. This technique has been adapted to piezoelectric crystals [43] and has been now much improved. Computerized complex U.S. machining systems have been designed, they allow to machine [45] a given surface even complex (introduced in computer by its equation $f(x, y, z) = 0$) with a given roughness (down to almost optical polish) and with a very small perturbation of material properties.

2. Chemical etching, polishing and machining. This technique, also introduced in the last decade [46], probably needs raw material highly homogeneous without given defects for instance tunnels to be fully efficient chemically polished [47] blanks are mechanically much stronger (i.e. much less dislocations are created) and complex geometries can be produced. The technique ranks in integrated techniques and much effort is still done [48] to investigate the kinetics of etching so as to master changes of surfaces with prolonged etching (control of surfaces is performed by S.E.M.).

B. Fixation of vibrating crystal

An ideal fixation would exhibit neither discontinuities nor stresses nor changes with time. This strongly encourage monolithic structures or automounted crystals [43]. The concept is valid for BAV and SAW devices as well.

C. Direct environment of Xtal

Last decade has seen continuing improvement in cleanliness of crystal, processing, including single step high vacuum processing bake out and sealing and U.V. cleaning procedures. Coldweld sealed metal enclosures and ceramic hermetic flatpacks have been developed for similar purposes.

4. Improvement in the "quality" of piezoelectric material is still needed

Recent improvements in resonator understanding and technique, radiation hardening requirements are strongly boosting research and development for "better" piezoelectric material. Better may also mean better availability and continuity in the supply of a given quality of material. Also, piezoelectric material suppliers have to consider industrial yield and this does not always encourage for highest quality material because the market may be too small.

A. Quality of quartz material

For those who work on the forefront of piezoelectric devices, availability of excellent material is still a problem. Nobody really knows where would be the limits of ultra high purity quartz with very few dislocations and growth defects, if that material was properly handled. Extensive attenuation measurements over a large temperature range have been done in the past, but they did not use extrahigh purity dislocation free material (and at 5 MHz results often came through resonators according to Warner's design). Recent work has been done on growth of high purity low dislocation quartz [49], [50]. Aluminium content level may be as low as 0.02 ppm or lower and a large degree of perfection is obtained (less than 10 disolocation lines per cm^2). Experiments demonstrate extreme importance of seed's origin selection and preparation. Best results seem to be obtained with high quality natural seeds prepared from areas selected for very low dislocation density, cutting damages beeing removed from the seed surfaces and all controls beeing done by X-ray topography.

B. New piezoelectric material

In fact, quartz has not yet been really challenged. However the last decade has seen further developments in Lithium Niobate and Lithium Tantalate applications. It has also seen quite a number of studies dealing with hydrothermally grown Berlinite crystals. Though crystals are still to be perfected interesting results have already been obtained on Berlinite resonators [51]. Compared to quartz, a much higher coupling is obtained together with a lower sensitivity of the temperature coefficients of frequency.

Finally, it is also to be pointed out that Lithium tetraborate has been introduced as a new piezoelectric material [52] and that Zn O or Al N films sputtered on to simple crystal Silicon begin to be used [53], [54] in composite resonator structures. The structures are small enough to be incorporated within silicon integrated circuits.

5. Non linear phenomena in quartz resonators

Several properties of resonators strongly depend on non linearities of quartz material. Harmonic generation, amplitude frequency effects and intermodulation correspond to propagation of a finite amplitude wave in a non linear medium. Sensitivities

to external or internal perturbations (temperature, force, pressure acceleration electric field) are due to the coupling between the high frequency wave and the non linear strained medium: they deserve a non linear treatment.

Fifteen years ago some non linear coefficients were still needed when measured by the author [55] to explain non linear effects in quartz resonators [56]. However it is clear that, to day, some important advances in the resonator field are due to success in non linear effects study and handling. Detailed information will be found in Ref. [56] or in a recent review paper [57] which also calls attention on the concept of lattice waves and phonons (leading to description of thermal conductivity) thermal expansion and acoustic attenuation by means of phonons interactions).

An interesting new non-linear analysis method has also been recently proposed [58] and caused to find out both theoretically and experimentally a so called "non-rationnal frequency division" [59].

The important part of the *SC* cut resonator is also to be pointed out in that field since amplitude frequency effect, intermodulation sensitivity to planar stresses are much reduced [57] [60].

Recently frequency and phase noise in quartz resonators have been studied [61] as a function of the driving power. At low power $1/f$ fluctuations are observed but at medium power (some mw) the non linearities of the crystal increase the phase fluctuations when at high powers thermal instabilities and chaotic behaviour occur (together with high level white noise).

6. Evolution in resonator or sensor design. New concepts

In this section, some advances of the last decade will be recalled. To begin with, the importance of effective production of doubly rotated thickness mode plates will be pointed out. Though introduced before world war II, doubly rotated resonators have really been developed after work by EERNISSE [62], [63] on *SC* cuts. In this paper we will basically refer to the exhaustive paper by BALLATO [64] and point out the exceptionnal advantages of doubly rotated plates (in particular for *SC* or *TTC* cuts, low sensitivities to stresses in cut's plane, excellent thermal behaviour including thermal transient [65] and low amplitude frequency effect [66]). This is the reason why intensive efforts on doubly rotated crystals have been reported during the five last years causing doubly rotated plates to be, now, commercially available.

Some new resonators or new concepts that appeared in the last decade will now be rapidly presented:

A. New resonators or techniques

1. Ceramic flat pack resonators [67], [68], [69], [70]. As pointed out by several authors, usual packaging techniques do not insure hermeticity thus exposing the crystal to contamination. The ceramic flat pack technique uses ceramic material

together with aluminium gaskets and allows mass production. This new configuration yields a small, highly reliable rugged crystal (polyimide bonding cans be used).

2. BVA techniques. This technique was introduced in Besançon, France, after 1975 [43], [44], [71], [72]. It is now well known and industrially produced [73], [74] though many models described are not yet in production line. The new BVA_n structures may use a rather conventionnal bonding and a special fixation (n odd) or may use "automounted" crystals i.e. crystal with monolithic fixations made out of quartz (n even). The crystals are usually "electrodeless" but electrodes can also be deposited on vibrating crystal (patent n° 77 17 309) so leading to BVA_4 or QAS designs [74]. Fig. 10 recalls some of the different designs proposed.

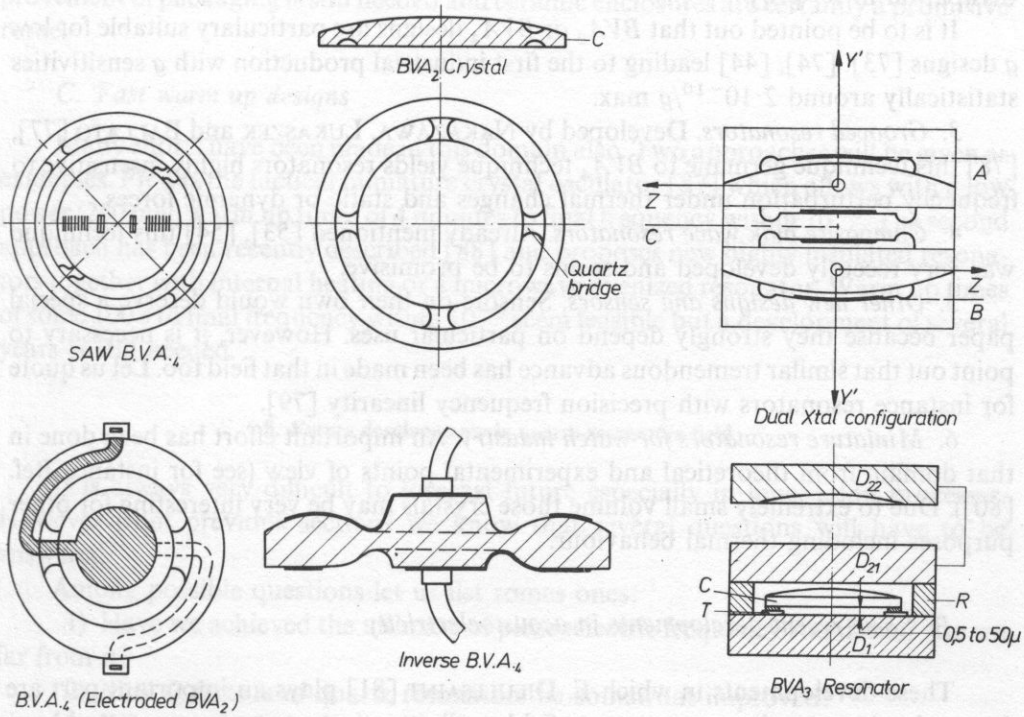

FIG. 10

At this point, BVA_2 units (5 to 100 MHz) and BVA_4 units, in particular, are in production lines. Among other advantages of BVA_2 designs [44], [71] we shall specially mention lower aging, much lower g sensitivity, higher drive levels and existence of zero aging drive levels [75]. More precisely, BVA_2 resonator allow much higher drive levels without degrading badly drift rates. Moreover theoretical considerations and experimental data [75] show that resulting aging a_r may be, as a first approximation,

modeled by:

$$a_r = a_i + kP\{1 + a\exp(-\sqrt{P/P_0}\, t/\tau) + \ldots\}$$

where: a_i is an intrinsic aging depending on material and cut, k is a constant depending on material and cut, a is a constant without dimension, P is the power dissipated in motional resistance R_1, P_0 is a reference power level, τ is a time constant; t is time.

This formula shows evidence of a drive level P_1 yielding on aging rate crossing zero. For natural Brazil quartz 5 MHz fifth overtone resonator P_1 is about 80 μw; 5 MHz third overtone *SC* correspond to 160 μw.

Using very high drive levels it is possible to "internally heat" the crystal by energy dissipation in R_1 [76].

It is to be pointed out that BVA_2 or BVA_4 designs are particulary suitable for low g designs [73], [74], [44] leading to the first industrial production with g sensitivities statistically around $2 \cdot 10^{-10}/g$ max.

3. Grooved resonators. Developed by NAKAZAWA, LUKASZEK and BALLATO [77], [78] this technique germane to BVA_4 technique yields resonators highly insensitive to frequency perturbation under thermal changes and static or dynamic forces.

4. Composite bulk wave resonators. Already mentioned [53], [54] this technique was very recently developed and seems to be promisive.

5. Other new designs and sensors. Sensors on their own would deserve a special paper because they strongly depend on particular uses. However, it is necessary to point out that similar tremendous advance has been made in that field too. Let us quote for instance resonators with precision frequency linearity [79].

6. Miniature resonators for watch industry. An important effort has been done in that domain from theoretical and experimental points of view (see for instance Ref. [80]). Due to extremely small volume those crystals may be very interesting for other purposes including thermal behaviour.

B. Some recent developments in acoustoelectricity

These developments in which E. DIEULESAINT [81] plays an important part are interesting because they open up new fields, call attention on new concepts and have practical consequences. Of importance is the mechanical excitation of a membrane by an optical beam which, in particular, leads to optical excitation of quartz resonators and optoacoustic oscillators [82] (piezoelectric material is not mandatory). On the other hand Raleigh waves can be generated by photo thermal effects [83] (generation of elastic waves by harmonic heating at the interface between an infinite medium and a backing material has also been studied). It has also been shown recently [84] that Lamb waves can be launched in glass plates and detected by bulk wave resonators placed between the arms of tongs.

7. Recent improvements of resonators in relation relation with different designs

A. Low a designs

This subject has already been investigated by many authors and in particular in France [85], [86]. The author simply stresses that the models described in reference [85] do yield low g sensitivities.

B. Reducing aging

This is certainly one of the most difficult subjects. However the efforts during the last decade have finally yielded a reduction of an order of magnitude. BVA_2 design provide lower aging rate and final aging established within days. Nevertheless improvement of packaging is still needed and ceramic enclosures are certainly a promisive route.

C. Fast warm up designs

Many efforts have been made in this domain also. Two approaches will be given as examples. First is the tactical miniature crystal oscillator [87] which allows with a low power (250 mw) warm up times of 4 minutes to final frequency within 10^{-8}. The second approach has been recently described [88] and proposes new highly insulated resonators together with internal heating or a microwave ovenized resonator. Warm up times of some 100 s to final frequency within 10^{-9} seem feasible but a development of several years is still needed.

8. Future developments in quartz resonators field

It is always very difficult to forecast future especially in innovation processes. However from previous sections we know that several questions will have to be answered.

Among possible questions let us list somes ones:

1) Have we achieved the ultimate of piezeoelectric frequency standards? Are we far from it?

2) May Q factors of quartz resonators be somewhat improved?

3) What kind of results could be obtained with "perfect" super lattice quartz material (properly handled)?

4) Which is the lowest g sensitivity feasible in the case of quartz Xtal resonators?

5) Which is the best resonator frequency range? Is it possible to use quasi electromagnetic waves instead of quasi electromechanical waves?

6) Have we paid enough attention to possible miniaturizations and use of monolithic structures?

7) Is energy trapping by spherical contours an optimal design?

8) Has resonator edge to be circular or rectangular?

9) Are nanotechnologies (in the Å range) of some use in quartz resonator design?

10) What is the future of non piezoelectric material for resonator design?

Of course some important questions are also related to the proper use of a resonator i.e. oscillator design theory and achievement.

One of the problems already pointed out is that there is not enough connection between the three trades involved in quartz oscillators achievement (i.e. material field, resonator field, electronics). Matching crystal to oscillator (or the reverse) is a very important task for success. Also oscillator design now benefits from computer aided design and various improvements including surface mounted components use and several others. Of course influences humidity have to be eliminated [89] through hermetically sealing (this also helps'emilinating pressure variations influence).

9. Conclusion: possible future trends (next 10 years)

Thanks to progress in resonator and oscillator fields as well, small, low cost, low consumption and rugged quartz oscillators or sensors are now available. Progress has yielded reduced aging, better short term stability, low thermal transient and small environmental dependance. Following table compares performances obtained 10 years ago with performances available to day for commercial precision crystals. From research area possible trands for near future are foreseen.

If we try tu summarize all the data obtained in the last 20 years, it is clear that 2 characteristics, aging and g sensitivity of oscillators, have been in constant progress while $\sigma_y(\tau)$ seemed to somewhat reach a limit in the vicinity of $7 \cdot 10^{-14}/10$ s at 5 MHz. Is is hard to predict what would happen with much better Q factors because it may depend on the type of Xtal (there is some evidence that part of the noise is correlated to proccesses in adhering electrodes) and obviously we still have to clear up various influences on noise processes (though in principle $\sigma_y(\tau)$ should vary as $1/Q^2$).

Some more confidence can be paid to improving and g sensitivity. An aging rate in the of $5 \cdot 10^{-11}$/year to $5 \cdot 10^{-10}$/year is probably in a reaching distance while a g sensitivity in the $10^{-11}/g$ range or better is probably achievable. Of course, such a low g sensitivity will also influence other parameters since an oscillator is never in a perfect mechanical environment. In other words we should see some more of the competition between high quality quartz standards and atomic rubidium references.

References

[1] A. E. Wainright, F. L. Walls et al., Proc. 28th Annual Frequency Control Symposium AFCS, pp. 117–180, (1974).

[2] S. R. Stein, C. M. Manney, Jr. et al., Proc. 32nd AFCS, pp. 527–530, (1978).

[3] V. E. Bottom, Proc. 35th AFCS, pp. 3–12, (1981).

[4] E. Hafner, IEEE transactions on Sonics and Ultrasonics, Vol. SU 21 n° 4, pp. 220–237, (1974).

[5] H. F. Tiersten, *Linear Piezoelectric Plate Vibrations*. Plenum Press, New York, (1969).

[6] H. F. TIERSTEN, Proc. 28th AFCS, 44, (1974).
[7] C. J. WILSON, J. Phys. D Appl. Phys., **7,** pp. 2449–2454, (1974).
[8] H. F. TIERSTEN and R. C. SMYTHE, Proc. 31st AFCS, pp. 44–47, (1977).
[9] R. J. BESSON, B. M. DULMET et al., Ultrasonics Symposium Proceedings, pp. 152–156, (1978).
[10] D. S. STEVENS and H. F. TIERSTEN, Proc. 35th AFCS, pp. 205–212, (1981).
[11] H. F. TIERSTEN and D. S. STEVENS, Proc. 36th AFCS, pp. 37–45, (1982).
[12] R. BOURQUIN and D. NASSOUR, C. R. Acad. Sc. Paris, **298,** Série II, n° 12, pp. 517–520, (1984).
[13] B. DULMET, Revue de Phys. Appl. **19,** pp 839–849, (1984).
[14] B. DULMET and F. FICHET, Proc. IEEE, Ultrasonics Symposium, (1984).
[15] B. DULMET, R. BOURQUIN, C. R. Acad. Sc. Paris, **294,** Série II, pp. 361 – 364, (1982).
[16] B. DULMET, R. BOURQUIN, Revue Phys. Appl. **18,** pp. 619–624, (1983).
[17] R. BOURQUIN, B. DULMET, Proc. Congrès International de Chronométrie Besançon, pp. 109–113, (1984).
[18] R. BOURQUIN, B. DULMET, G. GENESTIER, Proc. Ultrasonics Symposium, (1984).
[19] R. F. MILSOM, D. T. ELLIOTT et al., Proc. AFCS, pp. 174–186, (1981).
[20] R. D. MINDLIN, Proc. 36th AFCS, pp. 3–21, (1982).
[21] Z. NIKODEM, P. C. Y. LEE, Int. J. Solids Structure **10,** pp. 177–196, (1974).
[22] P. C. Y. LEE, Y. K. YONG, AFCS, (1984).
[23] A. BALLATO, IEEE trans. Sonics Ultrasonics, Vol. SU **25** n° 3, pp. 132–138, (1978).
[24] A. BALLATO, IEEE trans Sonics Ultrasonics, Vol. SU **25** n° 4, pp. 223–226, (1978).
[25] R. N. THURSTON, *Waves in solids*, Handbuch der Physik VI a/4 Springer Verlag, (1974).
[26] H. F. TIERSTEN Int. J. Eng. Sc. **9,** pp. 587–604 Pergamon, (1971).
[27] J. C. BAUMHAUER and H. F. TIERSTEN, J. Ac. Soc. Am, **54** n° 4, pp. 1017–1034, (1973).
[28] H. F. TIERSTEN, J. Acoust. Soc. Am. **57** n° 3, pp. 660–666, (1975).
[29] P. C. Y. LEE, KUANG-MING WU, Proc. 30th AFCS, pp. 1–7, (1976).
[30] P. C. Y. LEE, KUANG-MING WU, Proc. 34th AFCS, pp. 403–411, (1980).
[31] P. C. Y. LEE and Y. K. YONG, Proc. 37th AFCS, pp. 200–207, (1983).
[32] P. C. Y. LEE, Y. S. WANG et al., J. Acoust. Soc. Am. 57 n° 1, pp. 95–105, (1975).
[33] D. S. STEVENS, H. F. TIERSTEN, Proc. 37th AFCS, pp. 208–217, (1983).
[34] B. K. SINHA, H. F. TIERSTEN, J. App. Phys., **55** n° 9, pp. 3337–3347.
[35] J. P. VALENTIN, Doctoral Thesis n° 178, Besançon, (1983).
[36] J. P. VALENTIN, G. THEOBALD, J. J. GAGNEPAIN, Proc. 38th AFCS, (1984).
[37] J. P. VALENTIN, M. D. DECAILLIOT, R. J. BESSON, Proc. 38th AFCS, (1984).
[38] R. HOLLAND, IEEE Trans. SU 21, n° 3, p. 171, (1974).
[39] R. BECHMANN, A. D. BALLATO, T. J. LUKASZEK, Proc. IRE **50,** n° 8, (1962).
[40] G. GENESTIER, Doctoral thesis n° 127, ENSMM, Besançon, (1982).
[41] K. IIJIMA, Y. TSUZUKI et al., Proc. 30th AFCS, pp. 65–70, (1976).
[42] L. WIMMER, S. HERTL et al., Rev. Sci. Instrum. **55** (4), pp. 605–609, (April 1984).
[43] R. J. BESSON, Proc. 30th AFCS, pp. 78–82, (1976) and Proc. 31st AFCS, pp. 147–152, (1977).
[44] R. J. BESSON, J. M. GROSLAMBERT, F. L. WALLS, Ferroelectrics **43,** pp. 57–65(1982).
[45] P. MAITRE, ENSMM, Besançon, private communication.
[46] J. R. VIG, J. W. LEBUS et al., Proc. 31st AFCS, pp. 131–143, (1977).
[47] W. P. HANSON, Proc. 37th AFCS, pp. 261–264, (1983).
[48] C. R. TELLIER and al., Proc. 40th AFCS, (1986).
[49] D. F. CROXALL, I. R. CHRISTIE et al., Proc. 36th AFCS, pp. 62–65, (1982).
[50] J. F. BALASCIO, A. F. ARMINGTON, Proc. 40th AFCS, (1986).
[51] J. DETAINT, H. POIGNAUT et al., Proc. 34th AFCS, pp. 93–101, (1980).
[52] C. D. J. EMIN, J. F. WERNER, Proc. 37th AFCS, pp. 136–143, (1983).
[53] J. S. WANG, K. M. LAKIN et al., Proc. 37th AFCS, pp. 144–150, (1983).
[54] T. W. GRUDKOWSKI, J. F. BLACK et al., Proc., 36th AFCS, pp. 537–548, (1983).
[55] R. J. BESSON, Proc. 28th AFCS, p. 8, (1974).

[56] J. J. GAGNEPAIN, R. J. BESSON, Physical Acoustics WP Mason Ed. Vol. XI 245, Acad. Press, (1975).
[57] J. J. GAGNEPAIN, Proc. 35th AFCS, pp. 14–30, (1981).
[58] J. H. BALBI, J. A. DUFFAUD, R. J. BESSON, Proc. 32nd AFCS, pp. 162–168, (1978).
[59] J. H. BALBI, M. DULMET, A. THIRARD, Revue de Physique Appliquée, **17** n° 1, (janvier 1982).
[60] R. BOURQUIN, D. NASSOUR, D. HAUDEN, Proc. 36th AFCS, pp. 200–207, (1982).
[61] J. J. GAGNEPAIN, M. OLIVIER, F. L. WALLS, Proc. 37th AFCS, pp. 218–225, (1983).
[62] E. P. EERNISSE, Proc. 29th AFCS, pp. 1–4, (1975).
[63] E. P. EERNISSE, Proc. 30th AFCS, pp. 8–11, (1976).
[64] A. BALLATO, Physical Acoustics **13,** pp. 115–181, (1977).
[65] J. KUSTERS, IEEE Trans. Sonics Ultrasonics SU 23, pp. 273–276, (1976).
[66] J. J. GAGNEPAIN, J. C. PONCOT and C. PEGEOT, Proc. 31st AFCS, pp. 17–22, (1977).
[67] J. R. VIG, J. W. LEBUS et al., Proc. 29th AFCS, pp. 220–229, (1975).
[68] P. D. WILCOX, G. S. SNOW et al., Proc. 29th AFCS, pp. 202–219, (1975).
[69] R. D. PETERS, Proc. 30th AFCS, pp. 224–231, (1976).
[70] R. L. FILLER, J. M. FRONCK et al., Proc. 32nd AFCS, pp. 290–298, (1978).
[71] R. J. BESSON, Proc. 10th PTTI, pp. 101–130, (1978).
[72] *French patents* n° 7601035, 7717309, 7802261, 7828728, 7918553, 8110006, 8215351 and *corresponding patents or patents pending in other countries.*
[73] E. P. GRAF, U. R. PEIER, 37th AFCS, pp. 492–500, (1983).
[74] J. P. AUBRY, A. DEBAISIEUX, 38th AFCS, (1984).
[75] R. J. BESSON, D. A. EMMONS, Proc. 11th PTTI, pp. 457–469.
[76] J. P. VALENTIN, 34th AFCS, pp. 194–201, (1980).
[77] M. NAKAZAWA, T. LUKASZEK, A. BALLATO, Proc. 36th AFCS, pp. 513–516.
[78] M. NAKAZAWA, T. LUKASZEK, A. BALLATO, Proc. 35th AFCS, pp. 71–91, (1981).
[79] M. NAKAZAWA, H. ITO et al., Proc. 36th AFCS, pp. 290–296, (1982).
[80] A. E. ZUMSTEG, P. SUDA, Proc. 30th AFCS, pp. 196–201, (1976).
[81] E. DIEULESAINT, D. ROYER, *The mechanical behavior of electromagnetic solid continua,* pp. 3–15, G. A. Manguin editor Elsevier, (1984).
[82] E. DIEULESAINT, D. ROYER, Proc. Ultrasonics Symposium, pp. 793–795, (1982).
[83] D. ROYER, E. DIEULESAINT, J. de Phys. C6 suppl. **44,** n° 10 (oct. 1983).
[84] E. DIEULESAINT, A. BILLMANN et al., Proc. Ultrasonics Symposium, (1983).
[85] R. J. BESSON, J. J. GAGNEPAIN, D. JANIAUD, M. VALDOIS, 33rd AFCS, pp. 337–345, (1979).
[86] D. JANIAUD, Doctoral thesis Besançon, (1978).
[87] H. W. JACKSON, Proc. 36th AFCS, pp. 492–498, (1982).
[88] J. P. VALENTIN, M. D. DECAILLIOT, R. J. BESSON, Proc. AFCS, (1984) and Proc. 1rst European Frequency and Time Forum, (1987).
[89] F. L. WALLS, Proc. 42th AFCS, pp. 279–283, (1988).

Table 1.

(Commercial precision units)

	10 years ago	Now	Less than 10 years from now
$\sigma_y(\tau)$ 1s, 10 s	$4\ 10^{-13}$ to 10^{-12}	1 to $4\ 10^{-13}$	5 to 10×10^{-14}
Aging/year	2 to $3\ 10^{-8}$	3 to $6\ 10^{-9}$	5 to $9\ 10^{-10}$ predictible
g sens. max	$2\ 10^{-9}/g$	$3\ 10^{-10}/g$	4 to $7\ 10^{-11}/g$ SC 7 to $30\ 10^{-11}/g$ AT

ARCHIVES OF ACOUSTICS
16, 1, 53-72(1991)

MEASUREMENT OF QUARTZ CRYSTAL RESONATORS AND FILTERS IN THE PRODUCTION PROCESS

W. J. McCARTNEY

Transat Corporation
(31000 Bainbridge Road, Solon, Ohio 44118, USA)

1. Introduction

The crystal manufacturing industry has been plagued by measurement problems though out its history. Producers and customers have had problems monitoring product specifications with sufficient accuracy to insure the final product meets the customer requirement. This problem is getting more severe where manufacturers are being pushed to provide very small lot production runs with high precision and low cost. This paper outlines some practical issues present for crystal producers and users. Several directions are presented to help minimize the problem. Key among these suggestions are the use of measurement techniques, fixtures and equipment compatible with current industry standards.

2. History

The measurement equipment used in crystal manufacturing to produce a product meeting the customer requirement has developed from using the customers actual and product circuitry.

This approach, although it offered the best compliance with the customer requirement, is usually impractical in a production environment. The typical case might involve the customer sending specialized test equipment that the producer would actually install as final test equipment. The approach has several practical problems. One of the most severe is that the production process must be calibrated to a non-traceable standard. This creates severe manufacturing start-up and measurement repeatability problems. The calibration and drift of the instrument places pressure on the manufacturing process to "track" the drift.

The quality CI meters from a number of vendors have reduced this problem

somewhat, but the need for extended frequency range and good load capacitance correlation still plagued the industry.

Modern precision frequency synthesizers, vector voltmeters and high quality network analyzers have allowed the development of precision passive device measurement techniques based on them.

The need to measure devices accurately and reliably during the production process becomes more difficult at higher frequencies were the traditional measurement techniques are not accurate enough or the measurement technique does not have the bandwidth to track the device during an adjustment process.

A different set of difficulties occur in the frequency adjustment of monolithic filters. The production monitoring is more difficult because of the dynamics of the device can change as it is being adjusted. The problems of consistent measurement results and device mask alignment both must be resolved.

3. Measurement issues

The problems with correlating measurements can generally be divided into two areas, customers – the crystal end user – and producer – the crystal manufacturer. Measurement standards such as the IEC 444 and the EIA 512 utilizing precision measurement equipment help reduce some of these problems.

3.1. Crystal users

The crystal user wants to insure that the product he receives from the crystal manufacturer meets the design requirements. He should identify critical crystal device parameters early in the design process. This is often not the case. The equipment designer may have only a limited concept of the device and often must define the actual measurement equipment and technique for qualifying the part. This creates a problem with standardization in larger organizations as well as with consistency in how the product is specified internally and how the part is specified to the crystal manufacturer.

3.2. Crystal manufacturers

The crystal manufacturer wants to be able to correlate device monitors between each of his production steps as well as final inspection. It is essential for the multinational producer to have this capability to insure that devices manufactured around the world will comply with product specifications. This allows the manufacturer the flexibility produce the product at different facilities that may be optimized for lot sizes.

4. Crystal measurements

4.1. Active techniques

The oscillator measurement technique can be based upon designing a specialized test oscillator circuit or a CI meter. If a custom test circuit is designed with close attention to the target circuit design, this method offers the possibility of providing the best results for the application of the part. However, the penalty with this type of approach is that a "new" piece of test equipment may need to be introduced for each different part or class of part. Traceability and inter-facility correlation problems make this approach clearly undesirable.

The CI meter was developed to extract the motional parameters of the crystal. Although limited in precision at frequencies beyond 60 MHz, it provides a means to simulate the operation of the crystal in an active network. Problems with frequency range, load capacitance correlation and fixtures prevent the use at frequencies much beyond the 60 Mhz limit.

4.2. Passive techniques

Passive measurement techniques utilizing the *PI* networks or other fixtures have become widely acacepted in industry. Establishment of the IEC 444 (Ref. [7]) and EIA 512 (Ref. [6]) and their various extensions have enabled the producer and user of crystal units a much better measurement of the crystal device both in production final test and the device user's incoming inspection.

4.3. Test fixtures

The most widely accepted test fixture for measurement is the *PI* network (Fig. 1). A number of configurations are possible, the most widely accepted is the IEC 444 PI network. The use of computer calibration of these devices has improved the accuracy of

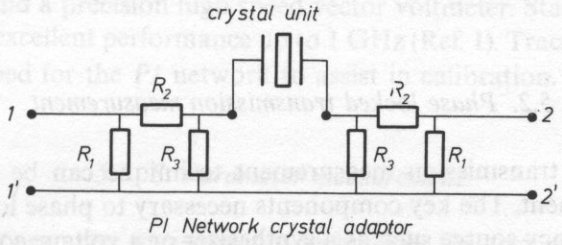

FIG. 1. *PI* Network

the network and reduced the precision requirement of the original IEC network (Ref. [1], [9], [12]).

Other networks hold some promise. The *T* network has some advantages for measurement of high frequency devices. Because of the possibility of coaxial construction, it may have future use as a standard crystal device adaptor.

Special *PI* networks are available that allow for insertion of load capacitances for measurement and final adjustment. These networks give the measurement system the capability to control whether the load capacitance is active by switching the load capacitance on or off by remote control (Fig. 2). This offers the potential for automation of the use of load capacitance measurements.

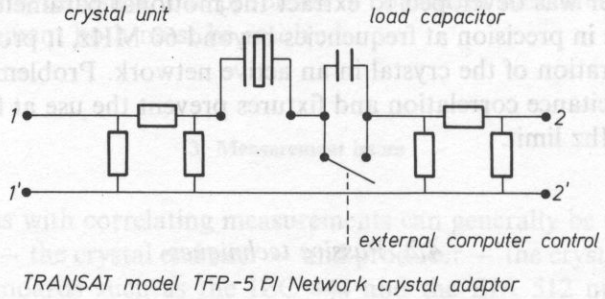

FIG. 2. Switching load CL *PI* Network

5. Current production equipment

5.1. *CI and oscillator based measurements*

These types of equipment typically suffer from poor measurement capability at higher frequencies. Some of this equipment offers high speed frequency tracking for fast frequency adjustment. Special fixtures are required for load capacitance measurements. The lack of a standard network makes it difficult to correlate measurements from site to site because of the strong dependance on electrical length of the circuitry contacting the crystal unit.

5.2. *Phase locked transmission measurement*

Phase locked transmission measurement technique can be implemented with a variety of equipment. The key components necessary to phase lock to a crystal are a sweepable frequency source such as a synthesizer or a voltage controlled oscillator, a vector voltmeter with a high speed phase measurement capability, and a phase lock module to couple the phaste data directly to the frequency sweep of the source. (Fig. 3)

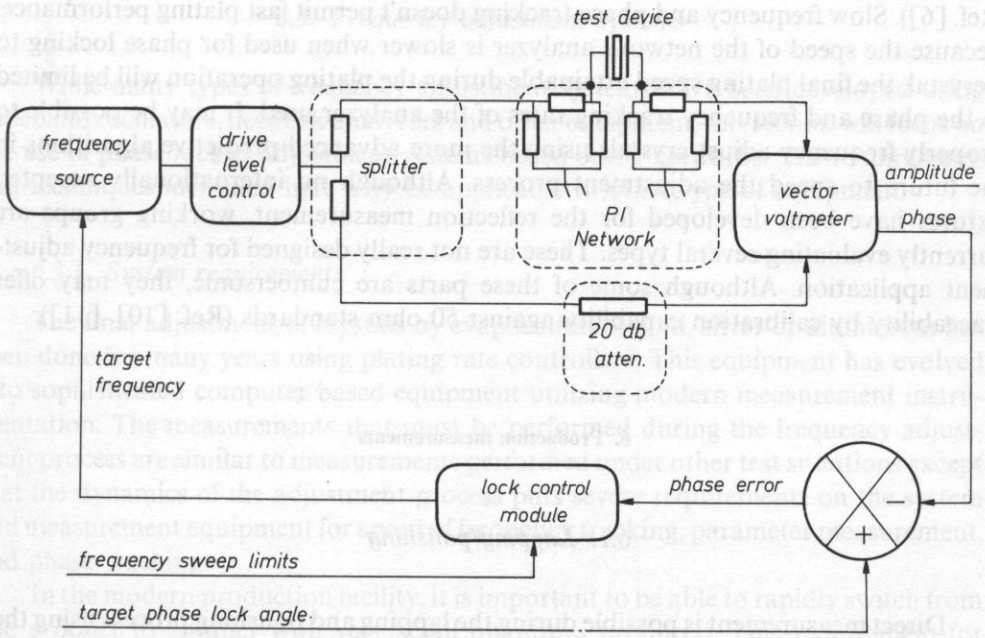

FIG. 3. Simplified phase locked transmission system

A matching *PI* network with well defined electrical parameters is typically used to couple the crystal to the measurement device.

The phase locked transmission measurement method has been widely accepted for measurement by international standard for accuracy. (Ref. [1], [2]). The addition of computer based error correction capability has increased the frequency range and accuracy of the *PI* network based transmission measurement up to nearly 1 GHz (Ref. [1], [12]).

High speed device tracking for good plating performance is possible with phase locked transmission measurement systems. The actual frequency tracking rates are dependant on the device the frequency sweep and phase lock equipment used. Practical adjustment systems with rates beyond 10 000 ppm per second are possible with an agile frequency source and a precision high speed vector voltmeter. Standard *PI* networks are available with excellent performance up to 1 GHz (Ref. 1). Traceable references are now being developed for the *PI* network to assist in calibration.

5.3. S. Parameter measurement

The use of *S* parameter measurement techniques for accurate measurement of crystals is supported in a number of publications. It is currently the basis of the EIA-512 crystal measurement standard and is well supported with measurement techniques

(Ref. [6]). Slow frequency and phase tracking doesn't permit fast plating performance. Because the speed of the network analyzer is slower when used for phase locking to a crystal, the final plating speed attainable during the plating operation will be limited to the phase and frequency tracking rates of the analyzer used. It may be possible to properly frequency adjust crystals using the more advanced predictive algorithms in the future to speed the adjustment process. Although no internationally accepted fixtures have been developed for the reflection measurement, working groups are currently evaluating several types. These are not really designed for frequency adjustment application. Although some of these parts are cumbersome, they may offer traceability by calibration capability against 50 ohm standards (Ref. [10], [11]).

6. Production measurements

6.1. Lapping/polishing

Direct measurement is possible during the lapping and polishing process using the automatic lap controllers (Ref. [21]). These units monitor the frequency of the lap load during lapping by utilizing a monitor electrode inserted in one of the lap plates. They operate by repetitively sweeping a frequency and observing the blanks as they pass above or beneath the electrode.

This instrument also offers the cappability of remote communication to a host computer. With this capability, lap load monitor information can be sent directly to a factory management system. Targeting information can be provided directly from the factory management system.

6.2. Etching

At present, control of temperature, time and acidity of the bath are used to try to control the etching process. This involves removing the blanks from the bath during the process to check the progress. A new type of instrument is now available for automatically monitoring the etching process without having to remove the blanks and individually test them. These instruments can use either a monitor blank or a blank from the etch load to monitor the progress of the etch. (Ref. [19], [22]).

The advantages for this instrument are immediately apparent. Close monitoring of the chemical and thermal characteristics of the etch bath can be relaxed. Remote communication capability to a factory management system is also possible to allow for external tracking of the etch process.

6.3. *Frequency adjustment systems*

While many types of frequency adjustment systems have been developed using wideband oscillators, network analyzers and other equipment, this section will focus on the use of phase locked adjustment systems based on *PI* networks. The requirements and techniques identified here may be applicable to other type of equipment.

6.3.1. *System requirements*

The final adjustment of crystals by evaporation of gold, silver or aluminium has been done for many years using plating rate controllers. This equipment has evolved into sophisticated computer based equipment utilizing modern measurement instrumentation. The measurements that must be performed during the frequency adjustment process are similar to measurements performed under other test situations except that the dynamics of the adjustment process puts severe requirements on the system and measurement equipment for speed of frequency tracking, parameter measurement, and phase tracking.

In the modern production facility, it is important to be able to rapidly switch from one product to another with very small quantities produced. This requirement for flexible manufacturing is directly reflected in the profitability of companies specializing in high precision, small lot size crystals. This forces the use of easily alterable systems that have the correct options and features quickly selectable.

6.3.2. *Targeting*

The process of targeting these systems must be rapid without requiring a great deal of calibration and tuning alignment. For the case of crystal units, the systems must be able to accept new frequency, load capacitance targets and process offsets directly. The key components in targeting are:

* target frequency, parameters
* process offset(s)
* specification limits
* load capacitance

6.3.3. *Load capacitance compensation*

The measurement and frequency adjustment of devices with load capacitances poses a difficult problem for production measurement equipment. The system must be able to measure devices in both the load and unloaded conditions without any operator intervention. In addition, the measurement system must allow for changing the physical load capacitance used if required.

A numerical measurement technique for evaluating the loaded impedance of a device have been described using a numerical compensation methods (Ref. [13]) and an actual equivalent reactance measurement technique (Ref. [3]). The equivalent reactance method provides a method of measurement without any physical load. This offers flexibility for inspection measurements. However, because the devices are measured far away from resonance on the reactance slope, it is not possible to maintain phase lock to track the device during fast frequency adjustment. This makes the direct equivalent reactance method ineffective for production plating measurements.

Methods for compensating the crystal unit for load capacitance are either too slow for plating or require plating to stop temporarily while a parameter measurement is performed. These methods suffer from the time penalty of having to stop the plating process, perform a parameter measurement and resume plating to a new offset target. This should not be a problem when small quantities are being produced. With larger production runs, the actual physical load capacitance should be inserted into the network.

Three types of compensation are:

FULL PHYSICAL LOAD CAPACITANCE COMPENSATION
FULL NUMERICAL LOAD CAPACITANCE COMPENSATION
PARTIAL NUMERICAL LOAD CAPACITANCE COMPENSATION

6.3.3.1. Full physical load capacitance compensation. This method is one where that actual load capacitor is installed in the network. This method offers the fastest throughput with the penalty of more difficult setup and calibration. It is best used for standard capacitance values or larger lot sizes.

6.3.3.2. Full numerical load capacitance compensation. Numerical load capacitance compensation method involves performing a parameter measurement to calculate. Numerical load capacitance compensation method can maintain phase lock and so can still track the device during the plating process. An actual parameter measurement is performed on the device and a frequency offset is applied to the target frequency using the following relationship:

$$F_T = F_s(1 + C_1/(C_0 + C_L))^{1/2} \tag{1}$$

where: F_T is the adjusted target frequency, F_s is the series resonance frequency of the crystal unit measured, C_L is the desired target load capacitance, C_1 is the measured motional capacitance of the crystal unit measured.

While this method is useful for overtone crystals and fundamental crystals with large C_L/C_0 ratio, errors can be significant when measuring fundamental crystals when the C_L/C_0 ratio gets small (Ref. [4]). The largest problem pertains to the measurement accuracy requirements on C_1 and C_0. Another problem in frequency adjustment systems is that the device could be measured a large distance from the target where measured C_1 and C_0 values might change with further plating. Either error present in the measurement of C_1 and C_0 can lead to poor selection of a final target. There are

techniques that can be used to overcome some of these limitations. The error caused by changes in the C_1 and C_0 parameters from subsequent plating can be reduced by offseting the initial frequency target closer to the actual final target. The errors present in the C_1 and C_0 measurements cannot be corrected.

The error present in the measurement can be modeled by assuming lossless crystals as:

$$E_1 = 25C_0/(n^2(C_0+C_L)) \tag{2}$$

where: E_1 is the error in ppm per % C_1 measurement error, n is the overtone number.

Let

$$K = C_L/C_0 \tag{3}$$

If KC_0 is substituted for C_L, then (2) becomes

$$E_1 = 25/n^2(1+K) \tag{4}$$

For this technique with fundamental crystals, as K gets small, the errors present in C_1 become more significant. For example, if a 1% C_1 measurement error is assumed, with a load capacitance of 20 pF and a C_0 of 4 pF, the targeting error would be 5 ppm. This limits the usefulness of this technique for fundamental crystals. Using the same parameters in the previous example, a third overtone would only have a targeting error of $5/n^2$ or 0.6 ppm.

The use of this technique in plating systems with the phase locked transmission measurement capability is:

a) phase lock to the crystal unit

b) plate the crystal to the offset target frequency, F_{T1} where F_{T1} is the target frequency derived from F_L, the loaded frequency target and any offsets.

c) perform a parameter measurement on the crystal unit and derive F_{s1}, C_{11}, and C_{01}; the crystal parameters measured at F_{T1}. Also calculate PH_1, the series resonance phase angle for F_{S1}.

d) calculate a final target frequency F_{T2} by:

$$F_{T2} = F_L/(1+C_{11}/(C_{01}+C_L))^{1/2} \tag{5}$$

e) phase lock the crystal at PH_1 and finish plating the crystal unit to the new target F_{T2}.

6.3.3.3. Partial numerical load capacitance compensation. Another approach for load capacitance plating is to allow for partial load compensation of devices using auxiliary load capacitors (Ref. [14]). With this technique, a load capacitance is placed in series with the device to partially compensate for the desired load capacitance. The parameters of this equivalent load device are recorded and a new offset target is developed in a similar fashion to the case of numerical load capacitance compensation except the measurement and targeting are adjusted for the effect of partial load capacitance compensation present in the network.

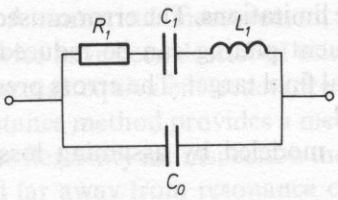

FIG. 4. Crystal equivalent circuit

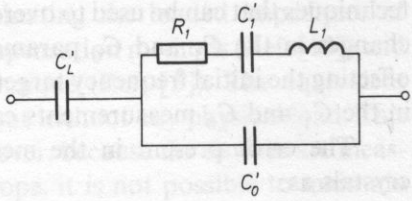

FIG. 5. Crystal equivalent circuit with load capacitor

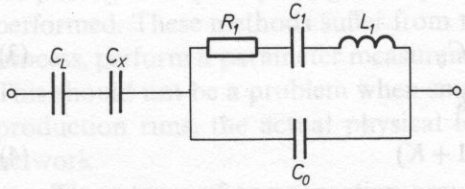

FIG. 6. Crystal equivalent circuit with load capacitor and partial load capacitance compensation

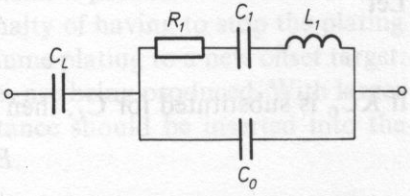

FIG. 7. Crystal equivalent circuit with partial load capacitor

In this approach, we develop a equivalent model (Figs. 6 and 7) of crystal incorporating C_X, where C_X is the partial load capacitance compensation using the following relationships:

$$C_1' = \{C_1(C_X+C_0)/(C_X+C_0+C_1)\} \tag{6}$$

$$C_0' = C_0C_X/(C_X+C_0) \tag{7}$$

$$C_L' = C_XC_L/(C_X-C_L) \tag{8}$$

and target frequency by:

$$F_X = F_L/(1+C_1'/(C_0'+C_L'))^{1/2} \tag{9}$$

where: F_X is the final target frequency for the crystal already partially compensated. Using this method, the plating would progress as:

a) phase lock to the crystal unit;

b) plate the crystal to the offset target frequency, F_{T1} where F_{T1} is the target frequency derived from F_L, the loaded frequency target and the offset;

c) perform a parameter measurement on the crystal unit for F_{s1}', C_{11}' and C_{01}'. Also calculate PH_1, the series resonance phase angle for F_{S1}';

d) calculate load capacitance C_L' of the crystal unit by (EQN 8);

e) calculate a final target frequency F_{T2} by:

$$F_{T2} = F_L/(1+C_{11}'/(C_{01}'+C_L'))^{1/2} \tag{10}$$

f) phase lock the crystal at PH_1 and finish plating the crystal unit to the new target F_{T2}.

6.3.4. *High frequency device plating*

High frequency or high resistance crystal units pose a special problem for frequency adjustment systems because zero phase frequency f_r (Fig. 8) is not located at series resonance. Under these conditions, the admittance circle is becomes elevated as susceptance w_sC_0 approaches the conductance $1/R_1$.

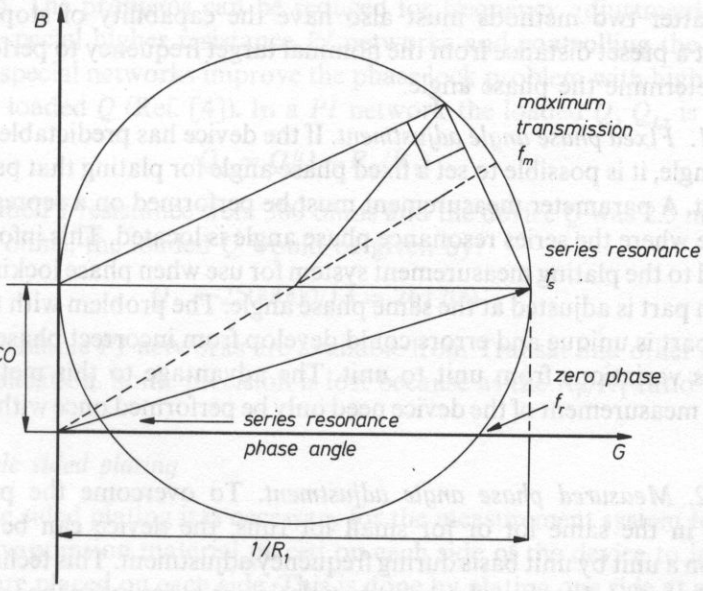

FIG. 8. Admittance circle representation

$$\begin{bmatrix} \Delta F_1 - F_2 \\ \Delta F_a \\ \Delta F_s \end{bmatrix} = \begin{bmatrix} \Delta F_1 - F_2 / \Delta F_1 & \Delta F_1 - F_2 / \Delta F_2 & \Delta F_1 - F_2 / \Delta F_s \\ \Delta F_a / \Delta F_1 & \Delta F_a / \Delta F_2 & \Delta F_a / \Delta F_s \\ \Delta F_s / \Delta F_1 & \Delta F_s / \Delta F_2 & \Delta F_s / \Delta F_s \end{bmatrix} \times \begin{bmatrix} F_1 \text{ plateback} \\ F_2 \text{ plateback} \\ F_s \text{ plateback} \end{bmatrix}$$

FIG. 9. Coupling matrix

To overcome this, the measurement system could phase lock to the crystal unit at series resonance f_S, at an angle above zero phase. Some devices will have no zero-phase series resonance frequency. This occurs when:

$$w_S C_0 R_1 \leqslant 1 \qquad (11)$$

In this case, the measurement system is not capable of being phase locked at the series resonance frequency. To successfully adjust the measurement system must evaluate the crystal unit parameters, phase lock to a phase angle larger than the f_S angle, and adjust the crystal for a series frequency f_S not directly measurable.

The following modes of operation should be available from the plating measurement system to adequately adjust these types of devices:

* FIXED PHASE ANGLE ADJUSTMENT
* MEASURED PHASE ANGLE ADJUSTMENT
* MEASURED PHASE ANGLE ADJUSTMENT, NUMERICALLY OFFSET

The latter two methods must also have the capability of stopping frequency adjustment a preset distance from the nominal target frequency to perform a measurement to determine the phase angle.

6.3.4.1. Fixed phase angle adjustment. If the device has predictable series resonance phase angle, it is possible to set a fixed phase angle for plating that particular type of crystal unit. A parameter measurement must be performed on a representative device to evaluate where the series resonance phase angle is located. This information is then transferred to the plating measurement system for use when phase locking to the crystal units. Each part is adjusted at the same phase angle. The problem with this approach is that each part is unique and errors could develop from incorrect phase settings due to parameters variations from unit to unit. The advantage to this method is that the parameter measurement of the device need only be performed once with no further time penalty.

6.3.4.2. Measured phase angle adjustment. To overcome the problem of unit variations in the same lot or for small lot runs, the device can be parametrically analyzed on a unit by unit basis during frequency adjustment. This technique allows for measurement of each unit and subsequent plating at series resonance of the individual device. The method avoids the problem of using a single phase angle as in the FIXED PHASE ANGLE ADJUSTMENT but suffers from a time penalty because a parameter measurement is done on each device.

6.3.4.3. Variable phase angle adjustment, numerically offset. Numerical offsets need to be added to the previous *S1* method when series resonance angle of the device is at a phase angle smaller than the minimum phase lock angle of the transmission measurement system. This typically arises with higher frequency units at frequencies beyond 150 MHz. In this situation the target frequency can be based on an projected offset from the current phase lock frequency. The frequency adjustment process is:

a) final or direct plate the crystal unit at an elevated phase lock angle to a frequency above the final target frequency, $F_0 = F_T + \text{offset}$.

b) make a parameter measurement of the device calculating the current series resonance of the device F_{S1}.

c) using the current phase lock frequency, F_0 actual (Note: This is below the

current series resonance frequency), offset the target frequency by:

$$F_T \text{ new} = F_0 \text{ actual} - (F_{S1} - F_T) \tag{12}$$

d) finish plating the unit to the new target.

6.3.5. High Q device plating

High Q devices pose difficult measurement problems during frequency adjustments two problems occur when planting high Q devices the first is the requirement for phase meter speed detecting the device to phase lock to it, the second the rate of the frequency sweep. The problems can be reduced for frequency adjustment measurements by using special higher resistance *PI* networks and controlling the frequency sweep rate. The special networks improve the phase lock problem with high Q devices by reducing the loaded Q (Ref. [4]). In a *PI* network the loaded Q, Q_L, is given by:

$$Q_L = Q/(1 + R_P/R_1) \tag{13}$$

For example, if the *PI* resistance were 300 ohms and the device Q was 2.5 million and resistance of 35 ohms, the loaded Q would be given by:

$$Q_L = 2500000/13 = 261200 \tag{14}$$

Commercially available *PI* networks are available from Transat and other sources to support this application. Some precision is lost because as the R_P/R_1 ratio gets large.

6.3.6. Double sided plating

With double sided plating it is necessary for the measurement system to monitor the amount of evaporation material placed on each side of the device to insure that equal amounts are placed on each side. This is done by plating one side at a time and tracking the change in frequency and switching to the other side when the plating process is fifty percent completed.

6.3.7. Direct plating

Direct or one shot plating of crystals is well described in (Ref. [9]). Direct plating requires the measurement system to attempt to monitor the device as the electrodes are initially placed on the device. To do this the system must wait for the device to "activate", then lock to the crystal unit as soon as is possible. Practically, this can be done by letting the measurement device monitor a frequency a predetermined distance above the target while plating the part. As the device "passes" this location, the system must immediately phase lock to the device and track it until plating is completed. This requires logic in the system to determine (1) when to stop waiting for the device, and (2) when to start frequency tracking. The speed of the phase lock system must be sufficient to capture the device as it passes the monitor frequency setting.

6.3.8. *Network communication*

Network communication capability with a host computer system has become a requirement in many installations where the plating system must retrieve configuration, targeting and model information from a factory management system. Also, lot tracking and process control parameters are often direct to and from the management system rather than being located on the frequency adjustment system.

6.3.9. *Configuration files*

The use of configuration or model files for the frequency adjustment systems is mandatory to allow rapid reconfiguration of the adjustment systems without recalibration.

6.4. *Monolithic two-pole filter measurement and adjustment*

A number of methods have been developed for adjusting monolithic twopole filters. One method is based on adjusting the short circuit amplitude versus frequency response. Another is based on oscillator measurements monitoring two resonator frequencies and bandwidth and adjust all three. A third method utilizes two short circuit and two open circuit measurements for deriving the filter frequencies (Ref. [17]). Each of these methods suffers when attempting to monitor and adjust higher frequency devices beyond about 50 MHz.

6.4.1. *Measurement techniques*

For high frequency twopole adjustment, the problem is divided into two areas, measurement and masking. Although effective measurement techniques have been developed for measuring the devices, they do not have the speed required for production frequency adjustment systems (Ref. [10], [18]).

Special networks and instrumentation must be utilized to monitor the filter under the dynamic adjustment situations. Commercially available networks have been developed for measuring and adjusting monolithic two-pole filters up to 100 MHz and beyond. These networks are available in commercial automatic frequency adjustment equipment (Ref. [20]). This network enables the individual monitoring of two resonator frequencies as well as bandwidth.

6.4.2. *Mask problem*

As the geometries of the high frequency filter get smaller, the mask positioning and alignment become critical. So much so that it becomes impractical to assume that the mask effects are consistent from one device to another or even on the same device as it is

adjusted. This places a severe strain on the frequency adjustment system attempting to adjust the device.

A solution to this problem is dynamic modeling of the crystal and the mask effects during the frequency adjustment process. To accomplish this, the measurement and adjustment system must rapidly and repeatedly characterize the device during the adjustment process.

6.4.3. Coupling matrix

If the system can rapidly measure the four characteristic frequencies of the device, a model of the mask effect can be developed called the coupling matrix (Fig. 10). In matrix form:

$$T = CPB \tag{15}$$

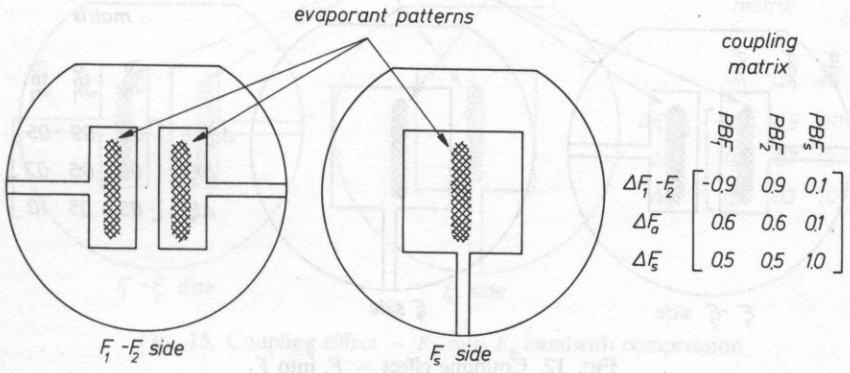

FIG. 10. Nominal two-pole adjustment pattern

where: T is the change in target error, C is the coupling matrix, PB is the plating amount on F_1, F_2 or F_S.

The coupling matrix defines the effect of plating F_1, F_2 or bandwidth, F_S on the target parameters; F_1, F_2 Symetry, F_a and F_s. The amount of plateback to use on a given resonator can be derived by:

$$C^{-1}T = PB \tag{16}$$

where: C^{-1} is the inverse of the coupling matrix.

Figures 11 through 18 show how the coupling matrix might shift for a given type of mask alignement.

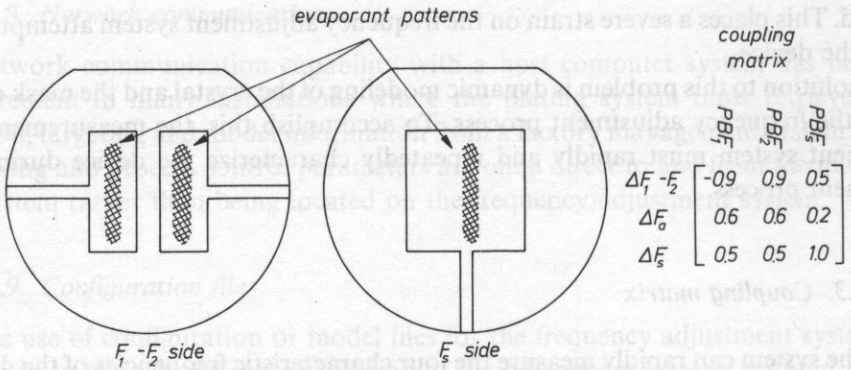

FIG. 11. Coupling effect — F_s into F_2

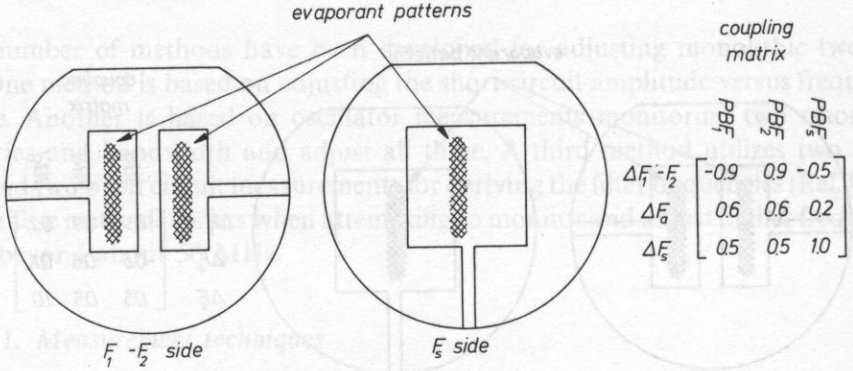

FIG. 12. Coupling effect — F_s into F_1

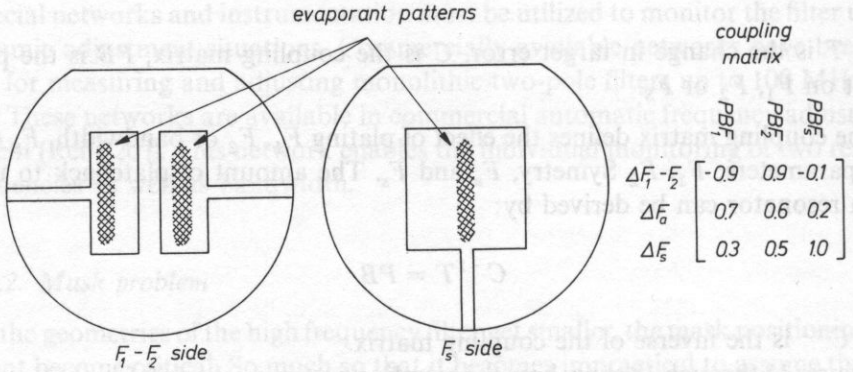

FIG. 13. Coupling effect — F_1 *into* F_a bandwith compression

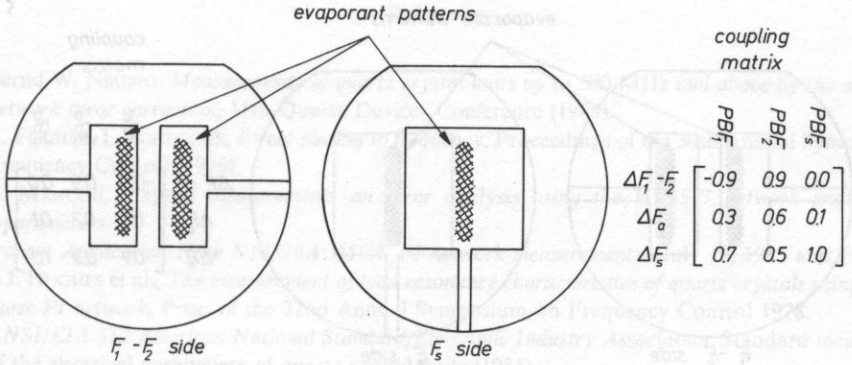

FIG. 14. Coupling effect — F_1 into F_s

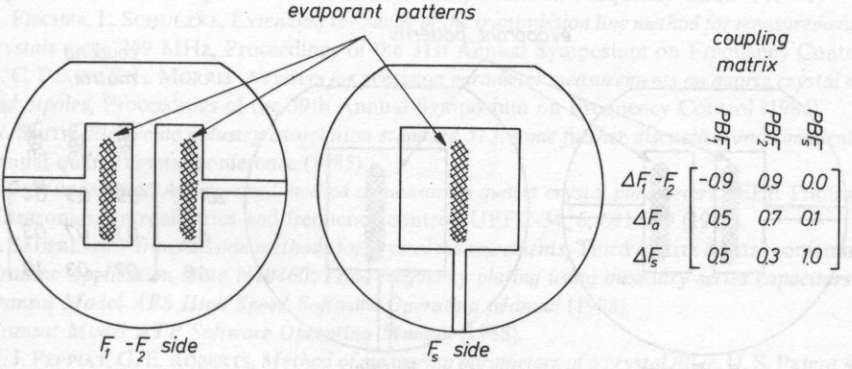

FIG. 15. Coupling efffect — F_2 into F_a bandwith compression

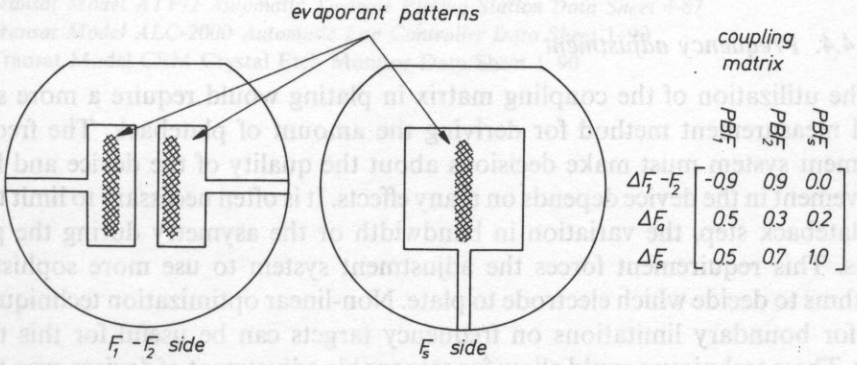

FIG. 16. Coupling effect — F_2 *into* F_s bandwith expansion

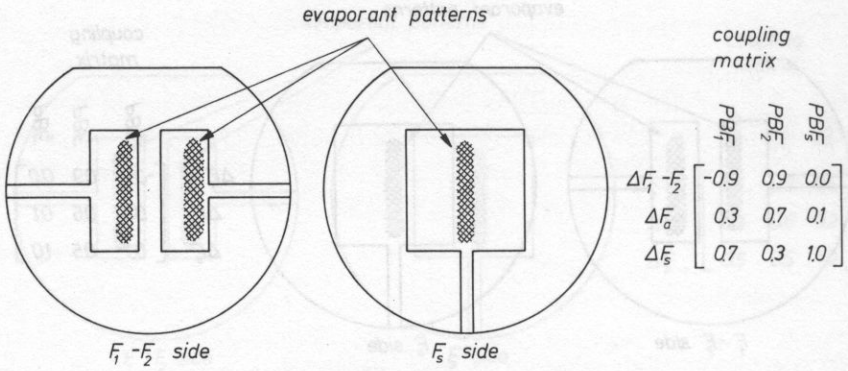

FIG. 17. Coupling effect — F_1, F_2 shifted

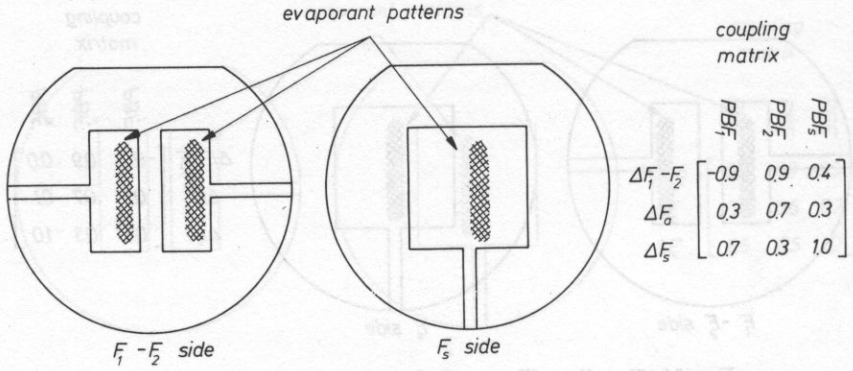

FIG. 18. Coupling effect — F_1, F_2, F_S *shifted mask shift effect*

6.4.4. Frequency adjustment

The utilization of the coupling matrix in plating would require a more sophisticated measurement method for deriving the amount of plateback. The frequency adjustment system must make decisions about the quality of the device and further improvement in the device depends on many effects. It is often necessary to limit the size of a plateback step, the variation in bandwidth or the asymetry during the plating process. This requirement forces the adjustment system to use more sophisticated algorithms to decide which electrode to plate. Non-linear optimization techniques that allow for boundary limitations on frequency targets can be useful for this type of system. These techniques could allow for reasonable adjustment of devices even though misalignment occurs.

References

[1] Bernd W. NEUBIG, *Measurements of quartz crystal units up to* 500 MHz *and above by the use of a PI network error correction*, 11th Quartz Devices Conference (1989).

[2] R. FISCHER, L. SCHULZKE, *Direct plating to frequency*, Proceedings of the 30th Annual Symposium on Frequency Control (1976).

[3] B. MANCINI, *Crystal measurement: an error analysis using the* HP3577 *network analyzer with S-parameters*

[4] *Transat Application Note N10379A: MCT PI network measurements*, (July 18, 1983 and Fe., 1989).

[5] S. J. HUGHES et al., *The measurement of load resonance characteristics of quartz crystals using the zero phase PI network*, Proc. of the 32nd Annual Symposium on Frequency Control 1978.

[6] *ANSI/EIA 512 American National Standard/Electronic Industry Association*, Standard measurement of the electrical parameters of quartz crystal units (1985).

[7] International Electrotechnical Commission, *Basic method for the measurement of resonance frequency and equivalent series resistance of quartz units by zero phase technique in a PI network*, Publication 444 1st Ed., (1973).

[8] W. J. HORTON et al., *Comparison of methods for measurement of quartz crystal resonators with load capacitance*, Proceedings of the 35th Annual Symposium on Frequency Control (1981).

[9] R. FISCHER, L. SCHULZKE, *Extending the range of the transmission line method for measurement of quartz crystals up to* 259 MHz, Proceedings of the 31st Annual Symposium on Frequency Control (1977).

[10] R. C. PEACH, S. E. MORRIS' *A system for precision parameter measurements on quartz crystal resonators and bipoles*, Proceedings of the 39th Annual Symposium on Frequency Control (1985).

[11] W. SMITH, *Electronic industry association standard 512: some further discussion and comment*, Seventh annual quartz crystal conference (1985).

[12] R. J. WILLIAMSON, *An improved method of measuring quartz crystal parameters.* IEEE Transactions on Ultrasonics, Ferroelectrics and frequency control, UFFC-34, 6, 681-689 (1987).

[13] F. SAUERLAND, *Transmission methods for crystal measurements*, Third quartz crystal conference (1981).

[14] *Transat Application Note N10460: Load frequency plating using auxiliary series capacitors* (1984).

[15] *Transat Model APS High Speed Software Operating Manual* (1988).

[16] *Transat Model ATP Software Operating Manual* (1988).

[17] H. J. PEPPIAT, G. E. ROBERTS, *Method of measuring parameters of a crystal filter*, U. S. Patent 4, 093, 914 (June 1978).

[18] R. KINSMAN, R. USKALI, *Equivalent circuit characterization of two-pole monolithic filters using S-parameters*, 8th quartz crystal conference (1986).

[19] F. SAUERLAND, *Automatic frequency control in chemical etching of quartz crystal blanks*, Paper to be presented Proceedings of the 44th Annual Symposium on Frequency Control 1990

[20] *Transat Model ATP-2 Automatic Twopole Plating Station Data Sheet 4-87*

[21] *Transat Model ALC-2000 Automatic Lap Controller Data Sheet* 1–90

[22] Transat Model CEM Crystal Etch Monitor Data Sheet 1–90

ARCHIVES OF ACOUSTICS
16, 1, 73-76(1991)

SPECTRAL THEORY OF NATURAL UNIDIRECTIONALITY OF SPUDT FOR BG WAVES

E. DANICKI

Institute of Fundamental Technological Research of the Polish Academy of Sciences
(00-049 Warszawa ul. Świętokrzyska 21)

A single-phase unidirectional interdigital transducer SPUDT is modelled by a system of periodic metal strips on a piezoelectric halfspace carrying Bleustein-Gulyaev BG wave. The dispersion relation for BG surface wave, as well as some relations between forward and backward waves in the system are discussed. Natural unidirectionality is explained in this way.

1. Introduction

In [1] a natural unidirectionality of a single-phase interdigital transducer was reported. The effect occurs for certain piezoelectric substrates only and only in the stop-band due to the cooperative mechanism of Bragg reflection of surface wave caused by electric, and mechanical interactions between the periodic strips of the transducer and the propagating surface acoustic wave.

In [2] a theory of propagation of BG wave was presented for quite general case of piezoelectric substrates, the strip property, and for frequencies including the stop-band. In fact, the theory includes the cases of both natural, and artificial [3] unidirectionality for BG waves, if only we put $\cos(\eta + 2\vartheta) = 0$ in relation (22) of [2]. The theory can be easily generalized to the case of Rayleigh surface acoustic wave (SAW).

2. Dispersion relation

Let's consider periodic metal strips arranged along x-axis on the surface of piezoelectric halfspace. The strip period is $\Lambda = 2\pi/K$, the strips have rectangular cross-section: thickness H and width $\Lambda/2$ and they are perfectly conducting, in this circumstance we have $\eta = 0$ [2]. The strip material is characterized by ϱ and μ, and the mechanical interaction between strips and BG wave is characterized by a parameter $g = (\varrho\omega^2 + k_s^2\mu)\, H/\pi$ [6], where $k_s = \omega/v_s$ approximates the wave vector of the wave, ω is its frequency.

The piezoelectric halfspace is characterized by the above mentioned cut-off wavenumber of bulk waves k_s and two dimensionless small parameters α and β, determining BG wave-numbers for metallized and free substrate surface, $k_s/\sqrt{(1-\alpha^2)}$ and $k_s/\sqrt{(1-\beta^2)}$, correspondingly. An effective surface permittivity of the substrate is $\varepsilon_0\varepsilon$, and effective surface stiffeness is γ [2]. For free substrate surface the BG wave is coupled to the electric potential with complex amplitude φ and particle displacement with the amplitude u on the substrate surface, the relation between them is $\varphi/u = [\gamma(\alpha-\beta)/\varepsilon_0\varepsilon]^{1/2}\exp(j\vartheta)$. In the case of natural unidirectionality we should have $\vartheta = \pi/4$ [4], and this value will be assumed in what follows.

In the stopband, the dependence of wave-number of a wave propagating under the short-circuited strips can be approximated as follows [2]

$$r_0 = \frac{K}{2} + \frac{1}{v_s}\sqrt{(\omega-\omega_1')(\omega-\omega_s)} \tag{1}$$

and similarly for free strips, where the wavenumber is r_∞ and stop-band frequencies ω_1 and ω_2 instead od ω_1' and ω_3 above.

In the case considered in [2], where we put $\cos(\eta+2\vartheta) = \pm 1$, it was $\omega_1' = \omega_1$, but this does not take place here, where we have $\cos(\eta+2\vartheta) = 0$. The stop-band frequencies ω_1', ω_s are determined by two solutions of the following equation [2]

$$S^2 - \frac{3\alpha+\beta}{4}SR + \alpha(\alpha+\beta)R^2 - |g|^2\gamma^2 = 0 \tag{2}$$

where $R = K/2$ and $S = \sqrt{(R^2-k_s^2)}$, $k_s = \omega/v_s$ (ω_1 and ω_2 are determined by (2) with replacement $\alpha \leftrightarrow \beta$).

The dependence of the stop-band frequencies is sketched in Fig. 1. As we see, the stop-bands are overlapping if $g \neq 0$, but they have not common stop-band frequency.

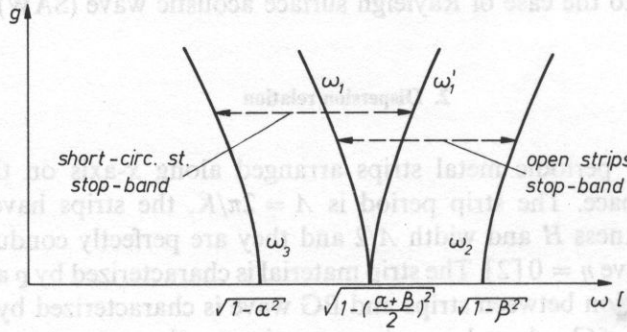

FIG. 1

3. Field components

As known, in periodic system two fundamental components of wave exist, namely forward, and backward propagating waves with wave-numbers r_0 and r_0-K, correspondingly ($Re(r_0) > 0$ here). On the substrate surface, the amplitudes of particle displacements of these two waves are u_0 and u_{-1}, where

$$u_{-1}/u_0 = \Gamma(r_0) = \frac{S_0 - R_0(\alpha+\beta)/4 + g^*\gamma\exp(-j2\vartheta)}{S_1 - R_1(\alpha+\beta)/4 + g\gamma\exp(j2\vartheta)}\exp(j2\vartheta) \tag{3}$$

where $R_0 = |r_0|$, $R_1 = |r_0-K|$, $S_n = \sqrt{(R_n^2 - k_s^2)}$, $n = 0, 1$.

It can be easily shown, that for certain frequency f_0 in the stopband, where $S_n - R_n(\alpha+\beta)/4$ is imaginary valued quantity, $\Gamma(r_0) = 0$. Similar relation for $\Gamma(-r_0)$ exists for surface wave propagating in opposite direction, where forward and backward waves have wave numbers $-r_0$ and $-r_0+K$. In this case the angle ϑ should be replaced by $-\vartheta$ and g by g^*. As the consequence, $\Gamma(-r_0) = \infty$ at frequency f_0.

The above relations are very important for explanation of the natural unidirectionality. Firstly note, that surface wave Poynting vector magnitude Π is determined by the magnitude of u as follows

$$\Pi = \frac{\omega|u|^2}{4(r/k_s)^2\gamma\sqrt{(r^2-k_s^2)}} \tag{4}$$

where r is the wavenumber and u is the amplitude of one of the above mentioned partial waves (the Poynting vector and the wave-vector have the same direction in the considered case).

It follows from the above, that the surface wave cannot propagate in $-x$ direction at frequency f_0, because there are not energy transported by partial waves with wave-numbers r_0-K and $-r_0$, simply because their amplitudes are zero at f_0.

Consider now a system, where all strips are grounded except one, which is supplied from an external voltage source. There is surface wave generated under this strip (see [5] for details of similar considerations for Rayleigh waves). The conclusion from the above reasoning is, that at the frequency f_0 the strip generate surface waves only in one direction (there are two partial waves generated, having wave-numbers r_0 and $K-r_0$). For frequencies different from f_0, but still in the stopband, surface waves are generated in both directions, however the generation in one direction still prevails ($|\Gamma(r_0)| < 1$ in stopband).

Outside the stopband, where $S_n - R_n(\alpha+\beta)/4$ has real value while $g\gamma\exp(-j2\vartheta)$ is imaginary valued, the symmetry of both directions are fully restored and the surface wave powers generated under the supplied strip in both directions are equal.

4. Some remarks on strip admittance

A surface wave propagating under the grounded strip induces electric current I flowing to it. The relation can be obtained

$$I \sim \sqrt{[\varepsilon_0 \varepsilon(\alpha-\beta)/\gamma]}\,(su_0 e^{j\vartheta} + (1-s)u_{-1}e^{-j\vartheta}) \tag{5}$$

where $s = r_0/K$. It is seen, that in the stopband where $s \approx 1/2$, both backward and forward waves contribute equally to the current, if only $|u_0| = |u_{-1}|$, so that there is not any further mechanism of unidirectionality.

Analogous theory as that presented in [5] for Rayleigh waves can be developed for the case considered. The main result is that the strip admittance Y is

$$Y \sim \frac{\alpha\omega + (\alpha^2-\beta^2)/2}{[(\omega-\omega_1')(\omega-\omega_3)]^{1/2}} \tag{6}$$

as compared to $Y \sim \sqrt{[(\omega-\omega_1')/(\omega-\omega_3)]}$ for bidirectional case [5].

The admittance of interdigital transducer having finite number of electrodes is similar to the above-mentioned strip admittance in the infinite system of periodic strips [5], but it is smoothed so that the transducer admittance does not exhibit singularites like pole or zero. The similarity of function (6) and the admittance of SPUDT presented in [4] may be noticed.

5. Conclusions

From the above spectral theory we may conclude that

– for cases where $\vartheta \neq \pi/4$, we can obtain unidirectionality if we apply complex value of g, by using the strips with trapezium cross-section [2], or split strips made from different metals [3],

– the natural unidirectionality takes place only in stopband, but strict unidirectionality takes place only for one frequency,

– the thickness of the strips does not effect the unidirectionality, however note that the average loading of the substrate by the strips can change ϑ [2].

References

[1] P. V. WRIGHT, *The natural single-phase unidirectional transducer, a new low-loss SAW transducer*, Ultras. Symp. Proc., 59–63 (1985).

[2] E. DANICKI, *Propagation of transverse surface acoustic waves in rotated Y-cut quartz substrates under heavy periodic metal electrodes*, IEEE Trans., SU–30, 5, 304–312 (1983).

[3] C. S. HARTMANN, P. V. WRIGHT, R. J. KANSY, E. M. GARBER, *An analysis of SAW interdigital transducer with internal reflections and the application to the design of single-phase unidirectional transducers*. Ultras. Symp. Proc., 40–45, (1982).

[4] T. THORVALDSSON, *Analysis of the natural single-phase unidirectional SAW transducer*, Ultras. Symp. (1989).

[5] E. DANICKI, *Unified theory of interdigital transducers an SAW reflectors*, J. Tech. Phys., **21**, 3, 387–403 (1980).

[6] E. DANICKI, *Perturbation theory of surface acoustic wave reflection from a periodic structure with arbitrary angle of incidence*, Arch. Mech., **36**, 5–6, 623–638 (1984).

ARCHIVES OF ACOUSTICS
16, 1, 79-90(1991)

INFLUENCE OF A BIASING STRESS ON THE SAW VELOCITY ON PIEZOELECTRIC SUBSTRATE

D. GAFKA

Institute of Fundamental Technological Research of the Polish Academy of Sciences
(00-049 Warszawa ul. Świętokrzyska 21)

The nonlinear differential equations and boundary conditions in small-field variables, for small fields superposed on large static biasing states, are obtained from general invariant nonlinear electroelastic equations. The influence on Surface Acoustic Wave (SAW) velocity of prestress (six independent tensor coefficients) is analyzed. Biasing stress tensor is involved directly into equations of motion, and the linearization about the static state is done. Change of mass density as well as the effective elastic constants of the piezoelectric substrate as a consequence of prestress is taken into account. Numerical results, given SAW velocity on prestressed substrate for different direction of stress and wave propagation are obtained for lithium niobate.

Developed theory and numerical program may be useful for analyzing and designing SAW sensors of temperature, pressure, acceleration and stress.

1. Introduction

In recent years, a number of workers [3, 5, 6, 7,9–12, 15, 17, 20, 21] have analysed and measured the change in acoustic surface wave (SAW) velocity due to applied static biasing stresses. The problem is interesting from three points of view. First, this effect can be easily used in SAW sensors of pressure, acceleration, force, temperature, gas existence and others [6, 12, 15, 16, 17]. Second, the main sources of frequency instabilities of SAW oscillators and other devices are temperature and forces effects [6, 16, 20]. Therefore it can be useful to describe stress sensitivity of SAW velocity. Third, the stress or strain may be utilized to control the performance of SAW devices for example selectivity of filters [6, 9] or temperature compensation of the devices.

In this paper a system of nonlinear electroelastic equations for small fields superposed on a bias [1, 2, 3, 13, 18, 21] is applied to the determination of the velocity of SAW in prestressed piezoelectric substrate. The influence of the biasing stress appears in the boundary conditions as well as the differential equations. The equations in the paper are written in the reference frame, connected with the material coordinates to make the boundary conditions easy to formulate, so the stress tensor is the Piola-Kirchhoff

tensor [13, 18]. Although the electric, electroelastic and elastic nonlinearities are included in the basic equations, only the elastic nonlinearities are included in the calculation, because the rest of coefficients and higher order constants can be negligible and have the second order meaning in the considered problem [13, 20].

Nonlinear system of equations is linearized involving decomposition of the stress and other field quantities into two parts, static biasing one, and dynamic connected with SAW. After that the well-known procedure is used to obtain final results and computer algorithm [19]. Numerical results for Y cut lithium niobate are presented using the published values of the second and third order elastic, piezoelectric and dielectric constants.

2. Nonlinear electroelastic equations

Velocity of SAW, having a harmonic form below

$$e^{-jbX_2} \cdot e^{j\omega(t-X_1/v)} \qquad (\mathrm{Im}\{b\} < 0) \tag{1}$$

on the surface of the piezoelectric halfspace is searched. The halfspace is under initial stress. The structure considered and used coordinate system is depicted in Fig. 1. The denotations are as follow: ω – angular frequency, v – wave velocity, b – decay constant of SAW, X_i – material coordinates.

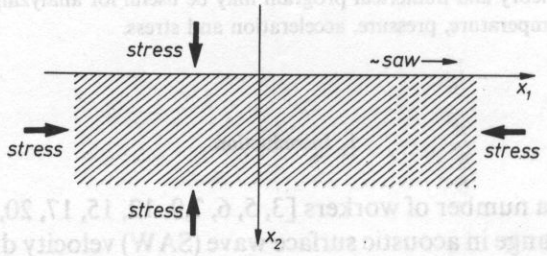

FIG. 1. Considered piezoelectric halfspace under biasing stress

The wave is assumed to propagate in the X_1 direction and decay in the X_2 direction and also SAW is a small amplitude wave, so it doesn't appreciably modify the bias. Propagation of SAW describes equation of motion with constitutive relations. In the case of biasing stress, which cannot be regarded as infinitesimally small, the general nonlinear equations should be taken into consideration as a starting point. They are written below in the reference frame with material coordinates (Lagrange's description), so stress tensor T is the Piola-Kirchhoff tensor [13, 18, 21]

$$\varrho u_j = \frac{\partial T_{ij}}{\partial X_i}, \tag{2}$$

$$T_{ij} = c_{ijkl}u_{k,l} + \gamma_{ijklmn}u_{k,l}u_{m,n} - e_{kij}E_k, \tag{3}$$

$$D_j = e_{jkl}u_{k,l} + \varepsilon_{ji}E_i. \tag{4}$$

In equation (2) ϱ is the mass density, and u is the displacement vector. It should be noted that ϱ is a function of stress $\varrho = \varrho(T)$ and this effect will be taken into account later. Constitutive relation (3) for a Piola-Kirchhoff stress tensor is composed of three parts. First component is linear elastic term with second order elastic tensor c_{ijkl} in the unprestressed state.The second is nonlinear elastic term with the third order effective (because in actual frame) elastic tensor γ_{ijklmn} and the third part is the piezoelectric term with the electroelastic tensor (linear only) e_{ijk}. The second constitutive relation (4) is usual for piezoelectrics and contains linear term of electroelasticity and electricity.

Effective elastic tensor γ_{ijklmn} can be obtained on the strength of thermodynamical considerations in the reference frame and has the form [13, 18, 21]

$$\gamma_{ijklmn} = c_{inkl}\delta_{jm} + 0.5c_{ijnl}\delta_{km} + 0.5c_{ijklmn}. \tag{5}$$

It depends on elastic material tensors of the second and third order given in tables of crystals [4, 13], δ is the identity tensor.

It should be noted that in equations (2)–(4) the nonlinearities between T and E, D and u, and also D and E are neglected. Dropt components have the second order meaning in comparison to elastic nonlinearity because of the character of piezoelectric phenomena [13, 20].

3. Boundary conditions

Presented system of equations (2)–(4) is valid for a piezoelectric space. For the case of SAW on the halfspace surface, to close mathematically the problem the boundary conditions must be added to the propagation equations. Because every field quantity is defined in the actual frame, they are valid even then if the boundary surface is deformed under biasing stress. It allows to formulate boundary conditions formaly the same as in the unprestressed case [8, 13, 14, 18, 19].

Mechanical boundary condition is vanishing of the SAW stress components on the surface

$$T_{2j} = 0 \quad \text{for} \quad X_2 = 0 \tag{6}$$

and electric boundary condition is vanishing of the SAW either electric strength

$$\mathrm{E} = 0 \quad \text{for } X_2 = 0 \tag{7}$$

or electric displacement

$$\Delta D_\perp = 0 \quad \text{for } X_2 = 0 \tag{8}$$

depending on that if the surface is shorted (metalized) or free (vacuum) respectively.

Involving (3), condition (6) can be written as

$$c_{2jkl}u_{k,l}+\gamma_{2jklmn}u_{k,l}u_{m,n}-e_{k2j}E_k=0 \tag{9}$$

what is now more complicated relation then in the unprestressed case (nonlinear).

Propagation equations (2)–(4) with boundary conditions (9) and (7) or (8) stand complete system of equations describing propagation of SAW on prestressed piezoelectric substrate.

4. Procedure of linearization

Formulated problem has been solved by a few authors using many different methods, for example making Talor expansion about the gradient of the static displacement [6, 13], using polynomial approximation or a multi-scale method [13]. The most known method is the perturbation method [7, 10, 11, 12, 13, 15], which gives the integral relation for the velocity variation. The comparison of obtained results to perturbation theory will be given at the and of the paper.

To find the linearized form of the equations (2)–(4) the decomposition of every quantity appearing in these equations has been done. It is assumed that displacements in the substrate can be separated into two parts: biasing static (or quasi-static) displacement denoted by u_i^s resulting from biasing stress T_{ij}^s and dynamic displacement connected with the SAW u_i^d

$$\begin{aligned} u_i &= u_i^s+u_i^d = x_i-X_i, \\ u_i^s &= X_i^s-X_i, \\ u_i^d &= x_i-X_i^s. \end{aligned} \tag{10}$$

Analogously stress is decomposed into two components

$$T_{ij}=T_{ij}^s+T_{ij}^d \tag{11}$$

and additionally the static part is assumed to be homogeneous

$$T_{ij}^s=\text{const}\,(X_i,\,t). \tag{12}$$

It should be written clearly now, that after biasing stress the mass density ϱ is changed into ϱ' because ϱ is a function of stress, so

$$\varrho'=\varrho\,(T_{ij}^s). \tag{13}$$

In piezoelectric substrate the initial electric field is conncted (because of nonzero tensor e) with the biasing stress. This effect gives some nonzero electric strength in the piezoelectric solid but doesn't perturb the SAW propagation, so it is neglected.

After substituting equations (10)–(13) into propagation equations (2)–(4) one can obtain separated relations for static biasing state and dynamic SAW propagation. The

equation of motion

$$\varrho' u_j^d = \frac{\partial T_{ij}^d}{\partial X_i} \tag{14}$$

contains only the dynamical quantities and new mass density ϱ'. The constitutive equations can be written as follows

$$T_{ij}^s + T_{ij}^d = c_{ijkl}(u_{k,l}^s + u_{k,l}^d) - e_{kij}E_k + \gamma_{ijklmn}(u_{k,l}^s + u_{k,l}^d)(u_{m,n}^s + u_{m,n}^d) \tag{15}$$

$$D_j = e_{jkl}u_{k,l}^a + \varepsilon_{ji}E_i. \tag{16}$$

(as it was mentioned above the static biasing part of electric quantities are neglected). Equation (15) can be separated into two independent equations, one for static state

$$T_{ij}^s = c_{ijkl}u_{k,l}^s + \gamma_{ijklmn}u_{k,l}^s u_{m,n}^s \tag{17}$$

and the other for SAW

$$T_{ij}^d = c_{ijkl}u_{k,l}^d + \gamma_{ijklmn}u_{kl}^d u_{m,n}^d + \gamma_{ijklmn}u_{k,l}^s u_{m,n}^d + \gamma_{ijklmn}u_{k,l}^d u_{m,n}^s - e_{kij}E_k. \tag{18}$$

Equation (17) can be made a little bit easier, but the biasing state must be assumed small, small enough to neglect the square term in (17). And because SAW is assumed to be a small amplitude wave the square term $u_{k,l}^d u_{m,n}^d$ in (18) can be neglected also. These two assumption are written together, as

$$|u_{k,l}^d| \ll |u_{k,l}^s| \ll 1. \tag{19}$$

Of course the mixed terms $u_{k,l}^s u_{m,n}^d$ must stay in (18). The linear elastic constitutive relation for the biasing state is obtained from (17)

$$T_{ij}^s = c_{ijkl}u_{k,l}^s \tag{20}$$

and for SAW such a constitutive relation is derived from (18)

$$T_{ij}^d = c_{ijkl}u_{k,l}^d + (\gamma_{ijklmn} + \gamma_{ijmnkl})u_{m,n}^s u_{k,l}^d - e_{kij}E_k. \tag{21}$$

The last equation can be written in a form

$$T_{ij}^d = c'_{ijkl}u_{k,l}^d - e_{kij}E_k \tag{22}$$

which is the same as in linear piezoelectricity [8, 14, 18, 19]. The only change in c'_{ijkl} instead of c_{ijkl}, where

$$c'_{ijkl} = c_{ijkl} + (\gamma_{ijklmn} + \gamma_{ijmnkl})u_{m,n}^s. \tag{23}$$

Due to stress the mass density changes its value also, what has been mentioned by ϱ' in (19). This is because of the change of the volume of the substrate, and though [1]

$$\varrho' = \varrho/(1 + u_{m,m}^s). \tag{24}$$

Appearing in (23) and (24) quantity $u_{m,n}^s$ can be derived inverting the matrix

equation (20)

$$u^s_{m,n} = c^{-1}_{stmn} T^s_{st}. \tag{25}$$

Concluding, making some additional assumptions such a linearized system of equations

$$\varrho' u^d_j = \frac{\partial T^d_{ij}}{\partial X_i} \tag{26}$$

$$T^d_{ij} = c'_{ijkl} u^d_{k,l} - e_{kij} E_k \tag{27}$$

$$D_j = e_{jkl} u^d_{k,l} + \varepsilon_{ji} E_i, \tag{28}$$

describing SAW propagation on prestressed piezoelectric substrate has been obtained. This system is formally identical to the system if the biasing stress doesn't exist. The coefficients are changed only: $c_{ijkl} \to c'_{ijkl}$ expressed in (23) with (25) $\varrho \to \varrho'$ expressed in (24), (25) and they are in fact functions of biasing stress.

The main advantage of presented reformulation is that one can use any well-known method or algorithm to solve the linear problem [8, 19] making small changes.

5. Numerical results

Taking ready made computer program for calculations SAW velocities on the unprestressed substrate surface, written by E. DANICKI [19], and changing the algorithm (e.g. involving third order elastic constants and biasing stress tensor values as new parameters) the author can calculate SAW velocities for different directions of propagation and different tensor of prestress.

The results for lithium niobate Y-cut are presented as an example. First material data of $LiNbO_3$ are rewritten basing on literature:

1/ mass density [13]

$\varrho = 4.7 \cdot 10^3$ kg/m^3

2/ second order coefficients (in Voigt's notation) [13]

– independent elastic constants [GPa]

$c_{11} = 203 \quad c_{12} = 53 \quad c_{13} = 75$

$c_{33} = 245 \quad c_{44} = 60 \quad c_{14} = 9$

– the other nonvanishing elastic constants

$c_{22} = c_{11} \quad c_{23} = c_{13} \quad c_{24} = -c_{14}$

$c_{55} = c_{44} \quad c_{56} = c_{14} \quad c_{66} = 0.5(c_{11} - c_{12})$

– independent piezoelectric constants [C/m^2]

$e_{15} = 3.7 \quad e_{22} = 2.5 \quad e_{31} = 0.2 \quad e_{33} = 1.3$

– the other nonvanishing piezoelectric constants

$e_{16} = -e_{22}$ $e_{21} = -e_{22}$ $e_{24} = e_{15}$ $e_{32} = e_{31}$

– nonzero electric constants [pF]

$\varepsilon_{11} = 389$ $\varepsilon_{33} = 257$ $\varepsilon_{22} = \varepsilon_{11}$

3/ third order elastic constants [GPa] (average) [4, 13]

$c_{111} = -512$ $c_{123} = 719$ $c_{144} = -37$ $c_{344} = -540$

$c_{112} = 454$ $c_{124} = 55$ $c_{155} = -599$ $c_{444} = -41$

$c_{113} = 728$ $c_{133} = -34$ $c_{222} = -478$

$c_{114} = -410$ $c_{134} = -1$ $c_{333} = -363$

$c_{223} = c_{113}$ $c_{233} = c_{133}$ $c_{234} = -c_{134}$

$c_{244} = c_{155}$ $c_{255} = c_{144}$ $c_{455} = -c_{444}$

$c_{355} = c_{344}$ $c_{356} = c_{134}$ $c_{466} = c_{124}$

$c_{122} = c_{111} + c_{112} - c_{222}$ $c_{256} = 0.5(c_{114} - c_{124})$

$c_{156} = 0.5(c_{114} + c_{124})$ $c_{266} = 0.5(2c_{111} - c_{112} - c_{222})$

$c_{224} = -c_{114} - 2c_{124}$ $c_{166} = 0.5(-2c_{111} - c_{112} + 3c_{222}$

$c_{366} = 0.5(c_{113} - c_{123})$ $c_{456} = 0.5(-c_{144} + c_{155})$

The SAW velocity V [km/s] depending on the biasing stress T [GPa] in the case of free surface V_∞ and metalized surface V_0 for three direction of putting initial stress: along wave propagation X_1, perpendicularly to cut surface X_2 and perpendicularly to wave propagation in the cut plane X_3 are presented in Fig. 2 for $LiNbO_3$ *Y*-cut *Z*-propagation ($X_1 = Z$).

Normalized velocity

$$(V(T) - V(T = 0))/(V(T = 0))$$

in relation to zero biasing state are presented for $LiNbO_3$ *YZ* ($X_1 = Z$) in Fig. 3, and for $LiNbO_3$ YX ($X_1 = X$) in Fig. 4. It doesn't matter if the surface is metalized or free, because the prestress doesn't change the electromechanical coupling coefficient $(V_\infty - V_0)/V_0$ of the piezoelectric substrate (with the 0.0003 precision).

In the next two figures, Fig. 5 and Fig. 6, relative change of decay of SAW propagating on the stressed surface versus stress

$$(t(T) - t(T = 0))/t(T = 0) = \Delta t/t(T)$$

is presented for the same cuts of $LiNbO_3$. The SAW velocity change are taken into account not only, but also the change of the length (the path of propagation) under biasing stress.

Additionally, the change of SAW velocity versus the angle of propagation in relation to *Z* axis of $LiNbO_3$ Y-cut under biasing stress $T = 2$GPa put in the X_1 direction are illustrated in Fig. 7. The picture presents SAW velocity for unprestressed substrate also.

The last Fig. 8 is made in the polar coordinates on the cut surface *Y* of $LiNbO_3$. Four SAW velocity curves for zero biasing stress $T = 2$GPa stress putting in the three different directions are presented.

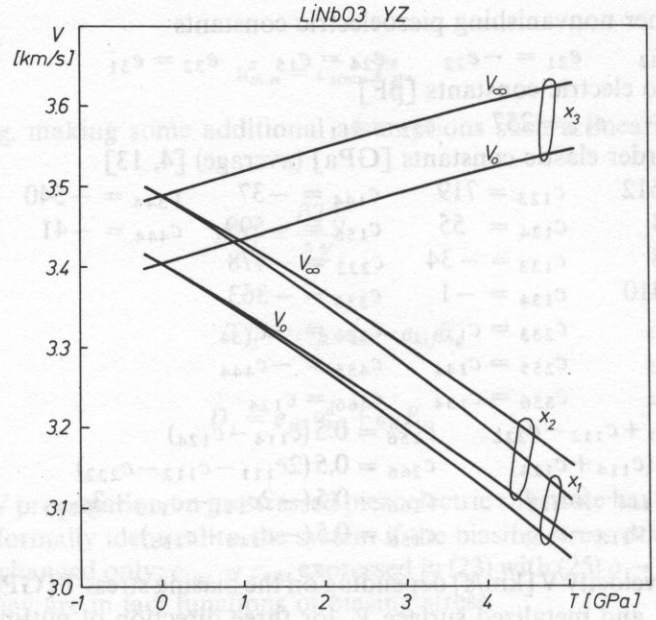

FIG. 2. SAW velocity as a function of prestress

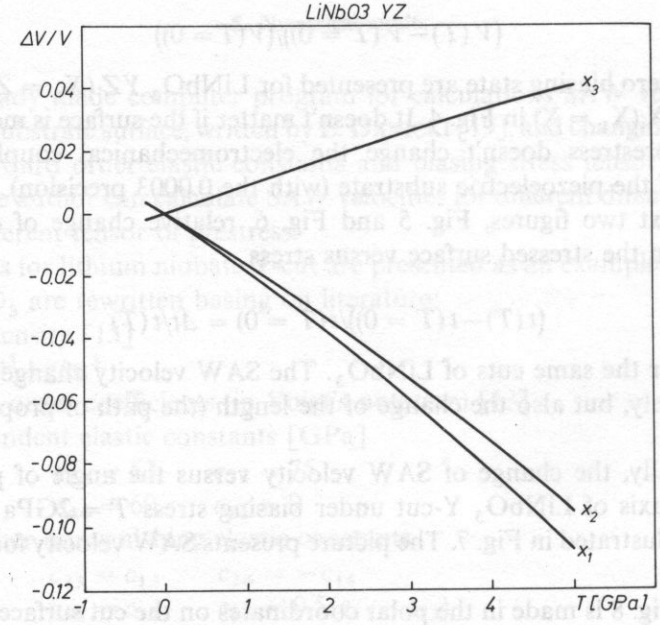

FIG. 3. Relative SAW velocity change versus static biasing stress

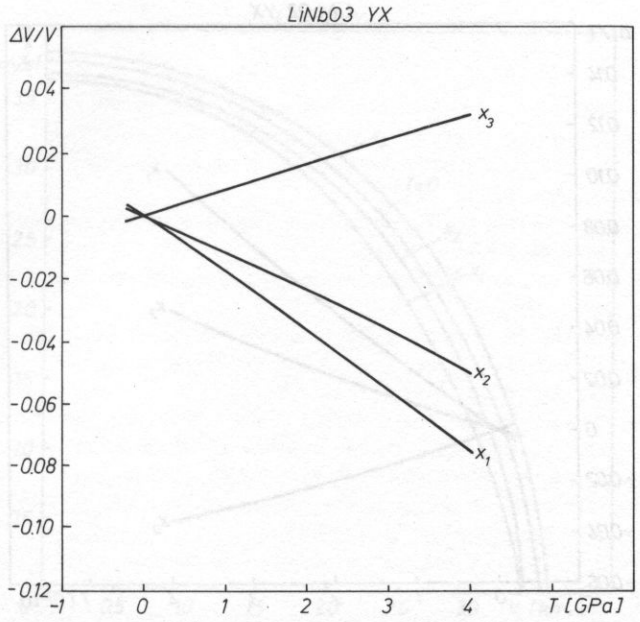

FIG. 4. Relative SAW velocity change versus static biasing stress

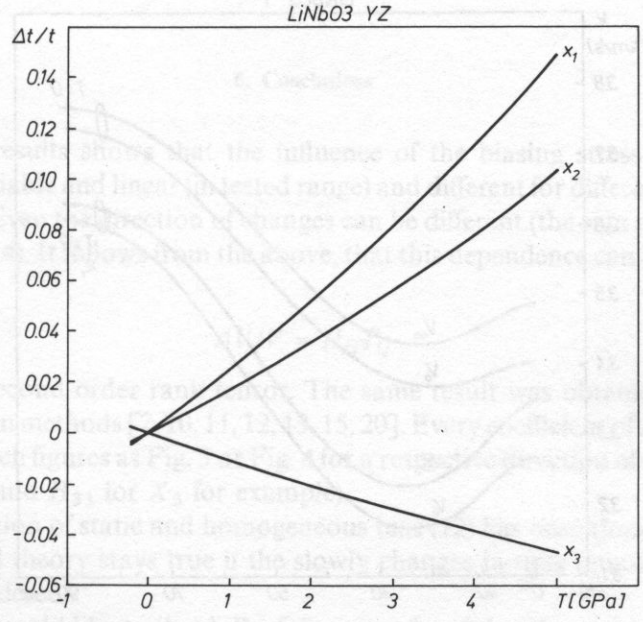

FIG. 5. Relative delay time of SAW as a function of prestress

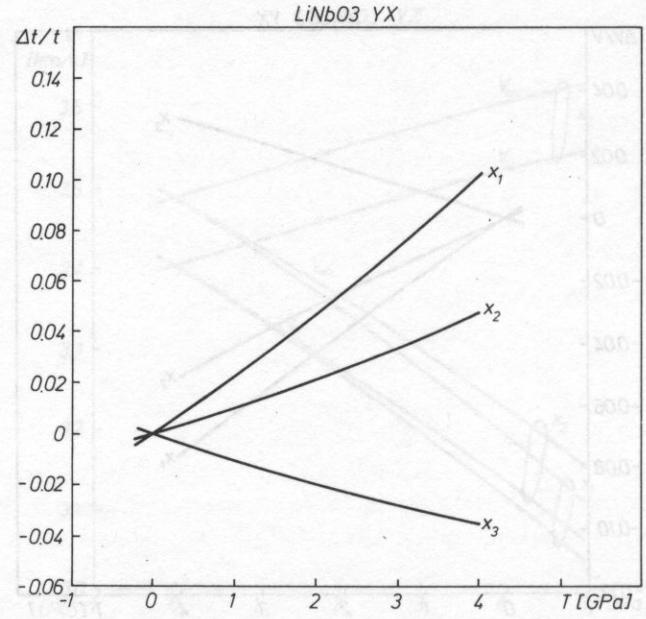

FIG. 6. Relative delay time of SAW as a function of prestress

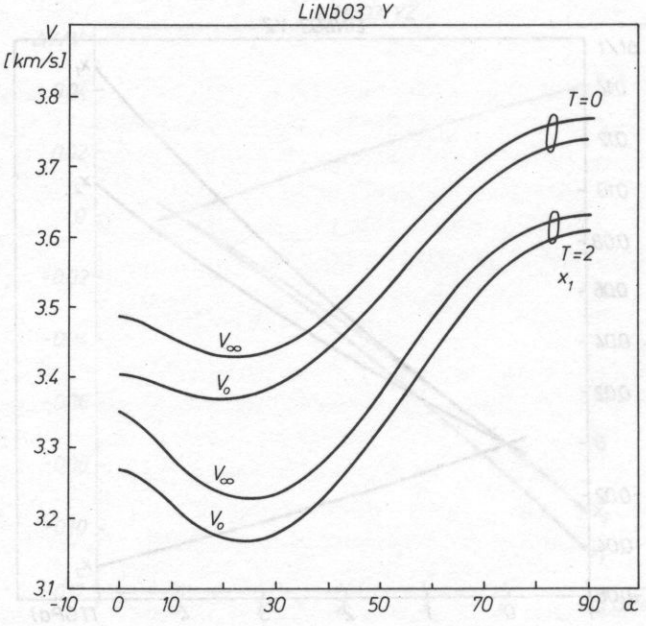

FIG. 7. SAW velocity as a function of angle of propagation for unprestressed and prestressed case

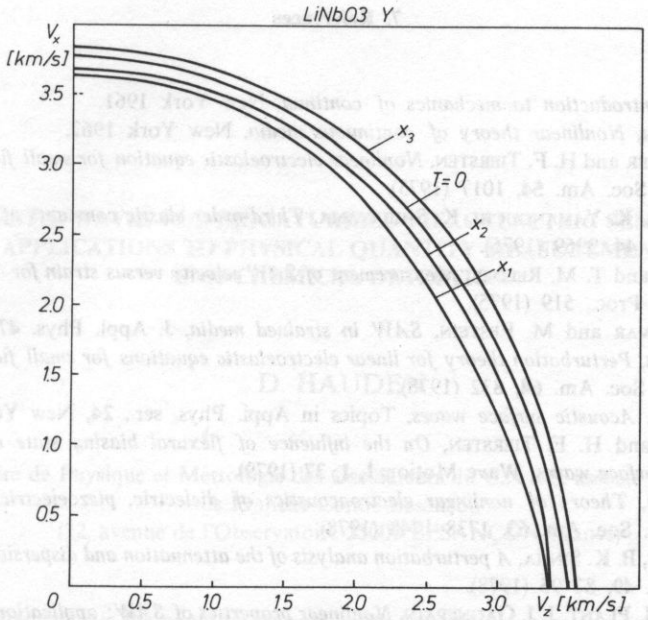

FIG. 8. SAW velocity as a function of angle of propagation for unprestressed and three directions of putting stress, in polar coordinates

6. Conclusions

Numerical results shows that the influence of the biasing stress on the SAW velocity is appreciable and linear (in tested range) and different for different direction of stress existence. Even the direction of changes can be different (the sign of curve slopes in Fig. 3 and Fig. 4). It follows from the above, that this dependence can be describe by the formula

$$\Delta V/V = H_{ij}T_{ij} \tag{29}$$

where H is the second order rank tensor. The same result was obtained by authors using perturbation methods [7, 10, 11, 12, 13, 15, 20]. Every coefficient of H_{ij} is the slope of the curve on such figures as Fig. 3 or Fig. 4 for a respective direction of stress (H_{11} for X_1, H_{22} for X_2 and H_{33} for X_3 for example).

The assumption of static and homogeneous bias (12) has been done in the paper, but the presented theory stays true if the slowly changes in time (quasistatics) of the prestress is considered.

The author would like to thank Prof. DANICKI for giving the computer program, which has been used, and for valuable remarks when doing this work.

7. References

[1] W. PRAGER, *Introduction to mechanics of continua*, New York 1961.

[2] A. C. ERINGEN, *Nonlinear theory of continuous media*, New York 1962.

[3] J. C. BAUMHAUER and H. F. TIERSTEN, *Nonlinear electroelastic equation for small fields superposed on a bias*, J. Ac. Soc. Am. **54**, 1017 (1973).

[4] Y. NAKAGAWA, K. YAMANOUCHI, K. SHIBAYAMA, *Third-order elastic constants of Lithium Niobate*, J. Appl. Phys. **44**, 3969 (1975).

[5] D. E. CULLEN and T. M. REEDER, *Measurement of SAW velocity versus strain for YX and ST quartz*, Ultras. Symp. Proc., 519 (1975).

[6] A. L. NALAMWAR and M. EPSTEIN, *SAW in strained media*, J. Appl. Phys. **47**, 43, (1976).

[7] H. F. TIERSTEN, *Perturbation theory for linear electroelastic equations for small fields superposed on a bias*, J. Ac. Soc. Am. **64**, 832 (1978).

[8] A. A. OLINER, *Acoustic surface waves*, Topics in Appl. Phys. ser., **24**, New York 1978.

[9] B. K. SINHA and H. F. TIERSTEN, *On the influence of flexural biasing state on the velocity of piezoelectric surface waves*, Wave Motion **1**, 1, 37 (1979).

[10] D. F. NELSON, *Theory of nonlinear electroacoustics of dielectric, piezoelectric, and pyroelectric crystals*, J. Ac. Soc. Am. **63**, 1738–1748 (1978).

[11] H. F. TIERSTEN, B. K. SINHA, *A perturbation analysis of the attenuation and dispersion of surface waves*, J. Appl. Phys. **49**, 87–95 (1978).

[12] D. HAUDEN, M. PLANT, J. J. GAGNEPAIN, *Nonlinear properties of SAW: applications to oscilators and sensors*, IEEE Trans. SU **28**, 5, 342–348, (1981).

[13] G. A. MAUGIN, *Nonlinear electromechanical effects and applications*, World Scientific 1985.

[14] D. P. MORGAN, *Surface-wave devices for signal processing*, Elsevier 1985.

[15] E. BIGLER, R. COQUEREL, D. HAUDEN, *Temperature and stress sensitivities of SAW quartz cuts*, Ultras. Symp. Proc., 285–288 (1987).

[16] R. L. FILLER, *The acceleration sensitivity of quartz crystal oscillators*: a review, IEEE Trans. UFFC **35**, 3, 297–305 (1988).

[17] H. F. TIERSTEN , D. V. SHICK, *An analysis of the normal acceleration sensitivity of contoured quartz resonators rigidly supported along the edges*, Ultras. Symp. Proc., 357–363 (1988).

[18] G. A. MAUGIN, *Continuum mechanics of electromagnetic solids*, North-Holland 1988.

[19] E. DANICKI, T. CZERWIŃSKA, *SAW parameters in piezoelectric crystals*, IFTR Reports 18/1988 (in Polish).

[20] E. BIGLER, G. THEOBALD, D. HAUDEN, *Stress-sensitivity mapping for SAW on quartz*, IEEE Trans. UFFC **36**, 1, 57–62 (1989).

[21] D. GAFKA, J. TANI, *Parametric constitutive equations for electroelastic crystals upon electrical or mechanical bias*, J. Appl. Phys. **70**, Dec. 1 (1991) (in press).

ARCHIVES OF ACOUSTICS
16, 1, 91-106(1991)

ELASTIC WAVES FOR MINIATURIZED PIEZOELECTRIC SENSORS: APPLICATIONS TO PHYSICAL QUANTITY MEASUREMENTS AND CHEMICAL DETECTION

D. HAUDEN

Laboratoire de Physique et Métrologie des Oscillateurs du C.N.R.S. associé à l'Université de Franche-Comté-Besançon
(32, avenue de l'Observatoire-25000 BESANÇON-France)

The frequency is the quantity measured with the best accuracy and time and length standards are defined with it. In the domain of the metrology closer of manufacturing applications (process control or instrumentation), sensors based on the frequency variation of oscillators, are potentially interesting because several reasons: high resolution, good sensitivity and digital signal by accounting.

This paper is dedicaced to an overview of oscillators used as sensor in which general principles and definitions are presented and illustrated with different devices built in SAW technologies (temperature, pressure, acceleration).

Different technological ways can be used to build the sensitive SAW sensor and chemical detector applications enable to describe the different possibilities as quartz or $LiNbO_3$ substrates or silicon substrate using Rayleigh waves or Lamb modes.

1. Introduction

Elastic nonlinearities in piezoelectric materials are responsible for the sensitivity of acoustic devices to external perturbations such as temperature, pressure, force, and electric field. The perturbations change the elastic properties of the medium and hence the phase velocity of the wave. If the elastic wave device is connected to a feedback amplifier to form a sensitive oscillator, a sensor results, when the frequency is the readout quantity.

Temperature, pressure, force and gas sensors that incorporate miniaturized BAW resonators and SAW devices are described. The technologies used, like photolithography and chemical etchnig processes, enable to mass-produce sensors with excellent reproducibility of the specifications.

2. Principles of elastic wave sensors

Bulk and surface elastic wave devices such as resonators and delay lines are sensitive to temperature, pressure, force, mass loading, and electric field. These physical quantities act on the device either directly (as in the case of temperature) or indirectly by means of a test body that transforms the mechanical quantity into quasistatic stress modifying the elastic properties of the substrate. The predeformation of the medium is superimposed on the particle displacement associated with the vibration. If the vibration does not influence the perturbation, the nonlinear phenomenon can be linearized so that the problem is the classical one but with modified elastic constants [1], [2], [3].

In an oscillator sensor the variation of the resonance properties of the devices caused by a physical quantity is translated into a frequency shift of the oscillator. Advantages of this type of sensor are the good short-term stability σ and hence its good intrinsic resolution. A typical curve of short-term stability of a SAW oscillator is presented in Fig. 1.

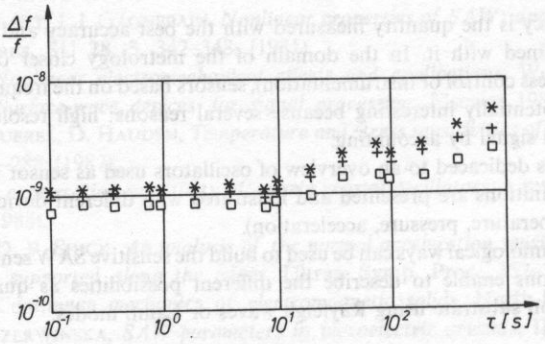

FIG. 1. Short-term stability of SAW delay line at 105 MHz used in force sensor

The sensitivity S to the external quantity determines the scaling factor of the sensor. The limiting resolution r is affected by the short-term stability over the time during which the frequency is measured and by the scaling factor.

$$r = \sigma \cdot f_0 / S$$

where f_0 is the oscillator frequency before applying the perturbation.

Though departure from linearity may no longer be a problem for sensors because of the digital electronics used with them, limitations are the frequency repeatability and the aging that are sometimes too large to permit reaching ultrahigh performances. Repeatability and aging have an influence on the unperturbed frequency and often on

the scaling factor. Moreover, it is still difficult to model their influences acccurately.

Typical values of short-term stability and aging are summarized in Table 1 for miniaturized BAW (MBAW) and SAW oscillators.

Table 1. Typical values of short-term stability σ, aging rate of SAW and miniaturized BAW oscillators used as sensors

Sensor Frequency	Short-Term Stability a	Aging Rate
100 MHz–1 GHz (SAW)	$2.10-10-10^{-9}$	few $\times 10^{-6}$/month
20 kHz–2 MHz (MBAW)	$8.10-11-10^{-9}$	few $\times 10^{-6}$/year

3. Temperature sensors

Different ultrasonic temperature sensors have been studied; the most popular is the HP–28 MHz temperature sensor [4]. Two ways have been used to miniaturize quartz temperature sensors: tuning-fork resonators have been used at low frequencies [5], [6] and SAW quartz oscillators employing doubly rotated cuts have operated at high frequencies. In both cases, the photolithographic technology used to realize the elastic devices enables one to improve the device reproducibility and the production yield.

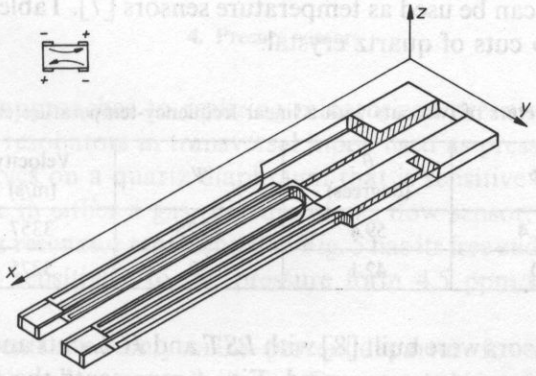

FIG. 2. Tuning-fork temperature sensor (after [3])

Figure 2 shows the **tuning-fork resonator** used as a temperature sensor. Its resonance frequency of 262 kHz varies linearly as a function of temperature, with a sensitivity of $34.6 \cdot 10^{-6}$ K and a linearity defect of 2.10^{-4} over 100 K due to the quadratic term (Fig. 3).

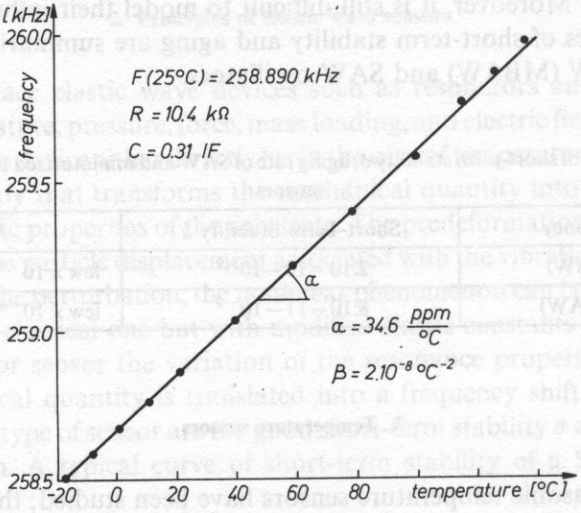

FIG. 3. Frequency shift versus temperature of tuning-fork resonator (after W. ZINGG)

However, an accuracy of $\pm 0.5°C$ can be reached after a preliminary calibration and a digital adjustment during operation. The complete oscillating sensor made in Switzerland is commercially available under the trade name "Thermopack".

In the case of **surface acoustic waves**, doubly rotated cuts with linear characteristics and high sensitivities can be used as temperature sensors [7]. Table 2 gives theoretical characteristics of two cuts of quartz crystal.

Table 2. Parameters of two cuts with a linear frequency-temperature characteristic

Quartz cuts	Φ	θ (degrees)	Ψ	Velocity (m/s)	TCF (10^{-6}/K)
LST	11.4	59.4	35.25	3357	33
JCL	0	42.1	39	3275	22

Temperature sensors were built [8] with *LST* and *JCL*-cuts and their sensitivities, resolutions and time constants measured. Fig. 4 represents the measured frequency-temperature (*F-T*) characteristics of both cuts. The *JCL* sensor had a sensitivity of 2.2 kHz/K, and the *LST*-probe a sensitivity of 3.4 kHz/K an oscillator-frequency of 100 MHz. Short-term stability of the SAW temperature oscillator is 10^{-8} over 1–3 sec. Thus the intrinsic resolution is about 0.1 mC°.

Time constants were measured under several types of heating: thermal diffusion form a contact point, convection and conduction. Table 3, summarizing the values of the time constants measured at 90 percent of the final value, enables comparison with Hewlett-Packard's temperature sensor under the same conditions.

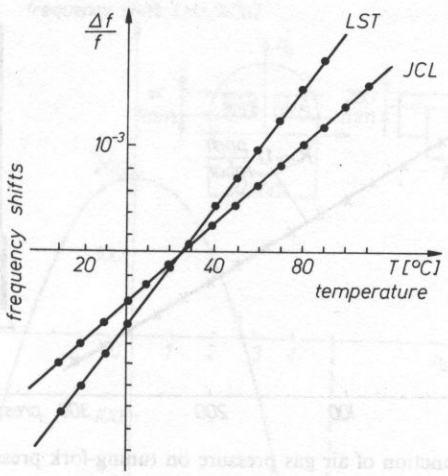

FIG. 4. Frequency shift versus temperature for *LST*-cut and *JCL*-cut quartz

Table 3. Time constants of BAW and SAW temperature sensors

Probes	Diffusion	Convection	Conduction
Bulk waves (H.P.)	1000 s	91 s	6 s
Surface waves	550 s	75 s	0,3 s

4. Presure sensors

Two different approaches to realizing minaturized pressure sensors have been studied: bulk-wave resonators in transversal mode used as pressure gas sensors, and surface acoustic waves on a quartz diaphragm that is sensitive to the bending force induced by pressure in either a gas pressure of gas flow sensor.

The **tuning-fork resonator** represented in Fig. 5 has its free ends grooved with holes to increase natural sensitivity to the pressure form 4.5 ppm/kPa to 11 ppm/kPa in air [6].

The measurements show only an 0.8–percent departure from linearity between 10 and 300 kPa and an excellent reproducibility. Frequency shifts of a sensor operating at 25 kHz as a function of air pressure are plotted on the same figure. Counting the frequency for 2.5 sec permits reaching a resolution of 1 Pa. One application is an altimeter because altitude can be measured with an accuracy of 1 m at 1000 m high, if temperature is well controlled.

Models of pressure sensitivity have been developed for optimizing SAW pressure sensors. The simplest device consists in directly applying pressure on a rectangular crystal plate fixed by epoxy on a rigid plane. When a *ST*–cut quartz SAW oscillator at 105 MHz is subjected to hydrostatic pressure from 0 to 300 kPa, the sensitivity is about

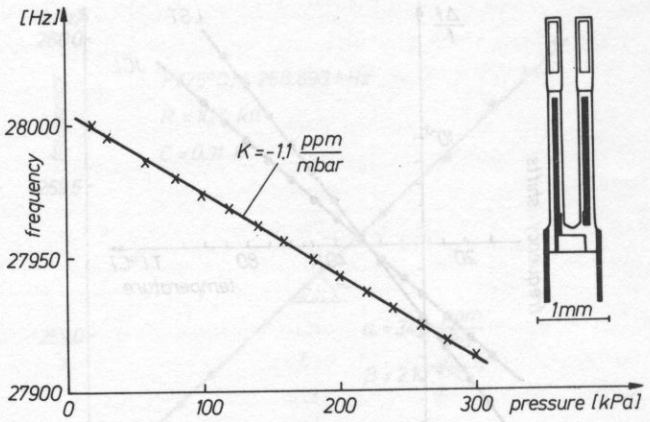

FIG. 5. Frequency shift as function of air gas pressure on tuning-fork pressure sensor (after W. ZINGG)

3 Hz/kPa and is rather low for sensor applications [3]. If instead a thin anisotropic plate is clamped at its edges and subjected to a pressure, it will be bent strongly [9], [10], [11]. The sensitivity can be increased further by using a thin circular diaphragm (Fig. 6).

Figure 7 gives the pressure sensitivity for a *Y*–cut quartz SAW sensor as a function of the mean position of the transducers along the a_3-axis. The diaphragm thickness is 250 μm and its diameter is 10 mm. The nominal oscillator frequency is 105 MHz. For

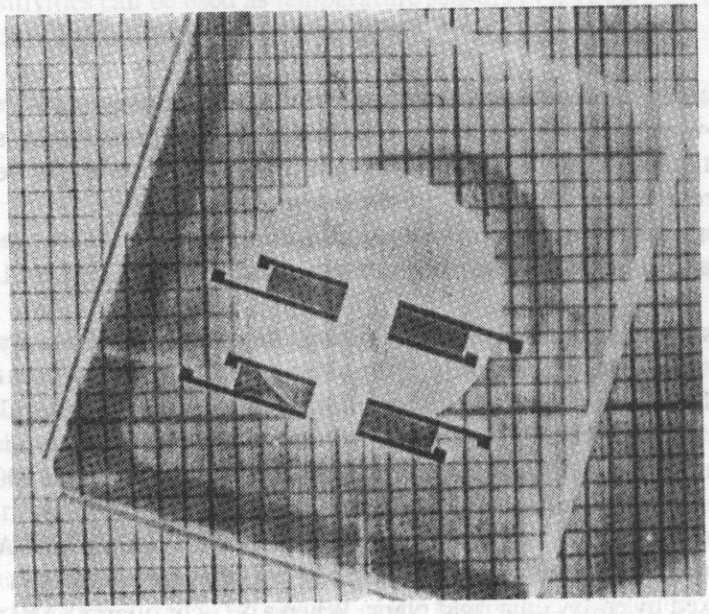

FIG. 6. Monolithic thin diaphragm for SAW pressure sensor

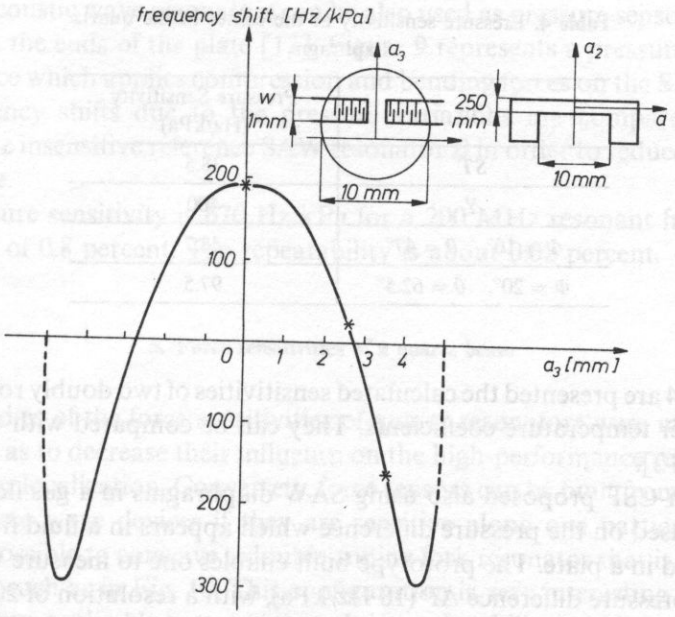

FIG. 7. SAW pressure sensor sensitivity as function of transducer position

a beamwidth $W = 1$ mm, three experimental points have been obtained. At the center of the diaphragm ($a_3 = 0$), the sensitivity is about 200 Hz/kPa and it is almost opposite that at $a_3 = 4$ mm. Using this result, a dual-channel sensor with a sensitivity twice as large has been built (400 Hz/kPa). The differential device also permits a large degree of temperature compensation. The measured frequency-temperature shifts are within 1 kHz over a temperature range from $-40°C$ to $80°C$. This corresponds to about 2 kPa over the total temperature range (Fig. 8).

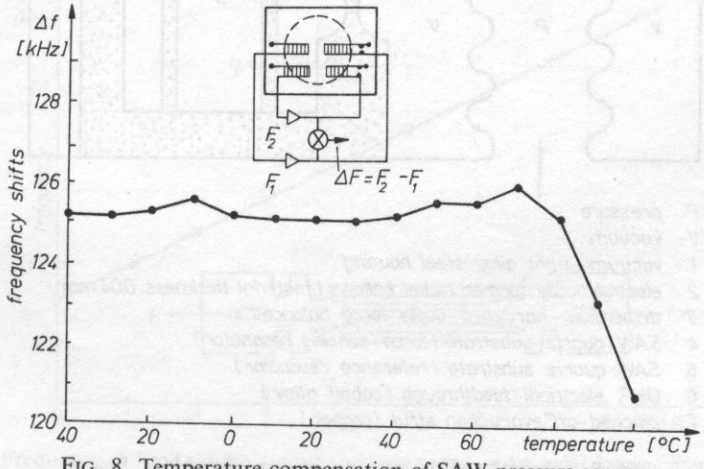

FIG. 8. Temperature compensation of SAW pressure sensor

Table 4. Pressure sensitivity at the center of the quartz diaphragm

Cut	Pressure Sensitivity (Hz/kPa)
ST	38.5
Y	400
$\Phi = 10°, \quad \theta = 47°$	48.7
$\Phi = 20°, \quad \theta = 62.5°$	97.5

In Table 4 are presented the calculated sensitivities of two doubly rotated cuts with zero first-order temperature coefficients. They can be compared with *Y*–and *ST*–cut sensitivities [12].

Thomson-CSF proposed also using SAW diaphragms in a gas flow sensor. The principle is based on the pressure difference which appears in a fluid flowing through a hole grooved in a plate. The prototype built enables one to measure with very good linearity the pressure difference ΔP (18 Hz/kPa), with a resolution of 20 Pa. Response time is less than 1 ms.

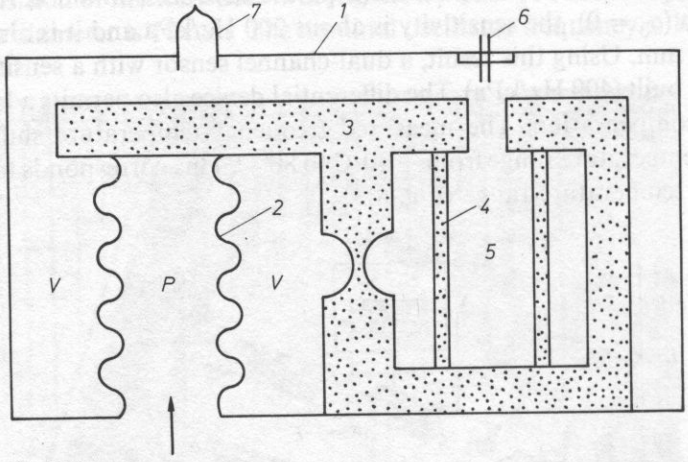

P pressure
V vacuum
1 vacuum - tight alloy steel housing
2 electrolytically formed nickel bellows (material thickness 0,04 mm)
3 dispersion - hardened CuBe force balance
4 SAW quartz substrate (force-sensing resonator)
5 SAW quartz substrate (reference resonator)
6 UHF electrical feedthrough (cobalt alloy)
7 pinched-off evacuation strut (copper)

FIG. 9. Schematic of the pressure sensor (after M. R. RISCH)

Surface acoustic wave resonators can be also used as pressure sensors if the forces are applied on the ends of the plate [13]. Figure 9 represents a pressure sensor using a balanced force which applies compression and bending forces on the SAW resonator *A*. The frequency shifts due to the pressure variations are compared with those obtained on the insensitive reference SAW resonator *B* in order to reduce the influence of temperature.

The pressure sensitivity is 670 Hz/kPa for a 200 MHz resonant frequency with a nonlinearity of 0.8 percent. The repeatability is about 0.02 percent.

5. Force sensitivities of a quartz beam

Many studies of the force sensitivities of quartz resonators were made to model these effects so as to decrease their influence on the high-performance resonators used in navigation or localization. Conversely, force sensors can be built from miniaturized bulk and surface wave devices if they are sensitive along one particular axis. For instance, it is possible to conceive a double-tuning fork resonator that is very sensitive to axial forces, such as in Fig. 10. This configuration is very interesting because of its excellent linearity, negligible hysteresis, good thermal stability, and low aging. Moreover, its sensitivity is very high: 10^{-3}/N between 0–10 N and a repeatability better than 6.10^{-4} over the force range [6].

The force sensitivities of a cantilever quartz beam on which surface acoustic waves are propagating have also been studied [14]. Forces are induced by acceleration acting on an inertial mass. The device consists of a thin rectangular plate of quartz clamped at an edge and subjected to compression and flexure forces at the opposite edge by means of an inertial mass *M*. Sizes of the device are given on Fig. 11 and the surface acoustic wave is propagating along the main axis of the plate (a'_1).

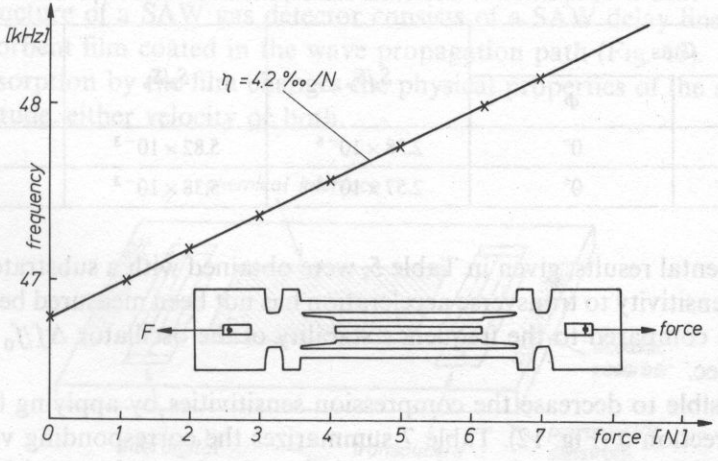

FIG. 10. Frequency shift od double tuning-fork resonator under axial forces (after W. ZINGG)

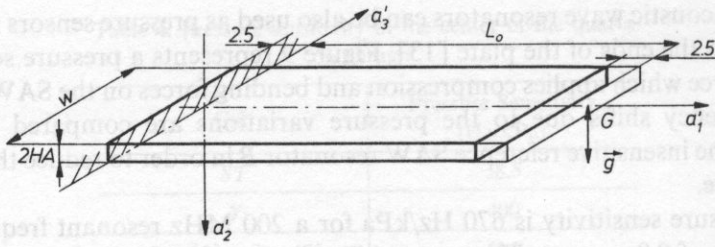

FIG. 11. Schematic of quartz cantilever beam ($LO = 200$ mm, $2HA = 0.5$ mm, $W = 10$ mm, $M = 2.6$ g)

Three different forces can be applied on the SAW substrate as the inertial mass is accelerated: main bending force F_2 along the a_2' axis, transverse bending force F_3 (a_3'), and compression foce F_1 (a_1').

Sensitivities are calculated for several cuts of quartz crystal which have a small temperature sensitivity.

Tables 5 and 6 give sensitivities S_p to the main bending force F_2, the ratio of the transverse bending force sensitivity to the main sensitivity S_t/S_p, and the ratio of the compression force sensitivity to the main sensitivity S_c/S_p for ST, X cut and AT, X cut.

Table 5. Acceleration sensitivities of quartz crystal cuts

ST-cut ($\Psi = 0$)	Theoretical Values (Hz/g)	Experimental Values (Hz/g)
Main bending force	1387	1318
Transverse bending force	3.3×10^{-3}	not measurable
Compression force	8	10

Table 6. Comparison of theoretical and experimental force responses

Cuts		S_t/S_p	S_c/S_p	S_p (Hz/g)
θ	Φ			
a) 42.75°	0°	2.38×10^{-6}	5.82×10^{-3}	1387
b) 35.25°	0°	2.57×10^{-6}	5.38×10^{-3}	1352

Experimental results, given in Table 5, were obtained with a substrate of ST-cut quartz. The sensitivity to transverse acceleration has not been measured because it has a small value compared to the frequency stability of the oscillator $\Delta f/f_0 = 2 \times 10^{-9}$ over 0.1–10 sec.

It is possible to decrease the compression sensitivities by applying forces in an azimuthal direction a (Fig. 12). Table 7 summarizes the corresponding values of S_p, S_c/S_p, S_t/S_p of ST-, AT-cuts when the azimuthal angle a is equal to a critical angle a_c.

Table 7. Force sensitivities at critical azimuthal angle a_c

Cuts	*ST, X*	*AT, X*
a_c	62.5°	53.5°
S_p (Hz/g)	90	85
S_c/S_p	$< 5 \times 10^{-6}$	$< 5 \times 10^{-6}$
S_t/S_p	1.7×10^{-3}	1.2×10^{-2}

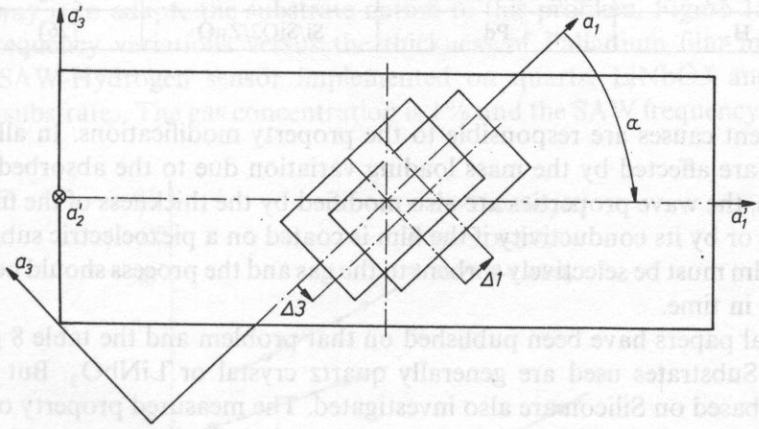

FIG. 12. Rotation α and translations $\Delta 1$, $\Delta 3$ of transducers

6. Gas sensors

The structure of a SAW gas detector consists of a SAW delay line with a thin selectively sorbent film coated in the wave propagation path (Fig. 13).

Gas absorption by the film changes the physical properties of the surface wave either amplitude, either velocity or both.

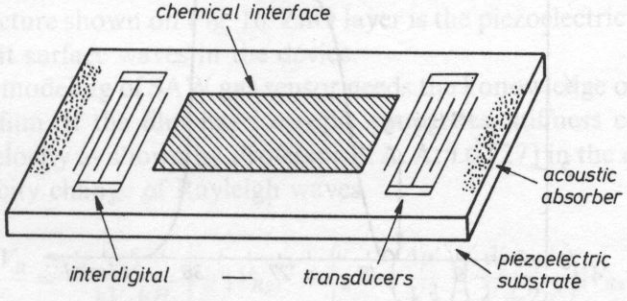

FIG. 13. Schematic of a SAW gas sensor

Table 8. Some gas sensor examples

Gas	Chemical film	Propagation Substrate and cut	Reference
H_2	Pd	Quartz–*ST*, *X*	[22]
NH_3	Pt	Quartz–*ST*, *X*	[23]
NO_2	Phtalocyanine	Quartz–*ST*, *X*	[21]
H_2S	WO_3	LiNbO3–*Y*, *Z*	[24]
SO_2	Triethanolamine	LiNbO3–*Y*, *Z*	[24], [18]
NO_2	Lead Phtalocyanine	LiNbO3–*Y*, *Z*	[25]
H_2	Pd	Si/SiO2/ZnO	[26]

Different causes are responsible to the property modifications. In all cases, the properties are affected by the mass loading variation due to the absorbed gas mass. Sometimes, the wave properties are also modified by the thickness of the film (dispersion effect) or by its conductivity if the film is coated on a piezoelectric substrate. The chemical film must be selectively sorbent to the gas and the process should be reversible and stable in time.

Several papers have been published on that problem and the table 8 gives some examples. Substrates used are generally quartz crystal or $LiNbO_3$. But composite structures based on Silicon are also investigated. The measured property of the SAW has been the velocity shift, then the frequency variation of an associated oscillator.

For example, describing the features of an hydrogen gaz sensor built by the italian team of Roma (E. VERONA et al.). An *ST*–cut of quartz crystal delay line is coated with wave propagation on path with a Palladium film, which is selectively sensitive to hydrogen. The film thickness is about 2000 Å and the wave frequency is close to 100 MHz.

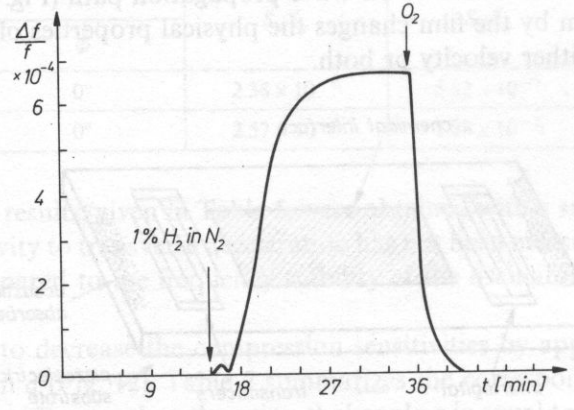

FIG. 14. Time response of a SAW H_2 sensor upon gas absorption and desorption (after E. VERONA)

Upon gas exposure, the phase velocity reaches in a few minutes a new steady state value (Fig. 14).

When the gaz exposure is switched off, desorption takes place and the velocity comes back to the initial value.

The different time constants (rise time, fall time) are depending on the temperature and the concentration of the gas.

Generally, if the gas concentration increases, velocity variations and the fall time increase and the rise time is decreasing.

To improve the resolution in relative velocity variation (or frequency variation), the film thickness could be thicker; but that also increases the rise time and the fall time. Another way is to adapte the substrate nature to this problem. Figure 15 shows the relative frequency variations versus the thickness of Palladium film measured on different SAW-Hydrogen sensor implemented on quartz, LiNbO3 and composite-Silicon substrates. The gas concentration is 1% and the SAW frequency is 80 MHz.

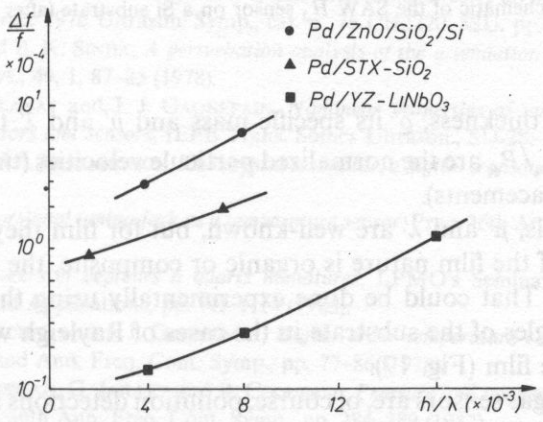

FIG. 15. Relative frequency shifts vs. Pd layer thickness for different SAW substrates (after E. VERONA)

If quartz and $LiNbO_3$ substrates are piezoelectric, then sensors have simple regular structure, but Silicon is not piezoelectric and gas sensor needs to implement composite structure shown on Fig. 16. ZnO layer is the piezoelectric film deposited on Si/SiO2 to excit surface waves in the device.

Complete modeling of SAW gas sensor needs the konowledge of elastic constants of the coated film. If the film has isotropic properties, stiffness constants leads to calculate the velocity as shown by Professor B. A. AULD [27] in the relation giving the fractional velocity change of Rayleigh waves

$$\frac{\Delta V_R}{V_R} = -\frac{1}{hV_R hP_R}\left[\varrho'|V_{Ry}|^2 + \left\{\varrho' - \left(\frac{4\mu'}{V_R^2}\right)\left(\frac{\lambda'+\mu'}{\lambda'+2\mu'}\right)|V_{Rz}|^2\right\}\right]$$

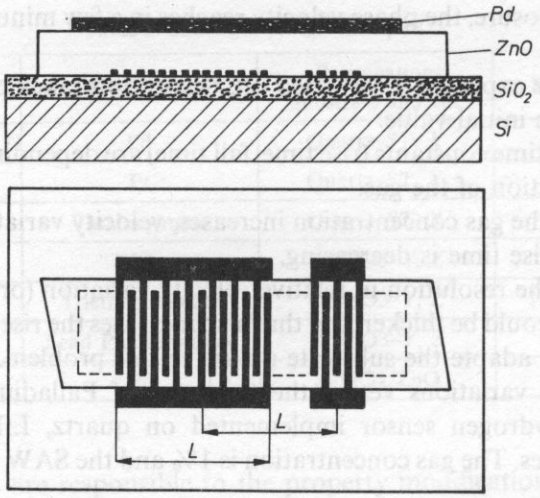

FIG. 16. Schematic of the SAW H_2 sensor on a Si substrate (after E. VERONA)

where h is the film thickness, ϱ' its specific mass and μ' and λ' the Lamé constants. $|V_{Rz}|/\sqrt{P_R}$ and $|V_R|/\sqrt{P_R}$ are the normalized particule velocities (time derivatives of the instantaneous displacements).

For bulk metals, μ' and λ' are well-known, but for film they are often undetermined. Moreover, if the film nature is organic or composite, the unknown constants must be measured. That could be done experimentally using the velocity variation value versus cut angles of the substrate in the cases of Rayleigh waves or bulk waves interacting with the film (Fig. 17).

Application of gas sensors are, of course, pollution detections in air, but also in the case of gas weapon detection, which is became a serious potential problem today.

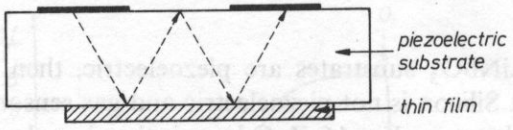

FIG. 17. Lamb wave device for measurement of film constants and for viscosity measurements

7. Conclusion

Surface acoustic devices or miniaturized bulk wave resonators are potentially efficient for sensor applications with different physical or chemical measurements. Some of them have been described in this paper.

Other applications studied in different laboratories include high-voltage probes, magnetic sensors, and deposited mass sensors. In the first application, $LiNbO_3$ is often used because of its strong piezoelectric coupling [15], [16], or because of the coupling with conduction electrons [17].

All of these sensors have frequency as output quantity, and so give digital information after frequency counting. In metrology and instrumentation, as in industrial activities, digital electronics is playing an increasing role in process and control, and new sensors will be necessary to use with new standards. With these sensors one obtains a direct value of the quantity from the frequency, or by determining frequency shift relative to a reference device, or measurement after frequency multiplication and mixing to increase sensitivity and resolution.

References

[1] B. K. SINHA, H. F. TIERSTEN, *On the influence of uniaxial biasing stresses on the velocity of piezoelectric surface waves*, in Proc. 1976 Ultrason. Symp., cat. n° 76 CH2220–5SU, pp. 475–479.

[2] H. F. TIERSTEN and B. K. SINHA, *A perturbation analysis of the attenuation and dispersion of surface waves*, J. Appl. Phys., **49**, 1, 87–85 (1978).

[3] D. HAUDEN, M. PLANAT and J. J. GAGNEPAIN, *Nonlinear properties of surface acoustic waves: applications to oscillators and sensors*, IEEE Trans. Sonics Ultrason., SU-28, 342–345 (1981).

[4] D. L. HAMMOND and A. BENJAMINSON, *The crystal resonator, a digital transducer*, IEEE Spectrum, **6**, 4, 53–60 (1969).

[5] R. J. DINGER, *The torsional tuning-fork as a temperature sensor*, Proc. 36th Ann. Freq. Cont. Symp., pp. 265–269 (1982).

[6] W. ZINGG, *Résonateurs et cepteurs à quartz miniatures*, LPMO's Seminar Frequency Standards: Characterisation and Applications, pp. N1–N14 (1985).

[7] D. HAUDEN, M. MICHEL and J. J. GAGNEPAIN, *Higher-order temperature coefficients of quartz SAW oscillators*, Proc. 32nd Ann. Freq. Cont. Symp., pp. 77–86 (1978).

[8] D. HAUDEN, S. ROUSSEAU, G. JAILLET and R. COQUEREL, *Pressure and temperature measurements with SAW sensors*, Proc. 36th Ann. Freq. Cont. Symp., pp. 284–289 (1982).

[9] J. F. DIAS and H. E. KARRER, *Stress effects in acoustic surface wave circuits and applications to pressure and force transducers*, Proc. 1974 IEEE Int. Solid-State Circuits Conf., pp. 166–170.

[10] T. M. REEDER, D. E. CULLEN and M. GILDEN, *SAW oscillator pressure sensors*, Proc. 1975 Ultrason. Symp. cat. n° 75 CH0994–4SU, pp. 264–268.

[11] D. HAUDEN, S. ROUSSEAU and J. J. GAGNEPAIN, *Sensitivities of SAW oscillators to temperature, forces and pressure: application to sensors*, Proc. 34th Ann. Freq. Cont. Symp., pp. 312–319 (1980).

[12] M. PLANAT and D. HAUDEN, *Nonlinear properties of bulk and surface acoustic waves in piezoelectric crystals*, Ferroelectrics, **42**, 117–136 (1982).

[13] M. R. RISCH, *Precision pressure sensor using quartz SAW resonators*, Sensors and Actuators, **6**, 127–133 (1984).

[14] D. HAUDEN, F. BINDLER and R. COQUEREL, *SAW cantilever-beam accelerometer sensitivities*, Proc. 1985 Ultrason. Symp. cat. n° 85 CH2209-5, pp. 486–489 (1985).

[15] S. JOSHI, *A temperature compensated high-voltage probe using surface acoustic waves*, Proc. 1982 IEEE Ultrason. Symp., pp. 317–320 (1982).

[16] R. INABA, Y. KASAHARA and K. WASA, *An electronic voltage sensor using surface acoustic waves*, Proc. 1982 IEEE Ultrason. Symp., 312–316 (1982).

[17] M. GILDEN and T. W. GRUDKOWSKI, *GaAs SAW resonator oscillators with electronic tuning*, Proc. 35th Ann. Freq. Cont. Symp., pp. 395–400 (1981).

[18] A. BRYANT, D. L. LEE and J. F. VETELINO, *A surface acoustic wave gas detector*, Proc. 1981 Ultrason. Symp., pp. 171–174 (1981).

[19] A. d'AMICO, A. PALMA and E. VERONA, *Hydrogen sensor using a palladium-coated surface acoustic wave delay line*, Proc. 1982 IEEE Ultrason. Symp., pp. 308-311 (1982).

[20] S. G. JOSHI and J. G. BRACE, *Measurement of humidity using surface acoustic waves*, Proc. 1985 Ultrason. Symp., cat. n° 85 CH2209–5, pp. 600–603 (1985).

[21] A. W. BARANDSZ, J. C. VIS, M. S. NIEUWENHUIZEN and E. NIEWKOOP, *A SAW-chemosensor for NO_2 gas concentration measurement*, Proc. 1985 Ultrason. Symp., cat. n° 5 CH2209–5, pp. 589–590 (1985).

[22] A. d'AMICO, M. GENTILI, P. VERARDI, E. VERONA, *Gas sensor based on improved SAW devices*, 2nd Int. Meeting on Chemical Sensors, Bordeaux, 743 (1985).

[23] A. d'AMICO, A. PETRI, P. VERARDI, E. VERONA, *NH_3 surface acoustic wave gas sensor*, Proc. 1987 IEEE Ultrason. Symp., p. 633 (1987).

[24] A. BRYANT, M. POIRIER, G. RILEY, D. L. LEE and Y. F. VETELINO, *Gas detection using surface acoustic wave delay lines*, Sensors and Actuators, **4**, 105 (1983).

[25] A. VENEMA, E. NIEWKOOP, A. J. WELLEKOOP, W. J. OHIJSEN, A. W. BARENDEEZ, M. S. NIEUWENHUIZEN, *NO_2 gas concentration measurement with a SAW chemisensor*, IEEE Trans. Ultrason., Ferroelectrics, Freq. Cont., UFFC–34, 148 (1987).

[26] C. CALIENDO, A. d'AMICO, P. VERARDI, E. VERONA, *Surface acoustic wave H_2 sensor on silicon substrate*, Proc. 1988 Ultrasonics Symp., p. 569 (1988).

[27] B. A. AULD, *Acoustic field and waves in solids*, vol. II, Wiley Interscience 1973.

ARCHIVES OF ACOUSTICS
16, 1, 107-119(1991)

NONLINEAR MATERIAL PROPERTIES OF QUARTZ DETERMINED BY THE RESONATOR METHOD

C. K. HRUSKA

Piezoelectricity Research Laboratory Department of Mathematics, York University
(Toronto, Ontario M3J 1P3, Canada)

Attempts to provide least-squares estimates of all 31 independent thrid-order nonlinear electromechanical constants of alpha quartz using the resonator method produce parameters containing third-order elastic constants linearly combined with the remaining three types of electromechanical nonlinearities: electroelastic, electrostrictive and dielectric.

To maximize the yield of the resonator method in terms of these latter three types of nonlinear constants, the third-order elastic constants must be "imported" from an external source. They can be introduced, with the same effect, before or after the least-squares process is executed. Their reliability is crucial for the quality of the electroelastic constants and apparently (considering the size of their respective standard errors) less important for the electrostrictive and third-order dielectric constants.

A comparison with the results of others, yielding in most cases an excellent agreement, is facilitated by introducing uniformity into the values of the linear constants used for their determination. This produces changes in the calculated nonlinear parameters but does not remove the few differences which were noted.

1. Introduction

Interactions between the dc electric field and alpha quartz provide valuable information about its material nonlinearities. One of the methods exploiting this principle is the resonator method. It is based on observations of the changes in the resonance frequency of quartz resonators induced by a dc electric field acting on the crystal material.

The current set of the experimental data provided by the resonator method has been used before (in part) e.g. by HRUSKA [7] and by HRUSKA and BRENDEL or (in total) by HRUSKA [8]. The last work resulted in the determination of the complete set electroelastic constants of quartz, several electrostrictive constants, some isolated and others in combination among themselves or with the (only) third-order permittivity of quartz.

In the process of all above applications of the resonator method the third-order

elastic constants of quartz were employed which were determined much earlier by THURSTON, MCSKIMMIN and ANDREATCH [18]. This was done so because the main thrust of the past work was directed towards the determination of other third-order material constants regarded as unknown or unverified. The third-order elastic constants were employed with little thought for whether or not it was actually necessary. The consequencies of this decision, in either case, have not been considered. To do so is the main objective of this work.

In the course of the work an attempt must be made to determine all four third-order electromechanical nonlinearities in quartz from the resonator method data. This produces results which are completely independent of all other nonlinear material constants determined earlier and invites a comparison with the results of others. In the past such comparisons were made without the benefit of assured independence of the compared quantities and, disregarding the fact that different authors use different sets of the linear material constants for their computation. In the comparisons made here this past omission is rectified.

The numerical values of all quantities (generated or referenced) in this paper are stated for right-hand quartz and its basic frame of reference according to the IEEE Standard 176 of 1978 [20].

2. Experimental data

The study of quartz nonlinearities made in this paper is done using the resonator method. It is based on observations of the linear coefficient L of the dependence of the resonance frequency f of quartz resonators on the dc electric field E applied to their body. This phenomenon has also been known as the polarizing effect or the electroelastic effect. The linear coefficient of the frequency–dc field dependence is defined as $L = (1/f) \cdot (df/dE)_{E=0}$.

The observations of the linear coefficient L used in this paper are the 184 values listed in [9]. They have been accumulated over a period of twenty years and originate from HRUSKA and KHOGALI [12], KINIGADNER [21], HRUSKA, MERIGOUX and KUCERA [13] and from HRUSKA and BRENDEL [11].

The observations of L were obtained for a variety of doubly rotated rectangular rods vibrating in length and plates vibrating in thickness. To describe their orientation an orthogonal frame of reference is used whose axes X'_1, X'_2 and X'_3 are fixedly connected with each resonator and parallel to its thickness t, width w and length l, respectively. This reference frame is related to the basic frame of reference X_1, X_2 and X_3 (denoted respectively X, Y, and Z in [20]) through the following matrix of the direction cosines

	X_1	X_2	X_3
X'_1	α_{11}	α_{12}	α_{13}
X'_2	α_{21}	α_{22}	α_{23}
X'_3	α_{31}	α_{32}	α_{33}.

The orientation of both the rods and the plates relative to the basic frame of reference is also stated in [9] and given using the IEEE rotational symbol $(XZlwt)\psi/\phi/\theta$ [20]. The values of the corresponding direction cosines α_{AB} which are needed later are fully calculable from the orientation angles ψ, ϕ and θ. The dc electric field E acting on the resonators is always in the direction of X_1' (resonator thickness) related to the basic reference frame by the direction cosines α_{11}, α_{12}, α_{13}.

3. The model of the linear coefficient L

The model linking the observations of the linear coefficient L to the nonlinear material tensors of quartz is based on the nonlinear theory of dielectrics. Its most recent version described in [8] is recorded as follows

$$L = A_{MIJKL} \cdot f_{MIJKL} + B_{MNIJ} \cdot l_{MNIJ} + C_{MRS} \cdot \varkappa_{MRS} + D_{IJKLMN} \cdot c_{IJKLMN} + E. \quad (1)$$

It relies on the earlier results by BAUMHAUER and TIERSTEN [2], BRENDEL [5], TIERSTEN and BALLATO [19], KITTINGER and TICHY [14], HRUSKA and BRENDEL [11], HRUSKA [7], and HRUSKA and BRENDEL [10].

The model presents the linear coefficient L as a linear function of four third-order nonlinear material tensors: c_{IJKLMN}, the third-order elastic stiffness tensor; l_{MNIJ}, the total electrostrictive tensor; f_{MIJKL}, the electroelastic tensor; and $\varkappa_{MRS}$, the third-order dielectric permittivity tensor. The electrostrictive tensor l_{MNIJ} is defined according to NELSON [17] and consists of the relative electrostrictive tensor and the Maxwell vacuum electric-stress tensor (Eq. (54), [17]). All these tensors are defined in the basic frame of reference of quartz according to [20]. They are defined for zero strain and zero electric field in the crystal material.

The coefficients A_{MIJKL}, B_{MNIJ}, C_{MRS}, D_{IJKLMN}, and the absolute term E in Eq. (1) are functions of the known second-order (linear) material constants of quartz and of the resonator orientation and mode of vibration. Their definition given in [8] will be restated below.

All uppercase indices used above and throughout the paper take on the values of 1, 2, 3. The Einstein summation rule is in effect everywhere except where explicitly stated otherwise.

Two types of resonators and vibrations, thickness modes of plates and the extensional mode of rods, provide the experimental values of L used in this paper. The definitions of the coefficients A_{MIJKL}, B_{MNIJ}, C_{MRS}, D_{IJKLMN}, and the absolute term E in Eq. (1) need to be given for each type of resonator separately. For the rods they are

$$A_{MIJKL} = \frac{1}{2} F'_{AB} s'_{33CD} \alpha_{1M} \alpha_{AI} \alpha_{BJ} \alpha_{CK} \alpha_{DL}, \quad (2)$$

$$B_{MNIJ} = 0, \quad (3)$$

$$C_{MRS} = 0, \quad (4)$$

$$D_{IJKLMN} = \frac{1}{2} F'_{AB} s'_{33CD} d'_{1EF} \alpha_{AI} \alpha_{BJ} \alpha_{CK} \alpha_{DL} \alpha_{EM} \alpha_{FN}, \tag{5}$$

$$E = \frac{1}{2} F'_{AB} s'_{33CD} (c'_{FBCD} d'_{1AF} + c'_{FDAB} d'_{1CF}), \tag{6}$$

where

$$F'_{AB} = (2\delta_{3A} - \delta_{3A}\delta_{3B} + \delta_{2A}\delta_{2B} + \delta_{1A}\delta_{1B} + \delta_{2A}\delta_{1B} + \delta_{1A}\delta_{2B}) s'_{AB33}/s'_{3333}, \tag{7}$$

$$s'_{AB33} = s'_{33AB} = \alpha_{AI}\alpha_{BJ}\alpha_{3K}\alpha_{3L} s_{IJKL}, \tag{8}$$

$$s'_{3333} = \alpha_{3I}\alpha_{3J}\alpha_{3K}\alpha_{3L} s_{IJKL}, \tag{9}$$

$$d'_{1AB} = \alpha_{1I}\alpha_{AJ}\alpha_{BK} d_{IJK}. \tag{10}$$

In Eq. (7) the Einstein summation rule is not in effect for the indices A and B on the right hand side of the definition of F'_{AB}.

The expressions for the coefficient D_{IJKLMN} and for the absolute term E in Eqs. (5) and (6), respectively, do not appear in [8] explicitly. However, they are obtained from the absolute term C there (Eq. (7), [8]) after it is recorded as a linear function of the third-order elastic stiffness tensor components c_{IJKLMN}

$$C = D_{IJKLMN} \cdot c_{IJKLMN} + E. \tag{11}$$

The above definitions (4)–(10) contain some material tensor components the meaning of which has not been defined. They represent: s_{IJKL}, the tensor of the elastic compliances, and d_{IJK}, the piezoelectric strain tensor. They are both related to the basic frame of reference. δ_{MI} is the Kronecker delta.

The definitions of the coefficients A_{MIJKL}, B_{MNIJ}, C_{MRS}, D_{IJKLMN}, and of the absolute term E in Eq. (1) for the three thickness modes of vibration of plates are

$$A_{MIJKL} = (1/2\lambda)\alpha_{1M}(\alpha_{1I}\alpha_{1L} l_J l_K - 2r\alpha_{1J}\alpha_{1R} l_I d_{RKL}), \tag{12}$$

$$B_{MNIJ} = (1/2\lambda)\varepsilon_0 \alpha_{1M}\alpha_{1N}(2r\alpha_{1J} l_I - r^2 \alpha_{1R} d_{RIJ}), \tag{13}$$

$$C_{MRS} = -(1/2\lambda) r^2 \alpha_{1M}\alpha_{1R}\alpha_{1S}, \tag{14}$$

$$D_{IJKLMN} = (1/2\lambda)\alpha_{1I}\alpha_{1L}\alpha_{1R} l_J l_K d_{RMN}, \tag{15}$$

$$E = (1/2\lambda)[\alpha_{1I}\alpha_{1E}(\alpha_{1J}\delta_{KM}\delta_{LN} + \alpha_{1L}\delta_{KN} l_J l_M + \alpha_{1L}\delta_{JN} l_K l_M) d_{EMN} c_{IJKL} + \alpha_{1J}\alpha_{1L}(2r\alpha_{1R} l_I d_{RIK} - \alpha_{1K}) e_{JKL}], \tag{16}$$

where

$$r = \alpha_{1I}\alpha_{1K} l_J e_{IJK}/(\alpha_{1A}\alpha_{1B}\varepsilon_{AB}). \tag{17}$$

The expressions for the coefficient D_{IJKLMN} and for the absolute term E in Eqs. (15) and (16), respectively, are obtained from the absolute term C (Eq. (11), [8]) after it is

recorded as a linear function of the third-order elastic stiffness tensor components c_{IJKLMN} as done previously for the rods (Eq. (11)).

Again, all quantities on the right-hand side of Eqs. (12)–(17) are defined in the basic frame of reference. Those that have not yet appeared in this paper are explained now. They are: c_{IJKL}, the elastic stiffness tensor, e_{NIJ}, the piezoelectric stress tensor; and ε_{MN}, the dielectric permittivity tensor. The constant ε_0 is the permittivity of free space.

The quantity λ and the amplitude vector (l_1, l_2, l_3) of the plate vibrations in Eqs. (12)–(17) are the respective eigenvalue and eigenvector of the matrix

where (Γ_{IK}),

$$\Gamma_{IK} = \alpha_{1J}\alpha_{1L}c_{IJKL} + \alpha_{1N}\alpha_{1J}\alpha_{1M}\alpha_{1L}e_{NIJ}e_{MKL}/(\alpha_{1A}\alpha_{1B}\varepsilon_{AB}).$$

The three generally existing eigenvalue-eigenvector pairs of the above matrix correspond to the three thickness modes of vibrations of the plates under consideration.

4. Calculation of the nonlinearities

Returning to Eq. (1) and its preparation for the calculation of the third-order material constants of quartz, the upper case tensor indices there have been contracted to their lower case matrix form. The interchange symmetry among the uppercase indices and the symmetry of quartz have been taken into account and the conventional choice of the independent material constants made. Eq. (1) has taken on the form

$$\begin{aligned} L_i = {} & a_{i1}\cdot f_{111} + a_{i2}\cdot f_{113} + a_{i3}\cdot f_{114} + a_{i4}\cdot f_{122} \\ & + a_{i5}\cdot f_{124} + a_{i6}\cdot f_{134} + a_{i7}\cdot f_{144} + a_{i8}\cdot f_{315} \\ & + b_{i1}\cdot l_{11} + b_{i2}\cdot l_{12} + b_{i3}\cdot l_{13} + b_{i4}\cdot l_{14} \\ & + b_{i5}\cdot l_{31} + b_{i6}\cdot l_{33} + b_{i7}\cdot l_{41} + b_{i8}\cdot l_{44} \\ & + c_i\cdot \varkappa_{111} \\ & + d_{i1}\cdot c_{111} + d_{i2}\cdot c_{112} + d_{i3}\cdot c_{113} + d_{i3}\cdot c_{114} + d_{i5}\cdot c_{123} \\ & + d_{i6}\cdot c_{124} + d_{i7}\cdot c_{133} + d_{i8}\cdot c_{134} + d_{i9}\cdot c_{144} + d_{i10}\cdot c_{155} \\ & + d_{i11}\cdot c_{222} + d_{i12}\cdot c_{333} + d_{i13}\cdot c_{344} + d_{i14}\cdot c_{444} + E_i, \end{aligned} \tag{18}$$

where

$$f_{111}, f_{113}, f_{114}, f_{122}, f_{124}, f_{134}, f_{144}, f_{315} \tag{19}$$

are the eight independent electroelastic constants, and

$$l_{11}, l_{12}, l_{13}, l_{14}, l_{31}, l_{33}, l_{41}, l_{44} \tag{20}$$

are the eight independent electrostrictive constants, and

$$\varkappa_{111} \tag{21}$$

is the (only) independent third-order permittivity constant of quartz, and

$$c_{111}, c_{112}, c_{113}, c_{114}, c_{123}, c_{124}, c_{133},$$
$$c_{134}, c_{144}, c_{155}, c_{222}, c_{333}, c_{344}, c_{444} \tag{22}$$

are the third-order elastic constants of quartz.

The conversion of Eq. (1) to Eq. (18) is straightforward but tedious and, for these reasons, its details are not given in this paper. The index i has been added to various quantities in Eq. (18) in preparation for its application to all 184 observations of the linear coefficient denoted now L_i, $i = 1, 2, \ldots, 184$.

All thirty-one material constants (19)–(22) are the fundamental material constants of quartz related to its basic reference frame. In agreement with the tensors in Eq. (1) they are defined for zero strain and zero electric field in the crystal material.

Aiming at the determination of the nonlinear constants (19)–(22) Eq. (14) was applied to all observations of the linear coefficient L_i. Due to random errors in the experimental values of L_i, this led to an overdetermined linear system

$$\begin{aligned} L_i - E_i = {} & a_{i1} \cdot f_{111} + a_{i2} \cdot f_{113} + a_{i3} \cdot f_{114} + a_{i4} \cdot f_{122} \\ & + a_{i5} \cdot f_{124} + a_{i6} \cdot f_{134} + a_{i7} \cdot f_{144} + a_{i8} \cdot f_{315} \\ & + b_{i1} \cdot l_{11} + b_{i2} \cdot l_{12} + b_{i3} \cdot l_{13} + b_{i4} \cdot l_{14} \\ & + b_{i5} \cdot l_{31} + b_{i6} \cdot l_{33} + b_{i7} \cdot l_{41} + b_{i8} \cdot l_{44} \\ & + c_i \cdot \varkappa_{111} \\ & + d_{i1} \cdot c_{111} + d_{i2} \cdot c_{112} + d_{i3} \cdot c_{113} + d_{i3} \cdot c_{114} + d_{i5} \cdot c_{123} \\ & + d_{i6} \cdot c_{124} + d_{i7} \cdot c_{133} + d_{i8} \cdot c_{134} + d_{i9} \cdot c_{144} + d_{i10} \cdot c_{155} \\ & + d_{i11} \cdot c_{222} + d_{i12} \cdot c_{333} + d_{i13} \cdot c_{344} + d_{i14} \cdot c_{444}, \end{aligned} \tag{23}$$

where $i = 1, 2, \ldots, 184$.

The thirty-one material constants (19)–(22) were sought by a least-squares fit to this system. Prior to this a brief analysis of the system matrix and of the random errors of its left hand sides was necessary.

The matrix of linear system (23), to be referred to as M, consists of four concatenated matrices, a_{ij}, $(j = 1, 2, \ldots, 8)$, b_{ik}, $(k = 1, 2, \ldots, 8)$, c_i, and d_{il}, $(l = 1, 2, \ldots, 14)$. Applicability of the least-squares procedure requires that the elements of matrix M be known with total accuracy. As they are functions of the linear material constants of quartz as well as of the resonator orientations this requires a concession that they all be regarded as known without errors. This concession naturally extends to the absolute term E_i in Eq. (23) which is a function of the same quantities (Eqs. (6) and (16)).

The experimental values in the observed coefficients L_i are thus regarded to be the only source of random errors of the left hand sides of system (23). Subsequent analysis suggested that the measure of random errors in L_i are the variations in this quantity among resonators of identical orientation rather than the standard deviations of observations made for individual resonator units. It was not possible to estimate these variations for about one third of the observations of L_i in system (23) as some of the

resonators were specimens of orientations dissimilar from other resonator used for this project. For this reason the least-squares procedure was executed using equal weighting of the left hand sides of system (23).

Two of the columns of matrix M, d_{i7} and d_{i12}, were found to be identically equal to zero. An additional fourteen columns, b_{i2}, b_{i8}, and d_{il}, $l = 1, 2, \ldots, 6, 8, 9, 10, 11, 13, 14$, were found to be linearly dependent on the remaining columns of matrix M. As a result the least-squares fit did not yield the values of all thirty-one sought constants (19)–(22) but rather only of fifteen parameters, most of them being linear combinations of these constants rather than their pure values.

The quality of the least-squares fit attained can be seen from the statistical indicators obtained during the least–squares process (MENDENHALL and SINCICH [22]): the sample multiple coefficient of determination $R^2 = 0.9976$ or the analysis of variance F test value = 4,707.

The values of the calculated parameters and their standard errors are placed in Table 1 and marked Solution 1. The definitions of the parameters in terms of the fundamental third-order material constants (19)–(22) are presented in Table 2.

Table 1. Third-order nonlinear material parameters and fundamental material constants of alpha quartz determined by the resonator method

Solution 1 nonlinear parameters this work		Solution 2 nonlinear constants according to [8]	
k_{111}	2.35 ± 0.05	f_{111}	2.16 ± 0.05
k_{113}	0.28 ± 0.07	f_{113}	-0.43 ± 0.07
k_{114}	0.60 ± 0.04	f_{114}	0.16 ± 0.04
k_{122}	-0.73 ± 0.03	f_{122}	-1.12 ± 0.03
k_{124}	1.37 ± 0.02	f_{124}	0.74 ± 0.02
k_{134}	1.72 ± 0.03	f_{134}	1.65 ± 0.03
k_{144}	-0.04 ± 0.03	f_{144}	0.01 ± 0.03
k_{315}	-0.78 ± 0.03	f_{315}	-0.78 ± 0.03
k_{11}	-3.0 ± 0.9	l_{11}	-3.1 ± 0.9
k_{13}	-8.7 ± 2.6	$l_{13} + 2.000\, l_{44}$	-9.1 ± 2.6
k_{14}	-2.4 ± 0.6	l_{14}	-2.3 ± 0.6
k_{31}	-11.2 ± 3.0	$l_{31} + 2.000\, l_{44}$	-11.2 ± 3.0
k_{33}	-7.7 ± 6.9	l_{33}	-7.7 ± 6.9
k_{41}	-4.7 ± 0.7	l_{41}	-4.7 ± 0.7
q_{111}	$(-2.4 \pm 2.5) \cdot 10^{-21}$	$\varkappa_{111} - 2.045 \cdot 10^{-23} l_{12}$	$(-2.4 \pm 2.5) \cdot 10^{-21}$

Parameters k_{ijk} and electroelastic constants f_{ijk} are in N/(V.m), parameters k_{ij} and electrostrictive constants l_{ij} are dimensionless, parameter q_{111} and third-order permittivity constant $\varkappa_{111}$ are in F/V. The numerical coefficient $2.045 \cdot 10^{-23}$ at l_{12} is also in F/V. The errors are standard errors. Given for room temperature, right-hand quartz and the frame of reference according to [20]. Solution 1 can be converted into Solution 2 using Table 2 and the third-order elastic constants according to [18]. Both solutions are calculated using the linear material constants of quartz taken from [3].

Table 2. Definition of third-order nonlinear material parameters of alpha quartz calculable by the resonator method

$$
\begin{aligned}
k_{111} &= f_{111} + 2.310\cdot10^{-12}c_{111} - 2.310\cdot10^{-12}c_{112} - 0.727\cdot10^{-12}c_{114}\\
k_{113} &= f_{113} + 2.310\cdot10^{-12}c_{113} - 2.310\cdot10^{-12}c_{123} - 0.727\cdot10^{-12}c_{134}\\
k_{114} &= f_{114} + 2.310\cdot10^{-12}c_{114} - 2.310\cdot10^{-12}c_{124} - 0.727\cdot10^{-12}c_{144}\\
k_{122} &= f_{122} + 2.310\cdot10^{-12}c_{111} + 2.310\cdot10^{-12}c_{112} + 0.727\cdot10^{-12}c_{114}\\
&\quad + 1.454\cdot10^{-12}c_{124} - 4.620\cdot10^{-12}c_{222}\\
k_{124} &= f_{124} + 2.310\cdot10^{-12}c_{114} + 6.930\cdot10^{-12}c_{124} - 0.727\cdot10^{-12}c_{155}\\
k_{134} &= f_{134} + 4.620\cdot10^{-12}c_{134} - 0.727\cdot10^{-12}c_{344}\\
k_{144} &= f_{144} + 2.310\cdot10^{-12}c_{144} - 2.310\cdot10^{-12}c_{155} - 0.727\cdot10^{-12}c_{444}\\
k_{315} &= f_{315}\\
k_{11} &= l_{11} + 1.205\cdot10^{-12}c_{111} - 0.603\cdot10^{-12}c_{112} - 0.379\cdot10^{-12}c_{114}\\
&\quad + 0.379\cdot10^{-12}c_{124} + 0.060\cdot10^{-12}c_{144} - 0.603\cdot10^{-12}c_{222}\\
k_{13} &= l_{13} + 2.00\,l_{44} + 1.205\cdot10^{-12}c_{113} - 1.205\cdot10^{-12}c_{123}\\
&\quad - 0.759\cdot10^{-12}c_{134} + 0.060\cdot10^{-12}c_{344}\\
k_{14} &= l_{14} - 2.411\cdot10^{-12}c_{124} - 0.379\cdot10^{-12}c_{144} + 0.379\cdot10^{-12}c_{155}\\
&\quad + 0.060\cdot10^{-12}c_{444}\\
k_{31} &= l_{31} + 2.00\,l_{44}\\
k_{33} &= l_{33}\\
k_{41} &= l_{41}\\
q_{111} &= \varkappa_{111} - 2.045\cdot10^{-23}l_{12} - 2.464\cdot10^{-35}c_{111} + 1.233\cdot10^{-35}c_{112}\\
&\quad + 0.777\cdot10^{-35}c_{114} - 2.326\cdot10^{-35}c_{124} - 0.367\cdot10^{-35}c_{144}\\
&\quad + 0.244\cdot10^{-35}c_{155} + 1.232\cdot10^{-35}c_{222} + 0.038\cdot10^{-35}c_{444}
\end{aligned}
$$

The parameters are combinations of the third-order nonlinear material constants of quartz including electroelastic constants f_{ijk}, third-order elastic constants c_{ijk}, electrostrictive constants l_{ij} and third-order permittivity $\varkappa_{111}$. The first eight parameters (k_{ijk}) are in N/(V.m), the next six (k_{ij}) are dimensionless, the last parameter (q_{111}) is in F/V. The numerical coefficients at c_{ijk} in parameters k_{ijk}, k_{ij} and q_{111} are in m^2/V, m^2/N and Fm^2/NV, respectively. The numerical coefficient at l_{12} in q_{111} is in F/V. The remaining numerical coefficients are dimensionless. The number and choice of indices of k_{ijk}, k_{ij} and q_{111} correspond to the first material constant in their definition.

The experimental values of the linear coefficient L and the linear material constants of quartz – the latter taken from BECHMANN [3] – needed in the above calculation are a mixture of quantities determined at 20 or 25°C. Consequently, the values of the nonlinear parameters in Table 1 are understood as valid for room temperature. Considering their existing accuracy (standard errors in Table 1) and their estimated temperature dependence [6] the temperature inconsistency of several degress Celsius is of no practical consequence. Similarly disregarded is the somewhat uncertain and probably nonuniform thermodynamic character of these quantitites which is not necessarily purely adiabatic.

A detailed numerical inspection of the solved system (23) has indicated that the standard errors in the individual parameters are commensurate with the standard errors in the experimental values of L (typically $\pm 0.26\cdot10^{-12}$ m/V). Large relative errors occur in the case of those parameters whose contribution to the measured quantity L is relatively small.

The above comments concerning the thermodynamic character of the results and their standard errors apply to the entire contents of Table 1 with the meaning of Solution 2 yet to be explained.

5. Discussion

One of the principal ideas which inspired this work was a desire to produce values of the third-order nonlinear material constants of quartz exclusively by means of the resonator method and completely independent of any other third-order constants determined earlier or by other methods. It was hoped that among the result would also be the third-order elastic constants. They were intended for an independent verification of their old and only existing values [18] which were never tested in a similar direct manner. However, in spite of abundance of experimental data, the linear system (23) failed to produce a single isolated value of these material constants. It appears that the third-order elastic constants will not be put to test using the present data provided by the resonator method.

The same linear system (23) was solved once before [8]. At that time the values of the third-order elastic constants were substituted into it from [18] and the least-squares procedure applied only to the remaining third-order constants. The solution obtained there is restated in the second part of Table 1 and marked Solution 2.

It is a direct consequence of the multicolinearity detected in the system matrix M that the two solutions in Table 1 are very simply interrelated. Solution 2 can be obtained from Solution 1 if the latter is stripped of the contribution of the third-order elastic constants defined in Table 2 using the values of the third-order elastic constants [18].

When Solution 2 was computed with the aid of the third-order elastic constants taken from [18] it was clear that it would depend, for its quality, on the reliability of the old third-order elastic constants [18]. The existing relationship between Solution 1 and Solution 2 makes it possible to estimate their potential distortive effect. As a function of these constants, the distortion would be a portion of the difference between the corresponding parts of Solution 1 and Solution 2; in relative terms it would be probably larger for the electroelastic constants f_{113} or f_{114} and smaller for the electrostrictive constants l_{11} or l_{14}, and definitely zero for the constants f_{315}, l_{33}, l_{41} and for the combination $l_{31}+2l_{44}$. At the same time, however, it is appropriate to say that there seems to be no evidence available indicating that the existing values of the third-order elastic constants are in any way compromised.

At the time when Solution 1 was sought, the principal objective was the determination of the electroelastic constants of quartz. The decision to use the "imported" values of the third-order elastic constants in the process was a natural one – these constants were already available – and the matter was not given much further thought.

However, had the linear system (23) been able to provide its own values for the third-order elastic constants, then Solution 1 would not have been so simply related to

(i.e. not directly convertible into) Solution 2. Depending on the difference between the imported third-order elastic constants and those provided by system (23) itself, the two solutions could have been in serious conflict and the question of using the values of third-order elastic constants external to the system (23) would have deserved much more attention.

It is only the result of this paper, namely the detected multicolinearity of the system matrix M, which provides a belated but vital reason to conclude that in trying to find the material constants determined in [8] it is impossible to do without the imported third-order elastic constants and that their use creates no conflict. In this sense this work validates the procedure adopted in [8].

Comparing Solution 1 and 2 further on, it is no coincidence that the standard errors for the two sets of quantitites are identical. Their interpretation requires an brief remark. First and foremost the stated standard errors apply to Solution 1, i.e. to the determined parameters k_{111} etc. Only if it is assumed that the third-order elastic constants from [18] are absolutely accurate, then the standard errors may be viewed as truly pertaining to quantites forming Solution 2, i.e. to the material constants f_{111} etc.

The results of this work are completely independent of all nonlinear material constants of quartz determined earlier or by other means. As such they are eminently suitable for comparisons with the results from other sources. This is of considerable interest not only for the sake of mutual verification of their immediate values but possibly also as a consistency test of the related applications of the nonlinear theory.

The comparison is made with a recent set of nonlinear constants listed by ADAM, TICHY and KITTINGER [1], whose values are taken over or derived from the work of BESSON and GAGNEPAIN [4], KITTINGER, TICHY and FRIEDEL [15] and THURSTON, MCSKIMMIN and ANDREATCH [18]. In preparation for the comparison, the values from [1] were substituted into the definitions of the parameters in Table 2. Substituting for the electroelastic constants f_{ijk} there, the third-order piezoelectric constants e_{ijk} from [1] were appropriately used with a reversed sign ($f_{ijk} = -e_{ijk}$). The results of the substitution were placed next to the results of this work into the last column of Table 3.

In most of the cases the differences between the results in Table 3 are comparable with the stated standard errors. This also seems to be the case with parameter q_{111}; however, the calculated standard error there is fairly large and the disagreement in sign is disturbing. On the other hand, there are parameters such as k_{13}, k_{31}, and, to a lesser degree, possibly others, which appear to be in conflict. Going just by the magnitude of their disagreement it is hard to classify it as insignificant.

On the whole the agreement in parameters k_{ijk} which are solely combinations of the third-order elastic and electroelastic constants appears to be better than that attained for the remaining parameters involving (apart from the third-order elastic constants) also electrostriction and third-order permittivity. This seems to agree well with the source of the current values of the electrostrictive constants [15] whose authors consider only one of their values as fairly reliable and advise caution regarding the rest of them.

Numerous comparisons between the nonlinear constants or their combinations

Table 3. Comparison of third-order nonlinear material parameters of alpha quartz obtained from independent sources

Nonlinear parameter	Resonator method this work	Other methods according to [1]
k_{111}	2.38 ± 0.05	2.37
k_{113}	0.29 ± 0.07	0.21
k_{114}	0.63 ± 0.04	0.72
k_{122}	-0.74 ± 0.03	-0.71
k_{124}	1.38 ± 0.02	1.41
k_{134}	1.71 ± 0.03	1.70
k_{144}	-0.03 ± 0.03	0.00
k_{315}	-0.79 ± 0.03	-0.90
k_{11}	-3.2 ± 0.9	-4.7
k_{13}	-8.6 ± 2.6	13.2
k_{14}	-2.4 ± 0.5	-2.2
k_{31}	-12.4 ± 3.0	3.4
k_{33}	-8.4 ± 6.8	-3.9
k_{41}	-4.4 ± 0.7	-4.1
q_{111}	$(-2.9 \pm 2.4) \cdot 10^{-21}$	$0.6 \cdot 10^{-21}$

Both parameter sets are calculated using the linear elastic constants according to [16] and the linear piezoelectric and dielectric constants according to [3]. Other relevant remarks are the same as for Table 1.

originating from various sources have been done before. As a rule the compared nonlinear constants were calculated using different sets of linear constants. This omission is rectified here. To achieve consistency with [1] the results of this work were recomputed using the elastic constants from McSKIMMIN, ANDEREATCH, and THURSTON [16] before they were entered into Table 3.

Given that a different set of elastic constants is used to make the comparison, the numerical coefficients in Table 2, depending on the linear material constants, have also changed. Their change is, however, very small, beyond the number of displayed decimal digits. As a result, no new version of Table 2 needs to be included in this paper. This entire comment is made only to assure the reader that such a possibility has been taken into account.

The effect of the linear constants on the nonlinear ones may be an interesting one but, at the same time, one that has been paid very little attention to. The comparison between the results of this work in Table 1 and 3 offer a qualitative preview of what can be expected.

6. Conclusion

This paper represents an attempt to determine simultaneously all four electromechanical nonlinearities existing in quartz: the third-order elasticity, the electroelasticity, the electrostriction and the third-order permittivity.

Fifteen parameters, for the main part linear combinations of the independent material constants describing these phenomena in quartz, have been determined using the least-square fit to one hundred and eighty-four experimental data provided by the resonator method.

The main reason for the number of determined parameters to be limited to 15 instead of the full number of 31 fundamental constants is a numerical one. The same numerical phenomenon provides a valuable insight into the function of the third-order elastic constants in the process of determination of the remaining nonlinearities (electroelasticity, electrostriction, third-order permittivity) by means of the resonator method. In particular, it shows that in order to determine these latter nonlinearities the use of third-order elastic constants from an external source cannot be avoided.

The work is a classical example of an independent verification process. The comparisons made with the nonlinearities determined separately by different authors and methods show an encouragingly high degree of agreement. At the same time, however, a few instances were noted with differences which may be statistically significant.

This study is based on a substantially larger number of observations (184) than is the total number of data (59) which have produced the values of the third-order electromechanical constants of quartz [1] external to this work. As such the present results carry some statistical weight. Any cases of disagreement between them and [1] are thus difficult to dismiss without an appropriate explanation which is yet to be found.

Acknowledgements

The author is obliged to Miss P. HRUSKA for her assistance with the final stages of preparation of this paper. This work was supported by a grant from the Faculty of Arts, York University and from the National Sciences and Engineering Research Council of Canada.

References

[1] W. ADAM, J. TICHY, E. KITTINGER, *The different sets of electrical, mechanical, and electromechanical third-order constants for quartz*, J. Appl. Phys., **64**, 5, 2556–2562 (1988).

[2] J. C. BAUMHAUER, H. F. TIERSTEN, *Nonlinear electroelastic equations for small fields superposed on bias*, J. Acoust. Soc. Am., **54**, 4, 1017–1034 (1973).

[3] R. BECHMANN, *Elastic and piezoelectric constants of alpha-quartz*, Phys. Rev., **110**, 5, 1060–1061 (1958).

[4] R. BESSON, J. J. GAGNEPAIN, *Determination des coefficients nonlineaires de polarisation electrique du quartz*, C.R. Acad. Sci., Paris **B274**, 835–838 (1972).

[5] R. BRENDEL, *Material nonlinear piezoelectric coefficient for quartz*, J. Appl. Phys., **54**, 9, 5339–5346 (1983).

[6] C. K. HRUSKA, *Temperature coefficients of the electroelastic constants of quartz*, IEEE Trans. UFFC, **35**, 5, 637–640 (1988).

[7] C. K. HRUSKA, *Determination of the third-order piezoelectric constants of quartz using the extentional mode of rods*, J. Appl. Phys., **66**, 3, 1071–1074 (1989).

[8] C. K. HRUSKA, *The electroelastic tensor of quartz determined by the resonator method*, J. Appl. Phys., **68**, (1990), in press.

[9] C. K. HRUSKA, *Determination of the complete tensor of nonlinear piezoelectricity of quartz using the resonator method*, Proc. of the 4th European Frequency and Time Forum, Communautes Scientifiques de Besançon (France) et Neuchatel (Switzerland), Neuchatel 1990, in press.

[10] C. K. HRUSKA, R. BRENDEL, *Combinations of the electroelastic and electrostrictive constants of quartz determined using the thickness modes of plates*, J. Appl. Phys., **67**, 4, 1676–1679 (1990).

[11] C. K. HRUSKA, R. BRENDEL, *The electroelastic constants of quartz determined by the resonator method*, J. Appl. Phys., **65**, 2, 715–717 (1989).

[12] K. HRUSKA, A. KHOGALI, *Polarizing effect with alpha-quartz rods and the electroelastic tensor*, IEEE Trans. SU, **18**, 2, 171–176 (1971).

[13] C. K. HRUSKA, H. MERIGOUX, M. KUCERA, *Linear frequency-dc field effect on the thickness modes of alpha-quartz plates*, J. Can. Ceram. Soc., **57**, 2, 53–57 (1988).

[14] E. KITTINGER, J. TICHY, *Electroelastic effect of crystal rods expressed by fundamental material constants*, J. Acoust. Soc. Am., **83**, 2, 647–651 (1988).

[15] E. KITTINGER, J. TICHY, W. FRIEDEL, *Nonlinear piezoelectricity and electrostriction of alpha quartz*, J. Appl. Phys., **60**, 4, 1465–1471 (1986).

[16] H. J. MCSKIMMIN, P. ANDREATCH Jr, R. M. THURSTON, *Elastic moduli of quartz versus hydrostatic pressure at 25°C and −195.8°C*, J. Appl. Phys., **36**, 5, 1624–1632 (1965).

[17] D. F. NELSON, *Theory of nonlinear electroacoustics of dielectric, piezoelectric, and pyroelectric crystals*, J. Acoust. Soc. Am., **63**, 6, 1738–1748 (1978).

[18] R. N. THURSTON, H. J. MCSKIMMIN, P. ANDREATCH Jr, *Third-order elastic coefficients of quartz*, J. Appl. Phys., **37**, 1, 267–275 (1966).

[19] H. F. TIERSTEN, A. BALLATO, *Nonlinear extentional vibrations of quartz rods*, J. Acoust. Soc. Am., **73**, 6, 2022–2033 (1983).

[20] *IEEE Standard on Piezoelectricity*, IEEE Std 176–1978, IEEE, New York, 1978, pp. 18–21, 25–27.

[21] A. KINIGADNER, *Elektromechanische Nichtlinearitaeten von Alpha Quarz*, Ph.D. Thesis, University of Innsbruck, Austria 1978, p. 91.

[22] W. MENDENHALL, T. SINCICH, *A second course in business statistics: Regression analysis*, Collier Macmillin Publishers, London, 2nd edition, 1986, pp. 150–159.

ARCHIVES OF ACOUSTICS
16, 1, 121-126(1991)

MONOLITHIC CRYSTAL FILTERS USING LITHIUM TANTALATE CRYSTAL

I. MATEESCU*, G. GACKOWSKA**, G. KORONY*, C. BORA*

* Institute of Physics and Technology of Materials Bucharest, Romania
** Institute of Fundamental Technological Research Polish Academy of Sciences
(00-049 Warszawa Świętokrzyska 21)

The characteristics of lithium tantalate crystal filters and the method of their design are described. The experimental results are presented and discussed.

1. Characteristics of $LiTaO_3$ filters

The large electromechanical coupling coefficient of lithium tantalate allow for a much wider band of filters than that achieved with quartz. Traditionally used in resonators and monolithic filters with good results. *AT*-cut quartz posses a low electromechanical coupling coefficient ($\sim 9\%$), which restricts the maximum available filter bandwith to approximately 0.3% of the centre frequency for the fundamental mode of operation.

Lithium tantalate has a coupling coefficient about 40%, which makes possible the construction of filters with a bandwith of up to 6% at fundamental frequency ([1], [2]).

For monolithic filters the vibrational mode structure of the plate should be dominated by a single thickness shear mode with strong electromechanical coupling, low temperature coefficient of frequency, freedom from competing modes.

These conditions are satisfied in $LiTaO_3$ crystals by *Y* 163°-cut. Having a strong shear mode with a good isolation from the competing mode, this cut has the disadvantage of having a poor temperature coefficient of resonance frequency. For *AT*-cut quartz it is ± 0.2 ppm/°C and for *Y* 163°-cut $LiTaO_3$, it is -22 ppm/°C ([3], [4]).

Figure 1 illustrates a $LiTaO_3$ *Y*-163° rotated *Y*-cut plate.

The direction of particle displacement lies within 3° of the *Z'* axis so that the mode is close to a pure shear mode. Because of this, the *TS* mode is along the *Z'*-axis for the lithium tantalate *Y* 163°-cut, but for *AT*-cut quartz the *TS* mode is along the axis.

Orientation precision of $LiTaO_3$ plates is less ($\pm 6'$) than for *AT*-cut quartz ($\pm 1'$).

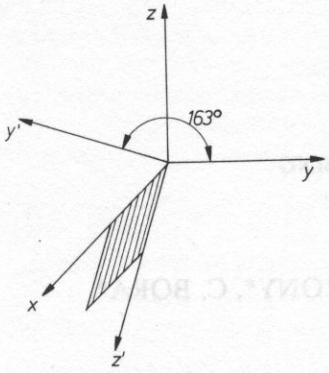

FIG. 1. The 163° rotated Y-cut $LiTaO_3$ plate

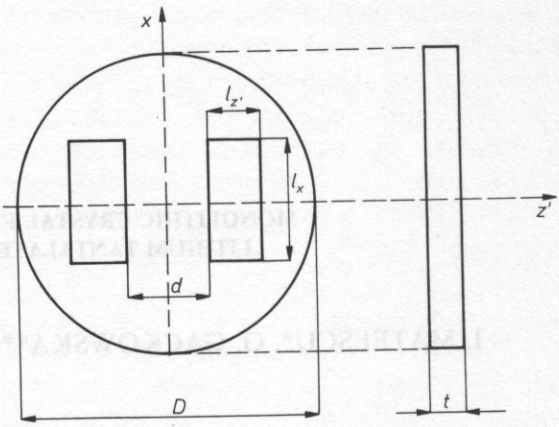

FIG. 2. Two-pole monolithic crystal filter

Lithium tantalate monolithic crystal filters provide a wide band of filters in the frequency range for centre frequency 10–100 MHz. $LiTaO_3$ plates require poling in a d.c. field. Lithium tantalate crystal is very sensitive to thermal shocks.

2. Design of monolithic $LiTaO_3$ crystal filters

The filtering operation is done on a single piezoelectric plate if a number of resonator pairs are deposited so that acoustic coupling can take place between them. Figure 2 presents a monolithic crystal filter with two resonators coupled in the Z'axis direction.

For lithium tantalate crystal in Z' coupling direction (*TS* mode) bandwith is wider than for coupling direction(*TT* mode).

Figure 3 shows the electrical equivalent circuit of a symmetric two-pole filter. It is compatible with that used for quartz filters. Filter network design with lithium tantalate crystal follows a similar procedure to the quartz approach.

There are three steps of monolithic filter design: synthesis, analysis and calculation of geometrical dimensions. For all steps we used the method and computing programme for quartz monolithic filters [5] adapted to $LiTaO_3$ crystals.

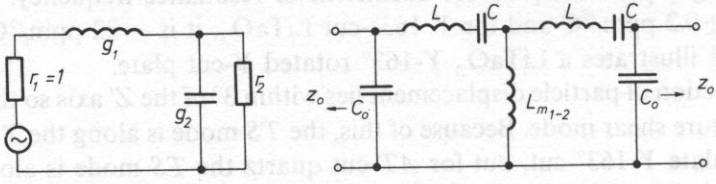

Fig. 3. Equivalent network for a high-coupling dual resonator

Specific piezoelectric, elastic and dielectric constants and relation between the electrical parameters of the network (Fig. 3) and the physical characteristics of the dual resonator are used in this programme.

The most important and useful relations are [6], [7]

$$L = \frac{0.154 N_m^2}{A f_m^3}\left[1 - \frac{0.224 m^2}{N_m^2}\right] \tag{1}$$

where A – area of electrode (mm^2), f_m – m^{th} order of frequency resonance (MHz), m – order resonance, N_m – frequency constant (MHz mm), L-inductance (H).

$$f_m = \frac{N_m}{t} \tag{2}$$

where t – thickness of the plate (mm).

The values of N_m for $LiTaO_3$ $Y\,163°$-cut are

$N_1 = 1.845$ MHz mm for fundamental frequency operation

$N_3 = 5.922$ MHz mm for third overtone frequency operation

$$A = l_x l_{z'} \tag{3}$$

where l_x and $l_{z'}$ are the dimensions of the electrodes. For fundamental frequency operation

$$\frac{l_{z'}}{t} \leq 9; \quad \frac{l_x}{t} \leq 5 \tag{4}$$

and for third overtone frequency operation:

$$\frac{l_{z'}}{t} \leq 8; \quad \frac{l_x}{t} \leq 4.5 \tag{5}$$

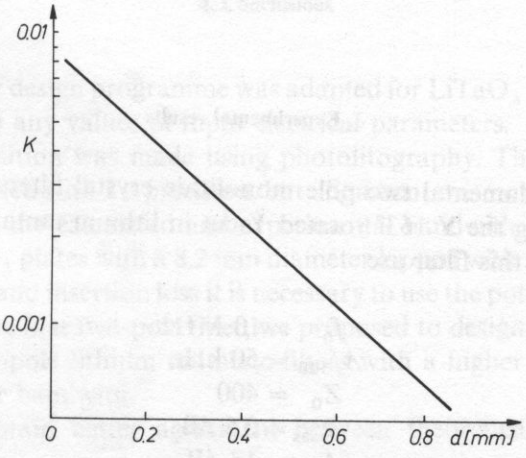

FIG. 4. Thickness shear inter-resonator coupling against electrode spacing

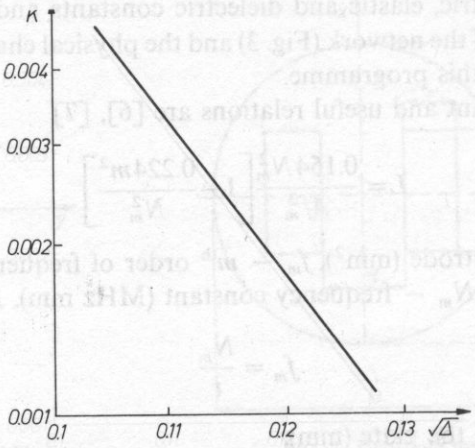

FIG. 5. Thickness shear inter-resonator coupling against square of plate back

The expression of inter-resonator coupling K has the form ([1], [8])

$$K = A\exp[-B(1-2\Delta^{1/2})\Delta^{1/2}d/t] \tag{6}$$

where A – function of electrode dimensions, d – inter-resonator spacing, A, B – functions of the coupling direction (TT or TS mode), Δ – plate back fractional frequency lowering produced by plating.

Figures 4 and 5 illustrate the dependence between the coupling coefficient and the distance d of the electrodes and plate back. From these curves we deduced the values for A and B.

3. Experimental results

Prototype fundamental two-pole monolithic crystal filters have been designed and fabricated using the Y 163° rotated Y-cut in lithium tantalate crystal.

Input data for this filter are:

$$\begin{aligned} f_0 &= 10 \text{ MHz} \\ \Delta f_{3\text{dB}} &= 50 \text{ kHz} \\ Z_0 &= 400 \\ A_{\max} &= 0.5 \text{ dB} \\ A_{\min} &= 18 \text{ dB}. \end{aligned}$$

The frequency response of this filter is shown in Fig. 6, the measuring specification being:

$$f_0 = 9{,}998 \text{ MHz}$$
$$f_{3\text{dB}} = 48 \text{ kHz}$$
$$A_{\max} = 0.8 \text{ dB}$$
$$A_{\min} = 20 \text{ dB}$$

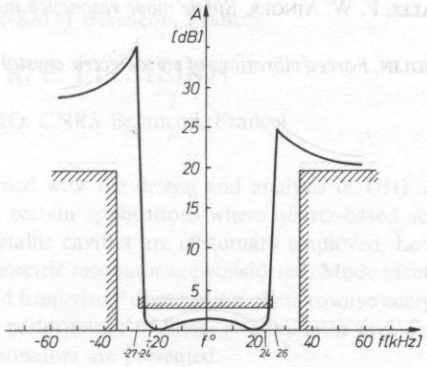

FIG. 6. Response of two-pole $LiTaO_3$ filter

4. Conclusions

The quartz filter design programme was adapted for $LiTaO_3$ $Y163°$-cut; it is good to design filters with any values of input electrical parameters.

Electrode deposition was made using photolitography. The dimensions of the electrode were obtained with 2 μ precision, but alignment was not too good; there was a difference between the calculated and experimental bandwith.

We used $LiTaO_3$ plates with a 8.2 mm diameter lapped with 3 μ abrasive powder, but to reduce the inband insertion loss it is necessary to use the polished crystal blanks.

Starting from the first two-pole filter, we proposed to design design and to make experimentally eight-pole lithium tantalate filters with a higher frequency overtone function and a wider bandwith.

We hope to obtain better agreement between theoretical and experimental resultas.

References

[1] M. C. HALES, T. W. BURGESS, *Design and construction of monolithic crystal filters using lithium tantalate*, Proc. of IEE, **123**, p. 657 (1976).

[2] B. GNIEWIŃSKA, Cz. KLIMEK, W. SOLUCH, *Rezonatory i generatory kwarcowe.*

[3] T. W. BURGESS, M. C. HALES, *Temperature coefficient of frequency in* $LiNbO_3$ *and* $LiTAO_3$ *plate resonators*, Proc. of IEE, **123**, p. 499 (1976).

[4] R. T. SMITH, F. S. WELSH, *Temperature dependence of the elastic, piezoelectric and dielectric constants of lithium tantalate and lithium niobate*, J. Appl. Phys., p. 2219 (1976).

[5] I. MATEESCU, *Filtre monolit cu cuart*, Teza de doctorat (1987).

[6] T. W. BURGESS, M. C. HALES, R. T. PORTER, *Equivalent circuit parameters for* $LiTaO_3$ *plate resonators*, Electr. Lett., **11**, p. 449, (1975).

[7] T. W. BURGESS, M. C. HALES, F. W. AINGER, *Single mode resonance in* $LiNbO_3$ *for filter design*, Electr. Lett., **9**, 251 (1973).

[8] H. F. TIERSTEN, R. D. MINDLIN, *Forced vibrations of piezoelectric crystal plates*, Q. Appl. Math., **20**, p. 107 (1962).

ARCHIVES OF ACOUSTICS
16, 1, 127-136(1991)

INVESTIGATIONS ON DIELECTRIC RESONATORS FOR APPLICATIONS BELOW 1 GHz

M. VALENTIN

(ENSMM Besançon, France)

R. E. ELCHEIKH

(LPMO: CNRS Besançon, France)

This paper is concerned with the design and analysis of UHF dielectric resonators operating below 1 GHz in certain applications where quartz-based acoustic resonators of modest performance or metallic cavities are customary employed. Lowest-order modes of circular and rectangular dielectric resonator are considered. Mode identification is obtained with a network analyzer and from visual observation of microwave energy detected by liquid crystal plates. Design and performance of filter, discriminator and oscillator using partly metallized $\lambda/4$ dielectric resonators are presented.

Introduction

Bulk Acoustic Wave Resonators (BAWR), Surface Acoustic Wave Resonators (SAWR), metallic cavities and Dielectric Resonators (DR) are used for filters, for the stabilization of fundamental frequency oscillators. In the 1 GHz frequency range, IF oscillators use crystal oscillators to achieve the necessary phase noise performance and the short term stability. The crystal oscillator frequency is increased to the required generator frequency by multiplication chains. In order to maintain the required long term stability the crystal oscillator has to be stabilized by means of an extremely stable low frequency reference signal (5 MHz). Multiplication increases the phase noise, requires filters with high out-of-band attenuation and provides spurious frequency lines. This method, in addition to being complex and costly, has a low efficiency and is possible only for low powers.

Because of these problems it would be better to utilise a highly stable source which is already in the IF frequency range.

Because of their size, metallic cavities are not very compatible with the structure of Microwave Integrated Circuits (MIC). Efforts have therefore long been made to replace these resonators by ceramic type and dielectric resonators have brought significant improvement in the design of microwave oscillators, filters and discriminators.

The existence of low-loss high dielectric resonators has been known for some time. A high dielectric material in free space exhibits radiation damping. If dielectric-constant is high ($\varepsilon_r \gg 1$) the relative damping is small enough to allow the dielectric to resonate. Compactness, light weight, temperature stability, relative low costs, integration are improvements brought by dielectric resonator in microwave components.

Dielectric resonators function as low as 1 GHz to as high as 35 GHz. At the low end, the dielectric resonator is relative large and is thus not conducive to compact designs; at the high end, losses and dimensions become difficult to control. For these reasons, most DR applications are in the range of 2 to 30 GHz.

In this paper circular and rectangular dielectric resonator are analyzed for applications in Microwave Integrated Circuits below 1 GHz. A dielectric waveguide is constructed from two parallel metallic strips and a dielectric slab of rectangular cross section between strips and contacting each of the strips. This line is capable of extremely brod-band and high power operation and is used for realizing compact dielectric resonator in 800/900 MHz frequency bands for land mobile satellite communication systems.

1. Natural resonant frequencies of dielectric resonators

1.1. Circular dielectric resonator

The study of electromagnetic waves in dielectric waveguide [1], [2], [3], [4] is very helpful in understanding the operation of dielectric resonators. The shape of a dielectric resonator is usually a short solid cylinder or a rectangular block.

The electromagnetic fields in dielectric resonator of high permittivity ($\varepsilon_r > 100$) satisfy well the open-circuit boundary condition (OCB) of a magnetic wall: at the OCB the normal component of electric field and the tangential component of magnetic field vanish. By duality principle, the TM field patterns with magnetic boundary conditions are the same as those for the TE modes with electric boundary conditions.

In the following experiments, used material (Zr, Sn) TiO_4 offers low temperature coefficient, a dielectric constant $\varepsilon_r = 37$. So, to obtain a better solution for circular dielectric resonator, the field is considered inside the rod and outside the rod. Unlike the components inside, the components outside are to be exponentially decaying in the radial direction. The eigenvalue equation for the dielectric rod waveguide of radius a is {2}:

$$\left[\frac{J'_m(x)}{x}+\frac{F(x)}{\varepsilon_r}\right]\left[\frac{J'_m(x)}{x}+F(x)\right]-\frac{\beta^2 a^2 m^2}{\varepsilon_r (k_0 a)^2}J_m(x)^2\left[\frac{1}{x^2}+\frac{1}{y^2}\right]^2=0 \tag{1}$$

where

$$F(x)=\frac{K'_m(y)J_m(x)}{yK_m(y)} \tag{2}$$

$$y = [(k_0 a)^2(\varepsilon_r - 1) - x^2]^{1/2} \tag{3}$$

$$x = [k_0^2 \varepsilon_r - \beta^2]^{1/2} a \tag{4}$$

J_m is the Bessel function of the first kind and mth order, K_m the modified Bessel function of the second kind, $k_0 = 2\pi/\lambda_0$ the wave number of free space, β the waveguide propagation constant and x_{mn} the eigenvalues.

The eigenvalue diagram of Fig. 1 which is a tool for identifying the various modes of a dielectric resonator, gives the eigenvalues as functions of the normalized frequency $k_0 a$ for TE_{mn}, TM_{mn} and hybride HEM_{mn} modes in the dielectric rod for the experiment value of $\varepsilon_r = 37$. The HEM_{11} mode is the dominant mode of the rod and has no low-frequency cut off. For a rod of radius $a = 1.74$ cm the wavelength obtained from the diagram is $\lambda_g = 6.9$ cm at frequency 1 GHz and $\lambda_g = 2.9$ cm at frequency 2 GHz.

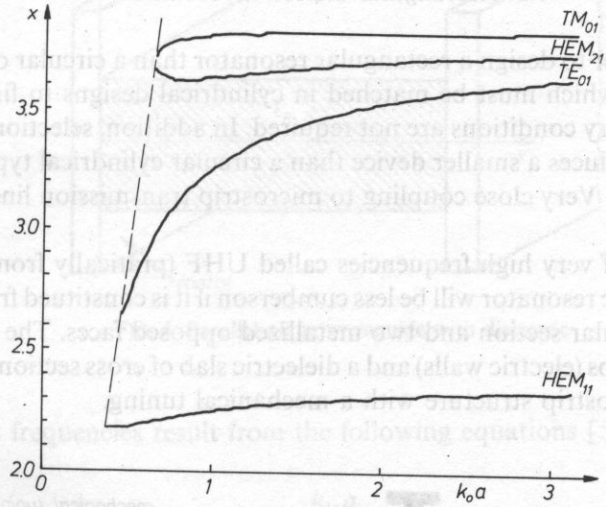

FIG. 1. Eigenvalue diagram of dielectric rod waveguide ($\varepsilon_r = 37$)

For a cylindrical rod of lenght I assuming that only flat surfaces satisfy the OCB condition, the value of x_{mnp} at resonance is:

$$x_{mnp} = \left[k_0^2 \varepsilon_r - \left(\frac{p\pi}{1} \right)^2 \right]^{1/2} a \tag{5}$$

The lowest resonance frequency belong to the HEM_{111} resonance and the next higher is TE_{011} mode. The most consistent results were obtained with the TE_{011} mode for which no electric field component existe normal to the dielectric surface. Fig. 2 shows resonant modes for a dielectric resonator ($a = 1.74$ cm, $l = 1.54$ cm) coulped in reaction to microstrip line.

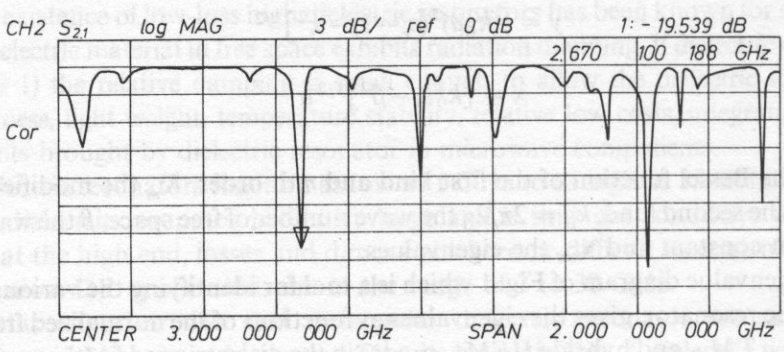

FIG. 2. Transmission coefficient of a circular dielectric resonator ($\varepsilon_r = 37$; $a = 1.74$ cm; $l = 1.54$ cm)

1.2. Rectangular dielectric resonator

It is much easier to design a rectangular resonator than a circular one: Bessel and Hankel functions, which must be matched in cylindrical designs to find a root that satisfies the boundary conditions are not required. In addition, selection of the proper resonant mode produces a smaller device than a circular cylindrical type designed for the same frequency. Very close coupling to microstrip transmission line can be easily obtained.

In the range of very high frequencies called UHF (pratically from 300 MHz to 3 GHz) the dielectric resonator will be less cumberson if it is constitued from a dielectric line with a rectangular section and two metallized opposed faces. The structure with two conducting strips (electric walls) and a dielectric slab of cross section $a \times b$ is shown on Fig. 3 in a microstrip structure with a mechanical tuning.

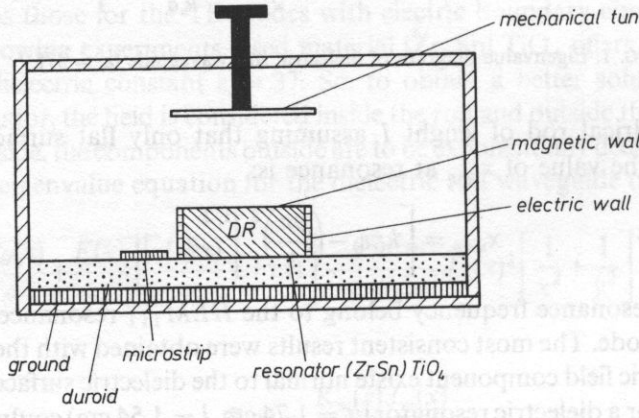

FIG. 3. Rectangular resonator in a microstrip structure

For high dielectric constant this line may be treated as a waveguide bounded by two magnetic walls and two electric walls. The fundamental mode is a quasi TEM mode. Small resonators ($b < \lambda_g/2$ where λ_g is the waveguide wavelength) are treated as line resonators and classified as quasi TEM resonator. A quarter wave resonator is obtained by metallizing an extremity of a $\lambda_g/4$ length line. With larger width b, resonances with a field dependence on the x as well as on the z coordinate can be excited. These resonances can be analyzed from the parallel plane waveguide partially filled with a dielectric (Fig. 4). TE and hybrid modes can propagate on this line. The lowest order TE_{10} mode, which is the dominant mode, has no cut off and is well suited for operation in UHF band.

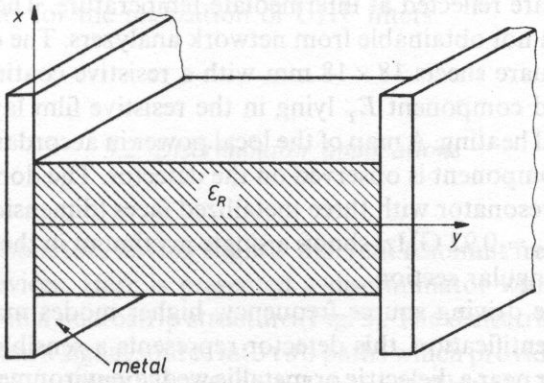

FIG. 4. Parallel plane waveguide with dielectric

Resonant frequencies result from the following equations [5]:

$$(k_0 a)^2(\varepsilon_r - 1) = \frac{k_{1e}a}{\cos k_{1e}a}, \quad \text{even modes} \tag{6}$$

$$(k_0 a)^2(\varepsilon_r - 1) = \frac{k_{10}a}{\sin k_{10}a}, \quad \text{odd modes} \tag{7}$$

where $k_1^2 = \omega^2 \mu_0 \varepsilon_1 - \beta^2$ is related to the propagation constant β, frequency ω and properties of the dielectric (μ and ε_1); $(k_{1e}a)$ must be between 0 and $\pi/2$, π and $3\pi/2$ ... and $(k_{10}a)$ must be between $\pi/2$ and π, $3\pi/2$ and 2π ... Single mode (TE_{10}) can exist if:

$$k_0 a < \frac{\pi}{2\sqrt{\varepsilon_r - 1}} \tag{8}$$

2. LIQUID crystal: an aid in the design and test of dielectric resonator

The evanescent nature of the field patterns requires that the resonator is screened by a metallic housing to avoid radiation losses and environmental influences. Providing the metallic walls are sufficiently distant from the resonator, conduction losses in housing are minimal. Much work has been undertaken in order to establish theories for resonant frequencies and in order to allow unambiguous identification of higher order mode pattern.

The technique of using liquid crystal detector plates for visual observation of microwave energy provide a quick and effective means to identify modes by looking the field map. The liquid crystal used in the present experiments is encapsulated with an active temperature range of 26–39°C. It reflects red light at 27°C and blue light at 33°C. Intermediate colors are reflected at intermediate temperature. The detector provides a type of information not obtainable from network analyzers. The devices used in this paper are several square sheets 18×18 mm with a resistive coating.

The electric field component E_T lying in the resistive film layer generates local currents causing local heating. A map of the local power in accordance with the square of the electric field component is observed on the detector. The dominant mode of the quarter wavelength resonator with three metallized faces (dimensions: $18 \times 6 \times 6$ mm, resonant frequency $f_0 = 0{,}92$ GHz) shows a single maximum in the electric field in the non metallized rectangular section.

By adjusting the driving source frequency, higher modes may be observed. In addition to mode identification, this detector represents a sensible test for radiation losses, field behaviour near a dielectric or metallic wedge, environmental influences and aid the designer in the dielectric resonator implementation.

3. Dielectric resonator applications

All resonators are made of (Zr Sn) TiO_4 ($\varepsilon_r = 37$) with a O ppm/°C $\pm$0.5 ppm/°C temperature coefficient [6]. Passive devices (filters, discriminators) and active devices (oscillators) containing dielectric resonators are presented.

At frequencies higher than 2 GHz, only circular cylindrical resonators are considered. At about 900 MHz the physical dimensions of circular dielectric resonator are too large: only partly metallized dielectric resonator are used. Resonators are on a dielectric substrat (RT Duroid 6010) in the vicinity of 50 Ω microstrip lines. Resonant frequencies of rectangular resonator of dimensions $10 \times 10 \times 18$ mm and $7 \times 8 \times 16.5$ mm are 0. 88 GHz and 1.01 GHz respectively. Size reduction is obtained but metallic losses are increased. An unloaded Q, $Q_u = 600$, is measured with additional conductor losses at 0. 88 GHz.

3.1. Filter applications [7] [8]

Band pass filters are provided by a section of evanescent waveguide in which dielectrics resonators are inserted and directly coupled to each other. A band pass filter operating at X Band was constructed utillizing circular cylindrical resonators. The mode – chart (eigenvalue diagram) is a useful first step for filter design. The resonant frequency of each resonator, coupling coefficients between adjacent resonators and external Q'_s were adjusted so as to produce the desired filter response. Bandwidths up to 1.5% are obtained with two coupled dielectric resonators in a monomode tuning configuration. Insertion losses smaller than 0.5 dB are obtained. For greater bandwidths, several resonant mode are used.

Rectangular dielectric resonators mounted in planar microstrip line circuitry provide an easy way for the realization of UHF filters.

3.2. Discriminator applications

Usually two resonators having slightly different resonant frequencies are utilized in discriminator devices. Here is presented a discriminator with only one dielectric resonator mounted in a microstrip structure (Fig. 5). The dielectric resonator splits the signal emanating from a signal source into two paths which provide signal inputs to the double-balanced mixer (DBM). A differential delay of the two signal paths for phase quadratur, together with the mixer and resonator functions as a frequency discriminator [9]. The resonator acts as a stop band filter between ports 1 and 2 and as pass band filter between ports 1 and 3. The phases $\phi_{21}(\omega)$ and $\phi_{41}(\omega)$ of $S_{21}(\omega)$ and $S_{41}(\omega)$ transmission coefficient at mixer inputs are represented on Fig. 6. The slope of "S" curve of the discriminator was measured to be 300 mV/MHz.

The device converts the frequency fluctuations into voltage fluctuations which can be monitored and measured with an appropriate spectrum analyzer.

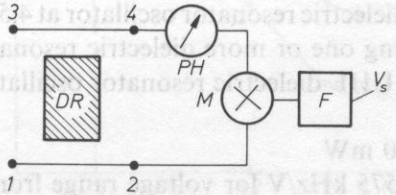

FIG. 5. Dielectric resonator discriminator

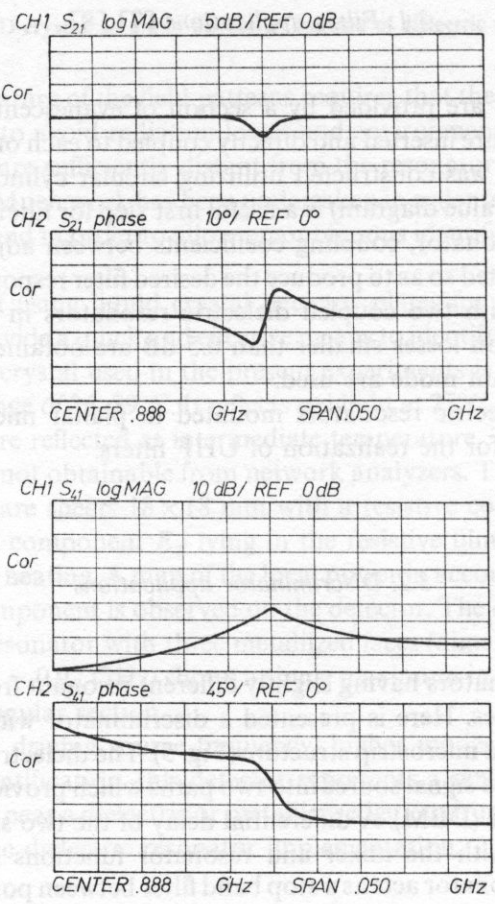

FIG. 6. $S_{21}(\omega)$ and $S_{41}(\omega)$ parameters of a four port dielectric resonator

3.3. *Oscillator applications*

Dielectric resonators can be directly used as an oscillator circuit element for feedback, matching, frequency determining, ... [10], [11], [12] [13]. PLOURDE [8] was the first to report a stable dielectric resonator oscillator at 4.5 GHz. New configurations have been developped using one or more dielectric resonators.

The performances of UHF dielectric resonator oscillator operating at 0.88 GHz are:

A output power of 50 mW
A pushing figure of 575 kHz/V for voltage range from 8 V to 11 V
A mechanical tuning over 51 MHz with output variation less 1 dB
An electrical tuning over 1.15 MHz with a varactor tuning
A frequency drift of $-$ 4 ppm/°C for temperature range from 20°C to 50°C

A frequency stability expressed as Allan's variance $\sigma_y(\tau)$ of $3.5\ 10^{-9}$ in the range 0.1 second to 10 seconds

A fractional frequency change < 3.6 ppm (observed during 12 days)

A frequency variation less than $-$ 13 kHz over the temperature range from 10°C to 50°C.

The short term stability is presented on Fig. 7, for a dielectric resonator (18 × 6 × 6 mm) which presents a common point of oscillation frequency corresponding to a bias voltage $V_B = 10.6$ V (Fig. 8).

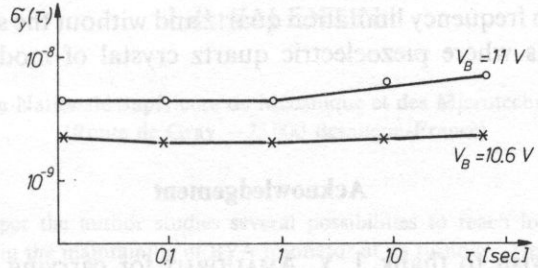

FIG. 7. Short term frequency stability: Allan's variance $< \delta_y(\tau) >$ versus the averaiging time

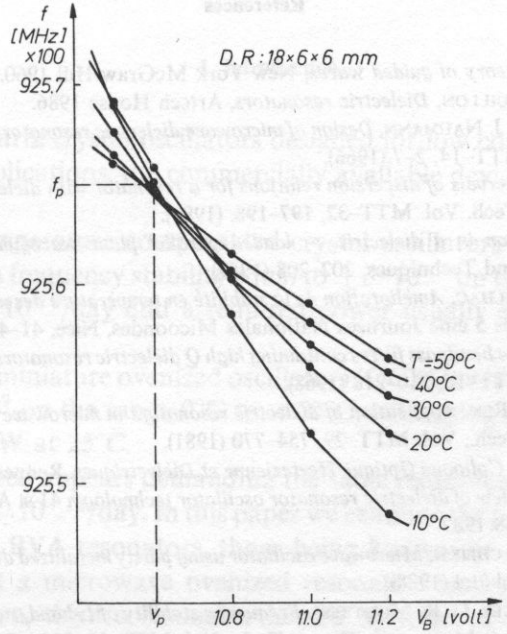

FIG. 8. Oscillation frequency as a function of the bias voltage V_B with the temperature T(°C) taken as parameter

For more frequency control, the same dielectric resonator can be used both as a feedback element and as dispersive element of a frequency discriminator. The DC output signal of the discriminator will be amplified and then applied to amplifier bias [14].

4. Conclusions

The dielectric resonators are readily applicable for compact, light weight, mobile systems used in the field of communication, surveillance and instrumentation. Results of experiments showed the feasibility of stable dielectric resonator at frequencies below 1 GHz without high frequency limitation quartz and without the supplying difficulty in certain applications where piezoelectric quartz crystal of modest performance are currently used.

Acknowledgement

The authors wish to thank J. Y. AMAUDRUT for carrying out numerically the evaluation of the eigenvalues for the hybride modes.

References

[1] R. E. COLIN, *Field theory of guided waves*, New York McGraw-Hill 1960.
[2] D. KAJFEZ and P. GUILLON, *Dielectric resonators*, Artech House 1986.
[3] J. C. SETHARES and S. J. NAUMANN, *Design of microwave dielectric resonators*, IEEE Trans. Microwave Theory Tech. Vol. MTT–14, 2–7 (1966).
[4] V. BILIK, *One-root intervals of dispersion relations for a resonator with dielectric sample*, IEEE Trans. Microwave Theory Tech. Vol. MTT–32, 197–198, (1984).
[5] M. COHN, *Propagation in a dielectric – loaded parallel plane waveguide*, IRE Transactions on Microwave Theory and Techniques, 202–208 (1959).
[6] J. C. MAGE, B. MARCILHAC, *Amélioration de la stabilité en température des matériaux pour résonateurs diélectriques*, Actes des 5 ème Journees Nationales Micoondes, Nice, 41–43 1987.
[7] S. B. COHN, *Microwave bandpass filters containing high Q dielectric resonators*, IEEE Trans. Microwave Theory Tech. Vol. MTT–16, 210–218 (1968).
[8] J. K. PLOUDRE, C. L. REN, *Application of dielectric resonators in microwave components*, IEEE Trans. Microwave Theory Tech., Vol. MTT–29, 754–770 (1981).
[9] M. VALENTIN, *10 ème Colloque Optique Hertezienne et Diélectriques*. Rennes – sept. 1989 p. 163–166.
[10] A. P. S. KHANNA, *Review of dielectric resonator oscillator technology*, 41 st Annual Frequency Control Symposium, pp. 60–68 1987.
[11] M. VALENTIN, R. E. ELCHEIKH, *Microwave oscillator using partly metallized dielectric resonator*. Proc, of the 2 nd EFTF, Neuchâtel (1988).
[12] J. LOBODA, T. E. PARKER, G. K. MONTRESS, *Frequency stability of L-band, two-port dielectric resonator oscillators*, IEEE Trans. Microwave Theory Tech., Vol. MTT–35, 1334–38 (1987).
[13] M. VALENTIN, *Bruit de phase et de fréquence de résonateurs diélectriques*, In: Interaction of radiation with matter a volume in honour of A. Gozzini, Scuolo Normale Superiore, Pise, 174–185, 1987.
[14] Z. GALANI et al., *Analysis and design of a single-resonator GaAs FET oscillator with noise degeneration.* IEEE Microwave Theory Tech., Vol. MTT 32, 1556–65 (1984).

ARCHIVES OF ACOUSTICS
16, 1, 137-148(1991)

LOW CONSUMPTION BVA RESONATORS

J.-P. VALENTIN

Ecole Nationale Supérieure de Mécanique et des Microtechniques
(Route de Gray – 25 000 Besançon-France)

In this paper the author studies several possibilities to reach low consumption of electrical power in the maintaining of BVA resonator at its turnover. Heatings by dielectric losses, by deposited resistors, by infrared radiations and by acoustic losses are examined. The results of calculations and experiments are presented and discussed. Two solutions are rejected because no convenient for low consumption or for weak aging. The retained solutions could open a new way for manufacturing of minature ovenized resonators.

1. Introduction

Concerning quartz crystal oscillators designed for low consumption, low power and low volume applications, the commercially available devices correspond to both following areas:

– first, the temperature compensated crystal oscillators (TCXO) providing, in the case of the best, a frequency stability equal to $\pm 3 \cdot 10^{-7}$ on the range $-40° + 70°C$, with an aging of $\pm 10^{-8}$/day and a required power usually equal to 70 mW at all temperatures.

– second, the miniature ovenized oscillators (OCXO) which provide a frequency stability of $\pm 5 \cdot 10^{-9}$ on the range 0°C to +50°C, with aging of $\pm 5 \cdot 10^{-10}$/day and power about 300 mW at 25°C.

Today a new need appears demanding the same requirements what the last one, but with aging of $\pm 5 \cdot 10^{-11}$/day. In this paper we examine the possibilities to reach the previous goal using BVA resonators, those being known for their weak aging. The possibilities are first a microwave ovenized resonator, second a resonator directly heated by conduction, third a resonator heated by infrared radiations and at last a resonator using an internal heating provided by acoustic losses.

For all these devices only the heart of the resonators is ovenized. Indeed, in the area of low consumption, the available heating power is very weak. So, heating is applied inside the can and not outside the can like is the case for usual ovens.

2. Microwave ovenized resonator

A basic idea is the quartz material can be heated by the means of dielectric loss. That last one occurs inside the bulk material in an homogeneous process and independently from thermal conductivity of the quartz crystal. First indication of that principle has been proposed by BESSON and DECAILLIOT [5]. The frequency range choosen is 2 to 4 GHz because of the commercial avaibility of microwave sources. For that frequency range the loss angle corresponds to $\mathrm{tg}\delta = 2.5 \cdot 10^{-4}$. The power P delivered per unit volume is given by

$$P = \pi f \varepsilon_r \varepsilon_0 \mathrm{tg}\delta E^2 \tag{1}$$

where f is the frequency, $\varepsilon_r \varepsilon_0$ the permittivity and E the electric field. The value of E can be calculated by the relation (1), P being equal to 300 mW (see Introduction) for a volume of half a cubic centimeter (central part and condensors of BVA resonator), f being 3 GHz and $\varepsilon_r = 4$. We obtain $E = 100$ kV/m. That result proves the faisability of a microwave ovenized resonator using an electromagnetic cavity and, particularly, a reentrant high Q cavity. That last one is schematically shown Figure 1. The crystal quartz resonator is set up inside central gap, the gaps of top and bottom providing thermal and electric isolations. If the dimensions of the cavity are correctly calculated, an intense microwave field is provided inside the gaps.

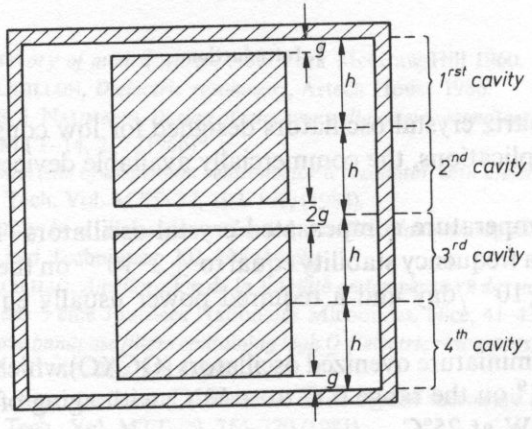

FIG. 1. Reentrant three gaps cavity

The design of the Fig. 1 is equivalent to four identical cavities with the same gap g for each cavity, under the condition the dielectric material is the same for all cavities. If a crystal quartz is set up inside the central gap, the quartz permittivity occurs and the central gap must be divided by ε_r.

In the case of a single cavity (high = h; radius = a), the TM_{mnp} general solution of

the Maxwell's equations written in cylindrical coordinates (r, θ, z) is given by [4]:

$$H_r = -j\sqrt{\frac{\varepsilon}{\mu}}\frac{\lambda_c}{\lambda}\frac{J_m\left(\frac{2\pi r}{\lambda_c}\right)}{\frac{2\pi r}{\lambda_c}} mE_0 \sin m\theta \cos p\pi \frac{z}{h} \tag{2}$$

$$H_\theta = -j\sqrt{\frac{\varepsilon}{\mu}}\frac{\lambda_c}{\lambda} J'_m\left(\frac{2\pi r}{\lambda_c}\right) E_0 \cos m\theta \cos p\pi \frac{z}{h} \tag{3}$$

$$H_z = 0$$

$$E_r = -\frac{\lambda_c}{\lambda_g} J'_m\left(\frac{2\pi r}{\lambda_c}\right) E_0 \cos m\theta \sin p\pi \frac{z}{h} \tag{4}$$

$$E_\theta = \frac{\lambda_c}{\lambda_g}\frac{J_m\left(\frac{2\pi r}{\lambda_c}\right)}{\frac{2\pi r}{\lambda_c}} mE_0 \sin m\theta \sin p\pi \frac{z}{h} \tag{5}$$

$$E_z = J_m\left(\frac{2\pi r}{\lambda_c}\right) E_0 \cos m\theta \cos p\pi \frac{z}{h} \tag{6}$$

$$\text{and } \frac{X_{mn}}{a} = \frac{2\pi}{\lambda_c}$$

where H_r, H_θ, H_z, E_r, E_θ and E_z are the magnetic and electric components of the magnetic field H and electric field E. J_m is the Bessel's function of first kind and m order, and X_{mn} the nth no null root of $J_m(x) = 0$. The derivative of J_m is noted J'_m.

The reentrant cavity of the Fig. 1 can be decomposed in single elements where fields are expressed by series of solutions like the equations (2) to (6), the continuity being assumed by the boundary conditions at bonds between those single elements. Only the Oz axisymmetrical solutions are kept, providing an homogeneous electric field inside the central gap. Same calculations has been developed by JAWORSKI [9]. The theoretical and numerical analysis has been performed by RAULIN [11]. One important of obtained results is shown Fig. 2. They are the electric field lines corresponding to the three gaps cavity of the Fig. 1.

It appears areas where the electric field is null. They will be advantageously used for setting the electrodes wires. That field configuration corresponds to the fondamental mode. For its, the electric field is more homogeneous inside the central gap and it presents the best efficiency to heat quartz crystal resonators. The total energy stored is located at half in the central gap. But it can be seen that the energy dissipated by dielectric losses inside the quartz crystal with respect to the energy dissipated by Joule effect in the metallic sides of the cavity is weak. Indeed that ratio is about 15% in the best case.

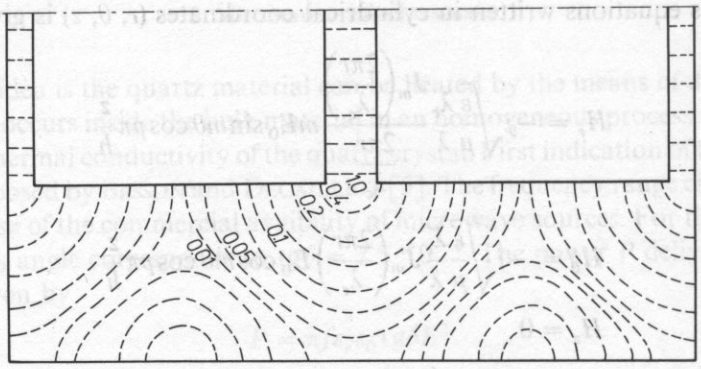

FIG. 2. Electric field of the three gaps cavity (fondamental mode)

Our experimental set-up [17] works up a V.C.O. type generator working between 2 and 4 GHz used together with an amplifier delivering a power of 2 W. A circulator separes incident wave from wave reflected by the cavity. Control is obtained by detection of reflected wave (see Fig. 3).

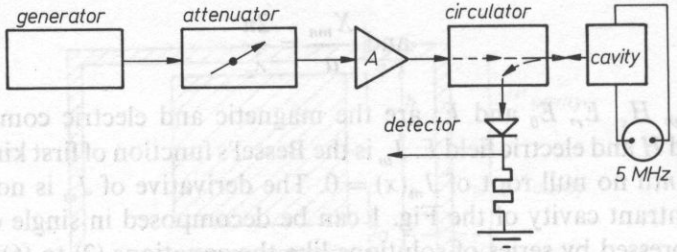

FIG. 3. Experimental set-up

The used crystal is a 5 MHz third overtone *SC* cut small BVA. The B mode is used as temperature sensor; the linear slope is $-$ 161 Hz/°C. The turn-over is obtained at 70°C. The cavity being thermally insulated and placed in vacuum at 20°C, the turn-over is reached for a power of 2 W corresponding to 240 mW applied on the quartz crystal. So, the theoretical analysis is confirmed. It is pointed out the weak ratio of energy usable for heating of the quartz crystal with respect to energy losses in the cavity sides. Let us precise the cavity sides were gilded with a gold thickness of two micrometers, i.e. greater than the skin effect thickness. The observed limitation of that ratio cannot be performed because of the very weak factor tgδ of the quartz material. There is the intrinsic limit of the principle of heating by dielectric losses.

3. Resonator heated by conduction

The principle of quartz crystal heating by resistors directly deposited on the edge of the crystal is for long time known [3], [10]. For BVA resonators BESSON [1] has proposed to deposite the heating resistors on the external sides of the BVA condensors. In 1989 GALLIOU and MOUREY [6] realize prototypes where the heaters are resistive paste printed on the condensors, on the opposite surfaces of the electrodes. The two condensors and the resonator are sandwiched together by insulating pieces manufactured in polytetrafluoroethyl. The whole is set up inside an evacuated enclosure.

The resistors are deposited on the condensors by serigraphy. It is not possible to serve the usual resistive pastes of electronic hybrid technology. Indeed, those mineral pastes must be heated at 800°C, temperature no convenient for quartz crystals. Only the pastes with carbon can be served, their baking temperature being 250°C. The thickness of the deposited resistors is 15 μm and procures a maximal power of 50 mW/mm^2.

In a first step the resonator temperature was measured with a thermistor sticked on the heaters and in a second step by the means of the B mode, for *SC* cut resonators.

The thermal study of the BVA resonator has been carried out by VALENTIN in 1985 [13]. The part of the radiative transfer heating was pointed out. For an usual BVA resonator the part of the radiative transfers is about one third by two thirds for the conductive transfers.

The Figs. 4 and 5 show the warmup and the heater power consumption for a BVA resonator heated by two resistors deposited on the condensors. Those results have been obtained for a 10 MHz *SC* cut resonator.

The previous results are very interesting for fast warmup and low consumption devices. The inconvenience of that heating method is the degazing of the heaters, which limites the aging performances about 10^{-9}/day. There is hard difficulty to perform that

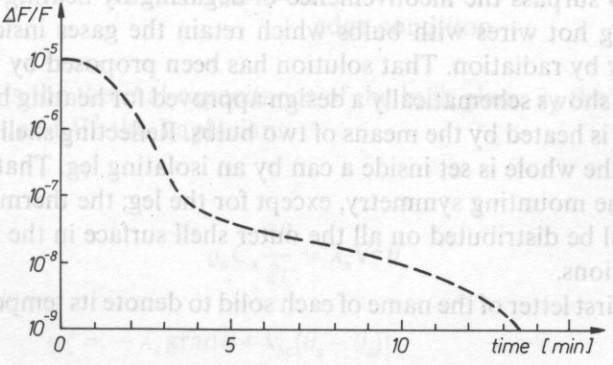

FIG. 4. Warmup for BVA resonator

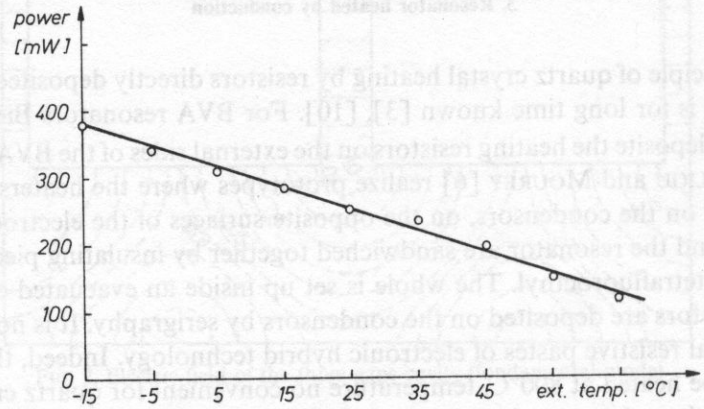

FIG. 5. Heater power consumption for BVA resonator

last aging because of the absorbing layer of the quartz crystal presents a thickness of two angströms for a frequency variation of one hertz (1 mm corresponds to 5 MHz for an *SC* cut, 3rd overtone). Now, two angströms are about the thickness of a monomolecular layer. Under those conditions it is preferable to research other solutions for low consumption heating of BVA resonator, particularly if we will turn to account its weak aging.

4. Infrared radiations oven

In order to surpass the inconvenience of degazing by heating layers, a solution consists in using hot wires with bulbs which retain the gases inside. Then the heat transfers appear by radiation. That solution has been proposed by VALENTIN in 1983 [14]. The Fig. 6 shows schematically a design approved for heating by radiation where a quartz crystal is heated by the means of two bulbs. Reflecting shell surrounds quartz and bulbs and the whole is set inside a can by an isolating leg. That simplified design clearly shows the mounting symmetry, except for the leg; the thermal conductance of this last one will be distributed on all the outer shell surface in the following thermal exchange equations.

Using the first letter of the name of each solid to denote its temperature (see Fig. 6), we can write:

for the hot wire

$$P = k_{wc}(\theta_w - \theta_c) + S_w \varphi_w \tag{7}$$

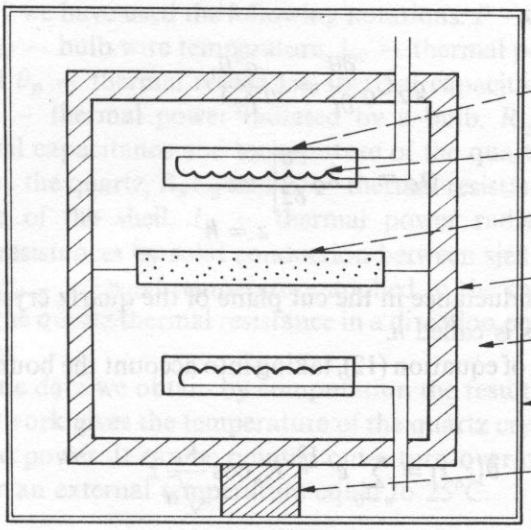

FIG. 6. Schematical infrared radiations oven

where P is the electrical power applied to the wire, k_{wc} the thermal conductance by solid conduction between the wire and the can, θ_i are temperatures, S_w the wire surface and φ_w the surfacic flux radiated by the wire. Here the thermal capacitance of the wire is neglected.

for the bulb glass

$$\varrho_B C_B \frac{\partial \theta}{\partial t} = \lambda_B \nabla^2 \theta \tag{8}$$

$$\varphi_B = -\lambda_B \operatorname{grad} \theta \Big| \quad \text{edge condition} \tag{9}$$

where $\varrho_B C_B$ is the thermal capacitance of the bulb glass, λ_B the thermal conductivity of the glass and ∇^2 the Laplacian.

for the shell

$$\varrho_s C_s \frac{\partial \theta}{\partial t} = \lambda_s \nabla^2 \theta \tag{10}$$

$$\varphi_s = -\lambda_s \operatorname{grad} \theta + k_{sc}(\theta_s - \theta_c) \Big| \quad \text{edge condition} \tag{11}$$

where the used notations are homogeneous with the previous.

for the crystal quartz

$$\varrho_Q C_Q \frac{\partial \theta}{\partial t} = \lambda_Q \frac{\partial^2 \theta}{\partial z^2} \tag{12}$$

$$\varphi_Q = -\lambda_Q \left.\frac{\partial \theta}{\partial z}\right|_{z=h} \tag{13}$$

Here the thermal conductance in the cut plane of the quartz crystal is neglected. The half crystal thickness is called h.

The general solution of equation (12), taking into account the boundary condition (13), is given by

$$\theta(z, t) = \sum_{n=0} e^{-k_n^2 t} K_n \cos \frac{k_n}{\sqrt{a}} z \tag{14}$$

$$\text{where } a = \frac{\lambda_Q}{\varrho_Q C_Q} \tag{15}$$

the constants k_n and K_n being calculated from the conditions at $t = 0$.

The main problem is the calculation of the radiated flux, according with the transparency of bulb glass and quartz in the range of wavelengths zero to four micrometers. The radiated flux expressions are strongly non-linear and depend on the fourth power of the temperatures. So it is convenient to use the electrical analogy for computer-aided analysis. Figure 7 shows the electrical equivalent circuit of thermal transfers [7].

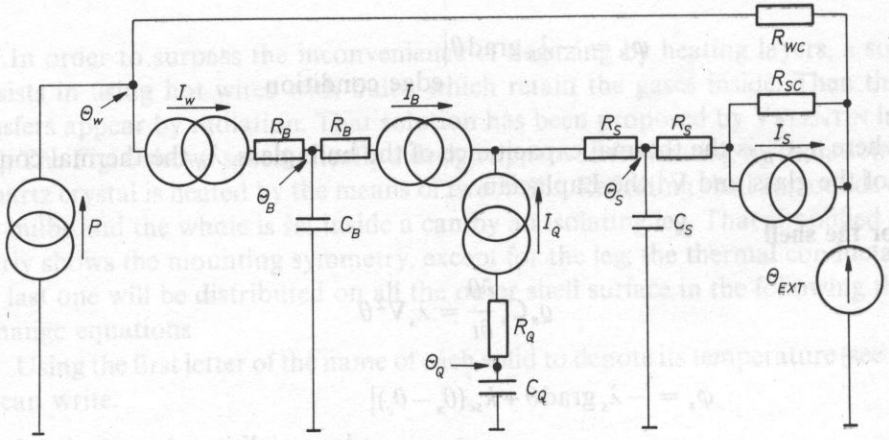

FIG. 7. Electrical equivalent circuit of thermal transfers

On the Fig. 7 we have used the following notations: P – electrical power applied to a bulb wire, θ_W – bulb wire temperature, I_W – thermal power radiated by a bulb wire, R_B, C_B and θ_B – thermal resistance, thermal capacitance and temperature of a glass bulb, I_B – thermal power radiated by a bulb, $R_Q C_Q$ and θ_Q – thermal resistance, thermal capacitance and temperature of the quartz crystal, I_Q – thermal power radiated by the quartz, $R_S C_S$ and θ_S – thermal resistance, thermal capacitance and temperature of the shell, I_S – thermal power radiated by the shell, R_{SC}, R_{WC} – thermal resistances by solid conduction between sjell and can (R_{SC}) and wire and can (R_{WC}), θ_{ext} – external temperature applied to the can.

R_Q denotes the quartz thermal resistance in a direction perpendicular to the plane of the crystal cut.

Using realistic data we obtain by computation the result of the Fig. 8, where the shown curves network gives the temperature of the quartz crystal versus the time and versus the applied power. It can be pointed out a turn-over of 90°C is obtained with only 200 mW for an external temperature equal to 25°C.

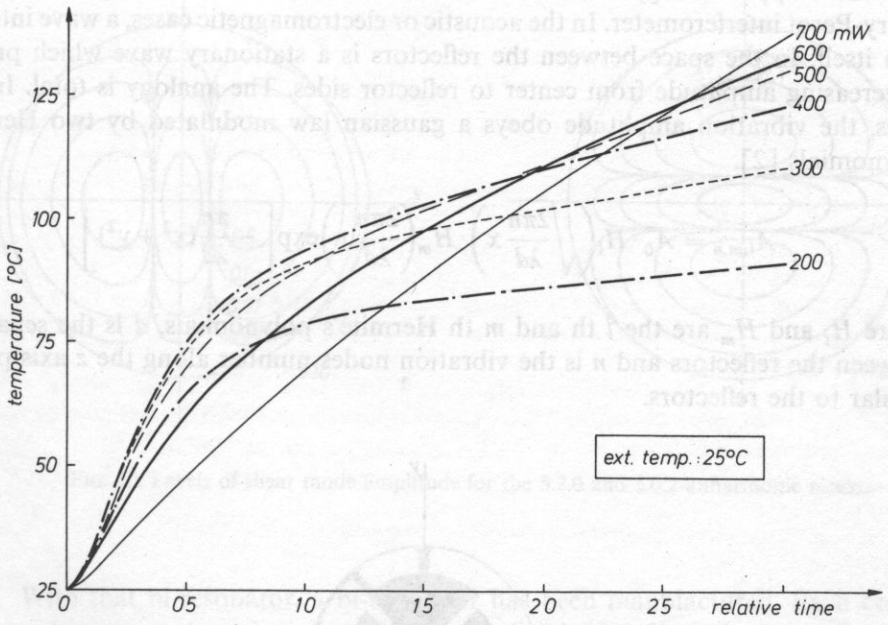

FIG. 8. Crystal temperature versus power in the case of heating by radiation

So, the simulation of heating by radiation shows it is possible to obtain low consumption for high turn-over. More, the heating is very homogeneous because of the thermal flux flows through the whole surfaces of the crystal and not only by two points (the holders). So the thermal dynamic effects are reduced. At last, the thermal resistance in the direction perpendicular to the cut plane is about thousand times less than the

thermal resistance in the cut plane. So, if a large heating step is applied on a cold crystal, the break down risk is very reduced. A precise study of oscillators heated by infrared radiations was exhibited in a recent paper [7].

5. Internal heating by acoustic losses

The internal heating of coated resonators and BVA resonators has been proposed by VALENTIN in 1980 [15]. The internal heating comes from the electrical energy dissipated by acoustic losses. The efficiency of that transformation is greater than 99%. Then, the thermal power equals the drive power. For heating by acoustic losses it is necessary to use a specific mode (overtone or anharmonic) providing a low coupling factor with the main mode and supporting high drive levels. Of course, the trapped energy resonators can be used for internal heating, and BVA resonators are particularly designed for that, since they accept very high levels, till several hundreds of milliwatts.

The trapped energy bulk wave acoustic resonators use the spherical mirror Fabry-Perot interferometer. In the acoustic or electromagnetic cases, a wave interferes with itself. In the space between the reflectors is a stationary wave which presents a decreasing amplitude from center to reflector sides. The analogy is total. In both cases, the vibration amplitude obeys a gaussian law modulated by two Hermite's polynomials [2].

$$A_{l,m,n} = A_0 \cdot H_l\left(\sqrt{\frac{2\pi n}{\lambda d}}\, x\right) \cdot H_m\left(\frac{2\pi n}{\lambda d}\, y\right) \exp\left[-\frac{\pi n}{\lambda d}(x^2 + y^2)\right] \tag{16}$$

where H_l and H_m are the l th and m th Hermite's polynomials, d is the separation between the reflectors and n is the vibration nodes number along the z axis perpendicular to the reflectors.

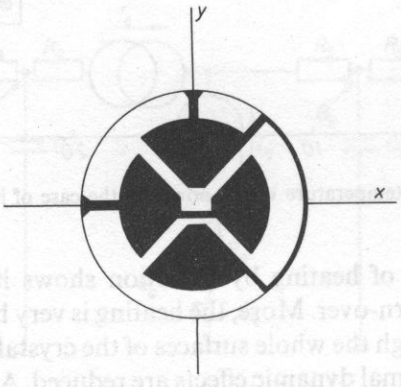

FIG. 9. Double electrodes system

WILSON in 1974 [18], next TIERSTEN and SMYTHE in 1977 [12] have proposed similar results in the case of trapped energy acoustic resonators. In the usual case, the vibration is located at the resonator central part and in peripheric spots corresponding to the Hermite's polynomials extrema. The energy is trapped inside these spots and inside the central part.

In a first step, we have realized a resonator provided a double electrodes system deposited on the condensors of a fifth overtone 5 MHz BVA resonator, *AT* cut. This work has been carried out by GILLET [8]. The double electrodes system is shown Fig 9.

Figure 10 shows the curves with same levels of shear vibration amplitude in the main plane of the resonator. These curves are obtained by computation in the case of the 5.2.0. and 5.0.2. modes. The subscripts *l* and *m* indicate the nodal lines number in the directions *x* and *y*. It can be pointed out the phase change of the amplitude is very fast, and in respect to that observation, the manufacturing of electrodes system must be realized with great care.

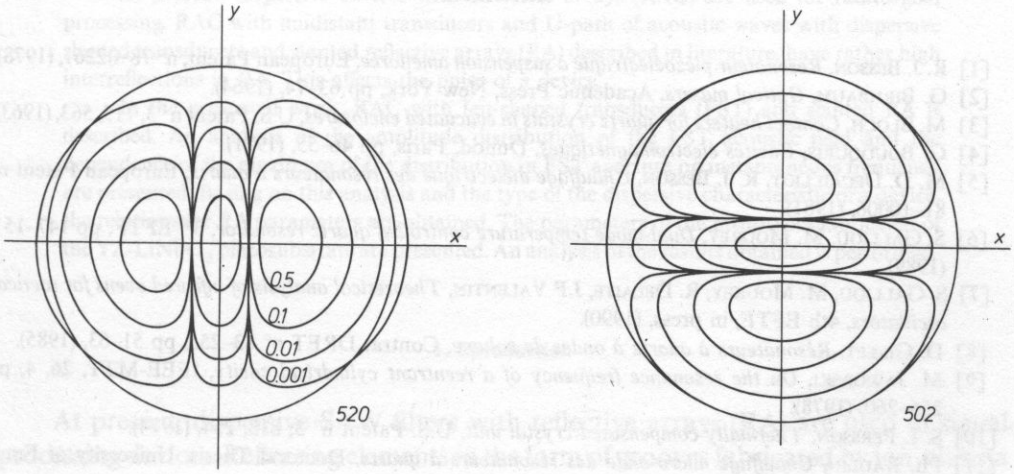

FIG. 10. Levels of shear mode amplitude for the 5.2.0 and 5.0.2 anharmonic modes

With that bi-resonator, a bi-oscillator has been manufactured. Each couple of electrodes was connected to an oscillator supplied by LC filter, the first at 5 MHz, the second at 7 MHz. Two signals were obtained. The frequencies were 5.1131 MHz for the 5.2.0. mode and 7.0878 for the 7.0.2. mode. The indirect amplitude frequency effect is minimized using anharmonics of different overtones [16].

The second step of that work is not realized today. The question is to know how to serve such a bi-resonator for providing a main mode and an internal heating mode. We consider this experiment is important. A success would open the way for a new miniature ovenized resonator.

6. Conclusions

We have examined four different possibilities to obtain low consumptions for BVA resonators.

By the means of the dielectric losses the necessary electrical power remains more high. The resistors deposited on the condensors bring on an unacceptable degazing, providing an aging largely greater than the usual aging of the BVA resonator. Probably the heating by infrared radiations is the best solution for low consumption; it could be turned to account in the future. The internal heating by acoustic losses is the more smart solution; it needs two very well uncoupled vibrations. In order to obtain such a result, it is possible to serve an even mode of vibration excited by parallel electric field. Then the even mode is very little affected by the vibrating state of the central part of the resonator and the discoupling between the modes can reach a nearly null value.

References

[1] R. J. Besson, *Résonateur piézoélectrique à suspension améliorée*, European Patent, n° 78–02261, (1978).
[2] G. Birnbaum, *Optical masers*, Academic Press, New-York, pp 63–74, (1964).
[3] M. Bloch, *Contact heaters for quartz crystals in evacuated enclosures*, U.S. Patent n° 3, 715, 563, (1963).
[4] G. Boudouris, *Cavités électromagnétiques*, Dunod, Paris, pp 46–55, (1971).
[5] M. D. Decailliot, R. J. Besson, *Chauffage diélectrique des résonateurs à quartz*, European Patent n° 81–10006, (1981).
[6] S. Galliou, M. Mourey, *Dual-mode temperature controlled quartz resonator*, 3rd EFTF, pp 147–151, (1989).
[7] S. Galliou, M. Mourey, R. Delaite, J.P Valentin, *Theoretical analysis of infrared ovens for tactical oscillators*, 4th EFTF, in press, (1990).
[8] D. Gillet, *Résonateurs à quartz à ondes de volume*, Contrat DRET n° 83–255, pp 51–63, (1985).
[9] M. Jaworski, *On the resonance frequency of a reentrant cylindrical cavity*, IEEE-MTT, **26**, 4, pp 256–260, (1978).
[10] S. I. Persson, *Thermally compensated crystal unit*, U.S. Patent n° 3, 818, 254, (1974).
[11] Ph. Raulin, *Chauffage micro-onde des résonateurs à quartz*, Doctoral Thesis, University of Franche-Comté, Besançon, (1984).
[12] H. F. Tiersten, R. C. Smythe, *An analysis of overtone modes in contoured crystal resonators*, 31st AFCS, pp 44–47 (1977).
[13] J.-P. Valentin, *Thermal gradient distributions in trapped energy quartz resonators*, J. Appl. Phys., **57**, 2, pp 492–497, (1985).
[14] J.-P. Valentin, *Résonateur à thermostat infrarouge intégré*, European Patent n° 83-07307, (1983).
[15] J.-P. Valentin, *Internal heating and thermal regulation of bulk quartz resonators*, 34th AFCS, pp 194–201, (1980).
[16] J.-P. Valentin, C. P. Guerin, R. J. Besson, *Indirect amplitude frequency effect in resonators working on two frequencies*, 35th AFCS, pp 122–129, (1981).
[17] J.-P. Valentin, M. D. Decailliot, R. J. Besson, *New approach of fast warmup for crystal resonators and oscillators*, 38th AFCS, pp 366–373, (1984).
[18] C. J. Wilson, J. Phys. D, 7, p. 2449, (1974).

ARCHIVES OF ACOUSTICS
16, 1, 149-156(1991)

$LINbO_3$ DISPERSIVE FILTER WITH FAN-SHAPED TRANSDUCERS AND REFLECTIVE ARRAYS

P. V. VIKTOROV, A. R. ZHEZHERIN, L. P. KONOVALOVA

Leningrad Institute of Aviation Instrument Making
(190 000, Leningrad, USSR)

At present, dispersive devices with reflective arrays (RAC) are used for radiosignal processing. RAC with unidistant transducers and U-path of acoustic waves with dispersive slanted transducers and slanted reflective arrays (RA) described in literature, have rather high interreflections in RA. This affects the pulse of a device.

In the presented work, RAC with fan-shaped transducers (FST) and slanted RA is described. An analysis of the amplitude distribution of the FST acoustic field and the dependence of the maximum of the distribution in FST aperture on instantaneous frequency are presented. Basing on this analysis and the type of the dispersive characteristic of a device, the relations for RA parameters are obtained. The parameters of the prototypes fabricated of the YZ-$LiNbO_3$ piezosubstrate are presented. An analysis of the results obtained is performed.

1. Introduction

At present, dispersive SAW filters with reflective arrays (RA) are used in signal processing devices. Reflecting elements in the form of grooves fabricated by ion-plazma etching in a piezosubstrate are most widely used. In the geometry of such filters, input and output unidistant interdigital transducers IDT and U-path RA ca be used [1] (Fig. 1a).

Propagating from the input transducer to the output one, an acoustic wave reflects on 90 deg two times (on the upper and lower gratings). To reduce multireflections inside the grating, the grooves are fabricated with low depth ($i/\lambda = 0.03$, where h-groove depth, λ – SAW wavelength). The drawbacks of this geometry are a relatively narrow band (30%) and high ripples of amplitude-frequency and phase-frequency responses due to SAW multireflections in RA. Increasing of device bandwith leads to the growth of insertion losses.

RAC with dispersive IDT and slanted RA are known [2]. The example of this device is shown in Fig. 1(b). This geometry of IDT has space-frequency selectivity. When the frequency of the exciting harmonic signal sweeps f_l to f_h, the acoustic beam of

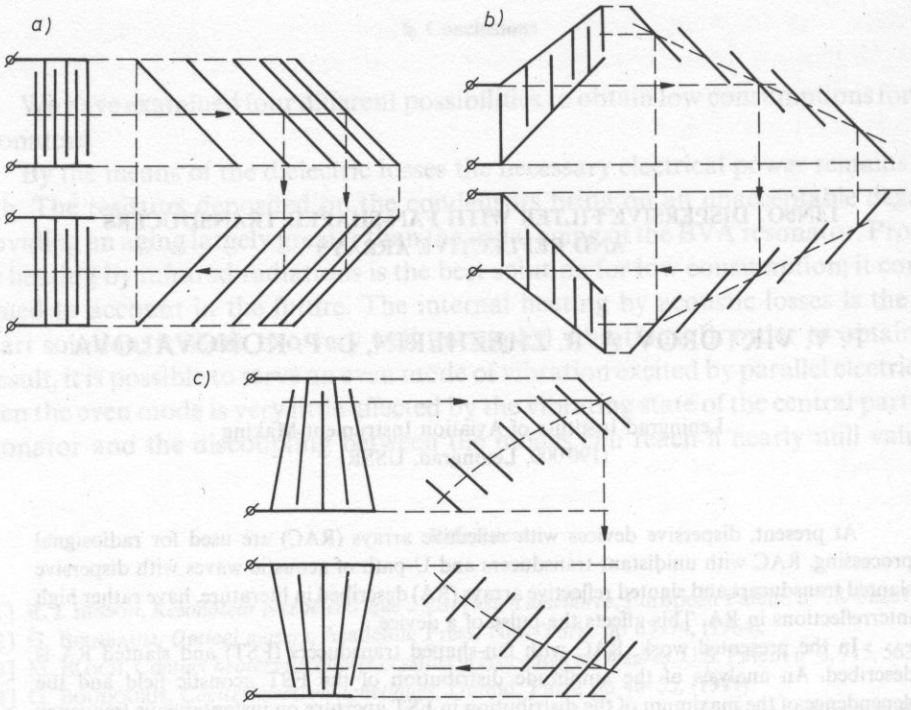

FIG. 1. Different RAC types

the slanted dispersive transducer shifts upwards in the transducer aperture. Beam width depends on the transducer's bandwith, aperture, and the angle of inclination of the transducer central line to the longitudinal axis of the device. The elements of RA are placed in a such way that in any longitudinal section it matches the condition

$$\Lambda_t = \Lambda_{RA},$$

where Λ_t is the distance between the adjacent fingers of IDT in an arbitrary section, Λ_{RA} the distance between the adjacent grooves in the same section. Space-frequency separation of reflecting channels reduces multireflections in RA. But the number of weak-dependent channels does not exceed 3–5. Also, in RAC slanted dispersive transducers and RA are used [3].

2. Analysis of FST acoustic field

In the designed dispersive filter, fan-shaped transducers FST and slanted RA are used. The geometry of the device is shown in Fig. 1(c). FST has high space-frequency selectivity [5]. Figure 2 shows the amplitude distribution, computed with a specially

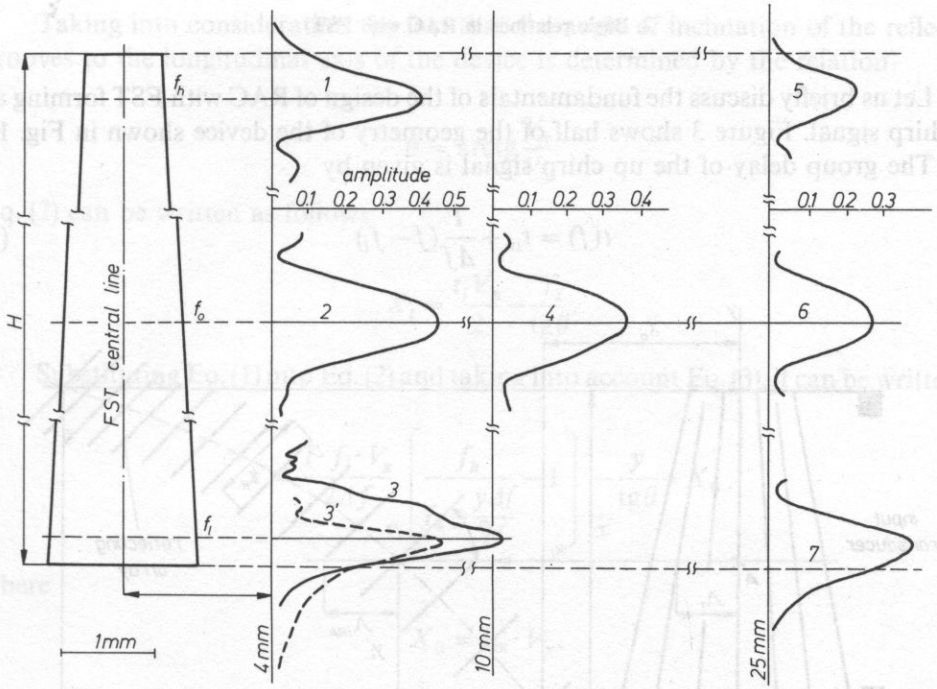

FIG. 2. Amplitude distribution of SAW FST acoustic field

written program, of the acoustic field in the aperture of FST at several distances from the longitudinal axis the distances are shown in brackets. The program accounts for SAW velocity anisotropy in the piezosubstrate (YZ-$LiNbO_3$). The field distribution on single frequency is characterized by the $\sin(x)/x$ function. The beam width can be estimated with a certain level of the function. The distribution (1) corresponds to high frequency of the exciting frequency band – f_h, 2 – to central frequency f_0, 3 – lower frequency f_l. The plots (1)–(5), (2)–(4)–(6) and (3)–(7) show changes in the distributions on the frequencies with the distance from the transducer's axis increasing. The relative bandwith of the transducer $\Delta f/f$ is 0.5 $f_h = 1.25\ f$, $f_l = 0.75\ f$. The fan's opening angle is 3 deg, the transducer aperture H is 7.7 mm. The plots show that in an aperture of FST, a great number actually 10–15 of weak-coupled acoustic channels can exist. Thus FST chances of being used to create RAC with reduced interreflections between RA elements are good.

However, as seen in Fig. 2 the drawbacks of the field structure are the decreased maximum value of the distribution function and broadening of the function. At great distances from the transducer's axis, the function can have be no explicit maximum on the frequency. In FST, the position of the acoustic beam in a device aperture depends on the frequency of an exciting harmonic signal hyperbolically [5]. That affects the RA geometry of the device.

3. Basic relations in RAC with FST

Let us briefly discuss the fundamentals of the design of RAC with FST forming an up chirp signal. Figure 3 shows half of the geometry of the device shown in Fig. 1c.

The group delay of the up chirp signal is given by

$$t(f) = t_{\text{in}} + \frac{T}{\Delta f}(f - f_l) \tag{1}$$

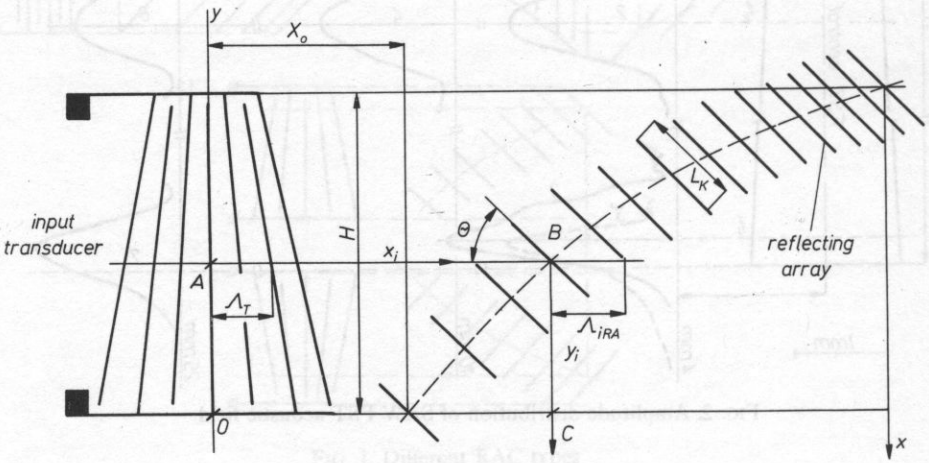

FIG 3. RAC-FST layout (one half represented)

where t_{in} – initial delay, T – signal duration, Δf – pulse frequency sweep, f_l – lower frequency.

In the coordinate system introduced in Fig. 3, any i-th delay is determined by the relation

$$\frac{t_i}{2} = \frac{AB}{V_x} + \frac{BC}{V_y} = \frac{X_i}{V_x} + \frac{Y_i}{V_y} \tag{2}$$

where V_x and V_y are the velocities in longitudinal and transverse directions.

For FST shown in Fig. 3 the following expressions is correct

$$f(y) = \frac{f_e}{1 - \dfrac{y\Delta f}{Hf_h}} \tag{3}$$

where f_l and f_h – lower and upper edges of the transducer's operating band f – instantaneous frequency, y – coordinate of acoustic beam position, H – transducer's aperture.

Taking into consideration the fact that the angle of inclination of the reflecting grooves to the longitudinal axis of the device is determined by the relation

$$\theta = \operatorname{arctg} \frac{V_y}{V_x}. \tag{4}$$

Eq. (2) can be written as follows:

$$X_i = \frac{t_i V_x}{2} - \frac{Y_i}{\operatorname{tg}\theta}. \tag{5}$$

Substituting Eq. (1) into Eq. (2) and taking into account Eq. (3), it can be written as

$$x = \frac{T \cdot f_l \cdot V_x}{2\Delta f} \left(\frac{f_h}{f_h - \dfrac{y\Delta f}{H}} - 1 \right) - \frac{y}{\operatorname{tg}\theta} + X_0 \tag{6}$$

where

$$X_0 = t_{in} \cdot V_x.$$

The relation (6) describes the shape of the central line of reflecting grating. The length of the k-th groove is determined by the width of the acoustic beam in groove position (on the transducer's aperture and at a distance from the fan axis).

The total signal duration is formed by both gratings, as shown in Fig. 1(c).

The layout of a compressive filter is shown in Fig. 4. The expansive and compressive devices shown in Figs. 1(c) and 4 realize the maximum dispersion in the pulse being formed. The minimum delay in the filters shown in Figs. 4 and 5 is determined by the path of the beam propagating along the trajectory *1*, and the maximum delay by the path along the trajectory *2*.

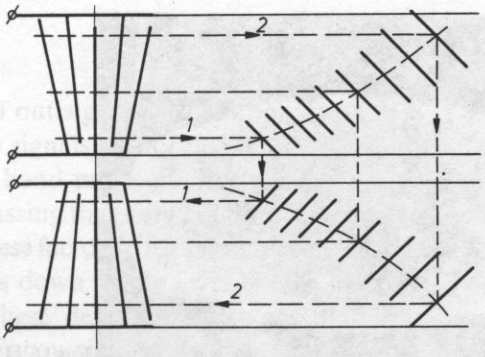

FIG. 4. Compression RAC with increased dispersion

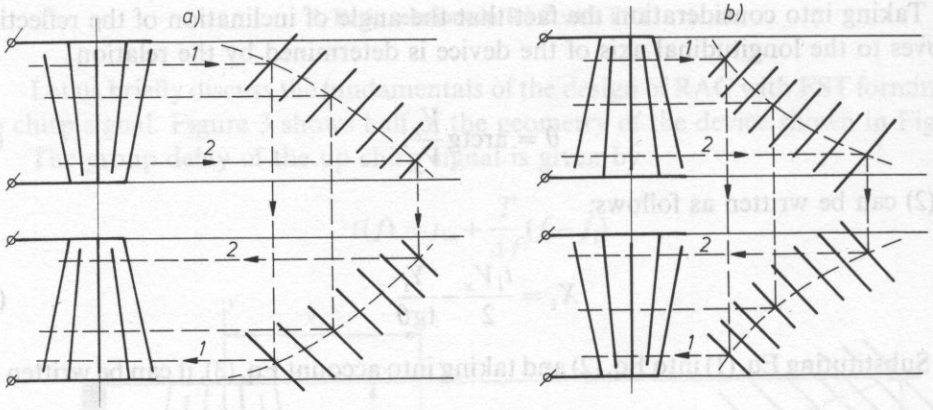

FIG. 5 a) Expansion RAC with decreased dispersion; b) Compression RAC with decreased dispersion

Dispersion in the signal being formed is the difference between these paths. Filters with the position of transducers and RA as shown in Fig. 5 realize the minimum pulse dispersion.

4. Experimental results

Dispersive devices with FST and slanted RA made on YZ-$LiNbO_3$ have been designed. The layouts of expansion and compression lines shown in Figs 1(c) and 4 have been used. In the compression line, RA has been apodized by changing the length of the reflective elements. Grooves with a constant relative depth $h/\lambda = 0.03$ are fabricated by ion-plasma etching. A radiopulse with duration $T = 16$ μs has been formed, the relative bandwith $\Delta f/f_0 = 40\%$. The pluse response of the expansion filter is shown in Fig. 6 (the scales 2 μs/div). Figure 7(a) shows the signal in the output of the compression filter the scales 50 ns/div. Figure 7(b) shows the same signal 20 times expanded vertically (the scales 25 ns/div). The estimated level of the side lobes is 28–30 dB.

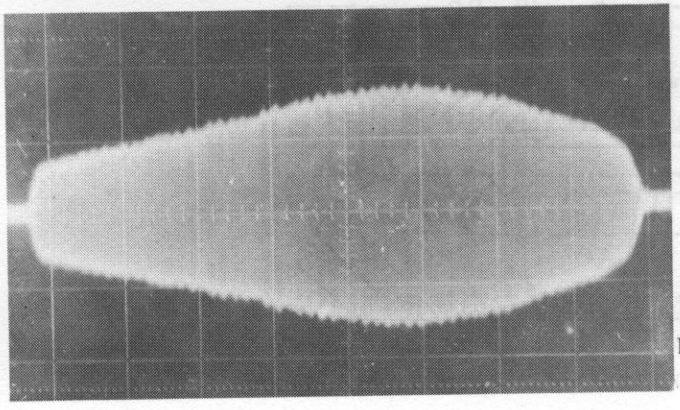

FIG. 6. Pulse response of the expansion filter. The scales: 2 μs/div.

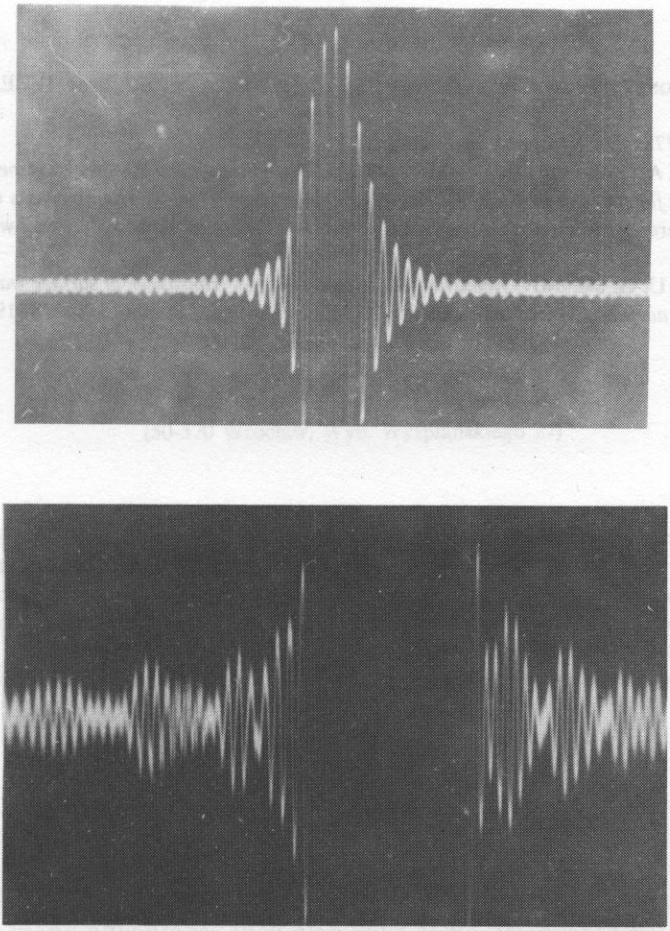

FIG. 7. a) Compressed signal in the output of the compression filter. The scales: 50 ns/div., 0.2 V/div.; b) Compressed signal in the output of the compression filter. The scales: 25 ns/div., 0.01 V/div.

The research carried out signals future application of FST in RAC. When wide-band (up to 100%) chirp signals are formed, FST transducers electric energy into an acoustic one in a whole band more effectively. FST increases the dynamic range of a device as a result of focussing the energy of the acoustic field into a narrow beam (Fig. 2). The combination of these factors with $LiNbO_3$ being used as a piezosubstrate allows to reduce insertion losses down to the level of (25–30 dB).

The drawback of these devices, is the fact that it is necessary to take into consideration changes of acoustic beam width along the distance from the fan's axis. This increases the drop of the pulse response of the "unweighed" device.

References

[1] R. C. WILLIAMSON, *Properties and applications of reflective-array devices*, Proc. IEEE, **64**, 5, 702–710 (1976).

[2] US Patent 4477784, SAW dispersive delay-line.

[3] P. V. VICTOROV, A. G. ZHEZHERIN, I. S. MITROFANOV, *Computation and design of a dispersive device with reflective arrays for forming and compression of wideband chirp signals.* The abstracts of the report on All-Union conference "Acoustoelectronic devices for information processing". Moscow, 379–380 (1988) (Russ).

[4] S. A. ZABUZOV, U. G. SMIRNOV, *Acoustic field of a fan-shaped transducer of surface waves. Radiosignal processing with acustoelectronic and acustooptic devices*, Nauka, Leningrad, 14–18 (1983) (Russ.).

ARCHIVES OF ACOUSTICS
16, 1, 157-160 (1991)

A QUARTZ RESONATOR FORCE TRANSDUCER

M. WERSZKO

Technical University of Wrocław
(50-370 Wrocław, Wyb. Wyspiańskiego 27)

The prototype of force transducer with the AT-cut quartz resonator serving as the sensitive to force element is described. The operating principle of this transducer is based on the relation between the resonator vibration frequency and the force acting on this resonator.

Since the quartz resonator is sensitive to ambient temperature, the force transducer has been also equipped by the LC-cut resonator, which plays the role of temperature sensor with frequency output signal. This signal is used to compensate the thermal influences.

1. Introduction

Currently, the force transducers with strain gauge are most often used in industry. Despite their many advantages they also have some disadvantages: relatively small sensitivity, analogue output signal not easily digitised. To avoid these disadvantages, the force transducers with quartz resonator representing the force-sensitive element are being developed today by some companies [1], [2], [3].

As we know, the resonance frequency of the resonator depends on Young's modulus E and density ϱ of quartz, and on the dimension of the resonator. For the AT-cut resonator this dependence is given by

$$f = 0.5\, n/h\sqrt{E/\varrho}, \tag{1}$$

where: n – vibration mode number, h – quartz thickness.

Parameters E, ϱ and h depend on the temperature, but modulus E additionally depends on the applied force F. This relation between modulus E and force F serves as a basis for the operating principle of the force transducer with quartz resonator (Fig. 1).

The steady-state characteristic of such force transducer (relation between the resonator frequency f and the measuring force F, applied to the resonator along the

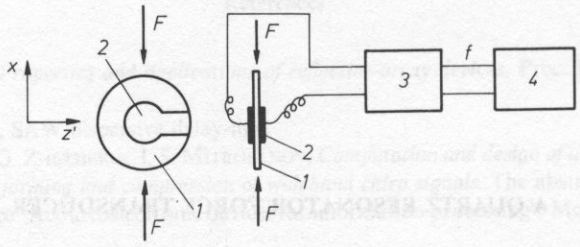

FIG. 1. Operating principle of the transducer. 1 – resonator, 2 – electrode, 3 – oscillator, 4 – frequency meter.

X-axis) is given by

$$f = f_0\sqrt{1+kF} \tag{2}$$

where: f_0 – resonator frequency at the starting point, when the measuring force is equal zero $F = 0$, k = scale factor.

The frequency deviation $\Delta f = f - f_0$ plays the role of the transducer output signal. For the AT-cut resonator the maximal value of this deviation (conditioned by the limiting range stress) referred to frequency f_0 equals about 0.5%.

Main advantages of the force transducer with quartz resonator are as follows:

- high sensitivity,
- frequency output signal; interference resistant and easily digitised,
- excellent stability,
- little drift, small hysteresis and time constant.

Disadvantages: sensitivity to changes of ambient temperature, steady-state characteristic non-linearity.

2. Force transducer design

The force transducer, developed at the Technical University of Wrocław, consists of an elastic frame *1* (Fig. 2), the *AT*-cut resonator *2* for the force measurement, the *LC*-cut resonator *3* for the temperature measurement, two oscillators *4* and *5*, the housing *6* and a microprocessor-based electronic unit *7*. The *AT*-cut resonator in form of the plane-convex plate is fitted into the steel frame *1* which reduces the measuring force F and transmits it to the resonator *2*. Under the action of this force the resonant frequency f of the resonator, connected with oscillator *4*, is changed. This frequency f is the output signal of the transducer.

In order to avoid the vapour condensation, air pressure inside the transducer housing *6* is reduced to the value of 7 kPa.

Main sources of the transducer errors are: ambient temperature and hysteresis. Variation of temperature influences, first of all, the resonator parameters E, ϱ, h (see Equation 1); moreover since the thermal expansion coefficients of the quartz resonator

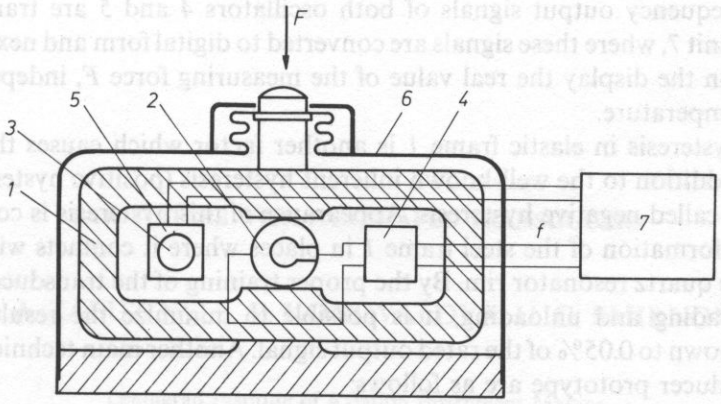

FIG. 2. Force transducer design 1 — elastic brame, 2 — *AT*-cut resonator, 3 — *LC*-cut resonator, 4 and 5 — oscillators, 6 — housing, 7 — electronic unit.

and the steel frame *1* are different, variation of ambient temperature produces additional tension in the quartz resonator and appropriate frequency change. As the steady-state characteristic shows (Fig. 3), the transducer error set up by ambient temperature can reach 0.2% of the rated output per 1°C.

The ambient temperature influence is compensated by means of the correction of the steady state transducer characteristic in the electronic unit 7. For this purpose serves the *LC*-cut resonator, which plays the role of the temperature sensor with frequency output signal. This resonator, connected with oscillator *5*, is placed near by the *AT*-cut resonator *2*.

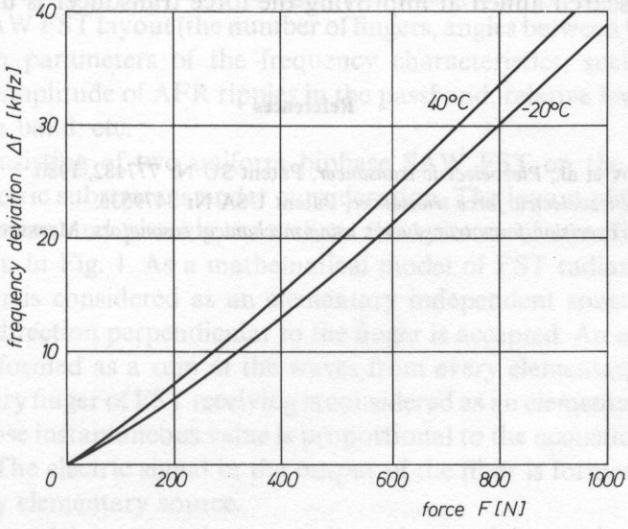

FIG. 3

The frequency output signals of both oscillators *4* and *5* are transmitted into electronic unit 7, where these signals are converted to digital form and next reprocessed to obtain on the display the real value of the measuring force F, independent of the ambient temperature.

The hysteresis in elastic frame *1* is another factor which causes the transducer errors. In addition to the well-known inherent hysteresis (positive hysteresis), there is also the so-called negative hysteresis. Appearance of this hysteresis is connected with inelastic deformation of the steel frame *1* in places where it contacts with very small areas of the quartz resonator rim. By the proper training of the transducer, its mutiple safe overloading and unloading, it is possible to minimize the resulting value of hysteresis down to 0.05% of the rated output signal. Another main technical data of the force transducer prototype are as follows:

- Rate load — 1000 N
- Sensitivity — 46 Hz/N
- Calibration accuracy — 0.2% of rated output
- Compensated temperature range — −20 to +40°C
- Temperature effect — 0.04% of rated output per 1°C.
- Rated output — 46 kHz.

3. Conclusion

The force transducer with quartz resonator described above seems to be very stable and sensitive. Compared e.g. with strain gauge force transducer, the quartz resonator force transducer needs two times smaller deformation of the elastic element and less sophisticated electronic device to convert the output signal to a digital form.

Further research aimed at improving the force transducer is under way.

References

[1] F. F. KOLPAKOV et al., *Piezoelectric transducer*, Patent SU Nr 777482, 1980.

[2] F. A. NORRIS, *Piezoelectric force transducer*, Patent USA Nr 3479536.

[3] T. UEDA et al., *Precision force transducers using mechanical resonators*, Measurement, **3**, Nr 2, 89–94 (1985).

ARCHIVES OF ACOUSTICS
16, 1, 161-165(1991)

SAW FILTERS WITH FAN-SHAPED TRANSDUCERS

S. A. ZABUZOW, L. P. KONOVALOVA, U. G. SMIRNOV

Leningrad Institute of Aviation Instrument Making
(190 000, Leningrad, USSR)

The results of the study of frequency characteristics of SAW filters with multifinger fan-shaped transducers (FST) are presented. Practically useful relations determining the FST directivity diagram and the main filter characteristics dependent on FST layout and the distance between them are obtained.

One way to design SAW piezoelectric bandpass filters is to use multifinger fan-shaped transducers (FST). FST forms an acoustic field as a rather narrow acoustic beam whose intensity maximum moves along the aperture of the transducer when the exciting frequency is varied [1]. On frequencies corresponding to aperture edges, a rather sharp decrease of intensity of the acoustic beam is observed; this makes it possible to create bandpass filters with a high squareness ratio of the amplitude-frequency response (AFR). But to design such filters, it is necessary to know the influence of the SAW FST layout (the number of fingers, angles between them, aperture, etc.) on the main parameters of the frequency characteristics, such as the AFR squareness ratio, amplitude of AFR ripples in the passband, relative level of the signal in the attenuation band, etc.

A system consisting of two uniform biphase SAW FST on the surface of the isotropic piezoelectric substrate is under consideration. The layout of fingers in every FST, their numbering and phasing, as well as the systems of coordinates used for analysis are shown in Fig. 1. As a mathematical model of FST radiating, the model where every finger is considered as an elementary independent source of flat SAW propagating in a direction perpendicular to the finger is accepted. An acoustic field of FST radiation is formed as a sum of the waves from every elementary source.

Similarly, every finger of FST receiving is considered as an elementary source of an electric signal whose instantaneous value is proportional to the acoustic field averaged along the finger. The electric signal in the output of the filter is formed summarizing signals from every elementary source.

Applying the model, an acoustic wave radiated by one finger with number n being

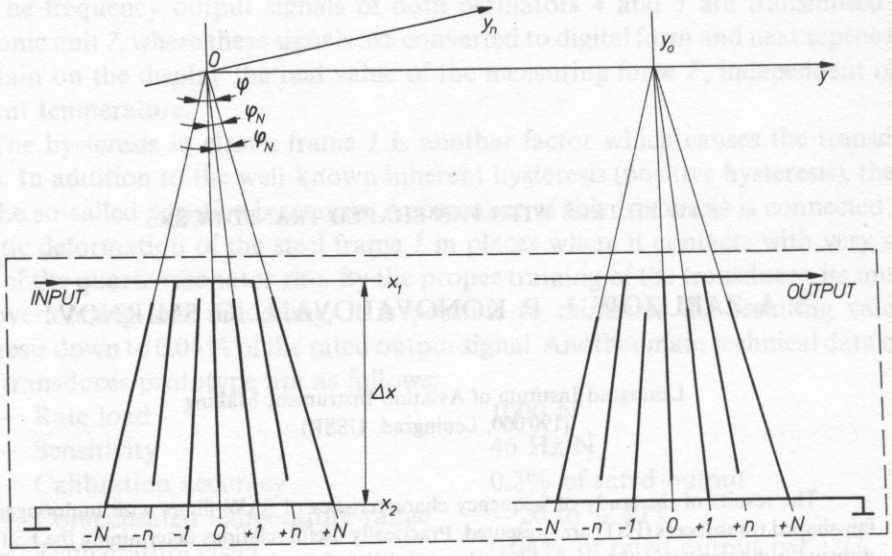

FIG. 1

fed with a harmonic signal with frequency f is described in the oordinates x, y by the following expression

$$a_n(x_n, y_n, t) = (-1)^n A_0 \exp j(2\pi f t - k x_n) \tag{1}$$

where A_0 and k – oscillation amplitude and wave number, respectively.

The instantaneous value of the acoustic field of radiating FST containing $2N+1$ fingers can be found transforming the coordinates x_n, y_n into x, y and summarizing the elementary waves..

$$a(x, y, t) = A_0 e^{j2\pi f t} \sum_{n=-N}^{+N} (-1)^n \exp\left[-jk(x \sin\varphi_n + y \cos\varphi_n)\right]. \tag{2}$$

The greatest value of the function $a(x, y, t)$ equals the sum of amplitudes of the elementary waves, i.e.,

$$a_{\max} = (2N+1) A_0 \tag{3}$$

can be seen in a point with the coordinates $y = 0$, $x = x_0$ only when the condition of synchronism is correct:

$$\sin\varphi_n = n \sin\varphi_1. \tag{4}$$

In accordance with it, FST angular dimensions must be chosen.

Normalized to the amplitude of the acoustic field of radiating FST, i.e. its

directivity diagram, is determined with the formula

$$D(x, y) = \frac{1}{2N+1} \text{Mod} \sum_{n=-N}^{+N} (-1)^n \exp[-jk(x \sin\varphi_n + y \cos\varphi_n)]. \quad (5)$$

Near FST the axis Ox i.e., when $y \approx 0$ as well as with small angles (assuming $\cos\varphi_n \approx 1$),the relation (5), taking into account the condition of synchronism (4), is a sum of geometrical progression and can be written as

$$D(x, 0) = \frac{1}{2N+1} \frac{\cos\left(\frac{2N+1}{2} kx \sin\varphi_1\right)}{\cos {}^1/_2 kx \sin\varphi_1}. \quad (6)$$

The relation (6) shows that as a result of interference of a great number of flat waves the acoustic field of radiating FST, gains the form of a rather narrow beam whose intensity maximum is seen along the line of synchronism, i.e., when

$$x = x_0 = \frac{\pi}{k \sin\varphi_1} = \frac{v}{2f \sin\varphi_1} \quad (7)$$

and shifts along the aperture when frequency is varied. The beam width at the level of 0.64 is equal to

$$\delta x = \frac{\lambda}{(2N+1)\sin\varphi_1} \approx \frac{\lambda}{\sin\varphi} \quad (8)$$

where λ and v–SAW wavelength and its phase velocity.

Frequency deviation corresponding to the beam shift of its width characterizes the frequency properties of FST and depends only on the number of fingers:

$$\delta f = \frac{2f}{2N+1} \approx \frac{f}{N} \quad (9)$$

The electric signal received by one finger of receiving FST is proportional to the value of the acoustic field averaged along the finger $a(x, y, t)$(2), i.e.

$$u_m(t) = \frac{1}{x_2 - x_1} \int_{x_1}^{x_2} a(x, y(x), t)dx, \quad (10)$$

where

$$y(x) = y_0 + x \text{tg}\varphi_m \quad (11)$$

– the equation of the straight line coinciding with the finger axis, m – rank number of the finger, x_1, x_2 – coordinates of the aperture's edges of receiving FST.

The electric signal of receiving FST containing $2N+1$ fingers can be found as the following sum:

$$u(t) = \sum_{m=-N}^{N} (-1)^m U_m(t) = Q(f)\exp(j\omega t). \quad (12)$$

As a result of integrating Eq. (11) and summarizing Eq. (12), the function $Q(f)$ is proportional to the complex voltage transmission coefficient of the filter:

$$Q(f) = \sum_{m=-N}^{+N} \sum_{m=-N}^{+N} (-1)^{n+m} \frac{\sin(\beta\pi f/f_0\gamma_{nm})}{\beta\pi f/f_0\gamma_{mn}} \times$$

$$\times \exp\left[j\pi \frac{f}{f_0}\left(\gamma_{nm} - M\sin^2\frac{\varphi_n}{2}\right) - j2\pi f\tau_0 \right], \quad (13)$$

where

$$\gamma_{nm} = n + m\frac{\cos\varphi_n}{\cos\varphi_m}; \quad \beta = \frac{\Delta x}{2x_0} \approx \frac{2\Delta f}{f_0};$$

$$f_0 = \frac{v}{2x_0\sin\varphi_1}; \quad x_0 = \frac{x_2 + x_1}{2};$$

$$\Delta x = x_2 - x_1; \quad M = \frac{4y_0 f_0}{v} = \frac{y_0}{\lambda_0}; \quad \tau_0 = \frac{y_0}{v},$$

In the formula (13) the following designations are found f_0 -frequency when the point of synchronism x_0 coincides with the center of aperture, λ_0 – SAW wavelength on frequency f_0, y_0 – the distance between the axes of symmetry of FST.

AFR and phase-frequency response PFR of the filter are respectively the absolute value and argument of the complex function $Q(f)$ and can be written as

$$K(f) = \sqrt{A^2 + B^2};$$

$$\varphi_k(f) = 2\pi f\tau - \operatorname{arctg}\frac{B}{A}, \quad (14)$$

where

$$A = \sum_{n=-N}^{+N} \sum_{m=-N}^{+N} (-1)^{n+m} \frac{\sin\beta\pi f/f_0\gamma_{nm}}{\beta\pi f/f_0\gamma_{nm}} \times$$

$$\times \cos\pi\frac{f}{f_0}\left(\gamma_{nm} - M\sin^2\frac{\varphi_n}{2}\right); \quad (15)$$

$$B = \sum_{n=-N}^{+N} \sum_{m=-N}^{+N} (-1)^{n+m} \frac{\sin\beta\pi f/f_0\gamma_{nm}}{\beta\pi f/f_0\gamma_{nm}} \times$$

$$\sin\pi\frac{f}{f_0}\left(\gamma_{nm} - M\sin^2\frac{\varphi_n}{2}\right).$$

Computation in accordance with Eqs. (14) and (15) show the following:

With small distances between FST axes of symmetry ($y_0 \ll y$) and small opening angles ($\varphi < 10°$), AFR and PFR actually do not depend on y_0 and φ. AFR shape is very close to rectangular and PFR shape – to straight. Actually, there are no AFR and PFR ripples in the filter's passband.

The transition coefficient in the passband is reversely proportional to frequency, and decreases proportionally to the square of frequency deviation outside the passband. The AFR slope on the edges of the passband is proportional to the number of fingers, that is in agreement with Eq. (9).

For example when $N = 20$ and $\varphi = 10°$, the passband $f/f_0 = 0.05$, and signal suppression with the frequency deviation of $2f$ reaches the level of 50 dB (0.3%). Such parameters whithout AFR and PFR ripples cannot be achieved in acoustic filters with apodized transducers having parallel fingers [2].

When the FST opening angle increases (i.e., when $\varphi > 10°$) signal suppression outside the filter's passband becomes worse. AFR and PFR ripples in the passband grow, the signal level in the suppression band increases.

With the distance y_0, between FST axes of symmetry increases, filter performance degrades. AFR and PFR ripples grow, signal suppression outside the passband decreases.

The filter's AFR close to rectangular is obtained only when the number of finger couples reaches a certain optimal value dependent on the relative bandwith in the FST aperture. When N is not great enough. AFR has a Gaussian line shape, and when N is too great i.e., when the FST opening angle is large, the AFR skew in the passband increases. If the FST aperture $\Delta x = 20\lambda$ and the relative passband $\Delta f/f_0 = 0.2$ then the optimal number of finger couples $N = 20 \ldots 25$.

An analysis of AFR and PFR SAW FST filters leads to the following conclusions:

– filters whose FST have a small opening angle lower than 10 and are placed as close to each other as possible, have the best performance;

– the AFR slope on the edges of the passband is determined by the number of finger couples in FST;

– the signal suppression level outside the passband and insertion losses in the passband are considerably dependent on the distance between FST.

References

[1] S. A. ZABUZOV, U. G. SMIRNOV, *Radiosignal processing with acustoelectronic and acoustooptic devices*, Nauka Leningrad, 14, 1983 [Russ.].

[2] S. S. KARINSKY, *SAW signal processing devices*, Sovetskoe radio Moskwa 1975 [Russ.].

ARCHIVES OF ACOUSTICS
16, 1, 167-171(1991)

NEW METHOD FOR THE CALCULATION OF THE TEMPERATURE BEHAVIOUR OF THE PIEZOELECTRIC RESONATOR PARAMETERS

J. ZELENKA

Technical University of Mechanical and Textile Engineering
(Hálkova 6, 461 17 Liberec, Czechoslovakia)

The derivatives $G^{(1)}_{ijkl}$ and $G^{(2)}_{ijkl}$ of the elastic stiffnesses which described the elastic properties of thermally deformated and with small-amplitude vibrated quartz plates were defined be LEE and YONG in 1985. The values of the derivatives were computed and are given in the paper. The relations for computing the temperature coefficients of frequency suitable for the more precise expression of the temperature behaviour of quartz plates vibrated in thickness modes are published.

1. Introduction

The described, new more precise, method for the calculation of resonant frequency temperature dependence of quartz resonators goes out from the LEE's and YONG's paper [1] and started from the preposition that the linear field equations for small vibrations have to be superposed on the thermally-induced deformations. It is necessary to consider the nonlinear field equations of thermoelasticity when the thermally-induced deformation is calculated.

2. Equations of motion and traction boundary condition

It follows from the solution of the mentioned system of equations derived by LEE and YONG for the thickness vibration of quartz plates that the incremental displacement equations of motions and traction boundary conditions can be considered in the form

$$G_{ijkl}u_{k,ji} = \varrho_0 \ddot{u}_i,$$
$$p_i = n_j G_{ijkl} u_{k,l} \text{ on } S \tag{1}$$

where ϱ_0 is the mass density in natural state, u_i are the displacement components, p_i are the incremental strain components, n_j are components of the unit outward normal to the faces of the plate in natural state and the effective elastic stiffnesses G_{ijkl} and their derivatives $G^{(n)}_{ijkl}$ are given by the relations

$$
\begin{aligned}
G_{ijkl} &= C_{ijkl} + G^{(1)}_{ijkl}\theta + G^{(2)}_{ijkl}\theta^2, \\
G^{(1)}_{ijkl} &= C_{sjkl}\alpha^{(1)}_{is} + C_{ijsl}\alpha^{(1)}_{ks} + C_{ijklmn}\alpha^{(1)}_{mn} + C^{(1)}_{ijkl}, \\
G^{(2)}_{ijkl} &= C_{sjtl}\alpha^{(1)}_{is}\alpha^{(1)}_{kt} + C_{sjkl}\alpha^{(2)}_{is} + C_{ijsl}\alpha^{(2)}_{ks} + C^{(1)}_{sjkl}\alpha^{(1)}_{is} + \\
&\quad + C^{(1)}_{ijsl}\alpha^{(1)}_{ks} + C_{sjklmn}\alpha^{(1)}_{is}\alpha^{(1)}_{mn} + C_{ijslmn}\alpha^{(1)}_{ks}\alpha^{(1)}_{mn} + \\
&\quad + C_{ijklmn}\alpha^{(2)}_{mn} + \frac{1}{2}\tilde{C}^{(2)}_{ijkl}.
\end{aligned} \tag{2}
$$

In the relations (2) $\alpha^{(n)}_{ij}$ are thermal expansion coefficients, C_{ijkl}, C_{ijklmn} are the second- and third-order elastic stiffnesses of the crystal, $C^{(1)}_{ijkl}$, $\tilde{C}^{(2)}_{ijkl}$ are the temperature derivatives of elastic stiffnesses given by LEE and YONG [1] and θ is the temperature change ($\theta = T - T_0$). As

$$G^{(n)}_{ijkl} = G^{(n)}_{klij},$$

Table 1. Calculated values of temperature derivatives $G^{(1)}_{ijkl}$ and $G^{(2)}_{ijkl}$ of effective elastic stiffnesses G_{ijkl}. $G^{(1)}_{ijkl}$ in 10^6 Nm^2 K^{-1}

	..11	..12	..13	..21	..22	..23	..31	..32	..33
11..	−7.879	0.000	0.000	0.000	−10.951	−2.309	0.000	−2.335	−6.598
12..		2.256	−2.309	2.256	0.000	0.000	−2.335	0.000	0.000
13..			−4.462	−2.309	0.000	0.000	−4.489	0.000	0.000
21..				2.256	0.000	0.000	−2.335	0.000	0.000
22..					−7.879	2.324	0.000	2.350	−4.279
23..						−5.285	0.000	−5.312	0.027
31..							−4.515	0.000	0.000
32..								−5.338	0.027
33..									−10.714

$G^{(2)}_{ijkl}$ in 10^3N m^{-2} K^{-2}

	..11	..12	..13	..21	..22	..23	..31	..32	..33
11..	−0.379	0.000	0.000	0.000	−0.738	−0.010	0.000	−0.011	−0.310
12..		0.199	−0.010	0.199	0.000	0.000	−0.011	0.000	0.000
13..			−0.069	−0.010	0.000	0.000	−0.057	0.000	0.000
21..				0.199	0.000	0.000	−0.011	0.000	0.000
22..					−0.379	0.011	0.000	0.011	−0.261
23..						−0.092	0.000	−0.074	0.001
31..							−0.044	0.000	0.000
32..								−0.056	0.000
33..									−0.278

but

$$G^{(n)}_{ijkl} \neq G^{(n)}_{jikl} \neq G^{(n)}_{ijkl} \tag{3}$$

generally 45 components of $G^{(1)}_{ijkl}$ and $\tilde{G}^{(2)}_{ijkl}$ must be considered when the resonant frequency temperature dependence is calculated. The computed components $G^{(1)}_{ijkl}$ and $G^{(2)}_{ijkl}$ are given in Table 1. They were calculated from the first and second temperature derivatives of the elastic stiffnesses for alpha quartz at 25°C which were published by LEE and YONG [1].

3. Resonant frequency temperature dependence of thickness vibrations of quartz plates

Let $2b$ be the thickness and n_i the components of the unit outward normal to the face of quartz plate in normal state. For traction-free face conditions the traction p_i on the surface of the plate is zero.

The solution for harmonic, antisymmetric thickness vibrations

$$u_k = A_k \sin \xi n_p X_p e^{j\omega t} \tag{4}$$

satisfies Eqs. (1) for $p_i = 0$ at $X_j = \pm b$ (X_j are crystallographical axes of quartz) provided that

$$(Q_{ik} - \lambda \delta_{ik}) A_k = 0$$

$$\xi = \frac{n\pi}{2b}, \qquad n = 1, 3, 5 \tag{5}$$

where

$$Q_{ik} = Q_{ki} = G_{ijkl} n_j n_l$$

$$\lambda = \varrho_0 \frac{\omega^2}{\xi^2} = \varrho_0 \left(\frac{2b\omega}{n\pi} \right)^2. \tag{6}$$

The amplitude A_k and the eigenvalue λ are function of the change θ of temperature ($\theta = T - T_0$)

$$A_k = A^{(0)}_k + A^{(1)}_k \theta + A^{(2)}_k \theta^2$$

$$\lambda = \lambda^{(0)} + \lambda^{(1)} \theta + \lambda^{(2)} \theta^2. \tag{7}$$

By inserting Eqs. (7) into Eqs (5) and comparing coefficients with the same powers of θ, can be obtained the system of Eqs.

$$[Q^{(0)}_{ik} - \lambda^{(0)} \delta_{ik}] A^{(0)}_k = 0, \tag{8}$$

$$[Q^{(0)}_{ik} - \lambda^{(0)} \delta_{ik}] A^{(1)}_k + [Q^{(1)}_{ik} - \lambda^{(1)} \delta_{ik}] A^{(0)}_k = 0, \tag{9}$$

$$[Q^{(0)}_{ik} - \lambda^{(0)} \delta_{ik}] A^{(2)}_k + [Q^{(1)}_{ik} - \lambda^{(1)} \delta_{ik}] A^{(1)}_k + [Q^{(2)}_{ik} - \lambda^{(2)} \delta_{ik}] A^{(0)}_k = 0, \tag{10}$$

where

$$Q_{ik}^{(m)} = G_{ijkl}^{(m)} n_j n_l \text{ for } m = 0, 1, 2. \tag{11}$$

The relations for solutions of $A_k^{(n)}$ and $\lambda^{(n)}$ were derived by LEE and YONG in [1] and here there will be given only the results of the derivation.

The zero order eigenvalue $\lambda^{(0)}$ can be derived from the relation

$$[Q_{ik}^{(0)} - \lambda^{(0)} \delta_{ik}] = 0. \tag{12}$$

The zero order amplitude $A_k^{(0)}$ can be normalized by the relation

$$A_k^{(0)} A_k^{(0)} = 1 \tag{13}$$

and calculated from the any two of Eqs. (8).

The first order eigenvalue $\lambda^{(1)}$ can be calculated from the relation

$$\lambda^{(1)} = A_i^{(1)} Q_{ik}^{(1)} A_k^{(0)}. \tag{14}$$

The first order amplitude $A_k^{(1)}$ is orthogonal to $A_k^{(0)}$

$$A_k^{(1)} A_k^{(0)} = 0 \tag{15}$$

and $A_k^{(1)}$ can be calculated from Eq. (9).

Finaly the second order eigenvalue $\lambda^{(2)}$ can be calculated from the relation

$$\lambda^{(2)} = A_i^{(0)} Q_{ik}^{(2)} A_k^{(0)} + A_i^{(0)} Q_{ik}^{(1)} A_k^{(1)}. \tag{16}$$

From second Eq. (6) follows

$$f = \frac{n}{2b} v \left[\frac{1}{\varrho_0} \lambda^{(0)} + \lambda^{(1)} \theta + \lambda^{(2)} \theta^2 \right] \tag{17}$$

and

$$f_0 = \frac{n}{2b} v \left(\frac{1}{\varrho_0} \lambda^{(0)} \right). \tag{18}$$

After substituting the first and second derivatives of the Eq. (17) with respect to temperature θ into the Bechmann's definition of the temperature coefficient of frequency

$$Tf^{(n)} = \frac{1}{n! f_0} \frac{\partial^{(n)} f}{\partial T^n} \bigg| T_0 \tag{19}$$

the relations for the first end second order of frequency temperature coefficients can be obtained

$$Tf^{(1)} = \frac{\lambda^{(1)}}{2\lambda^{(0)}},$$

$$Tf^{(2)} = \frac{1}{2\lambda^{(0)}} [\lambda^{(2)} - \lambda^{(0)} (Tf^{(1)})^2]. \tag{20}$$

4. Conclusion

The values of the derivatives $G^{(1)}_{ijkl}$ and $G^{(2)}_{ijkl}$ of the elastic stiffnesses G_{ijkl} convenient for the expression of the elastic properties of thermally deformated and with small-amplitude vibrated quartz plates are given in the paper. The derivatives were calculated from the temperature derivatives of elastic stiffnesses $C^{(1)}_{pq}$ and $\tilde{C}^{(2)}_{pq}$ for alpha quartz published by LEE and YONG [1]. The procedure for the more precise computation of the temperature coefficients of frequency of the thickness modes of vibrations of quartz plates is described. The piezoelectric properties of the plates were neglected in the published relations for the calculation of the temperature coefficients of frequency.

References

[1] P. S. Y. LEE, Y. K. YONG, *Temperature derivative of elastic stiffness derived from the frequency–temperature behaviour of quartz plates*, J. Appl. Phys., **56**, 5, 1514–1521 (1984).

ARCHIVES OF ACOUSTICS
16,1,173-179(1991)

NONLINEARITY OF THE FREQUENCY-TEMPERATURE CHARACTERISTICS OF *LC*-CUT QUARTZ RESONATORS

E. ŻUCHOWSKI, M. ŁYSAKOWSKA

Tele-and Radio Research Institute
(03-450 Warszawa, Ratuszowa 11)

On the basis of the classical theory of thickness vibrations, the formulas for the temperature coefficients and their angular derivatives of the frequency-temperature characteristics of quartz resonators with *LC*-cut are derived. Approximation of these characteristics by straight lines enables the evaluation of nonlinearity effects in a given range of temperature. A practical example is given.

1. Introduction

Accurate temperature measurement represent an important branch of modern metrology. For these purposes many kinds of temperature sensors are used, for instance the quartz resonators of appropriate e.g. *Y*, *LC* or *NL* angle cuts. The best linearity of the frequency-temperature characteristic is obtained in the case of a *LC*-cut.

2. Fundamental formulae

From the classical theory of thickness vibrations of a thin ideal crystal plate we obtain two well-known formulae [1]: for the resonance frequency

$$f = \frac{N}{2h}(\bar{c}^{(m)}/\varrho)^{1/2} \qquad N = 1, 3, \ldots \qquad m = 1, 2, 3 \tag{1}$$

where h – thickness of the plate, $\bar{c}^{(m)}$ – effective striffness, ϱ – quartz density and the secular relation for the effective stiffness

$$|c_{ijkl}m_jm_k - \delta_{il}\bar{c}^{(m)}| = 0 \qquad i, j, k, l = 1, 2, 3, \tag{2}$$

where c_{ijkl} – piezoelectrically-stiffened elastic constants, m_k, m_j – components of a unit normal vector perpendicular to the plane of the plate, δ_{il} – Kronecker's delta.

From these two relations the values of the temperature coefficients and their angular derivatives of the frequency-temperature characteristics may be obtained.

3. Nonlinearity of the frequency-temperature characteristic

The most important parameter of temperature sensors is the frequency-temperature characteristic which is almost a straight line. Therefore, in the analysis we consider a new parameter, the nonlinearity of this characteristic, which gives more interesting results.

The real characteristic is given by the known relation

$$\frac{\Delta f}{f_0} = a(T-T_0)+b(T-T_0)^2+c(T-T_o)^3 \tag{3}$$

while the approximate equation for the characteristic is assumed in the linear form

$$\left(\frac{\Delta f}{f}\right)_l = a_l(T-T_0)+b_l. \tag{4}$$

In the case when $b_l = 0$, the optimum value of a_l derived by the method of least squares can be obtained from the condition

$$\frac{\partial \delta^2}{\partial a_l} = 0$$

If $b_l \neq 0$, then a_l and b_l are obtained from

$$\frac{\partial \delta^2}{\partial a_l} = 0, \qquad \frac{\partial \delta^2}{\partial b_l} = 0$$

where

$$\delta^2 = \int_{x_d}^{x_g} (y_l - y)^2 dx,$$

$$y = \frac{\Delta f}{f_0}, \qquad y_l = \left(\frac{\Delta f}{f_0}\right)_l, \qquad x_d = T_d - T_0, \qquad x_g = T_g - T_0$$

T_d, T_g – lower and upper operating temperature, T_0 reference temperature.

Then the nonlinearity effect of the characteristic is defined as the differences $y_i - y$

$$\mathrm{N} = \mathrm{b}_l + (a_l - a)(T-T_0) - b(T-T_0)^2 - c(T-T_0{}^0)^2,$$

where b_l and $(a_l - a)$ are functions of b and c. The values of $a\,(T_f^{(1)})$, $b\,(T_f^{(2)})$ and $c(T_f^{(3)})$ and their angular derivatives will now be calculated.

4. Frequency-temperature coefficients and their derivatives

From Eq. (1), after differentiations with respect to the temperature, we obtain the following functional relation between the temperature coefficients of frequency and the temperature coefficients of $\bar{c}$, ϱ and h:

$$F(T_f^{(n)}) = \frac{1}{2}F(T_{\bar{c}}^{(n)}) - \frac{1}{2}F(T_{\varrho}^{(n)}) - F(T_h^{(n)}) \qquad n = 1, 2, 3$$

where

$$F(T_Y^{(n)}) = \frac{1}{n!}\frac{d^{n-1}\left(\frac{1}{Y}\frac{dY}{dT}\right)}{dT^{n-1}}$$

and

$$T_Y^{(1)} = \frac{1}{Y}\frac{dY}{dT}, \qquad Y \equiv f, \bar{c}, \varrho, h. \tag{7}$$

Hence, we obtain

$$T_f^{(1)} = G_1,\ T_f^{(2)} = G_2 + \frac{1}{2}G_1^2,\ T_f^{(3)} = G_3 + G_1 G_2 + \frac{1}{6}G_1^3 \tag{8}$$

where

$$G_n = \frac{1}{2}F(T_c^{(n)}) - \frac{1}{2}F(T_{\varrho}^{(n)}) - F(T_n^{(n)}). \tag{9}$$

The value of $T_c^{(n)}$ can be calculated on the basis of the formula (2). Further we can easily find that

$$T_{\varrho}^{(n)} = -(2\alpha_x^{(n)} + \alpha_z^{(n)}), \tag{10}$$

where α_x, α_z – linear thermal expansion coefficients of quartz. To obtain $T_h^{(h)}$ we write the plate thickness in the form of a vector

$$\mathbf{h} = ih_x + jh_y + kh_z. \tag{11}$$

Then for thickness vibrations

$$\mathbf{h} = h\mathbf{m} = h(im_x + jm_y + km_z) \tag{12}$$

where

$$h^2 = h^2x + h^2y + h^2z. \tag{13}$$

After calculations we obtain

$$T_h^{(n)} = \alpha_x^{(n)} + (\alpha_z^{(n)} - \alpha_x^{(n)})n_z^2, \qquad \alpha_y^{(n)} = \alpha_x^{(n)} \tag{14}$$

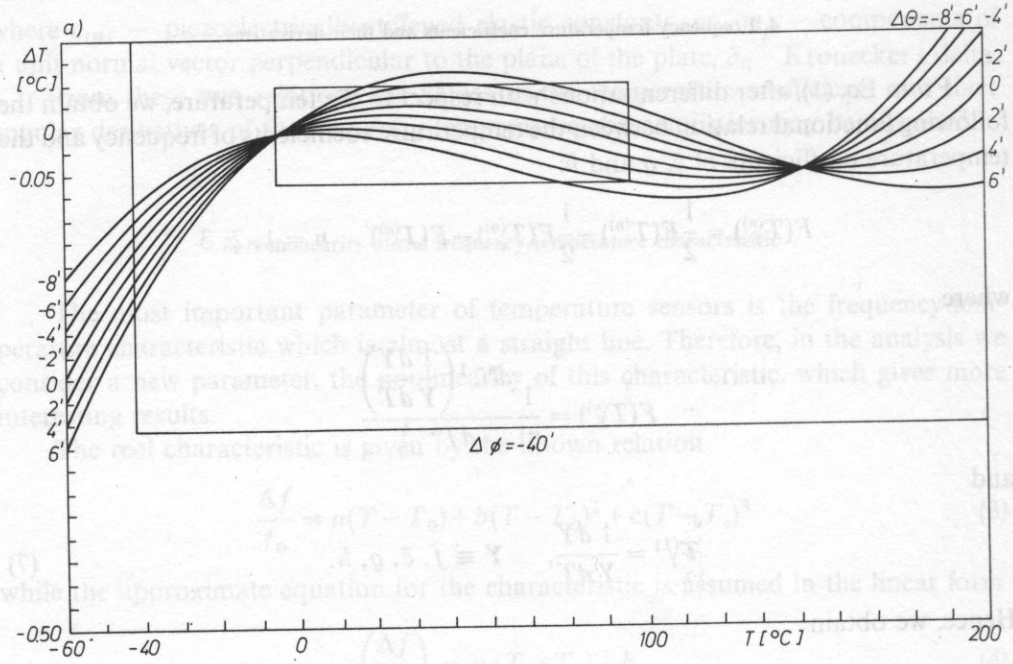
a)
ΔT [°C]
0
-0.05
-8'
-6'
-4'
-2'
0
2'
4'
6'
-0.50
-60
-40
0
100
T [°C]
200
ΔΘ=-8'-6'-4'
-2'
0
2'
4'
6'
Δφ=-40'

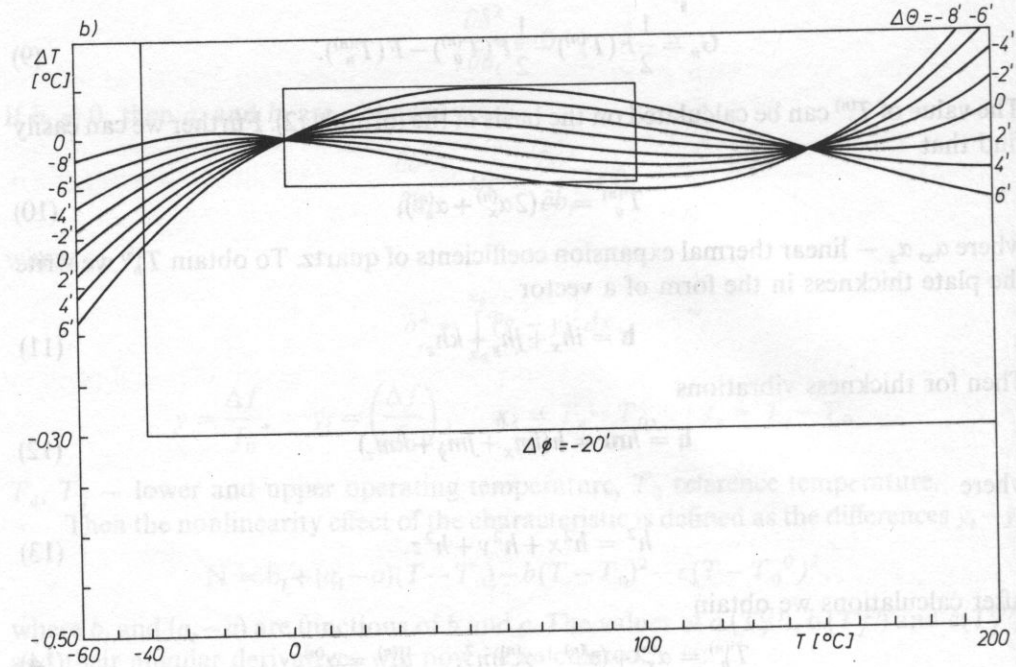
b)
ΔT [°C]
0
-8'
-6'
-4'
-2'
0
2'
4'
6'
-0.30
-0.50
-60
-40
0
100
T [°C]
200
ΔΘ=-8' -6'
-4'
-2'
0
2'
4'
6'
Δφ=-20'

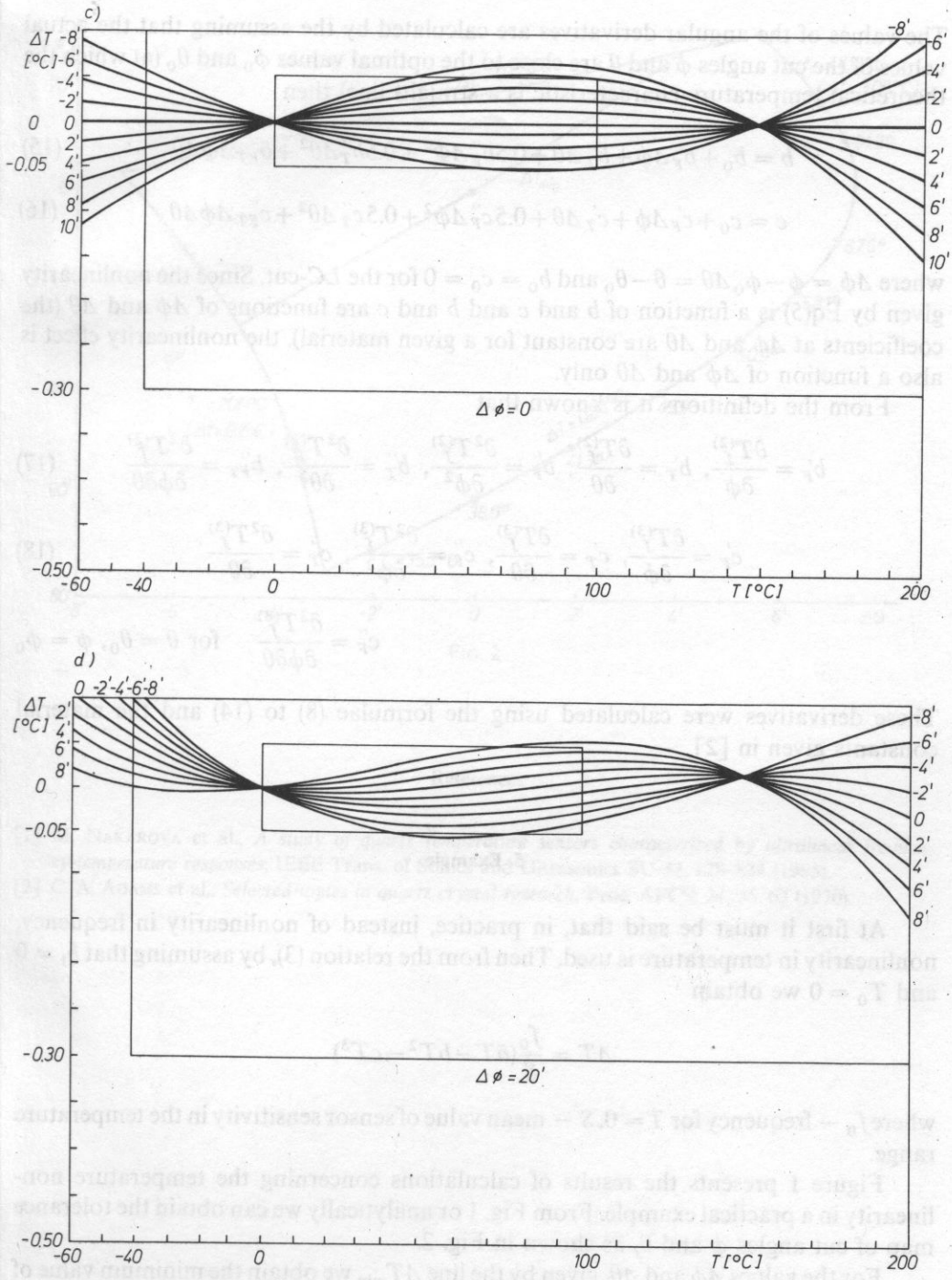
c)
ΔT [°C]
-8'
-6'
-4'
-2'
0
2'
4'
6'
8'
10'
0
-0.05
-0.30
-0.50
Δφ = 0
-60
-40
0
100
T [°C]
200

d)
ΔT [°C]
0 -2' -4' -6' -8'
2'
4'
6'
8'
0
-0.05
-0.30
-0.50
Δφ = 20'
-8'
-6'
-4'
-2'
0
2'
4'
6'
8'
-60
-40
0
100
T [°C]
200

FIG. 1

The values of the angular derivatives are calculated by the assuming that the actual values of the cut angles ϕ and θ are close to the optimal values ϕ_0 and θ_0 (at which the theoretical temperature characteristic is a straight line) then

$$b = b_0 + b'_F \Delta\phi + b'_T \Delta\theta + 0.5 b''_F \Delta\Phi^2 + 0.5 b''_T \Delta\theta^2 + b''_{FT} \Delta\phi \Delta\theta \tag{15}$$

$$c = c_0 + c'_F \Delta\phi + c'_T \Delta\theta + 0.5 c''_F \Delta\phi^2 + 0.5 c''_T \Delta\theta^2 + c''_{FT} \Delta\phi \Delta\theta \tag{16}$$

where $\Delta\phi = \phi - \phi_0 \Delta\theta = \theta - \theta_0$ and $b_0 = c_0 = 0$ for the LC-cut. Since the nonlinearity given by Eq(5) is a function of b and c and b and c are functions of $\Delta\phi$ and $\Delta\theta$ (the coefficients at $\Delta\phi$ and $\Delta\theta$ are constant for a given material), the nonlinearity effect is also a function of $\Delta\phi$ and $\Delta\theta$ only.

From the definitions it is known that

$$b'_F = \frac{\partial T_f^{(2)}}{\partial\phi},\ b'_T = \frac{\partial T_f^{(2)}}{\partial\theta},\ b''_F = \frac{\partial^2 T_f^{(2)}}{\partial\phi^2},\ b''_T = \frac{\partial^2 T_f^{(2)}}{\partial\theta^2},\ b''_{FT} = \frac{\partial^2 T_f^{(2)}}{\partial\phi\partial\theta} \tag{17}$$

$$c'_F = \frac{\partial T_f^{(3)}}{\partial\phi},\ c'_T = \frac{\partial T_f^{(3)}}{\partial\theta},\ c''_F = \frac{\partial^2 T_f^{(3)}}{\partial\phi^2},\ c''_T = \frac{\partial^2 T_f^{(3)}}{\partial\theta} \tag{18}$$

$$c''_F = \frac{\partial^2 T_f^{(3)}}{\partial\phi\partial\theta} \quad \text{for } \theta = \theta_0,\ \phi = \phi_0$$

These derivatives were calculated using the formulae (8) to (14) and the material constants given in [2]

5. Example

At first it must be said that, in practice, instead of nonlinearity in frequency, nonlinearity in temperature is used. Then from the relation (3), by assuming that $b_l = 0$ and $T_0 = 0$ we obtain

$$\Delta T = \frac{f_0}{S}(\bar{a}T - bT^2 - cT^3)$$

where f_0 – frequency for $T = 0$, S – mean value of sensor sensitivity in the temperature range.

Figure 1 presents the results of calculations concerning the temperature nonlinearity in a practical example. From Fig. 1 or analytically we can obtain the tolerance map of cut angles ϕ and θ, as shown in Fig. 2.

For the values $\Delta\phi$ and $\Delta\theta$, given by the line $\Delta T_{\min}$ we obtain the minimum value of nonlinearity (for a given value of $\Delta\phi$ or $\Delta\theta$).

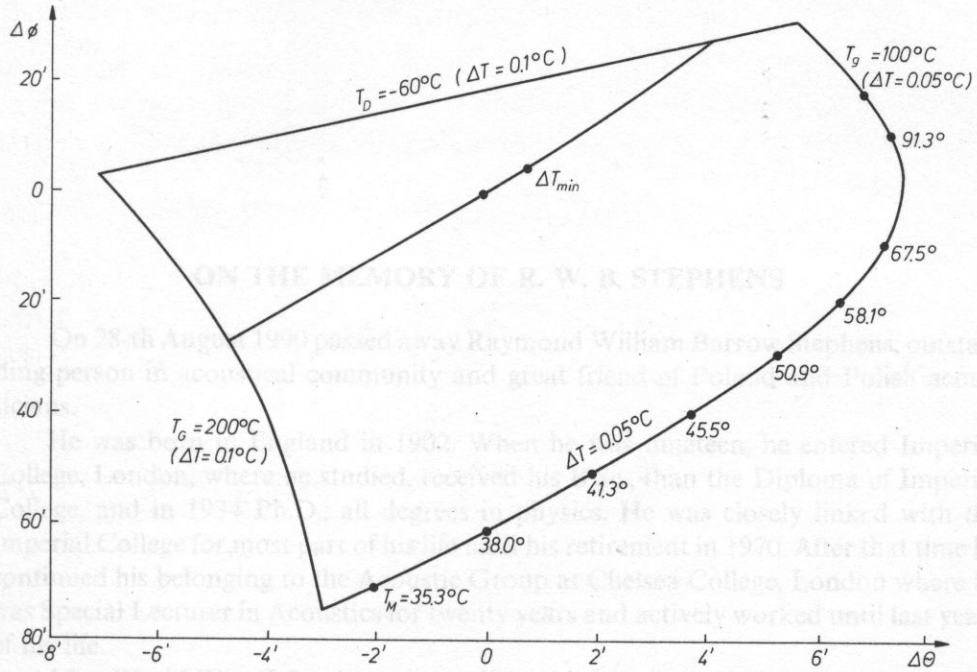

FIG. 2

References

[1] M. NAKAROVA et al., *A study of quartz temperature sensors characterized by ultralinear frequency-temperature responses*, IEEE Trans. of Sonics and Ultrasonics SU-32, 828–834 (1985).

[2] C. A. ADAMS et al., *Selected topics in quartz crystal research*, Proc. AFCS, 24, 55–63 (1970).

ON THE MEMORY OF R. W. B. STEPHENS

On 28-th August 1990 passed away Raymond William Barrow Stephens, outstanding person in acoustical community and great friend of Poland and Polish acousticians.

He was born in England in 1902. When he was nineteen, he entered Imperial College, London, where he studied, received his B.Sc., than the Diploma of Imperial College, and in 1934 Ph.D.; all degrees in physics. He was closely linked with the Imperial College for most part of his life until his retirement in 1970. After that time he continued his belonging to the Acoustic Group at Chelsea College, London where he was Special Lecturer in Acoustics for twenty years and actively worked until last years of his life.

After World War II Stephens was well established as a university teacher and his Acoustics Research Group begun to take shape. He was initiator and a supervisor of numerous degrees (more than 50 of them have been Ph.D. and D.Sc.) of students from U. K. and abroad. A great number of visiting scientists spent a shorter or longer periods of time working at his group. A number of Polish acousticians were among them and Stephens, along with his long life, always took care of them. Many other Polish acousticians visited Stephens Group during their scientific stays in U.K. On many occasions he had paid visits to Poland and was guest of Polish acousticians. Little known is the fact that his contacts with Polish Scientists date as far back as the World War II. During the war and just after the War he helped many Polish students studying at London University. During that time he was befriended with prof. Józef Mazur (Professor of Polish University College in London) who belonged to the staff of Imperial College until he came back to Poland in 1959 to guide the Institute of Low Temperatures in Wrocław.

In appreciation of his friendship and scientific achievements Dr R. W. B. Stephens was awarded a Honorary Membership of the Polish Acoustical Society in 1983.

Also, he was honored with numerous awards and distinctions of other acoustical societes around the world. He was the first foreigner honored by the highest american award: the Gold Medal by American Acoustical Society in 1977. He reccived also the Rayleigh Gold Medal of the British Acoustical Society, the Silver Medal of de Groupement des Acousticiens de Language Francaise in France and the honorary doctorate from the University of Cordoba in Argentina, as well as several honorary memberships in a number of other acoustical Societes.

He has been the author or co-author of six books and more than fifteen papers on acoustics and relative topics.

Raymond W. B. Stephens was active until last year of his life. He will be remembered by many of Polish acousticians as an ouststanding scientist a sincere friend and a nice person. He passed away in his 88-th year of life.

Jerzy K. Zieniuk, Antoni S. Śliwiński

The XXXVII OSA'90 Report

The annual conferences of Polish acousticians sponsored by the Committee on Acoustics of the Polish Academy of Sciences and by the Polish Acoustical Society, have been organized for thirty seven years, under a traditional name of the Open Seminar on Acoustics (OSA), actually by the seven regional branches of the Society, subsequently. This year the site of the OSA'90 was Gdańsk, and particularly its largest academic institution, widely known over the world for over eighty years, namely the Technical University of Gdańsk.

Thanks to the patronage of the Rector of the Technical University the debates were located in a well outfitted auditoria of the Shipbuilding Institute building, and all the participants were accomodated and boarded in a newly built students-hostel and students-restaurant nearby.

The OSA debates are annually the most important acoustical event in Poland, because, besides scientifical discussions covering all the branches of the largely interpreted field of acoustics, vital organizatory activities take place therein. This time, a day before the official opening of the OSA debates, the General Assembly of the Polish Acoustical Society took place, including elections of the Governing Bodies for the next three years term. The following colleagues have been elected:

President – Antoni Śliwiński (University of Gdańsk)
Vice-President – Aleksander Opilski (University of Silesia)
General Secretary – Tomasz Hornowski (University of Poznań)
General Treasurer – Mikołaj Łabowski (University of Poznań)
Body-Member – Marianna Sankiewicz (Techn. Univ. of Gdańsk)
Body-Member – Jerzy Ranachowski (Pol. Ac. of Sci. Warszawa)
Body-Member – Andrzej Gołaś – (Inst. of Vibroacoust. Kraków)
Body-Member – Henryk Idczak – (Techn. University of Wrocław)
Audit Chairman – Gustaw Budzyński (Techn. Univ. of Gdańsk)
Auditor – Zenon Jagodziński (Techn. Univ. of Gdańsk)
Auditor – Eugeniusz Soczkiewicz (Gliwice T. Univ.)
Dep. Auditor – Maria Leśniak (Techn. Univers. of Rzeszów)
Fellow Jury Chairman – Zygmunt Kleszczewski (Gliwice T.U.)
Fellow Jury Member – Andrzej Muszyński (Naval Acad. Gdynia)
Fellow Jury Member – Edmund Talarczyk (Techn. Univ. Wrocław)

On Tuesday, September 11, the OSA'90 debates started with the Opening Session. Marianna Sankiewicz, Chairman of the Organizing Committee, welcomed all and

introduced the Deputy Rector of the Technical University, Professor Wojciech Sobczak, who delivered an inaugural address to the participants.

The first plenary lecture was delivered by Professor Ignacy Malecki, Honorary Chairman of the OSA Scientific Committee. His lecture was devoted to the history of development of acoustics in the Gdańsk region. In the second plenary lecture, professor Jerzy Sadowski presented problems connected with acoustical planning of town areas.

There were five plenary sessions and fourteen technical sessions, where debates ran in two sections, in parallel. Technical sessions were devoted to several branches of acoustics: Acoustics of Speech, Environmental Acoustics, Noise Abatement, Physical Acoustics, Room Acoustics, Acoustical Measurements, Electroacoustics, Musical Acoustics, Psychological Acoustics, Sound Engineering, etc.

A specially structured session, named Practicum, was devoted to practical demonstrations of laboratory hardware and software in sound engineering. This session gained a vivid interest among the participants and aroused interesting discussions.

The late arrived papers were presented as posters; some of them were read during pauses due to some absent authors of contributed papers.

The exhibitors took advantage of the large foyer area foreseen for the exhibition. Bruel and Kjaer, as at every OSA Seminar, presented their latest achievements, "0,1 dB" from France and Elsinco from Warsaw exhibited their equipments.

The total number of papers presented during the OSA'90 debates was 78, including 5 plenary lectures, 68 contributed papers, 4 poster reports, and 1 Practicum lecture. The total number of participants was 110, including 56 authors from ten cities of Poland, 9 authors from seven cities from abroad, 38 participants and guests from Poland and 7 from abroad.

The Proceedings of the XXXVII Open Seminar on Acoustics edited and distributed among participants, prior to the debates opening, include in a two volume edition all the papers submitted by authors and approved by the Scientific Committee reviewers for publication. The edition contains texts of the 6 plenary lectures, 78 contributed papers, 6 poster reports, and an introduction to Practicum presentation, as well as subsidiary information concerning OSA organization. 124 authors and organizers are listed in the name index.

The excuted program of the Seminar contained:

1st plenary session: Chairman A. Śliwiński (Univ. of Gdańsk)

I. Malecki (Polish Academy of Sciences, Warszawa), *On the Opening of the XXXVII OSA'90* in Gdańsk.

J. Sadowski (Acoustical Dept. ITB, Warszawa), *Acoustical Designing of Urban Areas.*

Session A1: Chairman H. Harajda (WSP Zielona Góra)

A11 Z. Brachmański, W. Myślecki, K. Baściuk (Wrocław T. Univ.) *Relation between speech intelligibility and subjective scale of speech transmission quality for delta coding.*

A12 J. Zalewski (Wrocław Techn. Univ.), *Vowel recognition using connectionist network.*

A13 J. ZALEWSKI (Wrocław T.U.), *Comparison in the effectiveness in speaker recognition experiments using statistical pattern classifier and connectionist classifiier.*

Session B1: Chairman J. SADOWSKI (Acoust. Dept. ITB Warszawa)

B11 G. ENGLER (TH Zwickau), *Berechnung von Massnahmen zur Einhaltung zukunftiger Gerauschgrenzwerte für Fahrzeuge und Fahrzeugbaugruppen.*

B12 R. MAKAREWICZ, J. JARZĘCKI (Poznań Univ.), *Prediction of train noise in open terrain.*

B13 R. MAKAREWICZ, U. JORASZ, A. WŁOCH (Poznań Univ.), *Noise attenuation by barrier in terms of loudness level.*

Session A2: Chairman A. OPILSKI (Univ. of Silesia)

A21 K. BAŚCIUK, S. BRACHMAŃSKI (Wrocław T.U.), *The linear filtering of the complex cepstrum.*

A22 A. DOBRUCKI, C. SZMAL (Wrocław T.U.), *The influence of the geometry and material on the dynamic properties of loudspeaker spider and cone suspension.*

A23 M. GŁOWACKI, J. STANCLIK, M. PIERZCHAŁA (Wrocław T.U. HILMAR Wrocław), *Influence of type of compensation on generation of transient intermodulation distortion in audio power amplifiers.*

A24 J. BEDNAREK, T. GUDRA, E. TALARCZYK (Wrocław T.U.), *Airborne sandwich transducer.*

A25 W. Zawieska (CIOP Warszawa), *Active noise attenuation system in a duct – the laboratory stand.*

Session B2: Chairman W. STRASZEWICZ (Warszawa T.U.)

B21 R. MAKAREWICZ, Ł. KRASNOWSKA (Poznań Univ.), *Traffic noise propagation in a built-up area.*

B22 B. BOGUSZ, A. JAROCH, M. RABIEGA, B. RUDNO-RUDZIŃSKA (Wrocław T.U.), *Noise level pattern around a source of discrete low frequency component.*

B23 B. BOGUSZ, H. IDCZAK (Wrocław T.U.), *Random error determination by the confidence intervals method in sound power measurements using sound intensity measurements.*

B24 B. BOGUSZ, H. IDCZAK (Wrocław T.U.), *Analysis of estimation random error in sound power measurements using sound intensity method.*

B25 E. KOTARBIŃSKA, G. MAKAREWICZ (Warszawa T.U., – CIOP), *The pressure index – a basic parameter for acoustic estimation of industrial halls.*

B26 D. PLEBAN (CIOP Warszawa), *Investigation on sound absorption properties of materials in frequency range from 4 to 20 kHz.*

Session A3: Chairman W. RDZANEK (WSP Rzeszów)

A31 C. LEWA (Gdańsk Univ.), *NMR response in the presence of mechanical waves.*

A32 Z. KACZKOWSKI (Pol. Ac. Sci. Warszawa), *Magnetomechanical coupling in As-quenched and annealed... metallic glasses.*

A33 B. AUGUSTYNIAK, Z. KACZKOWSKI, L. MAŁKIŃSKI (Gdańsk T.U., Pol. Ac. Sci. Warszawa), *Relation between magnetomechanical Barkhausen effect and delta E effect in ... metallic glasses.*

A34 A. SIKORSKA, A. ŚLIWIŃSKI, S. ZACHARA (Gdańsk Univ.), *Photoacoustic studies on Europium Chelate powder.*

A35 A. SNAKOWSKA (WSP Rzeszów), *The acoustic field inside and outside the semi-infinitive unbaffled cylindrical wave-guide.*

A36 A. SNAKOWSKA (WSP Rzeszów), *The saddle point method applied to the problem of a far field outside the semi-infinitive cylindrical wave-guide.*

Session B3: Chairman J. ZALEWSKI (Wrocław T.U.)

B31 E. HOJAN (Poznań Univ.), *Subjective and objective evaluation of acoustic properties of concert halls based on their impulse response.*

B32 A. GOŁAŚ, J. WIERZBICKI (AGH Kraków), *Sound field modelling in rooms in various shapes using source image method.*

B33 J. TARGOŃSKI (Wrocław T.U.), *Sound column.*

B34 H. WINKLER (Bauakademie Berlin), *Influence on the reverberation time by slope of the side walls.*

B35 Z. WĄSOWICZ (Wrocław T.U.), *Investigations of the sound reflections time structure of the Wrocław Operetta hall.*

B36 H. IDCZAK, A. JAROCH, K. RUDNO-RUDZIŃSKI (Wrocław T.U.), *Properties of sound absorbing structure for anechoic chamber.*

2nd plenary session: Chairman E. SOCZKIEWICZ (Gliwice T.U.)

R. PANUSZKA (AGH Kraków), *Applications of intensity methods in vibroacoustical investigations.*

Session A 4: Chairman E. HOJAN (Poznań Univ.)

A41 W. HIRSCH, G. UHLMANN (Nucl. Inst. Rossendorf), *Methods for acoustic emission transducer calibration.*

A42 B. SMAGOWSKA, E. SUMOWSKA (CIOP Warszawa), *Testing the efficiency of vibration damping by protective gloves.*

A43 D. RUSER (Rostock Univ.), *Co-operation of the operator with a SONAR imaging system.*

B 4 Session: Chairman E. SOCZKIEWICZ (Gliwice T.U.)

B41 L. LENIOWSKA, W. RDZANEK, P. WITKOWSKI (WSP Rzeszów), *Mutual acoustical interactions of circular sources with parabolic velocity distribution for high frequency.*

B42 L. LENIOWSKA, W. RDZANEK, P. WITKOWSKI (WSP Rzeszów), *Mutual impedance of circular sources for high intereference parameters.*

B43 L. LENIOWSKA, W. RDZANEK (WSP Rzeszów), *The acoustical field of circular plate free vibrating in the planar finite baffle.*

B44 W. RDZANEK, P. WITKOWSKI (WSP Rzeszów), *Mutual acoustical interactions of circular sources with regard to damping effect.*

Session A5: Chairman R. PANUSZKA (AGH Kraków)

A51 E. SOCZKIEWICZ (Gliwice T.U.), *Scattering of acoustic waves and statistical characteristics of randomly inhomogeneous media.*

A52 H. GAWDA, H. TRĘBACZ (Med. Acad. Lublin), *Acoustical parameters of cancellous bone with different mineral content.*

A53 B. KOSTEK, G. PAPANIKOLAOU (Gdańsk T.U., Thessaloniki Univ.), *Multi-purpose acoustic analyzer.*

A54 D. GAFKA (IPPT PAN Warszawa), *Surface acoustic wave velocity on prestressed piezoelectric substrate.*

A55 J. FORTUNA, S. PIETREK (WAT Warszawa), *Accuracy of the wind velocity measurements of the atmospheric boundary layer by a Doppler sodar.*

Session B5: Chairman G. PAPANIKOLAOU (Thessaloniki Univ.)

B51 H. KUBIAK, J. BRĄGOSZEWSKI, S. WEYNA (Szczecin T.U.), *Computer aided presentation of results of acoustic field measurement, using sound intensity method.*

B52 J. REGENT (Gdańsk Music Ac.), *Practical usage of the method of diffraction integrals in the research of the acoustic field in a room.*

B53 A. ROZWADOWSKI ('0.1 dB' Villeurbanne), *PC based integrated acquisition and data processing system.*

B54 N. RUMMLER, V. GROSSER, C. BOMBACH (Ac. Sci. Chemnitz), RENO – *a computer program to investigate the sound emission from engine components by means of holographic vibration analysis.*

B55 A. KACZMARSKA, D. AUGUSTYŃSKA (CIOP Warszawa), *Some sources of infrasonic noise in steel plants and machine building industry.*

B56 J. KOTON (CIOP Warszawa), *The simplified mathematical model of noise emission of ultrasonic cleaners.*

Session A6: Chairman A. GOŁAŚ (AGH Kraków)

A61 S. BELOKON, E. VASILTSOV (Leningrad Res. Inst., Kiev T.U.), *Peculiarities of defining basic characteristics of acoustic field.*

A62 E. VASILTSOV, Y. OVCHAROV (Kiev T.U. Cherkassy Branch), *Peculiarities of reflectance evaluation by phase method.*

A63 E. BUDZYŃSKI (Gdańsk T.U.), *On sound-sources subjective localization theory.*

A64 G. BUDZYŃSKI, M. SANKIEWICZ (Gdańsk T.U.) *Problem of the aggravating hearing-loss in young people.*

A65 A. KULOWSKI (Gdańsk T.U.), *Modification of the ray method for modelling acoustic field in rooms.*

Session B6: Chairman J. CHWAŁEK (KUL Lublin)

B61 M. ISZORA, M. SANKIEWICZ (Gdańsk T.U.), *Acoustical investigation of S[t]Catherine carillon bells.*

B62 A. KACZMAREK (Gdańsk T.U.), *Comparative analysis of Gdańsk basilicas selected organ stops.*

B63 Z. PERUCKI (Gdańsk T.U.), *The feedback in flue pipes.*

B64 A. KACZMAREK (Gdańsk T.U.), *Methodology of organ stops analysis by means of multichannel sound registration system on IBM PC computer.*

B65 A. KACZMAREK (Gdańsk T.U.), *Polynomial approximation of the envelope spectrum of steady state organ sounds.*

B66 Z. PERUCKI (Gdańsk T.U.), *Investigations on the mechanism of sound generation in flue pipes.*

B67 B. KOSTEK, A. CZYŻEWSKI (Gdańsk T.U.), *Computer controlled pipe-organ instrument.*

3rd plenary session: Chairman M. SANKIEWICZ (Gdańsk T.U.)

A. CZYŻEWSKI *Digital procedures of sound engineering.*

B74 A. DYRO, A. CZYŻEWSKI (Gdańsk T.U.), *Implementation of digital filters for IBM.*

Session A7: Chairman M. SANKIEWICZ (Gdańsk T.U.)

A71 H. TYGIELSKI (WSP Zielona Góra), *Acoustic potential of a point source in a region limited by two parallel planes.*

Session B7: Chairman G. BUDZYŃSKI (Gdańsk T.U.)

B71 G. PAPANIKOLAOU, G. KALLIRIS (Thessaloniki Univ.), *Digital recovery of impulse noise affected signals.*

B72 K. CISOWSKI (Gdańsk T.U.), *Implementation of smoothing filters for the restoration of musical recordings.*

B73 W. KUCHARSKI, A. CZYŻEWSKI (Gdańsk T.U.), *Implementation of basic methods of sound synthesis for IBM-PC compatibles.*

B74 A. DYRO, A. CZYŻEWSKI (Gdańsk T.U.) *Implementation of digital filters for IBM PC compatibles*"

B75 M. IWANOWSKI, A. CZYŻEWSKI (Gdańsk T.U.), *Sound visualization using IBM PC compatibles.*

B76 G. GRAJA, A. CZYŻEWSKI (Gdańsk T.U.), *Computer aided standard console.*

B77 J. ZIAJKA, A. CZYŻEWSKI (Gdańsk T.U.), *Interfacing a digital tape recorder to a PC computer.*

B78 P. MRÓZ, A. CZYŻEWSKI (Gdańsk T.U.), *Digital sound editing system.*

4th plenary session: Chairman M. SANKIEWICZ (Gdańsk T.U.)

H. LASOTA (Gdańsk T.U.), *Spherical waves in acoustics.*

5th plenary session: Chairman M. SANKIEWICZ (Gdańsk T.U.) *Discussion and concluding debates*

Poster presentation included the following reports:

E. VASILTSOV, S. BELOKON (Kiev T.U., Leningrad Res. Ins.), *Combined acoustic receiver.*

A. WOLNIEWICZ (STILON Gorzów), *Physical chemistry of the gamma* Fe_2O_3 and *the electroacoustic characteristics of magnetic tapes.*

K. WÓJTOWICZ, W. GRUSZECKI, A. ORZECHOWSKI (Med. Ac. Lublin, MCS Univ. Lublin), *The application of ultrasonic velocity measurements in the observation of the liposomas phase transitions.*

G. BRZÓZKA, J. DEGÓRSKI, Z. KOZŁOWSKI, P. AULS, G. HAACK, (AGROMET-PROJEKT Poznań, RATIOPROJEKT Berlin), *Comparative analysis of the noise exposure assessment methods obligatory in Poland and in GDR, in the light of own experience.*

Soon after the closing of the Seminar the Jury of the competition dedicated to the memory of Marek Kwiek, made the decision concerning awards for young authors due to their best presented papers. Three awards have been assigned: the first one to Anna Snakowska (WSP Rzeszów), the second one to Henryk Tygielski (WSP Zielona Góra), the third one to Andrzej Kaczmarek (Gdańsk T.U.).

Sightseeing excursions to the City of Gdańsk included also acoustical events: live organ music and a lecture on organbuilding art presented by J. Chwałek and J. Gudel on the example of a beautiful baroque organ instrument in S'Nicolaus Basilica.

A common dinner-party on Thursday night permitted to establish or to strengthen the personal contacts among the participants, so important for the future development of the society of acousticians.

The Organizing Committee of the OSA'90 takes this opportunity to express once more its gratitude to all the person and institutions who helped at the realization of that task.

Marianna Sankiewicz

International congress on ultrasonics (ICU–90)

December 12–14, 1990, New Delhi, India

International Congress on Ultrasonics (ICU–90) was organised by National Physical Laboratory at New Delhi on December 12–14, 1990. The congress was sponsored by the Council of Scientific and Industrial Research, Indian Council of Medical Research, Central Scientific Instrument Organisation and Ultrasonic Society of India. This was second international conference being organised by National Physical Laboratory (NPL) in ultrasonics, after the one held in July 1980. The Chairman of the Advisory Board was Prof. Dr. S. K. Joshi, Director of NPL and the Secretary was Deputy Director of NPL, Dr. V. N. Bindal. The Chairman of Organising Committee was Dr. T. K. Saksena, Co-Chairman – Mr. S. C. Gupta and Secretary – Dr. Ashok Kumar. The Convenors of the Publication and Technical Programme Committee, Finance Committee and Reception Committee were Dr. S. K. Jain, Mr. Ved Singh, Dr. J. Singh and Dr. R. P. Tandon, respectively. The Chairman of the Souvenir and Exhibition Committee was Dr. S. P. Signal and Convenior – Dr. J. N. Som.

The ICU–90 was conducted in nine sessions (I. Ultrasound in Medicine (A), II. Underwater Acoustics (B), III. Ultrasonic Studies in Solids (C), IV. Non-Destructive Evaluation (D), V and VI. Ultrasonic Propagation in Liquids (E), VII, VIII and IX Ultrasonic Transducers, Instrumentation and Materials (F)

The congress was inaugurated by Prof. S. Z. Qasim, Vice-Chancellor of the Jamia Millia Islamia, New Delhi. A keynote address entitled "Acoustics-Infrasonics to Ultrasonics" was delivered by Dr. V. K. Aatres, Director of the Naval Physical and Oceanographic Laboratory, Cochin, during the Inaugural Session. The scientific programme included 9 invited contributions (3 was publishes as the abstracts and 1 as invited papers) and 56 research papers. The invited talks were presented by: Prof. V. R. Minicha (Lithotripsy – Issues and Perspective), Prof. Dubrovskii (Delphine acoustics), Prof. Z. Kaczkowski (Ultrasonic studies in metallic glasses), Prof. P. K. Raju (Non-destructive evaluation of the composites using acousto-ultrasonics), Prof. L. M. Lyamshev (Radiation acoustics), Prof. V. P. Bhatnagar (Modern trends in acousto-optics diffraction), Dr. R. S. Khandpur (Challenges in ultrasound hyperthermia). The list of participants contained 171 names from India and abroad.

An exhibition had been organised by the Ultrasonic Society of India, which also brough out the Souvenir containing the programme, abstracts of the accepted papers and lists of participants and exhibitors. The Proceedings of the ICU–90, edited by the Publication Committee with Dr. T. K. Saksena as the Chairman, were given to the 102

participants during registration. These proceedings were dedicated to Dr. V. N. Bindal on his 60th birthday (25.12.1990). The proceedings contained 49 papers (1 invited and 48 contributed) from India (39), Egipt (3), Spain (1), Italy (1), Soviet Union (1), Great Britain (1), and Poland (3). On Ultrasound in Medicine were published 7 papers (35 pages), on Underwater Acoustics – 3 papers (26 pages), on Ultrasonic Studies in Solids – 7 papers (6 contributed and 1 invited, 45 pages), on Non-Destructive Evaluation – 5 papers (29 pp.), on Ultrasonic Propagation in Liquids – 14 papers (86 pp.) and on Ultrasonic Transducers Instrumentation and Materials – 13 papers (79 pp.). The index of the proceedings contained 115 author names. On the list of exhibitors were Accutrol Systems Pvt. Ltd. New Delhi, Blue Star Ltd., New Delhi, Electronics Corporation India Ltd., Hyderabad, L & T – Gould Ltd., Mysore, Mekaster Electronic Service Centre Pvt. Ltd. and Systronics (Agency Division), Ahmebabad. As the co-chairmen of the Round Table Session were invited Dr. V. N. Bindal, Dr. T. K. Saksena, Professors: Dubrovski i, Raju Kaczkowski. As the introduction to the discussion Prof. Dubrovskii has talk on ultrasonic research in Acoustical Institute of the Academy of Sciences of the USSR, prof. Raju spoke on the non-destructive investigation at the Auburn University (USA) and prof. Kaczkowski spoke on the current research status and opportunities in ultrasound in Poland. In the discussion the delegates presented their institutions, organisations and factories.

Zbigniew Kaczkowski

25–29 May 1992 Gdańsk, Poland

5-th SPRING SCHOOL ON ACOUSTO-OPTICS AND ITS APPLICATIONS

GDAŃSK, POLAND

A. Śliwiński, P. Kwiek, A. Markiewicz
Institute of Experimental Physics,
University of Gdańsk, Wita Stwosza 57
80–952 Gdańsk, Poland

Application dead line 31.03.92,
fee US $ 350 (full accomodation included)